Scuola di Dottorato in Scienze della Natura e Tecnologie Innovative

Dottorato in Scienze Farmaceutiche e Biomolecolari (XXVI Ciclo)

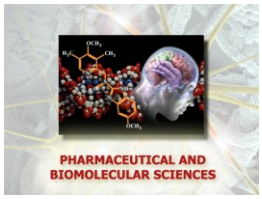

Dottorato in cotutela

Ecole Doctorale:425 Innovation Thérapeutique: du Fondamental à l'appliqué

Pôle: Pharmacotechnie et Physico-chimie
Année 2013-2014
Série Doctorat N°1271

Cotutelle de thèse

Targeted squalenoyl nanomedicines for pancreatic cancer treatment

Sabrina VALETTI

24 March 2014

JURY:

Pr. Gert STORM	*Rapporteur*
Dr. Gianfranco PASUT	*Rapporteur*
Pr. Giampaolo TORTORA	*Examinateur*
Dr. Didier DESMAELE	*Examinateur*
Pr. Patrick COUVREUR	*Co-tutor*
Dr. Barbara STELLA	*Co-tutor*
Dr. Simona MURA	*Co-tutor*

Università degli Studi di Torino – Facoltà di Farmacia
Université Paris-Sud 11 – Faculté de Pharmacie

Scuola di Dottorato in Scienze della Natura e Tecnologie Innovative

Dottorato in Scienze Farmaceutiche e Biomolecolari (XXVI Ciclo)

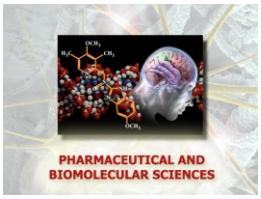

Dottorato in cotutela

Ecole Doctorale:425 Innovation Thérapeutique: du Fondamental à l'appliqué

Pôle: Pharmacotechnie et Physico-chimie
Année 2013-2014
Série Doctorat N°1271

Cotutelle de thèse

Targeted squalenoyl nanomedicines for pancreatic cancer treatment

Sabrina VALETTI

24 March 2014

JURY:

Pr. Gert STORM	*Rapporteur*
Dr. Gianfranco PASUT	*Rapporteur*
Pr. Giampaolo TORTORA	*Examinateur*
Dr. Didier DESMAELE	*Examinateur*
Pr. Patrick COUVREUR	*Co-tutor*
Dr. Barbara STELLA	*Co-tutor*
Dr. Simona MURA	*Co-tutor*

Table of Content

General Introduction……..…….....**6**

Part 1: Bibliographic study

Valetti, S.; Mura, S.; Stella, B.; Couvreur, P.
"Rational design for multifunctional non-liposomal lipid-based nanocarriers for cancer management: theory to practice."
Journal of Nanobiotechnology, 2013, 11 (Suppl 1):S6.....……...**10**

"Pancreatic cancer treatment and nanomedicine"…….....……**38**

Part 2: Experimental work

Chapter 1:
"Peptide-functionalized nanoparticles for selective targeting of pancreatic tumor" …….....……**43**

Chapter 2:
"How to functionalize squalene-based nanoparticles with a peptide: by conjugation before or after nanoparticle formation" …….....**78**

Chapter 3:
"Multi-therapeutic nanoparticles for synergistic combined therapy with gemcitabine and tyrosine kinase inhibitor" …….....…**104**

General Discussion…….…….....…**131**

General Conclusion and Future Perspectives…….....…**144**

Abbreviations…….……**147**

Annexe:

Synthèse du projet de thèse…….....**149**
Sintesi del progetto di dottorato…….....**158**

Semiramoth, N.; Di Meo, C.; Zouhiri, F.; Said-Hassane, F.; Valetti, S.; Gorges, R.; Nicolas, V.; Poupaert, J. H.; Chollet-Martin, S.; Desmaele, D.; Gref, R.; Couvreur, P. "Self-assembled squalenoylated penicillin bioconjugates: an original approach for the treatment of intracellular infections." *Acs Nano 2012, 6, 3820-31*

General Introduction

Pancreatic cancer is a lethal disease with the worst prognosis among all solid tumors. In the last decades, progresses in pancreatic cancer therapy had remained exceedingly slow and disappointing offering minimal benefits in median survival which remains of less than 6 months and the maximum of 5 years in the 6% of patients. The failure in pancreatic cancer therapy might be ascribed to both an inefficient drug delivery as a consequence of the complex tumor physio-phatology and the existence of multi-drug resistance phenomena which cause an increase of the doses required and the insurgence of an intolerable cytotoxicity on healthy tissues.
In this context, a great deal of attention focused on advanced nanoscale systems (*i.e.,* nanomedicines) with the aim to overcome the limits associated to the traditional drug delivery modalities. Nanomedicines can indeed enhance drug properties by (*i*) offering protection from degradation, (*ii*) enabling controlled release and distribution and (*iii*) increasing bioavailability while reducing undesired side effects.

This Ph.D. thesis was performed as a co-tutoring project between the University of Turin (Italy) and the University of Paris XI (France). The research was founded by the European Research Council under the European Community's Seventh Framework Program FP7/2007-2013 Grant Agreement N°249835 and by the MIUR (Ministero dell'Università e Ricerca Scientifica), Fondi Ricerca Locale (ex-60%).
In the current work we aimed to propose novel nanoscale-based strategies to optimize pancreatic cancer treatment taking into account the specific physio-pathology of this tumor. The first approach relied on the design of a targeted nanomedicine able to specifically bind receptors mainly expressed onto pancreatic cancer cells in order to selectively increase drug accumulation in these cells saving healthy ones.
In a second approach, by combining two therapeutic agents in the same nanoparticle we constructed a multi-therapeutic drug delivery system capable to increase the therapeutic index of the combined therapy.
In particular, taking advantages from the "*squalenoylation prodrug approach"*, the research activity of this Ph.D. work lead to the to design of (*i*) a novel peptide-functionalized squalenoyl gemcitabine nanoparticle and (*ii*) a tyrosine kinase inhibitor-loaded squalenoyl gemcitabine nanoparticle. Obtained nanoparticles were investigated with respect to their physico-chemical properties and *in vitro* antitumor activity. The efficacy of peptide-functionalized nanoparticles in impairing tumor growth was assessed *in vivo* on an experimental model of pancreatic cancer.

This Ph.D. thesis is divided in two main parts.
The first introducing part is composed by (*i*) a published bibliographic review on recent multifunctional non liposomal lipid-based nanocarriers that highlights the rational approaches used to improve cancer management and (*ii*) a short overview on the approaches used for pancreatic cancer treatment, with special attention on the nanomedicines.
The second part concerns the experimental work and it is divided in three chapters:

- the first chapter describes the design of targeted nanoparticles using a new peptide identified by phage display screening, the fine investigation of their surface properties and the selectivity for the biological target both *in vitro* and *in vivo;*
- the second chapter details the rational investigation of both the formulation parameters involved in the nanoparticles preparation and the physico-chemical properties of the resulting nanocarriers with the aim to design a ligand-targeted squalene-based nanoparticles showing the highest affinity for pancreatic tumor cells;
- the third chapter depicts the design of multi-therapeutic nanoparticles by combining the anticancer squalenoyl gemcitabine bioconjugate and tyrosine kinase inhibitors, their physico-chemical characterization and *in vitro* antitumor activity.

All chapters are in form of articles that have been published, already submitted or are currently in preparation.

Part 1: Bibliographic Study

Rational design for multifunctional non-liposomal lipid-based nanocarriers for cancer management: theory to practice

Journal of Nanobiotechnology, **2013**, 11(Suppl 1):S6

Sabrina Valetti [1, 2], Simona Mura [1], Barbara Stella [2] and Patrick Couvreur [1§]

[1] Univ Paris-Sud, Faculté de Pharmacie, 5 rue Jean-Baptiste Clément, 92296 Châtenay-Malabry cedex, France
CNRS UMR 8612, Institut Galien Paris-Sud, 5 rue Jean-Baptiste Clément, 92296 Châtenay-Malabry cedex, France

[2] Dipartimento di Scienza e Tecnologia del Farmaco, Università di Torino, via P. Giuria 9, 10125 Torino, Italy

[§] Corresponding author

Email addresses:

SV: sabrina.valetti@u-psud.fr

SM: simona.mura@u-psud.fr

BS: barbara.stella@unito.it

PC: patrick.couvreur@u-psud.fr

Astract

Nanomedicines have gained more and more attention in cancer therapy thanks to their ability to enhance the tumour accumulation and the intracellular uptake of drugs while reducing their inactivation and toxicity. In parallel, nanocarriers have been successfully employed as diagnostic tools increasing imaging resolution holding great promises both in preclinical research and in clinical settings. Lipid-based nanocarriers are a class of biocompatible and biodegradable vehicles that provide advanced delivery of therapeutic and imaging agents, improving pharmacokinetic profile and safety. One of most promising engineering challenges is the design of innovative and versatile multifunctional targeted nanotechnologies for cancer treatment and diagnosis. This review aims to highlight rational approaches to design multifunctional non liposomal lipid-based nanocarriers providing an update of literature in this field.

Keywords

lipid, nanocarrier, passive or active targeting, diagnosis, theranostic

Introduction

Cancer is the first leading cause of death in developed countries and the second one in developing countries, accounting for 7.6 million deaths (around 13% of all deaths) in 2008.[1] The World Health Organization predicts that by 2030 12 million of all deaths worldwide will be due to cancer.[1] Far from being a "modern" disease, cancer is one of the oldest maladies even if it start receiving more and more attention only when other severe killer diseases (such as tuberculosis, dropsy, cholera, smallpox, leprosy or pneumonia) had been eradicated. Despite an old and impatient battle, in which the international scientific and non-scientific committees are engaged, the knowledge of cancer's biology and the discovery of new molecules are unlikely to fully eradicate it. Even if new molecules are discovered to treat cancer, the efficacy of conventional chemotherapeutics is hampered by the following limitations: i) drug resistance at the tumour level due to physiological barriers (*i.e.;*non-cellular based mechanisms) ii) drug resistance at the cellular level (*i.e.,* cellular mechanisms) and iii) non-specific distribution, biotransformation and rapid clearance of anticancer drugs in the body.[2] The process that drives a drug to the target is indeed dependent on drug physico-chemical properties that affect its stability in the systemic circulation, the extravasation and the intratumoral distribution, also leading to undesired side effects.[2] To overcome these limits, the "magic bullet" theory, which refers to a drug which goes straight to its specific target, was postulated at the beginning of the XXth century.[3] In the past decades the application of this concept has led to the development of a plethora of colloidal systems aimed at deliver the drug exclusively to the diseased tissues, thus reducing systemic toxicity. In particular, in the past 35 years, cutting-edge research based on multidisciplinary approaches has been led to the development of nanoscaled drug carriers for medical application.[2,4] The first paper on nanoparticles was published in 1976 by Peter Speiser, a pioneer in the concept of nanoparticles: it focused on the development of nanoparticles for vaccination purposes, aiming at a slow release profile of the antigen, leading to a better immune response.[5] Later, Couvreur et al[6] discovered the lysosomo tropic effect of nanoparticles and for the first time published that nanocapsules were able to introduce compounds into cells which do not spontaneously accumulate intracellularly.
Rapidly, nanoparticles (NPs) found important application in cancer therapy due to numerous advantages that they offer over the free drugs [Table 1].[7-10]

Table 1 - Nanocarriers advantages and properties required for clinical translation [22]

Advantages offered by nanocarriers
• Prevention of undesired drug interaction with the biological environment (*i.e.,* drug inactivation by metabolization) • Control on pharmacokinetic/pharmacodynamic parameters • Enhanced drug accumulation at the tumor target site and improved intracellular uptake • Safety (*i.e.;* decrease of drug toxicity and side-effects).

Some engineered nanocarriers were been approved by the FDA (Doxil®[11], Daunoxome®[12], Abraxane®[13], Genexol®[14], Marqibo®[15]). Marqibo® is a vincristine loaded liposomal formulation made of sphingomyelin and cholesterol approved in 2012 for the treatment of adult patients with Philadelphia chromosome-negative (Ph –) acute lymphoblastic leukaemia.[15]
Aside from therapeutic use, in recent years nanocarriers have also been employed as imaging tools which hold great promises both in preclinical research and in clinical settings.[16-21] Nanoparticles for diagnostic purposes have now been marketed for 10 years.[4] The encapsulation of different imaging contrast agents (e.g., paramagnetic metal ions, superparamagnetic iron oxide

nanoparticles (SPIOs), Near Infra-Red (NIR) probes, radionuclides) in nanocarriers makes possible to enhance the signal to noise ratio in the targeted tissue compared to the surrounding health one. The increase of imaging resolution highlights small lesions which are undetectable with traditional methods.

At the moment, biodegradable polymers or lipid-based colloids are the only drug vehicles approved for clinical use. These materials offer promising possibilities to assure specific drug accumulation at the tumour site, improving the pharmacokinetic profile and safety of both drug and contrast imaging agents.[22]

The present review is focused on lipid-based nanocarriers which have classically received great attention due to their biodegradability, biocompatibility and targetability.[23] Lipid nanocarriers used for drug delivery purposes include liposomes, micelles, nanoemulsions, nanosuspensions, solid-lipid nanoparticles and lipoproteins-containing systems. Liposomal systems attract a great deal of interest and a simple research on the PubMed database reveals that more than 150 review articles have been published within this field in the last year alone. Consequently, we decided to limit the present review to non-liposomal lipid-based nanocarriers. After a short description of these drug nanocarriers, their applications as multifunctional tools for therapeutic and/or diagnostic applications in cancer management are reviewed.

Non-liposomal lipid-based nanocarriers

A broad range of lipid nanocarriers is currently used for drug delivery purposes. Although sometimes the boundaries between categories are not clearly defined, they can be classified into micelles, nanoemulsions, nanosuspensions, solid lipid nanoparticles, lipid nanocapsulesand lipoproteins (Figure 1).

Micelles are colloidal dispersions, which form spontaneously from amphiphilic or surfactant agents at certain concentrations and temperatures. They are characterized by two distinct portions with opposite affinities towards a given solvent. Lipid micelles are formulated adding phospholipids or long-chain fatty acids in the presence of appropriate surfactants.[24] At low concentrations, in an aqueous medium amphiphilic molecules exist separately and aggregation takes place within concentrations above to critical micelle concentration.[25]

Micelles possess a hydrophobic core and hydrophilic shell; they have been successfully used as pharmaceutical carriers for water-insoluble drugs or molecular imaging probes.[26] Thanks to their small size (from 5 to 100 nm) they demonstrated a very efficient and spontaneous accumulation in pathological areas with compromised vasculature. However, due to the limited size of their core they cannot load high amount of drugs. Lipid micelles are formulated adding phospholipids. The formation of micelles is driven by the decrease of free energy in the system because of the removal of hydrophobic fragments from the aqueous environment and the reestablishment of a hydrogen bond network in water. Lipid-based micelle preparation is a simple process, often base on a detergent or water-miscible solvent removal method that gives spontaneous formation of colloids with very similar diameters in aqueous media.

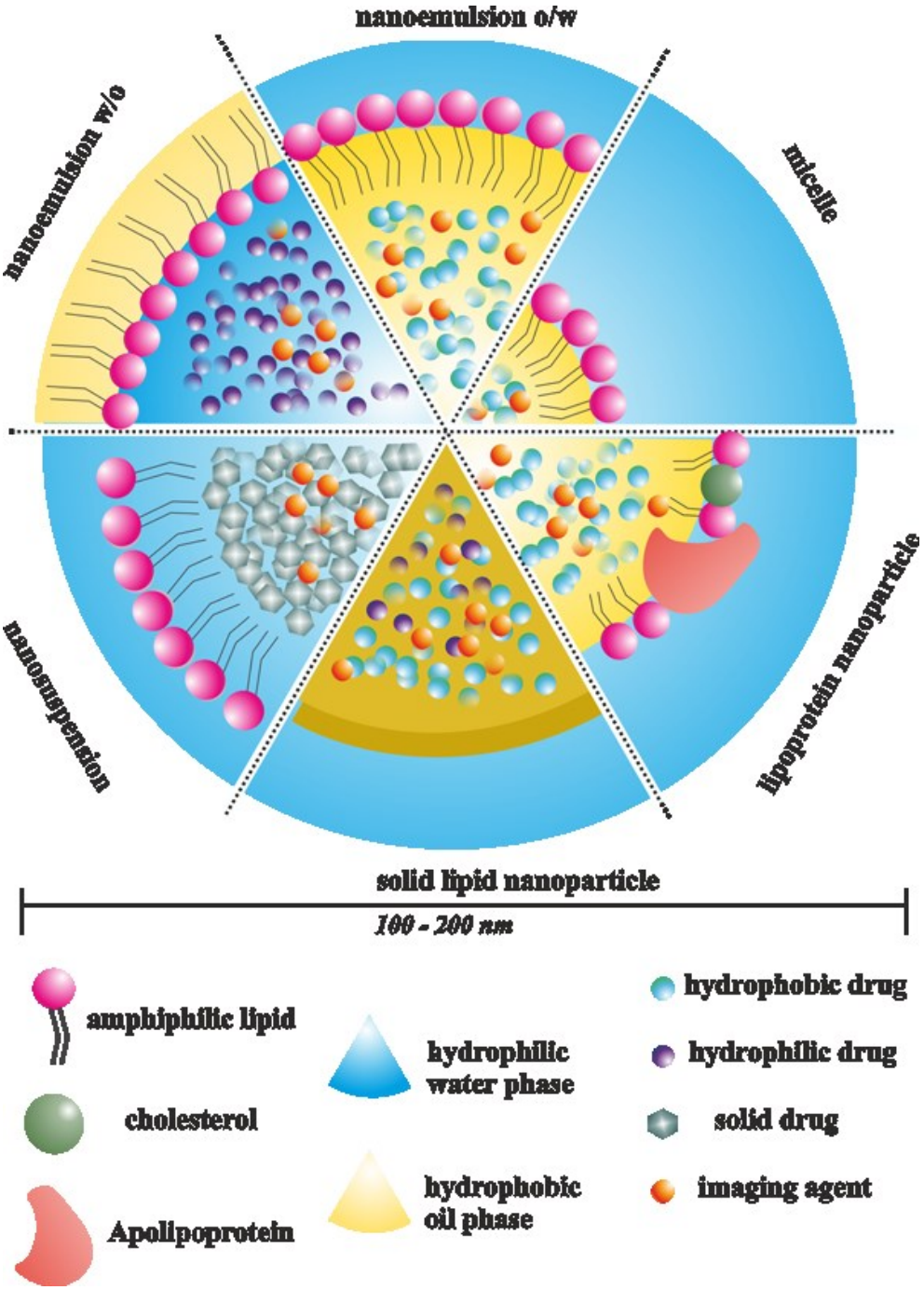

Figure 1 - Schematic representation of non-liposomal lipid-based nanocarriers

Nanoemulsions are transparent or translucent oil-in-water (o/w) or water-in-oil (w/o) droplets that can encapsulate either lipophilic and hydrophilic drugs or imaging agents, respectively in the oil or in the aqueous phase.[27-29] They are formulated from lipid components through high-energy methods (e.g., high-pressure homogenization, microfluidization or ultrasonification in order to obtain small size droplet) or through low-energy methods (e.g., spontaneous emulsification, solvent-diffusion method and phase-inversion temperature for labile drugs).[30]
Advantages of nanoemulsions over macroemulsions include higher surface areas and free energy without the inherent creaming, flocculation, coalescence and/or sedimentation.[27]
Likewise, nanosuspensions are sub-micron colloidal dispersions of particles of drug stabilized by surfactants (e.g., soya lecithin, mainly composed phospholipids). High pressure and multiple

high-energy passes are often required for their production, owing to the drug crystal binding and its stabilization in the colloidal system.[31] Even if they could be prepared directly by crystallization or precipitation, high pressure homogenization is the most frequently employed in large-scale production.[32] They are usually used as injectable dosage forms for poorly soluble drugs. In the case of high melting point compounds, the nanosuspensions allow preserving the crystalline state to obtain the small size required for an intravenous administration. Taking advantage from the absence of any solvent, the nanosuspensions possess higher drug loading compared to nanoemulsions.[27]

Solid lipid nanoparticles (SLN) can be considered as nanosuspensions with a solid lipid core stabilized by surfactants.[33] They are typically formed by heating an aqueous lipid mixture above the melting point of the lipid, adding drug, homogenizing and finally cooling to freeze the drug within the solid lipid spheres. Other procedures like microemulsification, high-pressure homogenization, solvent emulsification-evaporation and "coacervation" method have been proposed for the preparation of SLN.[34-36] A broad range of biocompatible and biodegradable lipids that remains in solid form at physiological temperatures has been used for SLN: fatty acids (e.g., stearic acid, palmitic acid), triglycerides (e.g., trilaurin, tripalmitin, and tristearin) and satured fatty acids (e.g., glycerol behenate, and cetylpalmitate).

SLN show a significant versatility for drug or contrast agents delivery since they can load lipophilic, hydrophilic, amphiphilic or charged molecules. They are characterized by an important physical stability that offers severals technological advantages, including (*i*) better storage stability in comparison to liposomes, (*ii*) easy management in large-scale production and (*iii*) possibility of lyophilization.[37,38] Numerous investigations have demonstrated that SLN can very efficiently control drug release, also improving drug accumulation into the tumour, along with a concomitant minimization of severe side effects and low toxicity of the carrier.[39,40] Despite these advantages, the solid crystalline core of SLN can present several drawbacks, such as problems of reproducibility in the particle growth, possibility of polymorphic transitions, which can induce drug expulsion during storage, and low drug incorporation capacities.[41]

Lipid nanocapsules (LNC) are constituted by an oily core surrounded by a tensioactive-based rigid membrane which represents a hybrid structure between polymeric nanocapsules and liposomes.[42] Empty or drug-loaded LNC, with a diameter below 100 nm and a narrow size distribution, can be prepared by a phase inversion temperature process and show long physical stability (> 18 months). [42] Different anticancer drugs,[43-45] nucleic acids[46]or, imaging agents[47-49]have been encapsulated in the lipid core of these nanoformulations. Surface modification with PEG chains has been also described.[44] Promising results have been obtained both *in vitro* on several cell lines and on *in vivo* models of experimental cancers.

Natural lipoproteins present in the blood as macromolecular carriers for hydrophobic lipids have also been employed as nanocarriers. Lipoproteins are classified in four categories depending on the density, from the largest diameters and lowest density: chylomicrons, very low-density lipoprotein (VLDL), low-density lipoprotein (LDL) and high density lipoprotein (HDL). They are basically formed by a core of triacylglycerides and cholesterol esters coated by a phospholipid and apolipoprotein shell.[50] By mimicking the endogenous shape and structure of lipoproteins, lipoprotein-inspirated nanocarriers could escape mononuclear phagocyte system recognition, thus remaining in the blood stream for an extended period of time,[51] ranging from 10 to 12 h in rodents[52] and up to 5 days in humans, as demonstrated by a clinical study in which autologous biotinyl-HDL3 was injected to five normolipidemic male volunteers as a probe for the determination of nanocarrier turnover.[52,53] LDL and HDL, mostly used for their diameters lower than 40 nm, can be loaded with drugs or imaging agents through covalent linkage with the phospholipid or protein material, intercalation of the molecules into the phospholipid shell or encapsulation in the nanoparticle core.

This approach provides a highly versatile natural nanoplatform for the delivery of poorly soluble drugs or imaging agents[54]; however, one potential hurdle in developing lipoproteins as a

clinically viable nanocarriers lies in the fact that lipoproteins are isolated from fresh-donor plasma, which might result in batch-to-batch variations thus posing several scale-up challenges.[55]

Targeted non-liposomal lipid-based nanocarriers

Nanoscaled systems appear as an attractive approach to overcome the limitations associated to conventional drug delivery strategies. However, the existence of endogenous self-defence mechanisms able to recognize either viral/bacterial or synthetic exogenous particles may hinder their effectiveness or cause side undesirable effects. The mononuclear phagocyte system is a part of the immune system that consists of the phagocytic cells (monocytes, macrophages and Kupffer cells) widely distributed and strategically placed in many tissues of the body (lymph nodes, spleen and liver) to recognize and neutralize foreign particles.[56] The recognition by these cells is promoted by the adsorption of specific proteins (renames "opsonins"), capable of interaction with specific plasma membrane receptors on monocytes and various subsets of tissue macrophages.[57-59]

In the case of infectious diseases, this mechanism provides an opportunity for the efficient delivery of therapeutic agents to these cells by using colloidal drug delivery systems.[60,61] However, in cancer treatment, the rapid sequestration of intravenously injected colloidal particles by liver and spleen decreases drug accumulation at the tumour site. Thus, the engineering of colloidal carrier systems which avoid rapid recognition by Kupffer cells and show long blood circulation time (i.e., Stealth® nanoparticles) is essential.[62] To this aim, several approaches have been investigated to modify the surface properties of the nanocarriers by using emulsifying agents or copolymer nonionic surfactants such as poloxamers and poloxamines, in order to block the opsonization process.[63,64] One of the most successful methods is the anchoring onto the nanoparticle surface, of a hydrophilic and flexible polymer, like polyethylene glycol (PEG) or its derivatives.[65-71]

Surface modification of nanoparticles not only confer significantly reduced mononuclear phagocyte system uptake, better stability and enhanced circulation time, but also result in an increased accumulation of the stealth particles in the tumour.[72,73] Compared to healthy tissues, tumours show high irregular vessels with abnormal heterogeneous density, large pores on the endothelial walls, reduced lymphatic drainage and higher interstitial pressure.[74] Due to this enhanced permeability and retention (EPR) effect, drug-loaded nanocarriers are able to accumulate at the tumour site by passive targeting (Figure 2A).[75,76]

However, PEGylation presents some important limits and drawbacks concerning the translation to the clinic. The observed discrepancy between preclinical and clinical results could, indeed, be attributed to the different progression rate of tumours models in animals and those of human patients, an important factor for EPR based anticancer nanomedicines.[77] In addition, it is already well known that the Doxil®, a PEGylated doxorubicin liposomal formulation, is able to trigger complement activation in human serum, leading to a pseudoallergic reactions called "complement activation-related pseudoallergy" (CARPA) which is associated with cardiopulmonary disturbance and other related symptoms of anaphylaxis.[78] For instance, a recent study showed that the extent of complement activation was correlated to the amount of methoxyPEG 2000(or 5000) at the surface of the lipid carrier.[79] Moreover, relying only on the EPR effect and therefore on tumour anatomy, in some cases passive targeting did not allow therapeutic drug amounts to reach the target site. Indeed, the physiology of tumours and especially fibrosis, hypovascularization [80,81] and the presence of extracellular matrix,[77] a highly interconnected network of collagen fibers, obstruct the nanoparticles to reach cancer cells. That seems to be the cause of the failure in pancreatic adenocarcinoma treatment.[82,83]

One of the major requirements for a successful cancer therapy is its ability to selectively kill cancer cells with minimal damage to healthy tissues.[84] In cancer cells, the extracellular leaflet of the plasma membrane is not characterized by unique molecular targets but rather by overexpressed antigens that are relatively down regulated in healthy cells.[85,86] Thus,

functionalization of nanocarrier surface with various targeting moieties that specifically bind the receptors mainly expressed on malignant cells has been widely investigated as valuable strategy to achieve an active targeting to cancer cells (Figure 2B).[87,88] Receptor-mediated internalization of nanocarriers would then allow efficient drug release inside the cell. Several ligands that belong to the families of small molecules, polysaccharides, peptides, proteins or even antibodies have been used for targeted nanocarriers. A broad range of techniques could be employed to investigate specific homing devices such as (i) antibody-based screens[89], (ii) cloning strategies[90], (iii) in vivo biotinylation and (iv) phage-displayed peptide libraries.[91] In literature, several synthesis methods and coupling strategies are described to achieve the desired macromolecular architecture and display the homing device on the surface of nanocarriers (for a systematic review see[88]). Furthermore, nanoparticles generally carry more than a single targeting ligand molecule thus allowing multivalent binding, which improves targeting efficacy with high binding constants.[92]

Lipid-based nanocarriers have been successfully employed for active targeting.

The first example was published in Science in 2002.[93] In this study, cationic NPs were prepared by self-assembly and polymerization of appropriate lipid molecules and then functionalized by conjugation of a trivalent lipid with the integrin αvβ3 ligand for endothelial cell targeting (αvβ3-NPs). The expression of αvβ3 integrins in 25% of human tumours (e.g., melanoma, glioblastoma, ovarian, breast cancer) makes them a successful choice for the design of targeted drug delivery systems.[94,95] These actively targeted SLNs enabled selective gene delivery both in vitro (towards αvβ3-expressing M21 human melanoma cells) and in vivo (towards angiogenic blood vessels in mice bearing αvβ3-negative M21-L melanomas). The therapeutic efficacy was then tested injecting NPs conjugated with the mutant Raf-1 gene (αvβ3-NPs/ Raf (–)) that blocks endothelial signalling and angiogenesis. Avβ3-NPs/ Raf (–) decreased angiogenesis, leading to tumour cell apoptosis and sustained regression of established primary and metastatic tumours. In a competitive assay experiment, treatment with 20-fold molar excess of soluble targeting ligand led to a tumour burden similar to that observed in control mice, demonstrating that the efficacy of targeted NPs resulted from αvβ3 specific recognition.[93] The well-known peptide sequence RGD (Arg-Gly-Asp), which recognizes the αvβ3 integrins, was identified 20 years ago.[96] Its cyclic form (cRGD), designed from the peptides developed by Kessler's group, provides easy conjugation to imaging and/or therapeutic moieties.[41,94] The importance of the peptide sequence for specific receptor targeting was demonstrated using negative control peptides which differ from the positive one only in few amino acids.[41] Lipid NPs were functionalized with both cRGD targeting ligand (SLN-cRGD) and cRAD peptide negative control (SLN-cRAD).[41] Results in vitro on HEK293(β3) cells line (human embryonic kidney genetically modified which strongly express αvβ3 integrins) showed specific targeting of SLN-cRGD in comparison with SLN-cRAD and non-functionalized SLN after incubation with cells at 4°C or 37°C. Nanoparticle internalization was inhibited by pre-saturation of cells with free cRGD, demonstrating the key role of αvβ3 integrins. Similarly, an active accumulation of cRGD-targeted particles was observed in HEK293(β3) xenografts-bearing mice after intravenous injection.[41] However, cRGD targeting failed in a murine mammary carcinoma model clearly demonstrating that cancer physiopathology is a crucial parameter for cRGD targeting efficacy.[41,97] Efficient drug targeting requires the increased accumulation of the drug at the tumour site thanks to the EPR effect, followed by a facilitated cellular uptake through ligand-mediated endocytosis.[22,98] The proof of concept has been provided by Wang et al.[98] using passively and actively targeted lipid-based-nanosuspensions (LNSs) loaded with docetaxel. LNS modification with PEG moieties conferred stealth properties while further conjugation of PEG chains with folic acid enabled to achieve active targeting properties.

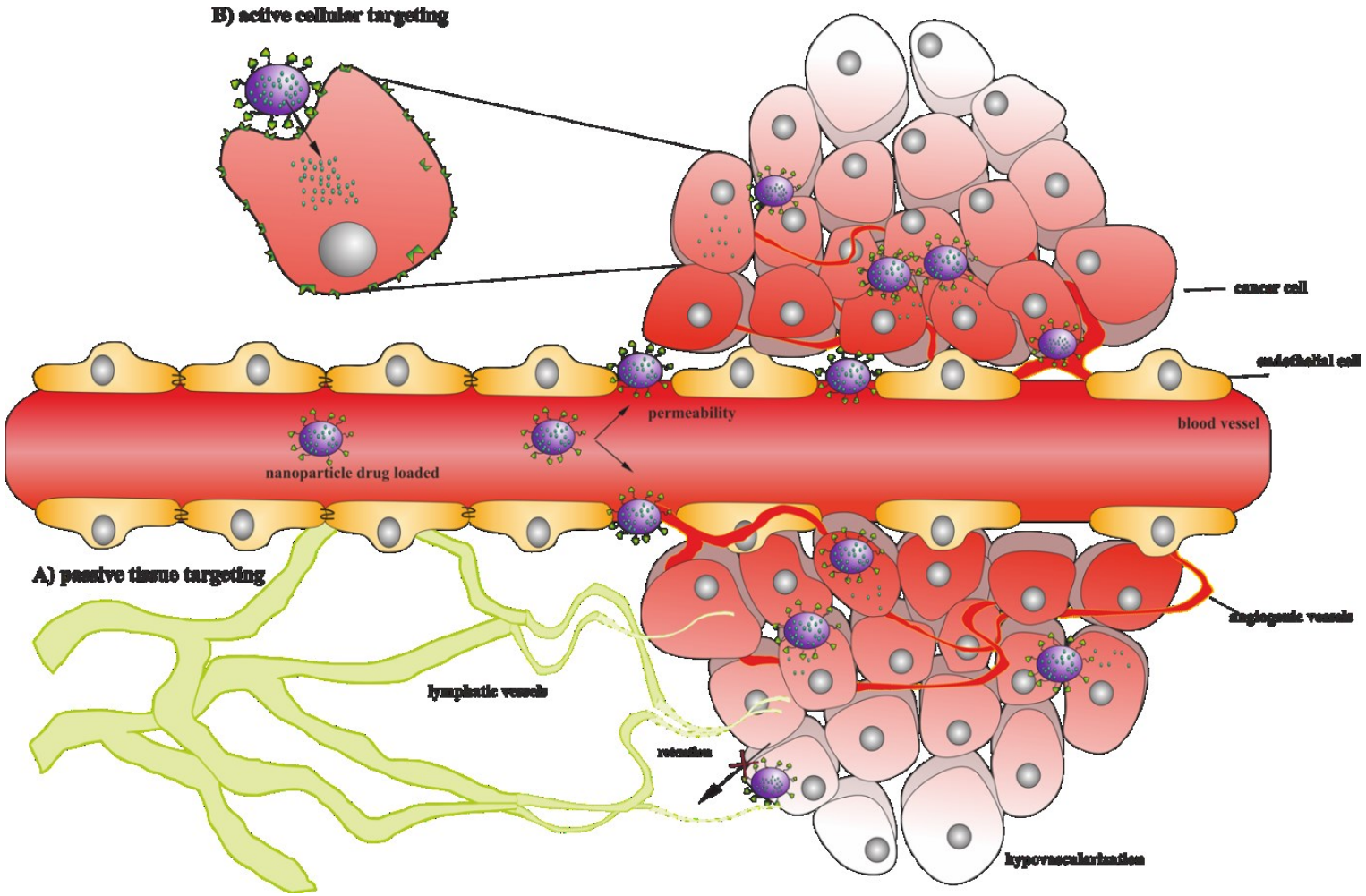

Figure 2. (a) Passive targeting. Healthy blood vessels are regular and continuous with tight endothelial junctions between cells. Conversely, the angiogenic vessels show gross architectural changes, such as large intracellular pore, presence of interrupted endothelium and incomplete basement membrane, allowing the extravasation of nanoparticles from blood vessels. In the tumour stromana noparticles remains trapped due to high-than-expected interstitial pressure, due to the lack of effective lymphatic drainage coupled with lower intravascular pressure. These pathophysiological characteristics enhance the tumour site accumulation of nanoparticles. However, aside to the well perfused and rapidly growing regions, a non-uniform tissue oxygenation due to the vascular heterogeneity led to the presence of poorly perfused, often necrotic areas in which the efficacy of the treatment is hampered. **(b)** Active targeting. In order to improve the intracellular delivery of the drug, nanoparticles could be functionalized with specific ligands that specifically bind receptors expressed primarily on malignant cells leading to receptor-mediated internalization, which is often necessary to release drugs inside the cell.

Folic acid (FA) is widely used as targeting ligand due to the overexpression of FA receptors (FR) in several human cancer cells, including malignancies of the ovary, brain, kidney, breast, lung and myeloid cells.[99] FR binding affinity (Kd = 1 × 1−10 M) does not appear to be affected by conjugation to the nanocarriers.[98,100] FA-functionalized systems represent an effective strategy for specific delivery of therapeutic agents to tumours.[98,101-105] Therefore, compared to non-functionalized LNS, targeted LNS showed a slightly higher toxicity on mouse melanoma B16 cells overexpressing FR, which was probably due to a synergy between the passive and active targeting.[98]

FA was also used to decorate lipid-based nanoparticles made of (DSPC)/triolein/cholesterol oleate/polyethylene glycol cholesterol (PEG-Chol) (40:40:18:2.5, mole: mole), in which a paclitaxel prodrug, the paclitaxel-7-carbonyl-cholesterol (Tax-Chol), was encapsulated in the lipid phase. In FA targeted formulations, 20% of the PEG-Chol was replaced by folate-PEG-Chol (f-PEG-Chol).[106] The incorporation of a lipid paclitaxel prodrug was chosen as strategy to overcome the paclitaxel propensity to precipitate and increase formulation stability. The FR-targeted LNPs showed enhanced activity against FR (+) tumour-bearing mice also inducing an effective extension of their survival.[106] FA has been also conjugated to the Lys residues of the apolipoprotein B (apoB-100) to develop an actively targeted LDL-based nanoplatform.[107] LDLs possess an intrinsic tumour targeting property due to the overexpression of the LDL receptor (LDLr) in various tumour cell lines, which was attributed to the large amount of cholesterol and fatty acids required for sustaining the rapid tumour proliferation.[108] Although this approach might provide a targeted delivery of drugs and diagnostic agents to tumours, the application of LDL-like NPs is clearly limited to the dysregulation of the LDLR associated with several disease.[107] Concerning FA-LDL, internalization studies performed on FR-overexpressing and in FR-nonexpressing cells confirmed that the FA-targeted LDL-like NPs uptake was driven by the FR receptor.[107]

EGFR is a transmembrane tyrosine kinase receptor overexpressed in a wide range of cancers including breast, ovarian, bladder, head and neck, glioma, pancreatic, kidney, lung and prostate, making it an attractive target for both therapeutic and diagnostic applications.[109-111] An example of EGFR-directed nanocarriers was provided through the functionalization of doxorubicin or carmustine-loaded cationic SLN with specific monoclonal antibody against EGFR for the treatment of brain glioblastoma multiforme.[112,113] Exposure to targeted nanoparticles resulted in higher inhibition of U87MG human glioblastoma-astrocytoma cells compared to non-targeted control NPs. Although these nanoparticles improved the administration of hydrophobic drugs, such as carmustine, allowing intravenously injection, an in vivo proof of evidence of the increased accumulation at the tumour site has not been provided yet. More recently, a new class of proteins known as affibody molecules has been introduced as an alternative approach to antibodies for EGFR-targeted systems.[114,115] These are composed of 58 amino acid residues bundled in a three-helix scaffold, a structure derived from the staphylococcal protein A Z-domain, which is an engineered variant of a gene encoding five highly homologous Ig-binding domains.[116] Taking inspiration from the advances in protein library technology, the Z domain was employed to design a novel class of high-affinity molecules. For example, the EGFR-binding Z domain was employed as homing device for the delivery of therapeutic agents towards a wide range of EGFR-overexpressing cancer cells.[84] To further improve binding efficiency, a heptameric EGFR-binding ligand was developed by fusing a heptamerization domain with an EGFR-binding Z domain. This heptameric EGFR-binding targeting ligand was used to decorate the surface of nickel-loaded lipid-based oil-filled nanoparticles (Ni-LNPs).[84] Nanoparticles were prepared from warm oil/water (o/w) microemulsion technique using polyoxyethylene (20) stearyl ether, D-alpha-tocopheryl polyethylene glycol 1000 succinate (TPGS) and a mixture of caprylic and capric fatty acid triglycerides. In vitro cell uptake studies showed up to 90% internalization of the EGFR-targeted Ni-LNPs into the EGFR overexpressing A431 human epidermoid carcinoma cells, while a significantly lower uptake (10%) was observed with untargeted Ni-LNPs. The targeting efficiency of the novel heptameric Z-EGFR domain was also

demonstrated in vivo with an almost two-fold increase of intracellular Ni accumulation in tumour cells.[84]

The CD44 receptor–hyaluronic acid (HA) interaction has also been investigated for cancer targeting.[117] HA is an anionic, non-sulphated glycosaminoglycan distributed throughout connective, epithelial and neural tissues.[118] Contrary to HA oligomer, the native high molecular weight HA is a "bioinert" component that does not induce inflammation, proliferation or proangiogenic effect.[119,120] HA has been used as homing device able to target CD44-expressing tumour initiating cells.[121] Moreover, due to its hydrophilicity it could prevent opsonin adsorption by steric repulsion, allowing to reduce mononuclear phagocyte system uptake.[122] Thus, HA-Ceramide-based self-assembled NPs loaded with docetaxel[118] and doxorubicin[123] was developed. Ceramides, which are composed of sphingosine and fatty acid triglycerides, are cellular membranes component which play a role as cellular signalling molecules involved in the regulation of differentiation, proliferation and programmed cell death.[124] In vitro studies on several cells lines showed that the cellular uptake of docetaxel and doxorubicin-loaded HA-ceramide nanoparticles was driven by CD44 receptor-mediated endocytosis.[118,123] The in vivo tumour targetability for the docetaxel-loaded nanoparticles labelled with a NIR fluorescence die (cyanine 5.5) showed interaction between HA and CD44 receptors in MCF-7/ADR tumour bearing mice. Doxorubicin-loaded HA-ceramide nanoparticles showing PEG chains at their surface demonstrated an increased therapeutic efficacy in tumour-bearing mice, probably due to the improved half-life and reduced clearance of doxorubicin together with its tumour accumulation by passive and active targeting.[123]

Galactose and galactosamine are also interesting ligands to target cancer cells which overexpress the asialoglycoprotein receptor (e.g., hepatic and cervical cancer cells).[88,125] For efficient hepatocyte targeting, galactose was linkedto the distal end of the PEG chains at the surface of DOTAP/DOPE lipid nanocapsules encapsulating DNA.[126] In primary hepatocytes, such functionalized lipid nanocapsules were found to increase by 18-fold the luciferase expression compared to non-galactosylated ones.[126]

Galactoside functionalization of SLN loaded with taspine, a bioactive aporphine alkaloid that inhibits tumour angiogenesis and controls tumour growth,[127] enabled a 3–4-fold increase of drug accumulation in the liver of healthy mice.[128] Docetaxel-loaded SLN were instead targeted to hepatic cells using the galactosylated dioleoylphosphatidyl ethanolamine (DCT-tSLN).[129] DCT-tSLN showed higher cytotoxicity on hepatocellular carcinoma cell line BEL7402 compared to Taxotere® and non-targeted nanoparticles (DCT-nSLN). In vivo studies in hepatoma-bearing mice showed that the DCT-tSLN had a better therapeutic index compared to Taxotere®. Moreover, histological analysis demonstrated that DCT-tSLN had no detrimental effect on both healthy and fibrotic-liver.[129]

Human and murine macrophages express mannose receptor on their surface,[130] and several studies confirmed the feasibility of using mannose- or mannan-modified nanocarriers to target macrophages.[131] Alveolar macrophages play a key role in the first-line host defence and lung cell homeostasis,[132] thus targeting macrophages may provide innovative therapeutic strategies against tumour invasion and metastasis for lung cancer which represents one of the most aggressive solid cancers. Polysaccharides or multiple oligosaccharides, such as mannan, which contains a large group of mannose residues, are recognized as having a much higher affinity than single sugar molecules because of the moiety density.[131] Indeed, surface of DNA-loaded cationic SLN was modified with L-α-phosphatidylethanolamine (PE)-grafted mannan-based ligand (Mannan-PE) obtaining mannan-targeted SLN-DNA (Man-SLN-DNA).[131] Transfection efficiency of Man-SLN-DNA was evaluated in vitro on RAW 264.7 cells (mouse leukemic monocyte macrophage cell line) and in vivo following pulmonary administration in rats. Man-SLN-DNA showed lower cytotoxicity than non-modified SLN-DNA and achieved higher gene expressions in comparison to Lipofectamine 2000-DNA. The above mentioned results indicated that mannan modification enhanced the active targeting ability of the carriers, and that Man-SLN-DNA may be a promising non-viral vector for targeted lung gene delivery.[131]

Finally, taking advantages of overexpressed transferrin receptor at the surface of brain tumour cells, the surface of lipid nanocapsules has been coated with the OX26 murine monoclonal antibody and the NFL-TBS.40-63 peptide derived from the light neurofilament subunit (NFL).[133] Intra-carotidal treatment with NFL-TBS.40-63 peptide functionalized nanocapsules was found to enhance the survival time (44 days versus 27 days) which was not obtained with non-targeted LNC. This suggests that this active targeting strategy may offer a promising approach for glioma treatment.[133]

Non-liposomal lipid-based nanocarriers for diagnostic (imaging) applications

The currently most accessible imaging techniques include magnetic resonance imaging (MRI), optical imaging, ultrasonography (US) and positron emission tomography (PET).

MRI is a powerful non-invasive technique based on magnetic properties, which offers the possibility of deep penetration into soft tissues. The human body consists by two-thirds of water molecules whose hydrogen atoms are able to act as microscopic compass needles susceptible to an externally applied magnetic field.[134,135] The different relaxation properties of various tissues allow using MRI to reconstruct images of structures, such as organs and lesions and to evaluate perfusion and flow-related abnormalities. MRI is optimized by using contrast agents able to increase the T_1 signal or decrease the T_2 signal, thus leading to a bright (positive) or dark (negative) contrast enhancement.[136]

The electronic configuration (seven unpaired 4f electrons) of the lanthanide ion Gd^{3+} allows to long electronic relaxation times or slower relaxation rates making it the most frequently T_1 positive contrast agents for T_1-weighted imaging in MRI.[136] The main drawback of Gd^{3+} is its similarity with endogenous metals (e.g., calcium and zinc) that might cause transmetallation or neuromuscular transmission arrest.[137] In order to sequester the ion for a safe administration, cyclic (*e.g.,*cyclen-based tetraacetic acid derivative complex DOTA) or acyclic (*e.g.,*diethylenetriaminepentaacetic acid complexes DTPA) chelating agents have been approved for clinical use. [136]Lipid-based nanoparticulate carriers able to carry multiple contrast agent moieties were developed (*e.g.,* Gd-DTPA was encapsulate in SLN [138] or incorporated into the lipid layer of LDL-based nanoparticles[139])with the aim to increase the accumulation of the contrast agent at the target site, consequently enhancing the signal intensity,.

Contrast agents could also use of the ferromagnetic properties of natural elements (*i.e.,* iron), which consist in both being attracted in the presence of an externally applied magnetic field and retaining the magnetization after its removal. Superparamagnetic iron oxide nanoparticles (SPIOs) have been investigated as a category of T_2 MRI contrast agents for both *in vitro* and *in vivo* imaging. They show a high magnetic moment that can increase proton relaxivities up to 10-folds.[136]

Magnetic nanoparticles (MNPs)-encapsulated SPIOs have already demonstrated broader applicability and improved efficacy for the detection of primary tumours, metastasis, sentinel lymph node invasion and for the visualization of biological processes (e.g., apoptosis, cell trafficking, and gene expression).[21,140-142] Biopharmaceutical performances, pharmacokinetics and toxicity depend on their composition and physicochemical properties as well as on the route of administration and dose (for review see [21]). Lipid-based nanocarriers have been suggested as a MRI contrast agent after encapsulation of MNPs.[28,143-145]

Optical imaging is a non-invasive technique based on the specific optical properties of tissue constituents at different wavelengths.[146] The "biological window" for optical imaging in NIR region (wavelengths 700-900 nm) is characterized by low absorption and low scattering in soft tissue that allow increasing the penetration depth, the major limit in optical imaging.[147]

Only two fluorophores (indocyanine green (ICG) and fluorescein) are currently approved by the FDA for medical use.[148] A successful optical molecular probe for medical imaging must show specific characteristics, such as absorption/emission wavelength in the deep or near infrared range, brightness, bio- and photo-stability and a successful pharmacokinetic profile (For review

see[148]). Application of ICG is limited by its numerous disadvantageous properties, including its concentration-dependent aggregation, poor aqueous stability *in vitro*, low quantum yield and high binding to nonspecific plasma proteins, leading to rapid elimination from the body. To overcome these problems, ICG has been effectively encapsulated in lipid micellar systems, such as glycocholic acid and phosphatidylcholine[149] or phospholipid-PEG[149,150] micelles, improving ICG optical properties and prolonging up to a few weeks its stability in aqueous buffer. "Lipidots™", a recent technology based on oil-in-water nanoemulsions, in which a soybean oil and wax are coated with lecithin and PEG[151,152], has also been investigated to encapsulate near infrared dyes obtaining highly bright fluorescent nanoprobes with very low cytotoxicity and good pharmacokinetic profile *in vivo.*[152,153] For example, in a first clinical trial, ICG was successfully evaluated as a new method for sentinel lymph node biopsy in breast cancer patients[154] that represents an efficient aid to eradicate the tumour or prevent further metastasis.[155] In parallel, HDLs[55,156] and LDLs[107,157] have been modified by the inclusion of lipophilic fluorophores, such as DiR (1,1'-Dioctadecyl-3,3,3',3'-Tetramethylindotricarbocyanine Iodide), DiR-bis-oleate[55,156,157], carbocyanine-based optical probe (DiI)[107] or novel fluorescent lipids (such as bacteriochlorinebisoleate (BchlBOA), a synthetic analog of Bacteriochlorophyll a (Bchl)).[55,156] Contrast generating materials can be included in the coating of the particle[157] or loaded in the hydrophobic core of lipoproteins.[55,158]

Ultrasonography (US) is a low cost and in real time clinical imaging modality based on the partial backscattering of ultrasound waves - frequency range from 2 to 15 MHz - by different structures of the body because of the impedance mismatch between different tissues.[159]

Due to the weak difference of echogenicity between different soft tissues, ultrasound contrast agents are usually needed to improve imaging and to distinguish between diseased and healthy tissues.

Perfluorocarbons (PFCs) are fluorinated aliphatic compounds that have been used as contrast agents for ultrasonography and magnetic resonance imaging (MRI) since the end of the 1970s.[160] Liquid PFCs (long perfluorinated carbon chain) have been used instead of gaseous PFCs (small perfluorinated carbon chain) due to higher resistance to pressure changes and mechanical stresses.[161,162] In order to administer liquid PFC by the parenteral route, nanoparticulate systems which encapsuled PFC droplets such as nanodroplets coated with phospholipid and cholesterol were designes.[163,164]

Based on the use of a radiolabeled compound, Positron Emission Tomography (PET) is a non invasive, nuclear imaging technique, capable of visualizing deep tissues with a high sensitivity and generating a three-dimensional image of living subjects. Using mathematical reconstruction methods and correction factors, quantitative information can be extracted from the images and radioisotope concentration can be measured in the specific region of interest.[165]

Radiolabel SLNs with positron emitter ^{64}Cu have been designed through the incorporation of a lipid-PEG-chelate (6-[p-(bromoacetamido) benzyl]-1,4,8,11-tetraazacyclotetradecane-N,N',N'',N'''-tetraacetic acid (BAT)), conjugated to a synthetic lipid, into the phospholipid monolayer forming the SLN surface.[165] The blood half-life of these SLNs was increased, comparatively to polymeric nanoparticles of similar size, due to reduced clearance in kidneys, liver and spleen.

Owing to the typical limitation for each technique, monomodal imaging was not enough for a successful diagnosis. In this context, multifunctional nanocarriers with plural imaging tools capabilities could be employed to exploit different modalities achieving molecular meaningful images at different levels of spatial resolution and dept. For example, functional multiplexed imaging with submicrometer resolution could be obtained using by optical imaging, although this technique does not provide quantitative concentration measurements and is basically restricted to biological objects no thicker than a few millimeters or centimeters. In contrast, PET allows quantitative whole body imaging with a low (a few mm) spatial resolution.[166] Taking advantage of multifunctional nanotechnology platforms, which include several contrast agents for multimodal imaging and tools for combining the different levels of observation, it was

possible to reconcile molecular images into a global picture in order to the overcome the limit of each technique.[28,166] In this view, quantum dots nano-crystals (QDs) were encapsuled in functionalized phospholipid micelles covalently labeled with fluorine-18, a commonly used fluorophore for clinical imaging, developing a novel bifunctional probe for fluorescence and nuclear imaging.[166] Phospholipid QD micelles exhibited long circulation half-time in the bloodstream and slow uptake by the mononuclear phagocyte system,in contrast with several previous studies using other polymer coatings.[166] In addition, this bifunctional micellar probe showed that a combination of PET and fluorescence imaging can be used to quantitatively and dynamically improve the monitoring of nanoparticles biodistribution and pharmacokinetics. Despite that, toxicity due to the presence of heavy metals such as cadmium and selenium is their major concern. Unless QDs can be made especially small (around 6 nm) and thus excreted via the kidneys, these particles typically have delayed clearance and are mostly excreted through the liver and into the bile without significant metabolism.[167]

Chen and co-workers have designed a novel multimodal tumour targeting molecular imaging probe encapsulating amphiphilic gadolinium chelates (Gd^{3+}- Gadolinium diethylenetriaminepentaacetate-di (stearylamide)) and fluorescent dyes (DiR) in HDL-RGD targeted nanoparticle.[168] *In vitro* observation showed that specific HDL-RGD nanoparticles were preferentially taken up by endothelial cells escaping macrophage phagocytosis. RGD-targeted, and untargeted HDL showed different accumulation/binding kinetics in mice bearing subcutaneous human EW7 Ewing's sarcoma tumours. The combination of NIR and MR imaging exploits the complimentary features of both techniques providing high sensitivity and high spatial resolution.[168]

Actively targeted contrast agent-loaded nanocarriers have also been developed to increase dye amounts at the tumour site. Since HDL's core lipid transfer is mediated through the interaction between ApoA-1, the major apolipoprotein, and the scavenger receptor class B type I (SR-BI), that is overexpressed in some cancer cell lines,[156,169] targeting this receptor represents a novel way to deliver imaging agents to tumours which overexpress this receptor. Furthermore, it is conceivable that a wide range of tumour-specific targets, such as epidermal growth factor (EGF), can be applied to HDL-like NPs.[55,107,157] A coordinated dual receptor (EGFR and SR-BI) targeting phenomenon leading to enhanced dye delivery has been shown by adding EGF targeting ligand to HDL-like NPs carrying DiR-BOA, a near-infrared fluorescent compound used as a model functional cargo.[55]

Furthermore as mentioned above, LDL nanoparticles could reroute away from their native receptors by conjugating tumour-homing ligands to their surface. Proof of this strategy has been demonstrated *in vitro* with fluorescent-labeled folic acid-conjugated LDL.[107] Later, DiR-LDL-FA (actively targeted LDL obtained by intercalation of DiR into the LDL phospholipid monolayer and conjugation of FA to ApoB-100) have successfully targeted FR expressing tumours, thus effectively validating the LDL rerouting strategy for enhanced cancer optical imaging *in vivo*.[157]

Theranostics applications of non-liposomal lipid-based nanocarriers

"Nanotheranostics" (i.e., theranostic nanomedicines) represent a novel extremely interesting versatile platform for both detection and cure of diseases, thanks to the development of multifunctional systems combing therapeutic and diagnostics functions(Figure 3).[16,170]

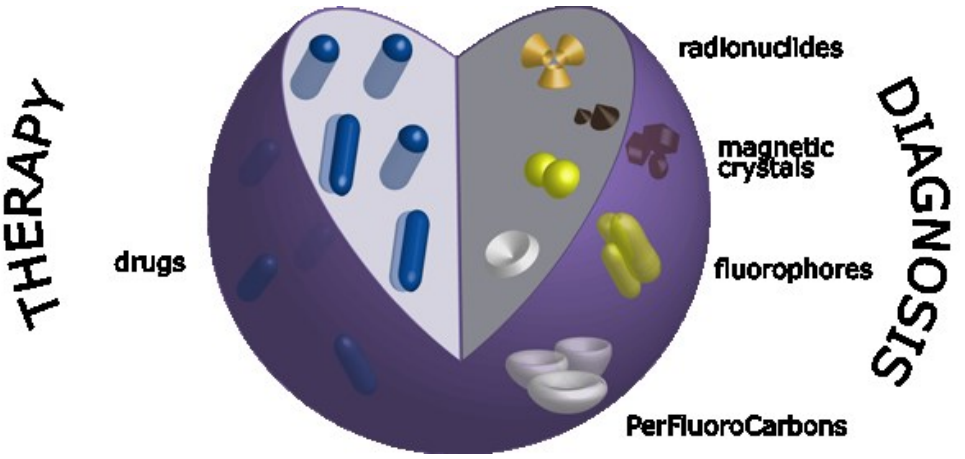

Figure 3 - Schematic representation of nanotheranostics

Taking advantage of the combination of simultaneous non-invasive diagnosis and treatment of diseases, one of the most promising aspects of the nanotheranostics is real time monitoring of pharmacokinetic drug profile to predict and validate the effectiveness of the therapy.[18,171,172] Due to these features, nanotheranostics are extremely attractive to optimize treatment outcomes in cancer, leading to the realization of a "personalized nanomedicine", which would enable to administer "the right drug to the right patient at the right moment".[173,174] Significant benefits in the management of cancers could be achieved combining the highest therapeutic efficiency with the best safety profile.[20]

HDL-like NPs for theranostic application were designed by incorporating a chemically stable bacteriochlorophyll analogue, a dye synthesized by the phototrophic bacteria, in their core.[55,156] This fluorescent photosensitizer can be tracked in vivo through NIR fluorescence imaging and can be activated to generate singlet oxygen upon light irradiation. NPs were successfully detected in epidermal carcinoma KB cells both in vitro and in tumour xenografts using the dorsal skinfold window chamber technique, which allows the monitoring of the nanoparticle tumour penetration with high spatial and temporal resolution.[156] Recently, Wang and co-workers proposed doxorubicin-loaded acoustic droplets containing a core of liquid perfluoropentane and lipid-based (DSPC, cholesterol, distearoylphosphatidylethanolamine (DSPE)-PEG2000) shell. High-intensity focused ultrasounds (HIFU) caused nanodroplets into an instant phase transition (i.e., acoustic droplet vaporization (ADV)) that led to the formation of gas bubbles, which mediated both mechanical cancer cell destruction and localized drug release, thus leading to significant cell toxicity.[175] Optical studies clearly illustrated the transient changes that occurred upon ADV of droplet-targeted and B-mode ultrasound imaging, revealing contrast enhancement by ADV in ultrasound images. Moreover, droplets were conjugated with aptamers, factitious oligonucleotides, providing the ability to specifically target CCRF-CEM human acute lymphoblastic leukaemia cells.

Gianella et al.[28] have developed a theranostic nanodevice composed of an oil in water nanoemulsion, loaded with iron oxide crystals, Cy7 dye and glucocorticoid prednisolone acetate valeranate, for MRI, NIR and therapeutic use respectively. The effectiveness of this nanotheranostic, which combined the high spatial resolution of MRI with the high sensitivity of optical fluorescence imaging, was evaluated on a colon cancer model. The massive uptake of NPs in the tumour was confirmed in vivo studies by MRI images, in which tumours appeared bright compared to the surrounding tissue, as well as by NIR imaging since the injection of Cy7-labeled nanoemulsions led to a strong fluorescent signal compared to Cy7-unlabeled ones. RGD peptide functionalized nanoemulsions resulted *in vivo* as active as the untargeted ones, due to the already extended tumour targeting of nanoparticles. Dayton and co-workers developed

perfluorocarbon emulsion nanoparticle containing a core of at least 50% liquid perfluorocarbons and a mixture of triacetin and soybean oils in which paclitaxel was encapsuled.[29] Another promising theranostic approach using ultrasound as imaging modality is represented by an oil in water emulsion made of liquid perfluoroctylbromide (PFOB) drops stabilized by a lipid layer in which the peptide melittin has been incorporated.[176] Melittin has already been proposed in the treatment of several cancers as cytotoxic agent that induces cell lysis through membrane permeabilization. [177,178] Feasibility as theranostic tool was investigated in vivo on xenograft models of breast cancer. Compared with control saline solution or mellitin free emulsion, the NPs treatment showed a significant inhibition of tumour growth. At the same time, they also provided a significant contrast enhancement, which enabled to monitor the therapeutic efficacy by ultrasound imaging.[28,29]

Recently, Couvreur and co-workers reported a novel nanotheranostic platform in which SPIOs are coated with squalene-based anticancer prodrugs.[144,145] Lipid–drug conjugates have gained considerable attention in recent years thanks to the improvement of the pharmacokinetic and of the therapeutic index of the associated drugs. Squalene (SQ), which is a natural acyclic triterpene, is the corner stone in the biosynthesis of most triterpenes including lanosterol and cycloartenol which in turn are the precursors of steroids.[179] In 2006 the covalent linkage of the anticancer drug gemcitabine to squalene was found to lead to the formation of amphiphilic bioconjugates which spontaneously self-assembled as nanoparticles in water.[180] This proof of concept has since been enlarged to other nucleoside analogue drugs (e.g.,ddI, ddC , AZT, ACV,Ara-C[180-184]), to more lipophilic drugs (e.g., paclitaxel[185,186]), to imaging transition metals (e.g.,ruthenium[187] or gadolinium[188]) as well as to antibiotics (e.g., penicillin [61])and nucleic acids (e.g., SiRNA[189]).

In general, these squalenoylated nanomedicines displayed an increased pharmacological activity in solid, metastatic and orthotopic experimental cancers (Figure 4).[190]

When the SPIOs/SQgemcitabine NPs were intravenously injected in tumour-bearing mice and guided using an extracorporeal magnetic field, an impressive anticancer activity was obtained at very low doses of the anticancer drug. Moreover, the magnetic responsiveness of embedded SPIOs coupled to their T2 imaging properties make them an efficient candidate for theranostic applications, because tumour collapse could be easily visualized by MRI.[145] This concept has also been found feasible by using Gd^{3+} for T1 positive imaging[188], showing that the squalenoylation is a versatile and safe nanotheranostic platform with high drug loading and controlled release properties.

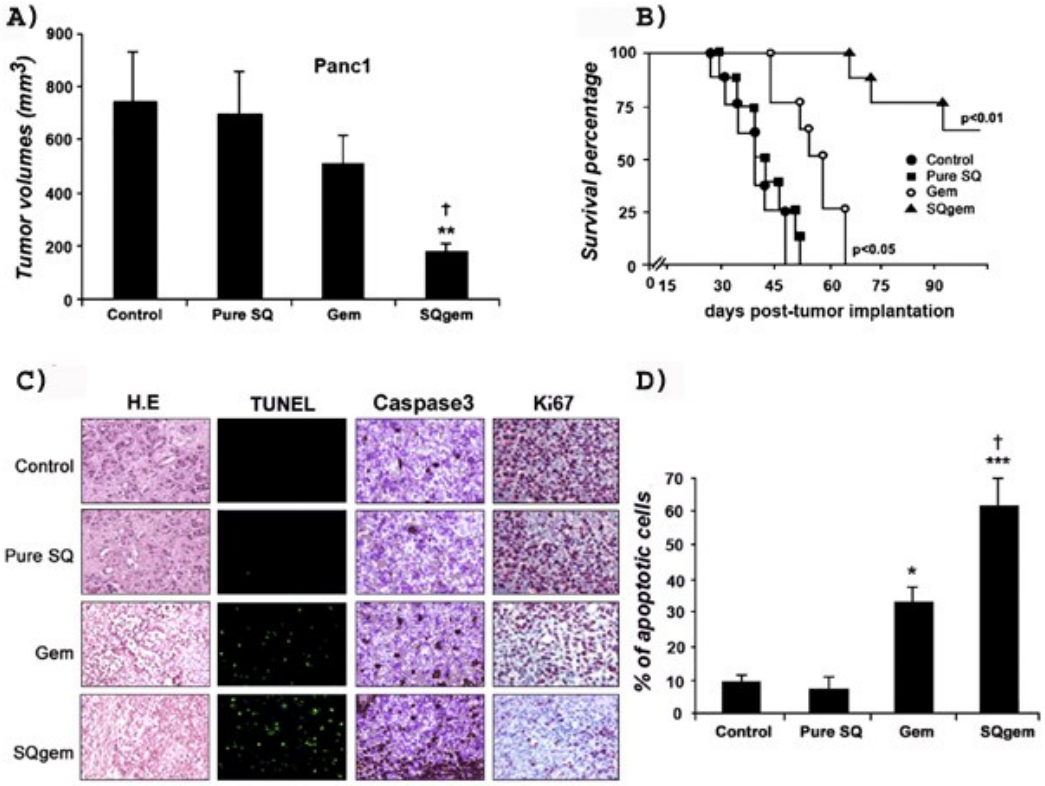

Figure 4 - *In vivo* antitumor efficacy of SQgemcitabine NP. **(A)** Mice bearing pancreatic chemoresistent Panc1 orthotopic tumour model were treated with equivalent drug dose of gemcitabine (dFdC) or SQgemcitabine (SQdFdC). After 1 month of treatment, volume of the primary tumour and tumour extension were significantly reduced by SQgemcitabine showing its superior antitumour efficacy compared to physiological solution or vehicle nanoparticles treated (pure SQ) or gemcitabine treated mice. **(B)** Mice survival curves showed a significant enhancement of the median survival after SQgemcitabine treatment. All the gemcitabine treated and untreated mice died respectively within 64 and 47 days following tumour implantation. Remarkably, mice treated with SQgemcitabine were still alive after 3 months and no tumours were detected after autopsy. **(C)** Tumour biopsy samples were collected from each group of mice and used for immunohistochemistry examination. Paraffin sections submitted to hematoxylin-eosin (H.E) from SQgemcitabine treated mice revealed an absence of mitotic figures and demonstrated enlarged cells with significant necrotic changes. Tissues staining with terminal deoxynucleotidyltransferase (TUNEL), for detecting DNA fragmentation, and (CASPASE3), aspartic acid-specific cysteine proteases, that are both present during apoptotic signaling cascades, revealed that apoptosis was most prominent in animals treated with SQgemcitabine. The number of Ki-67-positive tumour cells, a marker for proliferation, showed a significant decrease of the tumour proliferative activity in SQgemcitabine in comparison to gemcitabine treatment. **(D)** Quantitation rates of apoptotic cells confirmed the considerably increased apoptosis in the tumours from SQgemcitabine-treated mice and the statistically significant difference between SQgemcitabine and gemcitabine treatment. Adapted from ref 190. Copyright 2011 Nanomedicine.

Conclusions

Lipids are a class of natural or synthetic compounds with a range of structure and functions. Their supramolecular organization may be tailored to design nanoscaled structures able to be loaded with drugs or imaging agents or both ("nanotheranostics"). The proof of concept that such lipid nanocarriers may be used for cancer treatment and diagnosis is demonstrated in the present review.

Competing interests

The authors declare that they have no competing interests.

Acknowledgements

Authors thank Dr Victoria Franzinetti for her suggestions in revising the manuscript.
The authors would like to recognize that their work in this area has been
sponsored by the European Research Council under the European Community's Seventh Framework Programme FP7/2007-2013 Grant Agreement N°249835.
The authors acknowledge the Università ItaloFrancese/Université Franco Italienne (UIF/UFI) for the PhD co-tutoring agreement.

References

1. Ferlay J, S. H., Bray F, Forman D, Mathers; C, P. D. G. GLOBOCAN 2008 v2.0 (accessed Aug 2012) Cancer incidence and mortality worldwide: IARC CancerBase *Lyon, France: International Agency for Research on Cancer.* **2010**, 10.
2. Couvreur, P.; Vauthier, C. Nanotechnology: intelligent design to treat complex disease. *Pharm Res* **2006**, 23, 1417-50.
3. Strebhardt, K.; Ullrich, A. Paul Ehrlich's magic bullet concept: 100 years of progress. *Nat Rev Cancer* **2008**, 8, 473-80.
4. Kreuter, J. Nanoparticles--a historical perspective. *Int J Pharm* **2007**, 331, 1-10.
5. Birrenbach, G.; Speiser, P. P. Polymerized micelles and their use as adjuvants in immunology. *J Pharm Sci* **1976**, 65, 1763-6.
6. Couvreur, P.; Tulkens, P.; Roland, M.; Trouet, A.; Speiser, P. Nanocapsules: a new type of lysosomotropic carrier. *FEBS Lett* **1977**, 84, 323-6.
7. Sugibayashi, K.; Morimoto, Y.; Nadai, T.; Kato, Y.; Hasegawa, A.; Arita, T. Drug-carrier property of albumin microspheres in chemotherapy. II. Preparation and tissue distribution in mice of microsphere-entrapped 5-fluorouracil. *Chem Pharm Bull (Tokyo)* **1979**, 27, 204-9.
8. Widder, K. J.; Senyei, A. E.; Ranney, D. F. Magnetically responsive microspheres and other carriers for the biophysical targeting of antitumor agents. *Adv Pharmacol Chemother* **1979**, 16, 213-71.
9. Widder, K. J.; Morris, R. M.; Poore, G. A.; Howard, D. P.; Senyei, A. E. Selective targeting of magnetic albumin microspheres containing low-dose doxorubicin: total remission in Yoshida sarcoma-bearing rats. *Eur J Cancer Clin Oncol* **1983**, 19, 135-9.
10. Brasseur, F.; Couvreur, P.; Kante, B.; Deckers-Passau, L.; Roland, M.; Deckers, C.; Speiser, P. Actinomycin D absorbed on polymethylcyanoacrylate nanoparticles: increased efficiency against an experimental tumor. *Eur J Cancer* **1980**, 16, 1441-5.
11. Barenholz, Y. Doxil(R)--the first FDA-approved nano-drug: lessons learned. *J Control Release* **2012**, 160, 117-34.
12. FDA approves DaunoXome as first-line therapy for Kaposi's sarcoma. Food and Drug Administration. *J Int Assoc Physicians AIDS Care* **1996**, 2, 50-1.
13. Montero, A. J.; Adams, B.; Diaz-Montero, C. M.; Gluck, S. Nab-paclitaxel in the treatment of metastatic breast cancer: a comprehensive review. *Expert Rev Clin Pharmacol* **2011**, 4, 329-34.
14. Oerlemans, C.; Bult, W.; Bos, M.; Storm, G.; Nijsen, J. F.; Hennink, W. E. Polymeric micelles in anticancer therapy: targeting, imaging and triggered release. *Pharm Res* **2010**, 27, 2569-89.
15. Silverman, J. A.; Deitcher, S. R. Marqibo((R)) (vincristine sulfate liposome injection) improves the pharmacokinetics and pharmacodynamics of vincristine. *Cancer Chemother Pharmacol* **2012**.
16. Cai, W.; Chen, X. Nanoplatforms for targeted molecular imaging in living subjects. *Small* **2007**, 3, 1840-54.
17. Lee, H.; Yu, M. K.; Park, S.; Moon, S.; Min, J. J.; Jeong, Y. Y.; Kang, H. W.; Jon, S. Thermally cross-linked superparamagnetic iron oxide nanoparticles: synthesis and application as a dual imaging probe for cancer in vivo. *J Am Chem Soc* **2007**, 129, 12739-45.
18. Tsai, H. C.; Chang, W. H.; Lo, C. L.; Tsai, C. H.; Chang, C. H.; Ou, T. W.; Yen, T. C.; Hsiue, G. H. Graft and diblock copolymer multifunctional micelles for cancer chemotherapy and imaging. *Biomaterials* **2010**, 31, 2293-301.
19. Liu, F.; Laurent, S.; Fattahi, H.; Vander Elst, L.; Muller, R. N. Superparamagnetic nanosystems based on iron oxide nanoparticles for biomedical imaging. *Nanomedicine (Lond)* **2011**, 6, 519-28.

20. Mura, S.; Couvreur, P. Nanotheranostics for personalized medicine. *Adv Drug Deliv Rev* **2012**, 64, 1394-416.
21. Reddy, L. H.; Arias, J. L.; Nicolas, J.; Couvreur, P. Magnetic Nanoparticles: Design and Characterization, Toxicity and Biocompatibility, Pharmaceutical and Biomedical Applications. *Chem Rev* **2012**, 112, 5818-78.
22. Peer, D.; Karp, J. M.; Hong, S.; Farokhzad, O. C.; Margalit, R.; Langer, R. Nanocarriers as an emerging platform for cancer therapy. *Nat Nanotechnol* **2007**, 2, 751-60.
23. Arias, J. L.; Clares, B.; Morales, M. E.; Gallardo, V.; Ruiz, M. A. Lipid-based drug delivery systems for cancer treatment. *Curr Drug Targets* **2011**, 12, 1151-65.
24. Lukyanov, A. N.; Torchilin, V. P. Micelles from lipid derivatives of water-soluble polymers as delivery systems for poorly soluble drugs. *Adv Drug Deliv Rev* **2004**, 56, 1273-89.
25. Torchilin, V. P. Micellar nanocarriers: pharmaceutical perspectives. *Pharm Res* **2007**, 24, 1-16.
26. Reulen, S. W.; Dankers, P. Y.; Bomans, P. H.; Meijer, E. W.; Merkx, M. Collagen targeting using protein-functionalized micelles: the strength of multiple weak interactions. *J Am Chem Soc* **2009**, 131, 7304-12.
27. Constantinides, P. P.; Chaubal, M. V.; Shorr, R. Advances in lipid nanodispersions for parenteral drug delivery and targeting. *Adv Drug Deliv Rev* **2008**, 60, 757-67.
28. Gianella, A.; Jarzyna, P. A.; Mani, V.; Ramachandran, S.; Calcagno, C.; Tang, J.; Kann, B.; Dijk, W. J.; Thijssen, V. L.; Griffioen, A. W.; Storm, G.; Fayad, Z. A.; Mulder, W. J. Multifunctional nanoemulsion platform for imaging guided therapy evaluated in experimental cancer. *ACS Nano* **2011**, 5, 4422-33.
29. Dayton, P. A.; Zhao, S.; Bloch, S. H.; Schumann, P.; Penrose, K.; Matsunaga, T. O.; Zutshi, R.; Doinikov, A.; Ferrara, K. W. Application of ultrasound to selectively localize nanodroplets for targeted imaging and therapy. *Mol Imaging* **2006**, 5, 160-74.
30. Tadros, T.; Izquierdo, P.; Esquena, J.; Solans, C. Formation and stability of nano-emulsions. *Adv Colloid Interface Sci* **2004**, 108-109, 303-18.
31. Rabinow, B. E. Nanosuspensions in drug delivery. *Nat Rev Drug Discov* **2004**, 3, 785-96.
32. Trotta, M.; Gallarate, M.; Pattarino, F.; Morel, S. Emulsions containing partially water-miscible solvents for the preparation of drug nanosuspensions. *J Control Release* **2001**, 76, 119-28.
33. Mehnert, W.; Mader, K. Solid lipid nanoparticles: production, characterization and applications. *Adv Drug Deliv Rev* **2001**, 47, 165-96.
34. Wissing, S. A.; Kayser, O.; Muller, R. H. Solid lipid nanoparticles for parenteral drug delivery. *Adv Drug Deliv Rev* **2004**, 56, 1257-72.
35. Trotta, M.; Debernardi, F.; Caputo, O. Preparation of solid lipid nanoparticles by a solvent emulsification-diffusion technique. *Int J Pharm* **2003**, 257, 153-60.
36. Battaglia, L.; Gallarate, M.; Cavalli, R.; Trotta, M. Solid lipid nanoparticles produced through a coacervation method. *J Microencapsul* **2010**, 27, 78-85.
37. Faraji, A. H.; Wipf, P. Nanoparticles in cellular drug delivery. *Bioorg Med Chem* **2009**, 17, 2950-62.
38. Schubert, M. A.; Harms, M.; Muller-Goymann, C. C. Structural investigations on lipid nanoparticles containing high amounts of lecithin. *Eur J Pharm Sci* **2006**, 27, 226-36.
39. Reddy, L. H.; Adhikari, J. S.; Dwarakanath, B. S.; Sharma, R. K.; Murthy, R. R. Tumoricidal effects of etoposide incorporated into solid lipid nanoparticles after intraperitoneal administration in Dalton's lymphoma bearing mice. *AAPS J* **2006**, 8, E254-62.
40. Zara, G. P.; Cavalli, R.; Fundaro, A.; Bargoni, A.; Caputo, O.; Gasco, M. R. Pharmacokinetics of doxorubicin incorporated in solid lipid nanospheres (SLN). *Pharmacol Res* **1999**, 40, 281-6.

41. Goutayer, M.; Dufort, S.; Josserand, V.; Royere, A.; Heinrich, E.; Vinet, F.; Bibette, J.; Coll, J. L.; Texier, I. Tumor targeting of functionalized lipid nanoparticles: assessment by in vivo fluorescence imaging. *Eur J Pharm Biopharm* **2010**, 75, 137-47.
42. Huynh, N. T.; Passirani, C.; Saulnier, P.; Benoit, J. P. Lipid nanocapsules: a new platform for nanomedicine. *Int J Pharm* **2009**, 379, 201-9.
43. Peltier, S.; Oger, J. M.; Lagarce, F.; Couet, W.; Benoit, J. P. Enhanced oral paclitaxel bioavailability after administration of paclitaxel-loaded lipid nanocapsules. *Pharm Res* **2006**, 23, 1243-50.
44. Khalid, M. N.; Simard, P.; Hoarau, D.; Dragomir, A.; Leroux, J. C. Long circulating poly(ethylene glycol)-decorated lipid nanocapsules deliver docetaxel to solid tumors. *Pharm Res* **2006**, 23, 752-8.
45. Garcion, E.; Lamprecht, A.; Heurtault, B.; Paillard, A.; Aubert-Pouessel, A.; Denizot, B.; Menei, P.; Benoit, J. P. A new generation of anticancer, drug-loaded, colloidal vectors reverses multidrug resistance in glioma and reduces tumor progression in rats. *Mol Cancer Ther* **2006**, 5, 1710-22.
46. David, S.; Passirani, C.; Carmoy, N.; Morille, M.; Mevel, M.; Chatin, B.; Benoit, J. P.; Montier, T.; Pitard, B. DNA nanocarriers for systemic administration: characterization and in vivo bioimaging in healthy mice. *Mol Ther Nucleic Acids* **2013**, 2, e64.
47. Allard, E.; Hindre, F.; Passirani, C.; Lemaire, L.; Lepareur, N.; Noiret, N.; Menei, P.; Benoit, J. P. 188Re-loaded lipid nanocapsules as a promising radiopharmaceutical carrier for internal radiotherapy of malignant gliomas. *Eur J Nucl Med Mol Imaging* **2008**, 35, 1838-46.
48. Vanpouille-Box, C.; Lacoeuille, F.; Roux, J.; Aube, C.; Garcion, E.; Lepareur, N.; Oberti, F.; Bouchet, F.; Noiret, N.; Garin, E.; Benoit, J. P.; Couturier, O.; Hindre, F. Lipid nanocapsules loaded with rhenium-188 reduce tumor progression in a rat hepatocellular carcinoma model. *PLoS One* **2011**, 6, e16926.
49. Lemaire, L.; Bastiat, G.; Franconi, F.; Lautram, N.; Duong Thi Dan, T.; Garcion, E.; Saulnier, P.; Benoit, J. P. Perfluorocarbon-loaded lipid nanocapsules as oxygen sensors for tumor tissue pO(2) assessment. *Eur J Pharm Biopharm* **2013**.
50. Wasan, K. M.; Brocks, D. R.; Lee, S. D.; Sachs-Barrable, K.; Thornton, S. J. Impact of lipoproteins on the biological activity and disposition of hydrophobic drugs: implications for drug discovery. *Nat Rev Drug Discov* **2008**, 7, 84-99.
51. Ng, K. K.; Lovell, J. F.; Zheng, G. Lipoprotein-inspired nanoparticles for cancer theranostics. *Acc Chem Res* **2011**, 44, 1105-13.
52. Eisenberg, S.; Windmueller, H. G.; Levy, R. I. Metabolic fate of rat and human lipoprotein apoproteins in the rat. *J Lipid Res* **1973**, 14, 446-58.
53. Daerr, W. H.; Pethke, W.; Windler, E. T.; Greten, H. Biotinyl-high-density lipoproteins as a probe for the determination of high-density lipoprotein turnover in humans. *Biochim Biophys Acta* **1990**, 1043, 311-7.
54. Glickson, J. D.; Lund-Katz, S.; Zhou, R.; Choi, H.; Chen, I. W.; Li, H.; Corbin, I.; Popov, A. V.; Cao, W.; Song, L.; Qi, C.; Marotta, D.; Nelson, D. S.; Chen, J.; Chance, B.; Zheng, G. Lipoprotein nanoplatform for targeted delivery of diagnostic and therapeutic agents. *Adv Exp Med Biol* **2009**, 645, 227-39.
55. Zhang, Z.; Chen, J.; Ding, L.; Jin, H.; Lovell, J. F.; Corbin, I. R.; Cao, W.; Lo, P. C.; Yang, M.; Tsao, M. S.; Luo, Q.; Zheng, G. HDL-mimicking peptide-lipid nanoparticles with improved tumor targeting. *Small* **2010**, 6, 430-7.
56. Gordon, S. The macrophage. *Bioessays* **1995**, 17, 977-86.
57. Moghimi, S. M.; Davis, S. S. Innovations in avoiding particle clearance from blood by Kupffer cells: cause for reflection. *Crit Rev Ther Drug Carrier Syst* **1994**, 11, 31-59.
58. Patel, H. M.; Moghimi, S. M. Serum-mediated recognition of liposomes by phagocytic cells of the reticuloendothelial system - The concept of tissue specificity. *Adv Drug Deliv Rev* **1998**, 32, 45-60.

59. Gref, R.; Domb, A.; Quellec, P.; Blunk, T.; Muller, R. H.; Verbavatz, J. M.; Langer, R. The controlled intravenous delivery of drugs using PEG-coated sterically stabilized nanospheres. *Adv Drug Deliv Rev* **2012**, Volume 16, 215–233.
60. Fattal, E.; Pecquet, S.; Couvreur, P.; Andremont, A. Biodegradable microparticles for the mucosal delivery of antibacterial and dietary antigens. *Int J Pharm* **2002**, 242, 15-24.
61. Semiramoth, N.; Di Meo, C.; Zouhiri, F.; Said-Hassane, F.; Valetti, S.; Gorges, R.; Nicolas, V.; Poupaert, J. H.; Chollet-Martin, S.; Desmaele, D.; Gref, R.; Couvreur, P. Self-assembled squalenoylated penicillin bioconjugates: an original approach for the treatment of intracellular infections. *Acs Nano* **2012**, 6, 3820-31.
62. Moghimi, S. M.; Hunter, A. C.; Murray, J. C. Long-circulating and target-specific nanoparticles: theory to practice. *Pharmacol Rev* **2001**, 53, 283-318.
63. Moghimi, S. M. Prolonging the circulation time and modifying the body distribution of intravenously injected polystyrene nanospheres by prior intravenous administration of poloxamine-908. A 'hepatic-blockade' event or manipulation of nanosphere surface in vivo? *Biochim Biophys Acta* **1997**, 1336, 1-6.
64. Moghimi, S. M. Re-establishing the long circulatory behaviour of poloxamine-coated particles after repeated intravenous administration: applications in cancer drug delivery and imaging. *Biochim Biophys Acta* **1999**, 1472, 399-403.
65. Dunn, S. E.; Brindley, A.; Davis, S. S.; Davies, M. C.; Illum, L. Polystyrene-poly (ethylene glycol) (PS-PEG2000) particles as model systems for site specific drug delivery. 2. The effect of PEG surface density on the in vitro cell interaction and in vivo biodistribution. *Pharm Res* **1994**, 11, 1016-22.
66. Lin, W.; Garnett, M. C.; Schacht, E.; Davis, S. S.; Illum, L. Preparation and in vitro characterization of HSA-mPEG nanoparticles. *Int J Pharm* **1999**, 189, 161-70.
67. Gref, R.; Minamitake, Y.; Peracchia, M. T.; Trubetskoy, V.; Torchilin, V.; Langer, R. Biodegradable long-circulating polymeric nanospheres. *Science* **1994**, 263, 1600-3.
68. Monfardini, C.; Veronese, F. M. Stabilization of substances in circulation. *Bioconjug Chem* **1998**, 9, 418-50.
69. Peracchia, M. T.; Fattal, E.; Desmaele, D.; Besnard, M.; Noel, J. P.; Gomis, J. M.; Appel, M.; d'Angelo, J.; Couvreur, P. Stealth PEGylated polycyanoacrylate nanoparticles for intravenous administration and splenic targeting. *J Control Release* **1999**, 60, 121-8.
70. Peracchia, M. T.; Vauthier, C.; Puisieux, F.; Couvreur, P. Development of sterically stabilized poly(isobutyl 2-cyanoacrylate) nanoparticles by chemical coupling of poly(ethylene glycol). *J Biomed Mater Res* **1997**, 34, 317-26.
71. Pasut, G.; Veronese, F. M. State of the art in PEGylation: the great versatility achieved after forty years of research. *J Control Release* **2012**, 161, 461-72.
72. Milla, P.; Dosio, F.; Cattel, L. PEGylation of proteins and liposomes: a powerful and flexible strategy to improve the drug delivery. *Curr Drug Metab* **2012**, 13, 105-19.
73. Maeda, H.; Wu, J.; Sawa, T.; Matsumura, Y.; Hori, K. Tumor vascular permeability and the EPR effect in macromolecular therapeutics: a review. *J Control Release* **2000**, 65, 271-84.
74. Jain, R. K. Determinants of tumor blood flow: a review. *Cancer Res* **1988**, 48, 2641-58.
75. Takakura, Y.; Mahato, R. I.; Hashida, M. Extravasation of macromolecules. *Adv Drug Deliv Rev* **1998**, 34, 93-108.
76. Dreher, M. R.; Liu, W.; Michelich, C. R.; Dewhirst, M. W.; Yuan, F.; Chilkoti, A. Tumor vascular permeability, accumulation, and penetration of macromolecular drug carriers. *J Natl Cancer Inst* **2006**, 98, 335-44.
77. Taurin, S.; Nehoff, H.; Greish, K. Anticancer nanomedicine and tumor vascular permeability; Where is the missing link? *J Control Release* **2012**, 164, 265-75.
78. Moghimi, S. M.; Andersen, A. J.; Hashemi, S. H.; Lettiero, B.; Ahmadvand, D.; Hunter, A. C.; Andresen, T. L.; Hamad, I.; Szebeni, J. Complement activation cascade triggered

by PEG-PL engineered nanomedicines and carbon nanotubes: the challenges ahead. *J Control Release* **2010**, 146, 175-81.
79. Andersen, A. J.; Windschiegl, B.; Ilbasmis-Tamer, S.; Degim, I. T.; Hunter, A. C.; Andresen, T. L.; Moghimi, S. M. Complement activation by PEG-functionalized multi-walled carbon nanotubes is independent of PEG molecular mass and surface density. *Nanomedicine* **2013**, 9, 469-73.
80. Takahashi, Y.; Cleary, K. R.; Mai, M.; Kitadai, Y.; Bucana, C. D.; Ellis, L. M. Significance of vessel count and vascular endothelial growth factor and its receptor (KDR) in intestinal-type gastric cancer. *Clin Cancer Res* **1996**, 2, 1679-84.
81. Sofuni, A.; Iijima, H.; Moriyasu, F.; Nakayama, D.; Shimizu, M.; Nakamura, K.; Itokawa, F.; Itoi, T. Differential diagnosis of pancreatic tumors using ultrasound contrast imaging. *J Gastroenterol* **2005**, 40, 518-25.
82. Fuchs, C. S.; Mayer, R. J. Gastric carcinoma. *N Engl J Med* **1995**, 333, 32-41.
83. MacKenzie, M. J. Molecular therapy in pancreatic adenocarcinoma. *Lancet Oncol* **2004**, 5, 541-9.
84. Benhabbour, S. R.; Luft, J. C.; Kim, D.; Jain, A.; Wadhwa, S.; Parrott, M. C.; Liu, R.; DeSimone, J. M.; Mumper, R. J. In vitro and in vivo assessment of targeting lipid-based nanoparticles to the epidermal growth factor-receptor (EGFR) using a novel Heptameric ZEGFR domain. *J Control Release* **2012**, 158, 63-71.
85. deFazio, A.; Chiew, Y. E.; Sini, R. L.; Janes, P. W.; Sutherland, R. L. Expression of c-erbB receptors, heregulin and oestrogen receptor in human breast cell lines. *Int J Cancer* **2000**, 87, 487-98.
86. Ruoslahti, E. Specialization of tumour vasculature. *Nat Rev Cancer* **2002**, 2, 83-90.
87. Weitman, S. D.; Lark, R. H.; Coney, L. R.; Fort, D. W.; Frasca, V.; Zurawski, V. R., Jr.; Kamen, B. A. Distribution of the folate receptor GP38 in normal and malignant cell lines and tissues. *Cancer Res* **1992**, 52, 3396-401.
88. Nicolas, J.; Mura, S.; Brambilla, D.; Mackiewicz, N.; Couvreur, P. Design, functionalization strategies and biomedical applications of targeted biodegradable/biocompatible polymer-based nanocarriers for drug delivery. *Chem Soc Rev* **2012**, 42, 1147-235.
89. Jacobson, B. S.; Stolz, D. B.; Schnitzer, J. E. Identification of endothelial cell-surface proteins as targets for diagnosis and treatment of disease. *Nat Med* **1996**, 2, 482-4.
90. Carson-Walter, E. B.; Watkins, D. N.; Nanda, A.; Vogelstein, B.; Kinzler, K. W.; St Croix, B. Cell surface tumor endothelial markers are conserved in mice and humans. *Cancer Res* **2001**, 61, 6649-55.
91. Borgia, B.; Roesli, C.; Fugmann, T.; Schliemann, C.; Cesca, M.; Neri, D.; Giavazzi, R. A proteomic approach for the identification of vascular markers of liver metastasis. *Cancer Res* **2010**, 70, 309-18.
92. Montet, X.; Funovics, M.; Montet-Abou, K.; Weissleder, R.; Josephson, L. Multivalent effects of RGD peptides obtained by nanoparticle display. *J Med Chem* **2006**, 49, 6087-93.
93. Hood, J. D.; Bednarski, M.; Frausto, R.; Guccione, S.; Reisfeld, R. A.; Xiang, R.; Cheresh, D. A. Tumor regression by targeted gene delivery to the neovasculature. *Science* **2002**, 296, 2404-7.
94. Schottelius, M.; Laufer, B.; Kessler, H.; Wester, H. J. Ligands for mapping alphavbeta3-integrin expression in vivo. *Acc Chem Res* **2009**, 42, 969-80.
95. Beer, A. J.; Schwaiger, M. Imaging of integrin alphavbeta3 expression. *Cancer Metastasis Rev* **2008**, 27, 631-44.
96. Temming, K.; Schiffelers, R. M.; Molema, G.; Kok, R. J. RGD-based strategies for selective delivery of therapeutics and imaging agents to the tumour vasculature. *Drug Resist Updat* **2005**, 8, 381-402.

97. Lammers, T.; Kiessling, F.; Hennink, W. E.; Storm, G. Drug targeting to tumors: principles, pitfalls and (pre-) clinical progress. *J Control Release* **2012**, 161, 175-87.
98. Wang, L. L.; Li, M.; Zhang, N. Folate-targeted docetaxel-lipid-based-nanosuspensions for active-targeted cancer therapy. *International Journal of Nanomedicine* **2012**, 7, 3281-3294.
99. Low, P. S.; Henne, W. A.; Doorneweerd, D. D. Discovery and development of folic-acid-based receptor targeting for imaging and therapy of cancer and inflammatory diseases. *Acc Chem Res* **2008**, 41, 120-9.
100. Antony, A. C. The biological chemistry of folate receptors. *Blood* **1992**, 79, 2807-20.
101. Reddy, J. A.; Allagadda, V. M.; Leamon, C. P. Targeting therapeutic and imaging agents to folate receptor positive tumors. *Curr Pharm Biotechnol* **2005**, 6, 131-50.
102. Saul, J. M.; Annapragada, A. V.; Bellamkonda, R. V. A dual-ligand approach for enhancing targeting selectivity of therapeutic nanocarriers. *J Control Release* **2006**, 114, 277-87.
103. Stella, B.; Arpicco, S.; Peracchia, M. T.; Desmaele, D.; Hoebeke, J.; Renoir, M.; D'Angelo, J.; Cattel, L.; Couvreur, P. Design of folic acid-conjugated nanoparticles for drug targeting. *J Pharm Sci* **2000**, 89, 1452-64.
104. Lu, Y.; Low, P. S. Folate-mediated delivery of macromolecular anticancer therapeutic agents. *Adv Drug Deliv Rev* **2002**, 54, 675-93.
105. Low, P. S.; Kularatne, S. A. Folate-targeted therapeutic and imaging agents for cancer. *Curr Opin Chem Biol* **2009**, 13, 256-62.
106. Stevens, P. J.; Sekido, M.; Lee, R. J. A folate receptor-targeted lipid nanoparticle formulation for a lipophilic paclitaxel prodrug. *Pharm Res* **2004**, 21, 2153-7.
107. Zheng, G.; Chen, J.; Li, H.; Glickson, J. D. Rerouting lipoprotein nanoparticles to selected alternate receptors for the targeted delivery of cancer diagnostic and therapeutic agents. *Proc Natl Acad Sci U S A* **2005**, 102, 17757-62.
108. Shaw, J. M.; Shaw, K. V.; Yanovich, S.; Iwanik, M.; Futch, W. S.; Rosowsky, A.; Schook, L. B. Delivery of lipophilic drugs using lipoproteins. *Ann N Y Acad Sci* **1987**, 507, 252-71.
109. Mendelsohn, J.; Baselga, J. Status of epidermal growth factor receptor antagonists in the biology and treatment of cancer. *J Clin Oncol* **2003**, 21, 2787-99.
110. Nicholson, R. I.; Gee, J. M.; Harper, M. E. EGFR and cancer prognosis. *Eur J Cancer* **2001**, 37 Suppl 4, S9-15.
111. Real, F. X.; Rettig, W. J.; Chesa, P. G.; Melamed, M. R.; Old, L. J.; Mendelsohn, J. Expression of epidermal growth factor receptor in human cultured cells and tissues: relationship to cell lineage and stage of differentiation. *Cancer Res* **1986**, 46, 4726-31.
112. Kuo, Y. C.; Liang, C. T. Inhibition of human brain malignant glioblastoma cells using carmustine-loaded catanionic solid lipid nanoparticles with surface anti-epithelial growth factor receptor. *Biomaterials* **2011**, 32, 3340-50.
113. Kuo, Y. C.; Liang, C. T. Catanionic solid lipid nanoparticles carrying doxorubicin for inhibiting the growth of U87MG cells. *Colloids Surf B Biointerfaces* **2011**, 85, 131-7.
114. Tolmachev, V.; Orlova, A.; Nilsson, F. Y.; Feldwisch, J.; Wennborg, A.; Abrahmsen, L. Affibody molecules: potential for in vivo imaging of molecular targets for cancer therapy. *Expert Opin Biol Ther* **2007**, 7, 555-68.
115. Friedman, M.; Orlova, A.; Johansson, E.; Eriksson, T. L.; Hoiden-Guthenberg, I.; Tolmachev, V.; Nilsson, F. Y.; Stahl, S. Directed evolution to low nanomolar affinity of a tumor-targeting epidermal growth factor receptor-binding affibody molecule. *J Mol Biol* **2008**, 376, 1388-402.
116. Nygren, P. A. Alternative binding proteins: affibody binding proteins developed from a small three-helix bundle scaffold. *FEBS J* **2008**, 275, 2668-76.
117. Platt, V. M.; Szoka, F. C., Jr. Anticancer therapeutics: targeting macromolecules and nanocarriers to hyaluronan or CD44, a hyaluronan receptor. *Mol Pharm* **2008**, 5, 474-86.

118. Cho, H. J.; Yoon, H. Y.; Koo, H.; Ko, S. H.; Shim, J. S.; Lee, J. H.; Kim, K.; Kwon, I. C.; Kim, D. D. Self-assembled nanoparticles based on hyaluronic acid-ceramide (HA-CE) and Pluronic(R) for tumor-targeted delivery of docetaxel. *Biomaterials* **2011**, 32, 7181-90.
119. Noble, P. W. Hyaluronan and its catabolic products in tissue injury and repair. *Matrix Biol* **2002**, 21, 25-9.
120. Deed, R.; Rooney, P.; Kumar, P.; Norton, J. D.; Smith, J.; Freemont, A. J.; Kumar, S. Early-response gene signalling is induced by angiogenic oligosaccharides of hyaluronan in endothelial cells. Inhibition by non-angiogenic, high-molecular-weight hyaluronan. *Int J Cancer* **1997**, 71, 251-6.
121. Al-Hajj, M.; Wicha, M. S.; Benito-Hernandez, A.; Morrison, S. J.; Clarke, M. F. Prospective identification of tumorigenic breast cancer cells. *Proc Natl Acad Sci U S A* **2003**, 100, 3983-8.
122. Dufay Wojcicki, A.; Hillaireau, H.; Nascimento, T. L.; Arpicco, S.; Taverna, M.; Ribes, S.; Bourge, M.; Nicolas, V.; Bochot, A.; Vauthier, C.; Tsapis, N.; Fattal, E. Hyaluronic acid-bearing lipoplexes: physico-chemical characterization and in vitro targeting of the CD44 receptor. *J Control Release* **2012**, 162, 545-52.
123. Cho, H. J.; Yoon, I. S.; Yoon, H. Y.; Koo, H.; Jin, Y. J.; Ko, S. H.; Shim, J. S.; Kim, K.; Kwon, I. C.; Kim, D. D. Polyethylene glycol-conjugated hyaluronic acid-ceramide self-assembled nanoparticles for targeted delivery of doxorubicin. *Biomaterials* **2012**, 33, 1190-200.
124. Saddoughi, S. A.; Song, P.; Ogretmen, B. Roles of bioactive sphingolipids in cancer biology and therapeutics. *Subcell Biochem* **2008**, 49, 413-40.
125. Han, J. H.; Oh, Y. K.; Kim, D. S.; Kim, C. K. Enhanced hepatocyte uptake and liver targeting of methotrexate using galactosylated albumin as a carrier. *Int J Pharm* **1999**, 188, 39-47.
126. Morille, M.; Passirani, C.; Letrou-Bonneval, E.; Benoit, J. P.; Pitard, B. Galactosylated DNA lipid nanocapsules for efficient hepatocyte targeting. *Int J Pharm* **2009**, 379, 293-300.
127. Zhang, Y.; He, L.; Zhou, Y. Taspine isolated from Radix et Rhizoma Leonticis inhibits growth of human umbilical vein endothelial cell (HUVEC) by inducing its apoptosis. *Phytomedicine* **2008**, 15, 112-9.
128. Lu, W.; He, L. C.; Wang, C. H.; Li, Y. H.; Zhang, S. Q. The use of solid lipid nanoparticles to target a lipophilic molecule to the liver after intravenous administration to mice. *Int J Biol Macromol* **2008**, 43, 320-4.
129. Xu, Z.; Chen, L.; Gu, W.; Gao, Y.; Lin, L.; Zhang, Z.; Xi, Y.; Li, Y. The performance of docetaxel-loaded solid lipid nanoparticles targeted to hepatocellular carcinoma. *Biomaterials* **2009**, 30, 226-32.
130. Ezekowitz, R. A.; Williams, D. J.; Koziel, H.; Armstrong, M. Y.; Warner, A.; Richards, F. F.; Rose, R. M. Uptake of Pneumocystis carinii mediated by the macrophage mannose receptor. *Nature* **1991**, 351, 155-8.
131. Yu, W. Y.; Liu, C. X.; Liu, Y.; Zhang, N.; Xu, W. F. Mannan-Modified Solid Lipid Nanoparticles for Targeted Gene Delivery to Alveolar Macrophages. *Pharmaceutical Research* **2010**, 27, 1584-1596.
132. Wijagkanalan, W.; Kawakami, S.; Takenaga, M.; Igarashi, R.; Yamashita, F.; Hashida, M. Efficient targeting to alveolar macrophages by intratracheal administration of mannosylated liposomes in rats. *J Control Release* **2008**, 125, 121-30.
133. Laine, A. L.; Huynh, N. T.; Clavreul, A.; Balzeau, J.; Bejaud, J.; Vessieres, A.; Benoit, J. P.; Eyer, J.; Passirani, C. Brain tumour targeting strategies via coated ferrociphenol lipid nanocapsules. *Eur J Pharm Biopharm* **2012**, 81, 690-3.
134. Bertini, I. L., C. Chapter 1 Introduction. *Coordination Chemistry Reviews* **1996**, 150, 1-28.

135. Kruk, D.; Kowalewski, J. Nuclear spin relaxation in paramagnetic systems (S>/=1) under fast rotation conditions. *J Magn Reson* **2003**, 162, 229-40.
136. Villaraza, A. J.; Bumb, A.; Brechbiel, M. W. Macromolecules, dendrimers, and nanomaterials in magnetic resonance imaging: the interplay between size, function, and pharmacokinetics. *Chem Rev* **2010**, 110, 2921-59.
137. Bellin, M. F. MR contrast agents, the old and the new. *Eur J Radiol* **2006**, 60, 314-23.
138. Morel, S.; Terreno, E.; Ugazio, E.; Aime, S.; Gasco, M. R. NMR relaxometric investigations of solid lipid nanoparticles (SLN) containing gadolinium(III) complexes. *Eur J Pharm Biopharm* **1998**, 45, 157-63.
139. Corbin, I. R.; Li, H.; Chen, J.; Lund-Katz, S.; Zhou, R.; Glickson, J. D.; Zheng, G. Low-density lipoprotein nanoparticles as magnetic resonance imaging contrast agents. *Neoplasia* **2006**, 8, 488-98.
140. Gazeau, F.; Wilhelm, C. Magnetic labeling, imaging and manipulation of endothelial progenitor cells using iron oxide nanoparticles. *Future Med Chem* **2010**, 2, 397-408.
141. Al Faraj, A.; Luciani, N.; Kolosnjaj-Tabi, J.; Mattar, E.; Clement, O.; Wilhelm, C.; Gazeau, F. Real-time high-resolution magnetic resonance tracking of macrophage subpopulations in a murine inflammation model: a pilot study with a commercially available cryogenic probe. *Contrast Media Mol Imaging* **2013**, 8, 193-203.
142. Wilhelm, C.; Gazeau, F. Universal cell labelling with anionic magnetic nanoparticles. *Biomaterials* **2008**, 29, 3161-74.
143. Peira, E.; Marzola, P.; Podio, V.; Aime, S.; Sbarbati, A.; Gasco, M. R. In vitro and in vivo study of solid lipid nanoparticles loaded with superparamagnetic iron oxide. *J Drug Target* **2003**, 11, 19-24.
144. Arias, J. L.; Reddy, L. H.; Couvreur, P. Magnetoresponsive squalenoyl gemcitabine composite nanoparticles for cancer active targeting. *Langmuir* **2008**, 24, 7512-9.
145. Arias, J. L.; Reddy, L. H.; Othman, M.; Gillet, B.; Desmaele, D.; Zouhiri, F.; Dosio, F.; Gref, R.; Couvreur, P. Squalene based nanocomposites: a new platform for the design of multifunctional pharmaceutical theragnostics. *ACS Nano* **2011**, 5, 1513-21.
146. Costas, B. Review of biomedical optical imaging-a powerful, non-invasive, non-ionizing technology for improving in vivo diagnosis. *Meas. Sci. Technol.* **2009**, 20.
147. Schnall, M.; Rosen, M. Primer on imaging technologies for cancer. *J Clin Oncol* **2006**, 24, 3225-33.
148. Kobayashi, H.; Ogawa, M.; Alford, R.; Choyke, P. L.; Urano, Y. New strategies for fluorescent probe design in medical diagnostic imaging. *Chem Rev* **2010**, 110, 2620-40.
149. Kirchherr, A. K.; Briel, A.; Mader, K. Stabilization of indocyanine green by encapsulation within micellar systems. *Mol Pharm* **2009**, 6, 480-91.
150. Zheng, X.; Xing, D.; Zhou, F.; Wu, B.; Chen, W. R. Indocyanine green-containing nanostructure as near infrared dual-functional targeting probes for optical imaging and photothermal therapy. *Mol Pharm* **2011**, 8, 447-56.
151. Merian, J.; Gravier, J.; Navarro, F.; Texier, I. Fluorescent nanoprobes dedicated to in vivo imaging: from preclinical validations to clinical translation. *Molecules* **2012**, 17, 5564-91.
152. Gravier, J.; Navarro, F. P.; Delmas, T.; Mittler, F.; Couffin, A. C.; Vinet, F.; Texier, I. Lipidots: competitive organic alternative to quantum dots for in vivo fluorescence imaging. *J Biomed Opt* **2011**, 16, 096013.
153. Navarro, F. P.; Mittler, F.; Berger, M.; Josserand, V.; Gravier, J.; Vinet, F.; Texier, I. Cell tolerability and biodistribution in mice of indocyanine green-loaded lipid nanoparticles. *J Biomed Nanotechnol* **2012**, 8, 594-604.
154. Navarro, F. P.; Berger, M.; Guillermet, S.; Josserand, V.; Guyon, L.; Neumann, E.; Vinet, F.; Texier, I. Lipid nanoparticle vectorization of indocyanine green improves fluorescence imaging for tumor diagnosis and lymph node resection. *J Biomed Nanotechnol* **2012**, 8, 730-41.

155. Beri, A.; Janetschek, G. Technology insight: radioguided sentinel lymph node dissection in the staging of prostate cancer. *Nat Clin Pract Urol* **2006**, 3, 602-10.
156. Cao, W.; Ng, K. K.; Corbin, I.; Zhang, Z.; Ding, L.; Chen, J.; Zheng, G. Synthesis and evaluation of a stable bacteriochlorophyll-analog and its incorporation into high-density lipoprotein nanoparticles for tumor imaging. *Bioconjug Chem* **2009**, 20, 2023-31.
157. Chen, J.; Corbin, I. R.; Li, H.; Cao, W.; Glickson, J. D.; Zheng, G. Ligand conjugated low-density lipoprotein nanoparticles for enhanced optical cancer imaging in vivo. *J Am Chem Soc* **2007**, 129, 5798-9.
158. Cormode, D. P.; Jarzyna, P. A.; Mulder, W. J.; Fayad, Z. A. Modified natural nanoparticles as contrast agents for medical imaging. *Adv Drug Deliv Rev* **2010**, 62, 329-38.
159. Massoud, T. F.; Gambhir, S. S. Molecular imaging in living subjects: seeing fundamental biological processes in a new light. *Genes Dev* **2003**, 17, 545-80.
160. Liu, M. S.; Long, D. M. Perfluoroctylbromide as a diagnostic contrast medium in gastroenterography. *Radiology* **1977**, 122, 71-6.
161. Diaz-Lopez, R.; Tsapis, N.; Fattal, E. Liquid perfluorocarbons as contrast agents for ultrasonography and (19)F-MRI. *Pharm Res* **2010**, 27, 1-16.
162. Lanza, G. M.; Abendschein, D. R.; Hall, C. S.; Scott, M. J.; Scherrer, D. E.; Houseman, A.; Miller, J. G.; Wickline, S. A. In vivo molecular imaging of stretch-induced tissue factor in carotid arteries with ligand-targeted nanoparticles. *J Am Soc Echocardiogr* **2000**, 13, 608-14.
163. Diou, O.; Tsapis, N.; Fattal, E. Targeted nanotheranostics for personalized cancer therapy. *Expert Opin Drug Deliv* **2012**, 9, 1475-87.
164. Wang, C. H.; Kang, S. T.; Lee, Y. H.; Luo, Y. L.; Huang, Y. F.; Yeh, C. K. Aptamer-conjugated and drug-loaded acoustic droplets for ultrasound theranosis. *Biomaterials* **2012**, 33, 1939-47.
165. Andreozzi, E.; Seo, J. W.; Ferrara, K.; Louie, A. Novel method to label solid lipid nanoparticles with 64cu for positron emission tomography imaging. *Bioconjug Chem* **2011**, 22, 808-18.
166. Duconge, F.; Pons, T.; Pestourie, C.; Herin, L.; Theze, B.; Gombert, K.; Mahler, B.; Hinnen, F.; Kuhnast, B.; Dolle, F.; Dubertret, B.; Tavitian, B. Fluorine-18-labeled phospholipid quantum dot micelles for in vivo multimodal imaging from whole body to cellular scales. *Bioconjug Chem* **2008**, 19, 1921-6.
167. Burda, C.; Chen, X.; Narayanan, R.; El-Sayed, M. A. Chemistry and properties of nanocrystals of different shapes. *Chem Rev* **2005**, 105, 1025-102.
168. Chen, W.; Jarzyna, P. A.; van Tilborg, G. A.; Nguyen, V. A.; Cormode, D. P.; Klink, A.; Griffioen, A. W.; Randolph, G. J.; Fisher, E. A.; Mulder, W. J.; Fayad, Z. A. RGD peptide functionalized and reconstituted high-density lipoprotein nanoparticles as a versatile and multimodal tumor targeting molecular imaging probe. *FASEB J* **2010**, 24, 1689-99.
169. Acton, S.; Rigotti, A.; Landschulz, K. T.; Xu, S.; Hobbs, H. H.; Krieger, M. Identification of scavenger receptor SR-BI as a high density lipoprotein receptor. *Science* **1996**, 271, 518-20.
170. Brigger, I.; Dubernet, C.; Couvreur, P. Nanoparticles in cancer therapy and diagnosis. *Adv Drug Deliv Rev* **2002**, 54, 631-51.
171. Itaka, K.; Osada, K.; Morii, K.; Kim, P.; Yun, S. H.; Kataoka, K. Polyplex nanomicelle promotes hydrodynamic gene introduction to skeletal muscle. *J Control Release* **2010**, 143, 112-9.
172. Cabral, H.; Nishiyama, N.; Kataoka, K. Optimization of (1,2-diamino-cyclohexane)platinum(II)-loaded polymeric micelles directed to improved tumor targeting and enhanced antitumor activity. *J Control Release* **2007**, 121, 146-55.

173. Sadee, W.; Dai, Z. Pharmacogenetics/genomics and personalized medicine. *Hum Mol Genet* **2005**, 14 Spec No. 2, R207-14.
174. Bates, S. Progress towards personalized medicine. *Drug Discov Today* **2010**, 15, 115-20.
175. Wang, C. H.; Kang, S. T.; Lee, Y. H.; Luo, Y. L.; Huang, Y. F.; Yeh, C. K. Aptamer-conjugated and drug-loaded acoustic droplets for ultrasound theranosis. *Biomaterials* **2012**, 33, 1939-1947.
176. Soman, N. R.; Baldwin, S. L.; Hu, G.; Marsh, J. N.; Lanza, G. M.; Heuser, J. E.; Arbeit, J. M.; Wickline, S. A.; Schlesinger, P. H. Molecularly targeted nanocarriers deliver the cytolytic peptide melittin specifically to tumor cells in mice, reducing tumor growth. *J Clin Invest* **2009**, 119, 2830-42.
177. Tosteson, M. T.; Tosteson, D. C. The sting. Melittin forms channels in lipid bilayers. *Biophys J* **1981**, 36, 109-16.
178. Hansel, W.; Leuschner, C.; Enright, F. Conjugates of lytic peptides and LHRH or betaCG target and cause necrosis of prostate cancers and metastases. *Mol Cell Endocrinol* **2007**, 269, 26-33.
179. Desmaele, D.; Gref, R.; Couvreur, P. Squalenoylation: a generic platform for nanoparticular drug delivery. *J Control Release* **2012**, 161, 609-18.
180. Couvreur, P.; Stella, B.; Reddy, L. H.; Hillaireau, H.; Dubernet, C.; Desmaele, D.; Lepetre-Mouelhi, S.; Rocco, F.; Dereuddre-Bosquet, N.; Clayette, P.; Rosilio, V.; Marsaud, V.; Renoir, J. M.; Cattel, L. Squalenoyl nanomedicines as potential therapeutics. *Nano Lett.* **2006**, 6, 2544-8.
181. Bekkara-Aounallah, F.; Gref, R.; Othman, M.; Reddy, L. H.; Pili, B.; Allain, V.; Bourgaux, C.; Hillaireau, H.; Lepêtre-Mouelhi, S.; Desmaële, D.; Nicolas, J.; Chafi, N.; Couvreur, P. Novel PEGylated Nanoassemblies Made of Self-Assembled Squalenoyl Nucleoside Analogues. *Advanced Functional Materials* **2008**, 18, 3715-3725.
182. Caron, J.; Reddy, L. H.; Lepetre-Mouelhi, S.; Wack, S.; Clayette, P.; Rogez-Kreuz, C.; Yousfi, R.; Couvreur, P.; Desmaele, D. Squalenoyl nucleoside monophosphate nanoassemblies: new prodrug strategy for the delivery of nucleotide analogues. *Bioorg Med Chem Lett* **2010**, 20, 2761-4.
183. Stella, B.; Arpicco, S.; Rocco, F.; Burgalassi, S.; Nicosia, N.; Tampucci, S.; Chetoni, P.; Cattel, L. Nonpolymeric nanoassemblies for ocular administration of acyclovir: pharmacokinetic evaluation in rabbits. *Eur J Pharm Biopharm* **2012**, 80, 39-45.
184. Cosco, D.; Rocco, F.; Ceruti, M.; Vono, M.; Fresta, M.; Paolino, D. Self-assembled squalenoyl-cytarabine nanostructures as a potent nanomedicine for treatment of leukemic diseases. *Int J Nanomedicine* **2012**, 7, 2535-46.
185. Dosio, F.; Reddy, L. H.; Ferrero, A.; Stella, B.; Cattel, L.; Couvreur, P. Novel nanoassemblies composed of squalenoyl-paclitaxel derivatives: synthesis, characterization, and biological evaluation. *Bioconjug Chem* **2010**, 21, 1349-61.
186. Caron, J.; Maksimenko, A.; Wack, S.; Lepeltier, E.; Bourgaux, C.; Morvan, E.; Leblanc, K.; Couvreur, P.; Desmaele, D. Improving the Antitumor Activity of Squalenoyl-Paclitaxel Conjugate Nanoassemblies by Manipulating the Linker between Paclitaxel and Squalene. *Adv Healthc Mater* **2013**, 2, 172-85.
187. Dosio, F.; Stella, B.; Ferrero, A.; Garino, C.; Zonari, D.; Arpicco, S.; Cattel, L.; Giordano, S.; Gobetto, R. Ruthenium polypyridyl squalene derivative: A novel self-assembling lipophilic probe for cellular imaging. *Int J Pharm* **2013**, 440, 221-8.
188. Othman, M.; Desmaele, D.; Couvreur, P.; Vander Elst, L.; Laurent, S.; Muller, R. N.; Bourgaux, C.; Morvan, E.; Pouget, T.; Lepetre-Mouelhi, S.; Durand, P.; Gref, R. Synthesis and physicochemical characterization of new squalenoyl amphiphilic gadolinium complexes as nanoparticle contrast agents. *Org Biomol Chem* **2011**, 9, 4367-86.
189. Raouane, M.; Desmaele, D.; Gilbert-Sirieix, M.; Gueutin, C.; Zouhiri, F.; Bourgaux, C.; Lepeltier, E.; Gref, R.; Ben Salah, R.; Clayman, G.; Massaad-Massade, L.; Couvreur, P.

Synthesis, characterization, and in vivo delivery of siRNA-squalene nanoparticles targeting fusion oncogene in papillary thyroid carcinoma. *J Med Chem* **2011**, 54, 4067-76.

190. Rejiba, S.; Reddy, L. H.; Bigand, C.; Parmentier, C.; Couvreur, P.; Hajri, A. Squalenoyl gemcitabine nanomedicine overcomes the low efficacy of gemcitabine therapy in pancreatic cancer. *Nanomedicine* **2011**, 7, 841-9.

Pancreatic cancer treatment and nanomedicine

The pancreas is a glandular organ that regulates two major physiological processes: glucose metabolism and digestion. It is composed of (*i*) an endocrine gland that produces hormones including insulin, glucagon and somatostatin and of (*ii*) an exocrine portion made of acinar and duct cells that contribute to digestion and nutrient absorption in the small intestine by secreting pancreatic enzymes.

Cancer cells can arise from both parts evolving in four different tumor types (*i.e.*, pancreatic ductal adenocarcinoma, acinar-cell carcinoma, pancreatic endocrine tumor and serous cystadenoma) which show distinct clinical behavior and genetic profiles.[1]

Pancreatic ductal adenocarcinoma, a tumor type with ductal-cell histology, is a highly aggressive malignancy representing more than 85% of pancreatic neoplasms.[1] The etiology remains still poorly defined. It is associated with advancing age and approximately 10% of cases have an inherited predisposition mainly due to hereditary pancreatitis, which represent the major risk factor.[2] According to the National Cancer Institute, 1 out of 68 men and women will be diagnosed with cancer of the pancreas during their lives.[3] The only potentially curative therapy is surgical resection that is unfortunately possible only for 20% of patients making this tumor the fourth leading cause of cancer-related death.[2] Gemcitabine, a nucleoside analogue that blocks the DNA replication, is the major chemotherapic agent for pancreatic cancer treatment since 1996.[4] Although its weak response rate of 5% and the modest overall survival benefit, this drug still remains the first-line treatment in the clinical practice.[5] Gemcitabine drawbacks mainly arise from its rapid blood inactivation and consequently short plasma half-life[6] and from the downregulation of its membrane transporter that decreases cellular internalization.[7] In addition, chemotherapy of pancreatic cancer is hampered by the tumor physio-pathological complexity.[2,8] Indeed, recent clinical evidences have revealed that pancreatic cancer is a complex entity composed by several distinct elements including pancreatic-cancer cells, stem cells and a dense, poorly vascularized stroma.[2,9] Moreover, pancreatic cancer cells carry on average 63 genetic alterations[10] thus, each treatment may display efficacy only in subgroups of patients with specific molecular phenotypes.

As a consequence of this physio-pathology, the latest clinical trials evaluated targeted agents able to interact with (*i*) signaling pathways genetically altered in most of the tumors such as KRAS2, TNF-α and hedgehog, IGF-IR type I, SPARC secreted protein, mucin-1, death receptor, PSCA (prostate stem-cell antigen), mesothelin, FGFR (fibroblast growth factor receptor), PDGFR (platelet-derived growth factor), MEK (mitogenactivated protein kinase–extracellular-signal–regulated kinase) and Src kinases.[2,5,8]

In parallel, combined therapy with gemcitabine and others agents was ascertained as an alternative good approach to overcome pancreatic heterogeneity issue by synergistically countering different biological signaling pathways. The FOLFIRINOX combination chemotherapy regimen (*i.e.*, oxaliplatin, leucovorin,irinotecan and 5-fluorouracil) has shown improvement in overall survival over the gemcitabine as single agent event thought, owing to the increased toxicity, this protocol is a treatment option only for of patients with metastatic pancreatic cancer and a good performance status.[11] On the contrary, several evidences showed that a significant enhancement of the efficacy of the monotherapy, without toxicity increase, can be achieved by combination of chemotherapy with molecular targeted treatments.[2,12]

Proof of concept is the FDA approval of the erlotinib, a small-molecule tyrosine kinase inhibitor, as first-line treatment in advanced, unresectable or metastatic pancreatic carcinoma in combination with gemcitabine.[13] However, improvements in overall survival remain limited to few weeks.[14]

In this context, nanocarrier drug delivery systems hold a big potential to further improve the efficacy of targeted chemotherapy in pancreatic carcinoma treatment. For instance, successful

results have been obtained with albumin-bound paclitaxel nanoparticles (nab-paclitaxel - Abraxane®), approved in 2013 for late-stage pancreatic cancer.[15] As for targeted drug therapy, nanotechnology-based drug delivery systems with ligands grafted to the nanocarrier surface were developed to improve targeting efficacy *via* multivalent binding with the receptor.[16] Nanoparticles decorated with several ligands such as the epidermal growth factor (EGF)[17], the arginine-glycine-aspartic acid (RGD) peptide[18] or antibodies towards the transferrin receptor[19] have been developed for targeting of pancreas (for review see[20-22]). However, functionalization with such ligands, that were not specific for pancreatic cancer led to limited targeting efficiency.

As observed for the combined drug therapy, controlled drug release from nanocarriers can tune the pharmacokinetic and biodistribution of chemically dissimilar drug molecules that independently have disparate pharmacological behaviors.[23,24]

In the above delineated context, the discovery of novel ligands specific for pancreatic cancer, which would allow to design efficient targeted nanomedicines and/or the development of nanotechnology-based more adequate combined therapies, capable to significantly increase antitumor efficacy and survival rate, represents important challenge.

References

1. Bardeesy, N.; DePinho, R. A. Pancreatic cancer biology and genetics. *Nature Reviews Cancer* **2002**, 2, 897-909.
2. Hidalgo, M. Pancreatic cancer. *N Engl J Med* **2010**, 362, 1605-17.
3. Jemal, A.; Siegel, R.; Xu, J.; Ward, E. Cancer statistics, 2010. *CA Cancer J Clin* **2010**, 60, 277-300.
4. http://www.clinicaltrials.gov/. http://www.clinicaltrials.gov/.
5. Oberstein, P. E.; Saif, M. W. First-line treatment for advanced pancreatic cancer. Highlights from the "2011 ASCO Gastrointestinal Cancers Symposium". San Francisco, CA, USA. January 20-22, 2011. *JOP* **2011**, 12, 96-100.
6. Storniolo, A. M.; Allerheiligen, S. R.; Pearce, H. L. Preclinical, pharmacologic, and phase I studies of gemcitabine. *Semin Oncol* **1997**, 24, S7-2-S7-7.
7. Rauchwerger, D. R.; Firby, P. S.; Hedley, D. W.; Moore, M. J. Equilibrative-sensitive nucleoside transporter and its role in gemcitabine sensitivity. *Cancer Res* **2000**, 60, 6075-9.
8. Corbo, V.; Tortora, G.; Scarpa, A. Molecular Pathology of Pancreatic Cancer: From Bench-to-Bedside Translation. *Current Drug Targets* **2012**, 13, 744-752.
9. Olive, K. P.; Jacobetz, M. A.; Davidson, C. J.; Gopinathan, A.; McIntyre, D.; Honess, D.; Madhu, B.; Goldgraben, M. A.; Caldwell, M. E.; Allard, D.; Frese, K. K.; Denicola, G.; Feig, C.; Combs, C.; Winter, S. P.; Ireland-Zecchini, H.; Reichelt, S.; Howat, W. J.; Chang, A.; Dhara, M.; Wang, L.; Ruckert, F.; Grutzmann, R.; Pilarsky, C.; Izeradjene, K.; Hingorani, S. R.; Huang, P.; Davies, S. E.; Plunkett, W.; Egorin, M.; Hruban, R. H.; Whitebread, N.; McGovern, K.; Adams, J.; Iacobuzio-Donahue, C.; Griffiths, J.; Tuveson, D. A. Inhibition of Hedgehog signaling enhances delivery of chemotherapy in a mouse model of pancreatic cancer. *Science* **2009**, 324, 1457-61.
10. Jones, S.; Zhang, X.; Parsons, D. W.; Lin, J. C.; Leary, R. J.; Angenendt, P.; Mankoo, P.; Carter, H.; Kamiyama, H.; Jimeno, A.; Hong, S. M.; Fu, B.; Lin, M. T.; Calhoun, E. S.; Kamiyama, M.; Walter, K.; Nikolskaya, T.; Nikolsky, Y.; Hartigan, J.; Smith, D. R.; Hidalgo, M.; Leach, S. D.; Klein, A. P.; Jaffee, E. M.; Goggins, M.; Maitra, A.; Iacobuzio-Donahue, C.; Eshleman, J. R.; Kern, S. E.; Hruban, R. H.; Karchin, R.; Papadopoulos, N.; Parmigiani, G.; Vogelstein, B.; Velculescu, V. E.; Kinzler, K. W. Core signaling pathways in human pancreatic cancers revealed by global genomic analyses. *Science* **2008**, 321, 1801-6.
11. Conroy, T.; Desseigne, F.; Ychou, M.; Bouche, O.; Guimbaud, R.; Becouarn, Y.; Adenis, A.; Raoul, J. L.; Gourgou-Bourgade, S.; de la Fouchardiere, C.; Bennouna, J.; Bachet, J. B.; Khemissa-Akouz, F.; Pere-Verge, D.; Delbaldo, C.; Assenat, E.; Chauffert, B.; Michel, P.; Montoto-Grillot, C.; Ducreux, M.; Unicanc, G. T. D.; Intergrp, P. FOLFIRINOX versus Gemcitabine for Metastatic Pancreatic Cancer. *New Engl J Med* **2011**, 364, 1817-1825.
12. Shi, S.; Yao, W. T.; Xu, J.; Long, J.; Liu, C.; Yu, X. J. Combinational therapy: New hope for pancreatic cancer? *Cancer Lett* **2012**, 317, 127-135.
13. http://www.accessdata.fda.gov/drugsatfda_docs/appletter/2013/021660Orig1s037ltr.pdf
14. Moore, M. J.; Goldstein, D.; Hamm, J.; Figer, A.; Hecht, J. R.; Gallinger, S.; Au, H. J.; Murawa, P.; Walde, D.; Wolff, R. A.; Campos, D.; Lim, R.; Ding, K.; Clark, G.; Voskoglou-Nomikos, T.; Ptasynski, M.; Parulekar, W. Erlotinib plus gemcitabine compared with gemcitabine alone in patients with advanced pancreatic cancer: a phase III trial of the National Cancer Institute of Canada Clinical Trials Group. *J Clin Oncol* **2007**, 25, 1960-6.
15. http://www.fda.gov/newsevents/newsroom/pressannouncements/ucm367442.htm.

16. Reulen, S. W.; Dankers, P. Y.; Bomans, P. H.; Meijer, E. W.; Merkx, M. Collagen targeting using protein-functionalized micelles: the strength of multiple weak interactions. *J Am Chem Soc* **2009**, 131, 7304-12.
17. Kudgus, R. A.; Szabolcs, A.; Khan, J. A.; Walden, C. A.; Reid, J. M.; Robertson, J. D.; Bhattacharya, R.; Mukherjee, P. Inhibiting the growth of pancreatic adenocarcinoma in vitro and in vivo through targeted treatment with designer gold nanotherapeutics. *PLoS One* **2013**, 8, e57522.
18. Ji, S.; Xu, J.; Zhang, B.; Yao, W.; Xu, W.; Wu, W.; Xu, Y.; Wang, H.; Ni, Q.; Hou, H.; Yu, X. RGD-conjugated albumin nanoparticles as a novel delivery vehicle in pancreatic cancer therapy. *Cancer Biol Ther* **2012**, 13, 206-15.
19. Camp, E. R.; Wang, C.; Little, E. C.; Watson, P. M.; Pirollo, K. F.; Rait, A.; Cole, D. J.; Chang, E. H.; Watson, D. K. Transferrin receptor targeting nanomedicine delivering wild-type p53 gene sensitizes pancreatic cancer to gemcitabine therapy. *Cancer Gene Ther* **2013**, 20, 222-8.
20. Yu, X.; Zhang, Y.; Chen, C.; Yao, Q.; Li, M. Targeted drug delivery in pancreatic cancer. *Biochim Biophys Acta* **2010**, 1805, 97-104.
21. Yang, F.; Jin, C.; Subedi, S.; Lee, C. L.; Wang, Q.; Jiang, Y.; Li, J.; Di, Y.; Fu, D. Emerging inorganic nanomaterials for pancreatic cancer diagnosis and treatment. *Cancer Treat Rev* **2012**, 38, 566-79.
22. Sykes, P. D.; Neoptolemos, J. P.; Costello, E.; Halloran, C. M. Nanotechnology advances in upper gastrointestinal, liver and pancreatic cancer. *Expert Rev Gastroenterol Hepatol* **2012**, 6, 343-56.
23. Parhi, P.; Mohanty, C.; Sahoo, S. K. Nanotechnology-based combinational drug delivery: an emerging approach for cancer therapy. *Drug Discov Today* **2012**, 17, 1044-52.
24. Ma, L.; Kohli, M.; Smith, A. Nanoparticles for combination drug therapy. *Acs Nano* **2013**, 7, 9518-25.

Part 2: Experimental work

Chapter 1:

“Peptide-functionalized nanoparticles for selective targeting of pancreatic tumor”

Peptide-functionalized Nanoparticles for Selective Targeting of Pancreatic Tumor

*Sabrina Valetti [a,b], Federica Maione [c], Simona Mura [a], Barbara Stella [b], Didier Desmaële [a], Magali Noiray [a], Juliette Vergnaud [a], Christine Vauthier [a], Luigi Cattel [b], Enrico Giraudo [b,c], Patrick Couvreur [a]**

(Article submitted to *Biomaterials)*

[a] Université Paris-Sud, Faculté de Pharmacie, 5 rue Jean-Baptiste Clément, 92296 Châtenay-Malabry cedex, France
CNRS UMR 8612, Institut Galien Paris-Sud, 5 rue Jean-Baptiste Clément, 92296 Châtenay-Malabry cedex, France

[b] Dipartimento di Scienza e Tecnologia del Farmaco, Università di Torino, 9 via Pietro Giuria 10125 Torino, Italy

[c] Laboratory of Transgenic Mouse Models, Institute for Cancer Research at Candiolo (IRCC), Strada Provinciale 142, Km. 3.95 10060 Candiolo (Torino), Italy

*To whom correspondence should be addressed.
E-mail: patrick.couvreur@u-psud.fr
Tel: +33 1 46 83 53 96
Fax: +33 1 46 83 55 11

Abstract

Chemotherapy of pancreatic cancer is hampered by the tumor physio-pathological complexity. Here we show a targeted nanomedicine using a new ligand, the CKAAKN peptide, which had been identified by phage display, as efficient homing device within the pancreatic pathological microenvironment. Taking advantages from the squalenoylation platform, the CKAAKN peptide was conjugated to squalene (SQCKAAKN) and then co-nanoprecitated with the squalenoyl prodrug of gemcitabine (SQdFdC) giving a near monodisperse nanoparticles (NPs) for safe intravenous injection. By interacting with a novel target pathway, the Wnt-2, the CKAAKN functionalization enabled: (*i*) to specifically increase cell uptake and cytotoxicity in pancreatic cancer cells, saving healthy cells and (*ii*) to improve efficacy in impairing tumor growth, thanks to the activity on both cancer and tumor vasculature cells. All together, these results make this approach a first successful example of pancreatic cancer targeted nanosized materials with unique selectivity and multiple mechanism of action.

Keywords

Targeted nanoparticles, tumor-targeting peptide, squalene-based materials, pancreatic cancer, gemcitabine.

Introduction

Pancreatic cancer is a devastating disease which represents the fourth leading cause of cancer-related death in the European Community and in North America.[1] The median survival is less than 6 months and the maximum is 5 years for the 6% of patients.[2] Despite this high mortality, pancreatic cancer represents only the 10th most common cause of new cancers. This imbalance between frequency and mortality is because most patients are diagnosed at an unresectable, advanced and metastatic stage for which, at the moment, only palliative treatments are available, due to the lack of sensitivity of pancreatic cancer to many chemotherapeutic drugs.[2] Despite the decline over the past decade in the global mortality related to lung, colon, prostate and breast cancer, the progresses in pancreatic cancer therapy had remained exceedingly slow and disappointing without impairing the death rate. Since 1996, gemcitabine (dFdC), a nucleoside analogue that blocks the DNA replication, is the major chemotherapic agent for pancreatic cancer treatment.[2] Although its weak response rate of 5% and the modest overall survival benefit, this drug still remains the first-line treatment in the clinical practice. Several combined protocol therapies with gemcitabine have been tested in randomized clinical trials with no important outcomes.[3,4] Only erlotinib, an inhibitor of the epidermal growth factor and recently (September 2013) Abraxane (paclitaxel albumin-bound nanoparticles) have been approved by the FDA in combination with gemcitabine due to the small, but statistically significant improvement in patient survival and delay in tumor growth.[5,6] Due to its rather hydrophilic character, gemcitabine is unable to passively diffuse across the plasma membrane but it is transported into the cell, by either human equilibrative (hENT) or sodium-gradient nucleoside transporters. The resistance to gemcitabine treatment often arises from the down regulation of these nucleoside transporters which impairs gemcitabine membrane transport, as shown both in pre-clinical experimental models and in the clinic.[7] Gemcitabine is also rapidly inactivated into the blood, due to the fast metabolization by blood deaminases, into the inactive difluorouracil. Thus, frequent administration schedule at high drug dose (usually 800-1000 mg/m^2, 30 min infusion) is required. Additionally, the poor tumor tissue perfusion resulting from deprived vascularization, the formation of a dense stroma and the important heterogeneity of pancreatic cancer cells dramatically hampers drug efficacy and bioavailability in the tumor tissue, also leading to significant side effects.[8] Drug nanocarriers decorated with hydrophilic and flexible polymers, such as poly(ethylene glycol) (PEG), have been proposed to improve drug accumulation at the tumor target site through the so-called Enhanced Permeability and Retention (EPR) effect that takes advantages from the high irregular tumor vasculature with abnormal heterogeneous density, the large pores on the endothelial walls and the reduced lymphatic drainage in tumor tissue.[9,10] However, in the case of pancreatic cancer, such "passive" targeting is inefficient due to the presence of the above mentioned dense and poorly vascularized stroma. As a consequence of this physio-pathological complexity, the development of targeted therapeutic approaches, using nanosized materials able to specifically bind to receptors mainly expressed onto malignant cells and relatively down regulated in healthy ones [11] , represents an attractive therapeutic alternative.[12-14] To date, there are very few examples of drug-loaded nanoparticles functionalized with specific ligands showing a therapeutic efficacy in experimental pancreatic cancer models. For instance, nanocarriers were decorated with the epidermal growth factor (EGF) [15], the arginine-glycine-aspartic acid (RGD) peptide[16] or antibody towards the transferrin receptor.[17] However, apart from the fact that these nanodevices exhibited poor drug loading[16,17] and/or were constructed with non-biocompatible gold materials,[15] they were functionalized with homing devices not specific for pancreatic cancer since typically expressed also on several other types of healthy or cancer cells. This explains the inability of these materials to reach the pancreatic cancer tissue, even at a low concentration.[18] Therefore, the discovery of more specific ligands for pancreatic tumor targeting is urgently needed and represents an important challenge.

In this context, we have taken advantage of previous findings that, starting from a phage-displayed peptide library screening on mouse models of cancer, described peptides that selectively bind tumor vasculature.[19] The major advantage of this approach consists in the identification of novel peptide ligands, able to specifically interact with the target disease marker proteins, which are accessible *via* the systemic circulation within a definite pathological microenvironment. This represents a major concern in pancreatic cancer, in which many molecular targets are inaccessible due to the unique physio-pathological conditions explained before (that is, poor tumor vasculature and abundant extracellular matrix). In particular Joyce *et al.*[19] identified a linear peptide composed by 6 aminoacids (*i.e.* CKAAKN) which specifically bound tumor vessels in the RIP1-Tag2 transgenic mice, a prototypical mouse model of multistage pancreatic islet cell carcinoma.[19,20] Remarkably, the CKAAKN peptide was found capable of homing progenitor angiogenic cells, as well as pancreatic stroma and cancer cells.
Motivated by this finding, we have constructed a novel efficient targeted nanomedicine for pancreatic cancer treatment, using squalene, a natural and biocompatible lipid as carrier material[20], gemcitabine as anticancer drug and the CKAAKN peptide as homing device. After chemical modification, the squalene was conjugated to either gemcitabine (SQdFdC) or to CKAAKN peptide (SQCKAAKN).

Materials and Methods

Materials

1,1',2-Trisnor-squalenic aldehyde were obtained from squalene as previously described.[21] Gemcitabine hydrochloride (difluorodeoxycytidine (dFdC)) was purchased from Sequoia Research Products Ltd (UK). 4-(*N*)-trisnorsqualenoyl-gemcitabine (SQdFdC) was obtained as previously reported[21]. CKAAKN peptide was purchased from CASLO Laboratory Aps (Denmark). Squalene, dextrose and all other reagents were obtained by Sigma-Aldrich Chemical Co. (Italy). All solvents used were of analytical grade from Carlo Erba Reagenti (Italy) or VWR (France). The ^{1}H NMR and ^{13}C NMR spectra were recorded on Bruker Avance 300 (300 MHz, 75 MHz) or Bruker Avance 400 (400 MHz, 100 MHz) spectrometers in $CDCl_3$, CD_3COCD_3, CD_3OD or D_2O. Multiplicities of resonances are described as broad (b), singlet (s), doublet (d), triplet (t), or multiplet (m). Recognition of methyl, methylene, methine, and quaternary carbon nuclei in 13C NMR spectra rests on the J-modulated spin-echo sequence. Mass spectra were obtained using electrospray ionization (ESI) conditions in a positive-ion or a negative-ion mode either on Finnigan-MAT TSQ 700 spectrometer (CA) or Esquire LC Bruker spectrometers. All reactions involving air- or water-sensitive compounds were routinely conducted in glassware which was flame-dried under a positive pressure of nitrogen. The reactions were monitored by thin-layer chromatography (TLC) on F254 silica gel pre-coated plates; after development, the plates were viewed under UV light (254 nm) and visualized with I_2 or Kägi-Misher reagents. Flash-column chromatography was performed on CombiFlash® Rf systems (Teledyne ISCO, Italy) on appropriate columns (silica or RP18). All solvents were distilled prior to flash chromatography.

Synthesis and characterization of 6-(maleimidyl)-hexanoic acid (trisnor-squalenylidene)-hydrazide (9)

A solution of 1,1',2-trisnor-squalenic aldehyde **(8)** (0.334 g, 0.868 mmol) in CH_2Cl_2 was added to dry methanol (15 mL). The resulting mixture was sonicated few minutes until complete dissolution. [6-(maleimido)hexanamido]azanium trifluoroacetate (**7**)[22] (0.306 g, 0.868 mmol) and 4 Å molecular sieves (200 mg) were then added and the reaction mixture was stirred for 1 h at room temperature under nitrogen. The formation of the desired product **(9)** was monitored by TLC (petroleum ether/ethyl acetate 1/1 v/v, R_f: 0.65). The mixture was filtered and concentrated under reduced pressure. The residue was taken into water (5 mL) and was extracted with CH_2Cl_2 (3 x 15 mL). The combined organic phases were dried over anhydrous $MgSO_4$ and concentrated *in vacuo*. Purification by flash-chromatography on silica column eluting with a gradient of petroleum ether to petroleum ether/ethyl acetate 60/40 v/v gave the product as a light yellow waxy material (0.211 g, 63% yield).

^{1}H NMR ($CDCl_3$) δ: 8.39 (s, 1H, C*H*=NN), 7.05 (t, *J* = 5.2 Hz, 1H, N*H*CO), 6.68 (s, 2H, CO-C*H*=C*H*CO), 5.14-5.07 (m, 5H, *H*C=C(CH_3)), 3.54-3.49 (t, *J* = 7.2 Hz, 2H, CH_2N), 2.70-2.50 (m, 2H, CH_2CONH), 2.40-1.90 (m, 20H, =C(CH_3)CH_2CH_2), 1.80 (s, 3H, HC=C(CH_3)$_2$), 1.76-1.65 (m, 12H, HC=C(CH_3)CH_2), 1.62-1.60 (m, 4H, NCH_2CH_2CH_2CH_2CON), 1.41-1.33 (m, 2H, NCH_2CH_2CH_2CH_2CH_2CON). ^{13}C NMR ($CDCl_3$) δ: 171.2, 166.3, 147.3, 135.8, 135.7-132.0, 125.9-124.7, 42.5, 39.7-26.4, 38.2, 36.6, 31.0, 26.9, 25.9, 24.6-16.4, 22.4. MS (EI): *m/z(%)* 81 (70), 110 (100), 192 (55), 591 (3). HPLC analysis: Symmetry C18 column, 5 μm (Merck, Italy) equipped with a C18 column guard, elution with 100% methanol, detection

by UV adsorption measurement at 237 nm (flow rate 1 mL/min, t_r=5.79 min). Peak heights were recorded and processed on a CBM-10A Shimadzu interface.

Synthesis and characterization of the Michael adduct of CKAAKN and 6-(maleimidyl)-hexanoic acid (trisnor-squalenylidene)-hydrazide (SQ-CKAAKN, (5))

A mixture of **(9)** (13.5 mg, 0.0229 mmol) and CKAAKN peptide (**4**) (7.25 mg, 0.0114 mmol) in dimethylformamide DMF/H_2O 3/1 v/v (2 mL) was stirred for 3 h at 40 °C. The reaction mixture was then concentrated under reduced pressure and the crude product was taken into diethyl ether to remove unreacted maleimide. The supernatant was withdrawn after decantation (3 times). In order to eliminate unreacted peptide, the solid was dissolved in methanol and filtered through a sintered glass funnel. The product was obtained as a translucent waxy material (10 mg, 0.0082 mmol, 70% yield); MS (+ESI): *m/z* (%) = 1226.0 (100) $[MH]^+$, 614.5 (2) (Fig.1).

Preparation of nanoparticles (NPs)

SQdFdC and SQdFdC/SQCKAAKN nanoparticles were prepared by the nanoprecipitation technique.[23] Practically, for SQdFdC NPs, SQdFdC was dissolved in ethanol (40 mg/mL) and then added dropwise under magnetic stirring into 1 mL of MilliQ® water (ethanol/water 0.1/1 v/v). Formation of the nanoparticles occurred spontaneously without using any surfactant. After solvent evaporation under reduced pressure, an aqueous suspension of pure SQdFdC nanoparticles was obtained (final SQdFdC concentration 4 mg/mL). For SQdFdC/SQCKAAKN NPs the two compounds were dissolved in 0.1 mL of ethanol at 1:0.01 SQdFdC/SQCKAAKN molar ratio. The organic solution was then added dropwise under magnetic stirring into 1 mL of MilliQ® water (ethanol/water 0.1/1 v/v). After solvent evaporation under reduced pressure, an aqueous suspension of SQdFdC/SQCKAAKN NPs was obtained (final SQdFdC concentration: 3.4 mg/mL). For fluorescent NPs (unconjugated or linked to CKAAKN), 1% w/w of the hydrophobic green dye cholesteryl BODIPY FL C12 (BChol-green, Life Technologies, Molecular Probes, France) or the hydrophobic red dye cholesteryl BODIPY RED 542/563 C11 (BChol-red, Life Technologies, Molecular Probes, France) was added to the ethanolic solution. The nanoprecipitation occurred as described above. All the formulations were stored at room temperature.

Nanoparticle characterization

The mean particle size and polydispersity index of SQdFdC NPs and of SQdFdC/SQCKAAKN NPs were measured by dynamic light scattering (DLS) with a Nano ZS from Malvern (UK) (173° scattering angle) at 25 °C. The measurements were performed after dilution of the NPs suspensions to 1:25 in MilliQ® water. The NPs surface charge was investigated by zeta potential measurements at 25°C after dilution with 0.05 mM KCl solution or 0.02 M phosphate buffer at pH values ranging from 7.4 to 9.8, applying the Smoluchowski equation and using the same apparatus. Measurements were carried out in triplicate. The colloidal stability was investigated by measuring the nanoparticle mean diameter over a period of 72 hours (Supplement Fig. S1). The morphology of the nanoparticles was examined by cryogenic transmission electron microscopy (cryoTEM). Briefly, one drop (5 µL) of the nanoparticles suspensions (5 mg/mL) was deposited on a 200-mesh electron microscopy grid. Most of the drop was removed with a blotting filter paper and the residual thin film remaining within the holes was vitrified by plunging into liquid ethane. The specimen was then transferred using liquid nitrogen to a cryo-specimen holder and observed using a JEOL 2100HC microscope.

Surface plasmon resonance analysis

Interaction analyses were performed on a BIAcore T100 instrument including CM5 Series S sensor chip (GE Healthcare Life Sciences Europe, France). All experiments were carried out at 25 °C in Dulbecco-PBS (D-PBS) running buffer. The immobilization process was performed with 150 mM phosphate buffer, pH 7.4 at a flow rate of 10 µL/min. The carboxymethylated dextran matrix was activated for 7 min with a mixture 1:1 *N*-ethyl-*N*'-(3-diethylaminopropyl)-carbodiimide (EDC) 0.1 M/ *N*-hydroxysuccinimide (NHS) 0.4M (GE Healthcare Life Sciences Europe, France). The sFRP-4 receptor was then injected over the activated surface at 10 µg/mL in 10 mM sodium acetate buffer at pH 4.4 during 7 min, giving an average immobilization level of 2800 resonance units (RU). Unreacted sites of the matrix were finally blocked by a 7-min injection of 1 M ethanolamine hydrochloride at pH 8.5. For reference, additional blank flow channel was prepared according to the same process without injecting the receptor over the surface. Binding capacities of the functional surfaces were tested with 180 s injections of CKAAKN peptide solution, nanoparticles or nanoparticles functionalized with the CKAAKN peptide at different concentrations. All experiments were carried out in duplicate on the IPSIT platform (Châtenay-Malabry, France).

Evaluation of the activation of C3 protein of the complement system

The activation of the complement system (highlighted by the conversion of plasmatic C3 protein into C3b and C3a fragments) induced by the different nanoparticles was evaluated by 2-D immunoelectrophoresis using a polyclonal antibody to human C3.[24] Human serum was obtained after calcifying plasma from healthy donors (EFS Ile-de-France, France) and stored at −80 °C until use. Veronal-buffered saline (VBS) containing 0.15 mM Ca^{2+} and 0.5 mM Mg^{2+} ions (VBS^{2+}) and VBS containing 40 mM ethylenediaminetetraacetic acid (VBS–EDTA) were prepared as described by Kazatchkine *et al.*[25] Complement C3 antiserum rose in goat was purchased from Sigma-Aldrich (France). To ensure a valid comparison of the different nanoparticles, each sample was concentrated up to 6 mg/mL to obtain a sufficient specific surface ($S_{specif} = 6$ m/Dd, where m is the mass contained in the sample, D is the average diameter and d is the density). 100 µL of nanoparticles (corresponding to an equivalent surface area of 167 cm^2) were incubated under gentle agitation for 1 h at 37 °C with 50 µL of human serum and 50 µL of VBS^{2+}. 100 µL of water were used as control of spontaneous activation of C3 protein and 100 µL of redox radical emulsion polymerization (RREP) dextran (0.5%)-coated poly(isobutylcyanoacrylate) (PIBCA) nanoparticles[26] were used as positive control in the experimental conditions used (Supplement Fig. S2). All experiments were performed with the same human serum whose functionality was tested before use (Supplement Fig. S2). After incubation, 7 µL of each sample were subjected to a first electrophoresis (600 V, 16 mA, 100 W, 70 min) on 1% agarose gel in tricine buffer, then the 2-D electrophoresis (500 V, 12 mA, 100 W, 18 h) was carried out on Gelbond® film coated with agarose gel containing a polyclonal antibody to human C3 at 0.1 mg/mL for detection of native and activated form of C3. Films were fixed in 0.15 M NaCl, further dried and stained with coomassie blue to reveal the presence of native C3, and lower molecular weight activated fragments C3a and C3b precipitated with the antibody. Activation of the C3 protein was expressed as the complement activation factor (CAF) defined as the ratio of the peak surface of C3a+C3b detected on the plate over the sum of the peaks surface of C3 and C3a+b. For the nanoparticles the CAF was then normalized (CAF_n) on a scale ranging from 0 to 100 in which 100 indicated total activation and 0 the spontaneous activation measured in absence of nanoparticles. Areas under the peaks were measured using ImageJ® software. All experiments were set up in triplicate or more to determine mean and SD.

Cell culture

Human pancreatic carcinoma cell lines MIA PaCa-2, BxPC3, PANC-1, breast cancer cell line MCF-7 and embryonic murine fibroblasts NIH/3T3 were obtained from the American Type Culture Collection (France) and maintained as recommended. Briefly, MIA PaCa-2, PANC-1, MCF-7 and NIH/3T3 cells were grown in Dulbecco's Modified Eagle Medium (DMEM) supplemented with 10% heat-inactivated (56 °C, 30 min) fetal bovine serum (FBS). In addition, MIA Paca-2 cells medium was supplemented with 2.5% heat-inactivated horse serum (Gibco, France). BxPC3 cells were maintained in Roswell Park Memorial Institute medium (RPMI 1640 Lonza, Belgium) supplemented with 10% heat-inactivated FBS. All media were further supplemented with 50 $U.mL^{-1}$ penicillin and 50 $U.mL^{-1}$ streptomycin (Lonza, France). Cells were maintained in a humid atmosphere at 37 °C with 5% CO_2. Cells were used between passage 3 and 12 after thawing.

Western Blot

Pancreatic adenocarcinoma (BxPC3, MIA PaCa-2, PANC-1), breast cancer (MCF-7) and embryonic fibroblast cells (NIH/3T3) were lysed in RIPA Buffer (Sigma-Aldrich, France) supplemented with Pierce™ phosphatase and protease inhibitor cocktail (Thermo Fisher Scientific, Perbio Science, France), vortexed and then centrifuged 5 min at 3000 g. The protein concentration in the supernatant was then measured using a colorimetric assay (Bio-Rad Protein Assay Dye, Bio-Rad Laboratories, France). Equal amount of proteins (30 µg) were boiled for 10 min with the same volume of Laemmli Sample Buffer supplemented with 5% beta-mercaptoethanol (Bio-Rad Laboratories, France) separated in sodium dodecylsulphate (SDS)-polyacrylamide gels (Mini-Protean - TGX 4-15% - Precast Gels BIO-RAD) and electrically transferred to PVDF membrane using a semi-dry transfer system (20 V, 1 h). The membrane was blocked with 5% dry milk suspension in 0.1% Tween 20 in PBS (blocking buffer), then incubated for 2 h at room temperature with the primary antibody solution in blocking buffer and, after 30 min washing in PBS-Tween 20 0.1%, incubated for 1 h at room temperature with the secondary antibody solution in blocking buffer. Antibodies were used at the following dilutions: polyclonal rabbit anti-FZD-5 diluted 1/1000 (Millipore, France), mouse anti-β-actin diluted 1/3000 (Sigma-Aldrich, France), goat anti-mouse secondary antibody conjugated to horse radish-peroxydase diluted 1/2000 (SantaCruz Biotechnology, Clinisciences, France) and goat anti-rabbit secondary antibody conjugated to horse radish-peroxydase diluted 1/5000 (SantaCruz Biotechnology, Clinisciences, France). Detection of chemiluminescence was performed using the Clarity™ Western ECL substrate (Bio-Rad Laboratories, France) and images were captured by the ChemiBIS system from DNR Bioimaging Systems. MCF-7 cell line was used as a positive control.[27]

Confocal laser scanning microscopy

Observations were made by sequential acquisition with a Zeiss LSM-510 confocal laser microscope equipped with a 1 mW argon laser and 1 mW helium neon laser, using a Plan-Apochromat 20X or 63X objective lens (NA 1.40, oil immersion). Green fluorescence (CMFDA) was observed with a band-pass 505 and 550 nm emission filter and under a 488 nm laser illumination. Red fluorescence (BChol-red) was observed with a long-pass 560 nm emission filter and under a 543 nm laser illumination. The pinhole diameter was set at 98 µm for CMFDA and 106 µm for BChol-red and an optical section thickness of 0.4 µm was fixed. Twelve bit numerical images were acquired with Carlo Zeiss ZEN 2011 software version 7.1.

Cytotoxicity studies

The *in vitro* cytotoxicity of NPs was investigated on MIA PaCA-2 and NIH/3T3 cell lines through the determination of the mitochondrial activity, using the 3-(4,5-dimethylthiazol-2-yl)-2,5-diphenyl tetrazolium bromide test (MTT, Sigma-Aldrich). Briefly, cells were seeded in 100 µL of growth medium (MIA PaCa-2 (1 x 10^4 cells/mL), NIH/3T3 (0.75 x 10^4 cells/mL)) in 96-well plates and preincubated for 24 h. Cells were then treated with 100 µL of the different nanoparticle suspensions for 72 h. Before, the colloidal stability of the nanoparticle in the cell culture medium was investigated by measuring mean diameter (Supplement Fig. S1). Initial cell density and incubation time were determined to allow cells to remain in exponential growth and to undergo two cell-doubling times during the assay. At the end of the incubation period 20 µL of a 5 mg/mL MTT solution in phosphate buffered saline were added to each well. After 1 h of incubation, the culture medium was removed and replaced by 200 µL of dimethyl sulfoxide (DMSO), in order to dissolve the formazan crystals. The absorbance of the solubilized dye was measured spectrophotometrically with a microplate reader (LAB System Original Multiscan MS) at 570 nm. The percentage of viable cells for each treatment was calculated from the ratio of the absorbance of the well containing the treated cells *versus* the average absorbance of the control wells (i.e., untreated cells). All experiments were set up in triplicate.

Cell-internalization of NPs

MIA PaCa-2 and NIH/3T3 cells (5 x 10^4 cells/mL) were cultured in 12-well plates for 24 h to achieve approximately 40% confluence. Cells were then incubated at 37 °C with 5% CO_2 for 6 h with 1 µM of fresh dispersion of either BChol-green-labeled SQdFdC NPs or SQdFdC/SQCKAAKN NPs. Free fluorophore was used as control. After treatment supernatants were discarded, cells rinsed twice with PBS and harvested for measurement. Cell suspensions were analyzed by flow cytometry (Accuri C6, BD Biosciences, France) and mean fluorescence intensities were collected between 515 and 545 nm, using the 488-nm line of an argon laser for excitation. For all experiments 10000 cells were measured from each sample.
For low temperature experiments, the cells were incubated in the cold room at 4 °C for 5 h. Results were expressed as the ratio of the mean fluorescence intensity of each sample to the mean fluorescence intensity of non-treated cells. This value was then corrected by the fluorescence factor of each NP suspension. All measurements were performed in triplicate or more to determine mean and SD.

Coculture

NIH/3T3 fibroblasts (7.5 x 10^4 cells) were plated onto microscopic glass slides and incubated for 18 h at 37°C with 5% CO_2 in complete medium. To visualize and distinguish between NIH/3T3 fibroblasts and MIA PaCa-2 cells in coculture, NIH/3T3 cells were stained with 5 µM CellTracker green 5-chloromethylfluorescein diacetate (CMFDA, Life Technology, Molecular Probes) according to the manufacturer's protocol. After staining, cells were left to rest for 2 h at 37 °C with 5% CO_2 in cell culture medium, and then unstained MIA PaCa-2 cells (15 x 10^4 cells) were co-incubated. The seeding ratio between MIA PaCa-2 and NIH/3T3 cells was 2:1 due to the faster doubling time of the latter. After 18 h, the coculture was incubated with BChol-red-labeled SQdFdC NPs and BChol-red-labeled SQdFdC/SQCKAAKN NPs diluted in fresh cell culture medium at 10 µM. At different time points (2, 6, and 24 h) nanoparticles were withdrawn and cells washed with pre-warmed culture medium before imaging. Free fluorophore was used as control.

Transgenic tumor model

The RIP-Tag2 transgenic mouse model has been previously reported.[28] Transgenic mice were generated by backcrossing transgenic males with C57Bl/6 females (Jackson Laboratory, USA). All animal procedures were approved by the Ethical Commission of the University of Turin and by the Italian Ministry of Health in compliance with the international laws and policies.

In vivo: therapeutic efficacy

Tumor-bearing RIP-Tag2 mice were treated for two weeks, starting from 12 until 14 weeks of age. Mice were randomized and assigned to 4 groups of 8 mice each and all groups received four intravenous injections in the lateral tail vein on days 0, 3, 7 and 11 with either (*i*) 15 mg/Kg dFdC; (*ii*) SQdFdC NPs at dFdC equivalent dose of 15 mg/kg; (*iii*) SQdFdC/SQCKAAKN NPs at dFdC equivalent dose of 15 mg/kg or (*iv*) saline control solution. In order to obtain 5% w/w isosmotic solution, dextrose was added to the nanoparticle suspensions and their colloidal stability was investigated by measuring mean diameter (Supplement Fig. S1). Mice were monitored regularly for changes in weight and health status. Mice were humanely sacrificed on day 12. A pre-treatment with 5mg/kg of dexamethasone (Decadron®, CABER S.p.A., Italy) was performed by intramuscular injection 4 h before the treatment. None toxicity of nanoparticles or gemcitabine was observed at the doses tested.

Tissue preparation and histology

Tumor tissues were fresh frozen in Optimum Cutting Temperature (O.C.T. Tissue Tek) and cut in 10 µm thick sections using a Leica CM1900 cryostat. Sections were air-dried, fixed in zinc fixative (6.05 g Tris, 0.35 g Ca $(C_2H_3O_2)_2$, 2.5 g Zn $(C_2H_3O_2)_2$, 2.5 g ZnCl, 3.8 mLHCl 37%) for 10 min and they were blocked with 1% bovine serum albumin and 5% serum (donkey serum) in PBS. Tissues were then subjected to immunostaining with the following appropriate primary antibodies: purified rat monoclonal anti-Panendothelial cell antigen (Meca32) (clone Meca32, BD Pharmingen, USA), diluted 1/100; rabbit polyclonal anti-α-SMA (Abcam, UK), diluted 1/100; rabbit monoclonal anti-cleaved caspase-3[29] (asp175, clone 5A1, Cell Signaling, USA), diluted 1/50 or rabbit polyclonal anti-Frizzled 5 (Abcam, UK) diluted 1/100. The secondary antibodies used were: anti-rabbit Alexa Fluor®488 or Alexa Fluor®555 and anti-rat Alexa Fluor®488 or Alexa Fluor®555 (1/400, Molecular Probes, USA). Nuclei were counterstained with DAPI (Invitrogen, USA). All immunofluorescence images were captured by using a Leica TCS SP2 AOBS confocal laser-scanning microscope (Leica Microsystems) maintaining the same laser power, gain and offset settings. All immune-localization experiments were performed on multiple tissue sections and included negative controls for determination of background staining, which was negligible.

Confocal microscopy quantifications

Quantifications of tumor vasculature were performed with MacBiophotonics ImageJ. The total area occupied by vessels was quantified as percentage of Meca32 positive staining on the tumor tissue area. For each animal, the total vessel area of 5 fields/mouse was quantified. To quantify pericyte coverage (α-SMA, red channel) in each image, a region of interest (ROI) close to each blood vessel (Meca32, green channel) was drawn and then the mean fluorescence intensity (MFI) of red and green channels was quantified using the Leica Confocal Software Histogram Quantification Tool. The ratio between red and green channel MFI was then calculated; values

were expressed as percentage of red-green co-staining. To determine the expression levels of caspase-3 (red channel), in each analyzed image the number of cleaved caspase-3 positive cells on the total number of cells present in the tissue area was measured.

Immunohistochemistry analysis

Frozen tumor sections were processed as previously described in the above "Tissue preparation and histology" section. Then, slides were permeabilized in 0.1% PBS, treated for 30 min with 3% hydrogen peroxide (Sigma-Aldrich, Italy) to quench endogenous peroxidases and saturated with protein block serum-free (Dako, Denmark). Tissues were stained with the rabbit polyclonal anti-Ki67 (Abcam, UK) primary antibody, diluted 1:100. Anti-rabbit horse radish-peroxydase-conjugate secondary antibody (EnVision; DakoCytomation, Denmark) was used, and the reaction was visualized with the AEC kit (DakoCytomation). Tissues were counterstained with Mayer hematoxylin (Vector Laboratories), mounted on glass slides, and visualized with a BX-60 microscope (Olympus) equipped with a color Qicam Fast 1394-digital CCD camera (12 bit; QImaging). The number of proliferating cells was evaluated by using ImageJ and considering 5 different fields/mouse. Values are presented as percent of Ki67 positive cells on total cell number.

Statistical analysis

The results of all experiments are expressed as mean ± SD. Statistical analyses were performed using a 2-tailed, unpaired Mann-Whitney U test. A p value below 0.05 was considered significant.

Results and discussion

Design and characterization of CKAAKN-functionalized nanoparticles

SQdFdC **(3)** was synthesized as reported elsewhere[21] by acylation of the C-4 nitrogen atom of the cytosine nucleus with 1,1',2- trisnor-squalenic acid **(2)** prepared from squalene (Fig. 1).

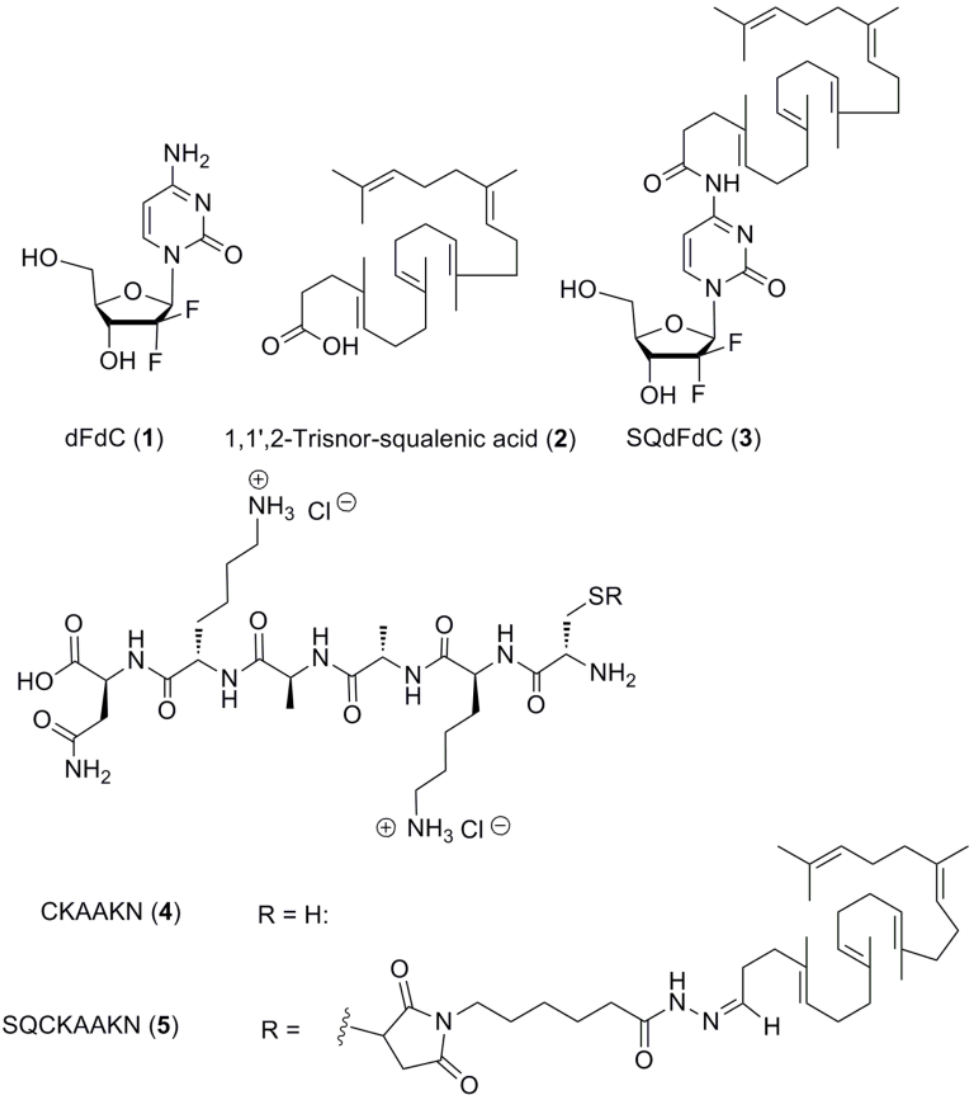

Fig. 1 | Squalenoyl derivatives. Structure of dFdC **(1),** CKAAKN peptide **(4)** and their squalenoyl conjugates SQdFdC **(3)** and SQCKAAKN **(5)**.

The obtained amphiphilic bioconjugate is able to spontaneously self-assemble in water into nanoparticles (NPs).[21] The thiol group of the N-terminal cysteine of the CKAAKN peptide **(4)** enabled the conjugation of the peptide to squalene, previously modified by the introduction of a 6 carbon atoms lipophilic chain with a maleimide terminal group, which allowed to establish a hydrolysable bond with the squalene moiety and a relatively stable thioether bond with the peptide **(5)**. In spite of the difficulty to allow the highly hydrophilic peptide to react with the lipophilic squalene derivative, the thiol-maleimide Michael-type addition allowed to obtain the desired conjugate with a satisfactory 70% yield (Supplement Fig. S3). Thanks to their similar squalenoyl moiety, the simple addition of an ethanolic solution of the two materials (that is,

SQdFdC/SQCKAAKN in 1/0.01 molar ratio) to water led to the spontaneous formation of nanoparticles without requiring any surfactant (ethanol/water 0.1/1 v/v). The obtained nanoparticle suspension was characterized by a high drug loading (40%) and a narrow size distribution (average diameter of 130-170 nm with polydispersity index of 0.1) as confirmed by dynamic light scattering (DLS) and Cryo-transmission electron microscopy (Fig. 2a,c).
Interestengly, the higher zeta potential value of SQdFdC/SQCKAAKN NPs, as compared with SQdFdC NPs (ZP average of -6 mV *vs* -22 mV), probably relies to the protonation of the lysine amino groups present in the CKAAKN structure, suggesting the presence of the peptide onto the nanoparticle surface which is a crucial aspect to obtain an efficient cancer cell targeting.

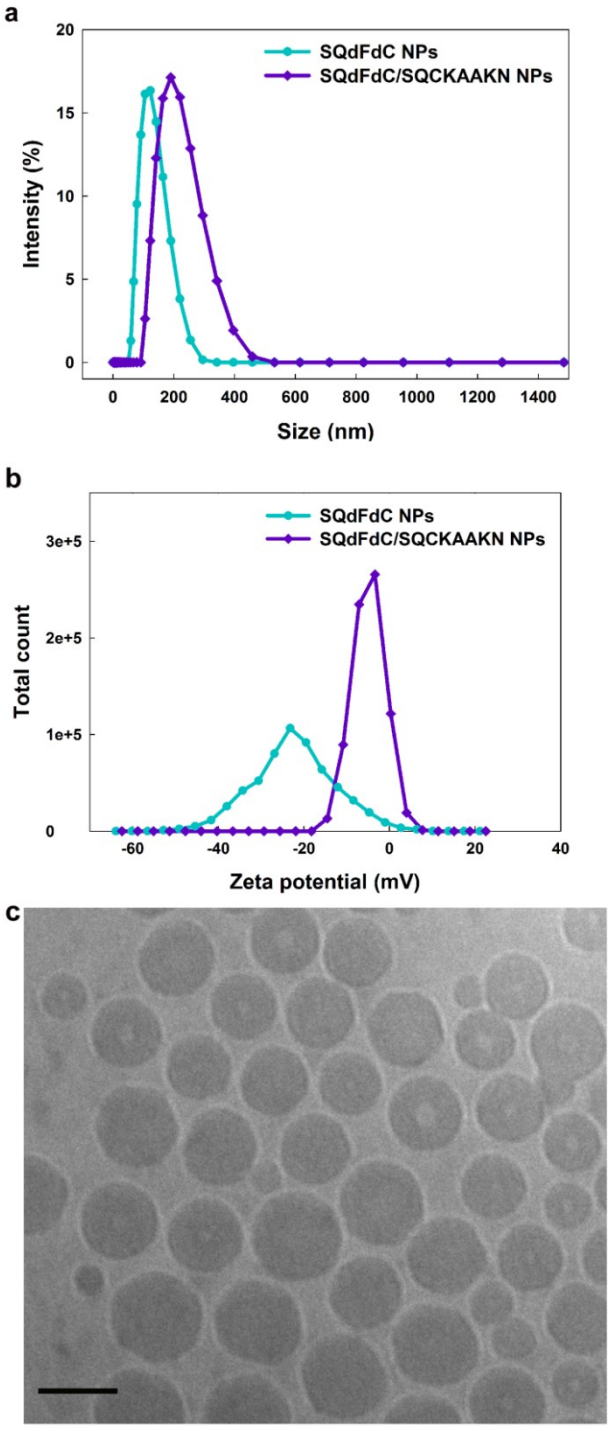

Fig. 2 | Characterization of SQdFdC and SQdFdC/SQCKAAKN NPs. Dynamic light scattering (DLS) data giving **(a)** the average diameter in intensity and **(b)** the zeta potential (ZP)

of SQdFdC and SQdFdC/SQCKAAKN NPs. **(c)** Cryogenic transmission electron microscopy of SQdFdC/SQCKAAKN NPs. Scale bar: 100 nm.

Ligand-receptor interaction

In order to further confirm the surface localization of the CKAAKN peptide and to evaluate its targeting ability, the ligand-receptor binding of the peptide was investigated. Since it was reported by Joyce *et al*[19], that the sequence CKA-K shared motifs with the Wnt-2 protein, we tested if CKAAKN could act as Wnt-2 mimetic interacting with the Frizzled (FZD) receptors by surface plasmon resonance (SPR). Among the FZD family, we focused our attention on the FZD-5 because it has been correlated with the development of vascular abnormalities and angiogenesis processes.[30,31] Since the receptor immobilization on the SPR biosensor could altered its conformation affecting the ligand binding, we chose to use the sFRP-4, a secreted frizzled-related protein with high FZD-5 sequence alignment (BLAST analysis) that was already successfully used to this aim keeping its recognition ability. [32]
Interestingly, the CKAAKN peptide was able to specifically interact with the sensorchip-immobilized sFRP-4 confirming the correlation indicated previously (Supplement Fig. S4).[19] Remarkably, a more important plasmonic signal was obtained with SQdFdC/SQCKAAKN NPs, whereas no signal was observed under identical experimental conditions with non-functionalized SQdFdC NPs (Fig. 3).
Moreover, SQdFdC/SQCKAAKN NPs showed a concentration-dependent sensorgram profile (Supplement Fig. S5). The more important ligand-receptor interaction observed with CKAAKN-functionalized nanoparticles, as compared with the free peptide, demonstrate that the affinity of phage-display-derivates peptides can be significantly enhanced thanks to the multivalent interactions offered by a scaffold-like nanosized material in concordance with previous observations.[33, 34]

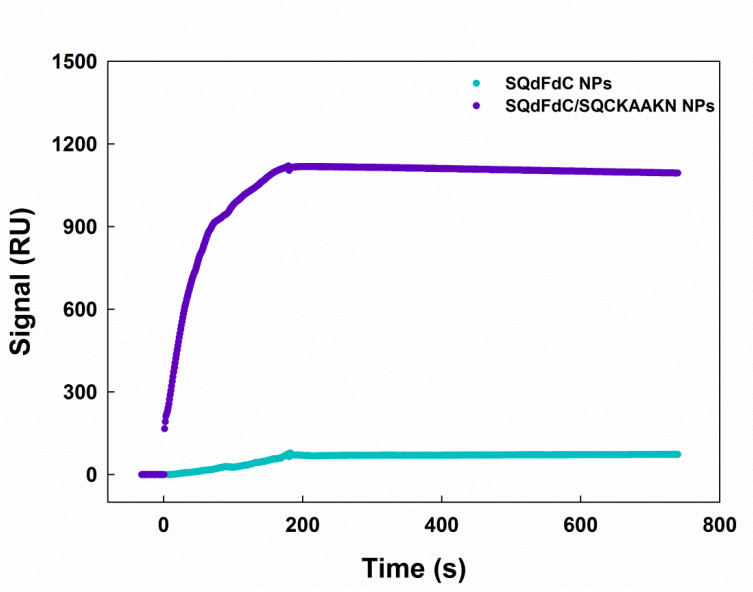

Fig. 3 | Surface plasmon resonance analysis of SQdFdC and SQdFdC/SQCKAAKN NPs. SPR sensorgrams (resonance units (RU) *versus* time) obtained by simultaneous injection of SQdFdC and SQdFdC/SQCKAAKN NPs (180 µM eq SQ) over sFRP-4 immobilized on two parallel channels of the same sensor chip.

Despite peptides present several advantages in comparison to other targeting homing devices (i.e., easy of synthesis and low immunogenicity), they usually possess modest target affinity. Indeed, the conjugation of multiple copies of targeting ligand onto the nanocarrier surface, allows overcoming this limitation by enabling multivalent interaction with high binding constants and improving targeting efficacy.[33] These results allowed identifying the biological target of the CKAAKN peptide confirming also its surface localization. The Wnt-2 belongs to a family of secreted lipid-modified signaling glycoproteins principally involved in embryonic development and tissue homeostasis.[35] Wnt-signaling pathway has been shown to regulate also the pancreatic β-cell endocrine function[36], proliferation, migration and differentiation.[30] Moreover, its overexpression in pancreatic tissue has been recently correlated to tumorigenesis, driving the self-renewal and differentiation of cancer stem cells and promoting the angiogenesis process.[11,35,37-39] On the basis of these observations, CKAAKN peptide, a specific Wnt-2 mimetic, may be considered as a novel promising homing device to tailor targeted nanosized material towards pancreatic cancer cells.

Targeting of cancer cells by CKAAKN-functionalized NPs.

The targeting ability of SQdFdC/SQCKAAKN NPs was investigated in cell cultures, using healthy and pancreatic tumor cells. Western blot analysis on several cell lines allowed identifying the NIH/3T3 (fibroblast cell line) and the MIA PaCa-2 (pancreatic tumor cell line) as low and high FZD-5 expressing cells, respectively (Supplement Fig. S6). Cytotoxicity studies clearly demonstrated that peptide functionalization of nanoparticles specifically increased toxicity toward pancreatic cancer cells MIA PaCa-2 (Supplement Fig. S7). For instance, exposure of these cells to 30 nM (eq. dFdC) SQdFdC/SQCKAAKN NPs maintained more than 93% of viable healthy NIH/3T3 cells but led to a reduction of malignant MIA PaCa-2 cells viability to 55%, as compared with non-treated cells (Fig. 4a). Of note, SQdFdC non functionalized NPs were not efficient in killing cancer cells and 100% cell viability was still observed after incubation at the same concentration (30 nM eq. dFdC). The cell internalization of peptide-functionalized and non-functionalized nanoparticles was further investigated by flow cytometry using green fluorescently-labeled nanoparticles. After 6 h, incubation with MIA Paca-2 cells, the cell capture of SQdFdC/SQCKAAKN NPs was found 14–fold higher than the one of SQdFdC NPs. Moreover, the peptide-functionalization caused a 6-fold decrease of nanoparticles uptake by healthy NIH/3T3 cells (Fig. 4b). These results suggest that both types of NPs were internalized *via* an energy-dependent process but using different pathways (Supplement Fig. S8). Non functionalized NPs were taken-up by both cell lines in a non-specific manner, resulting in higher accumulation in NIH/3T3 fibroblasts. On the contrary, SQdFdC/SQCKAAKN NPs were internalized in the cells by a receptor-mediated mechanism, allowing to achieve highly selective tumor cell uptake, while decreasing non-specific accumulation into healthy cells. The selective capture of SQdFdC/SQCKAAKN NPs by cancer cells was further confirmed in a coculture experiment of healthy NIH/3T3 cells (stained in green) and MIA PaCa-2 cells (unstained) incubated with red fluorescently-labeled nanoparticles (Fig. 4c,d). Confocal images clearly showed similar uptake of non-functionalized NPs in both tumor and normal cells (Fig. 4c), whereas SQdFdC/SQCKAAKN NPs were selectively captured by tumor cells while healthy cells were saved from nanoparticles recognition (Fig. 4d).

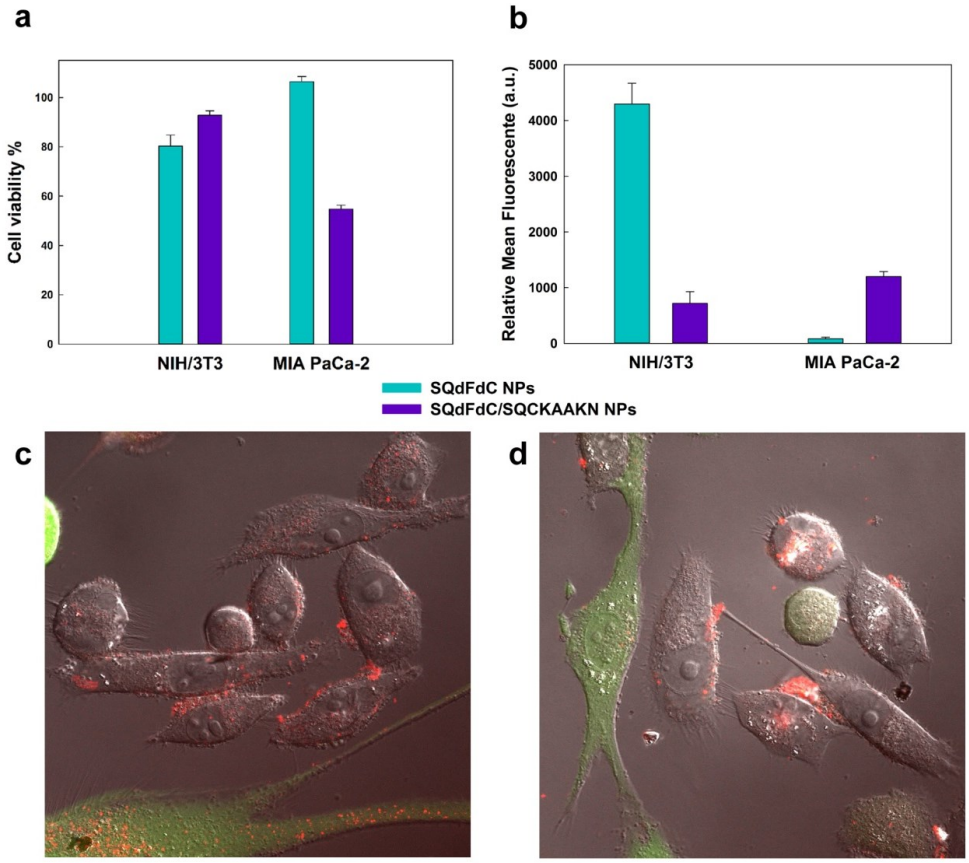

Fig. 4 | Targeting of pancreatic cells. (a) Viability of MIA Paca-2 and NIH/3T3 cells treated for 72 h with SQdFdC NPs and SQdFdC/SQCKAAKN NPs at same concentration in squalenoyl prodrugs (30 nM eq. dFdC). **(b)** Quantification of cellular uptake of BChol-green-labeled SQdFdC NPs and BChol-green-labeled SQdFdC/SQCKAAKN NPs in NIH/3T3 and MIA PaCa-2 cells at 37°C. **(c)** 3D reconstruction images obtained from confocal z scans of a coculture of NIH/3T3 (green) and MIA PaCa-2 cells (unstained) after incubation with BChol-red-labeled SQdFdC NPs and **(d)** BChol-red-labeled SQdFdC/SQCKAAKN NPs. Values represent mean ± SEM. Scale bars = 20 μm.

Antitumor efficacy of CKAAKN-functionalized NPs in RIP-Tag2 mice

Taken together, these results clearly demonstrated the potential of CKAAKN-functionalized squalene-based materials to specifically target pancreatic cancer cells. However, it has been reported that high ligand density at the nanoparticle surface may promote idiosyncratic reactions based on complement activation and lead to a pseudo-allergic reaction (CARPA effect), which is responsible for thrombocytopenia, cardiopulmonary and hemodynamic changes that could conduce to death.[40-42] Therefore, SQdFdC/SQCKAAKN NPs and SQdFdC NPs were investigated for their ability of activating the complement C3 component, a key player in the activation of complement system.[43] It was observed that both types of NPs were very weak activators of the complement C3 component in human serum. Non-functionalized and CKAAKN-functionalized nanoparticles displayed, indeed, normalized Complement Activating Factor (CAF_n) values of 10 ± 2.1% and 10 ± 2.8%, respectively (Fig. 5), thus supplement the hypothesis of a safe intravenous administration.

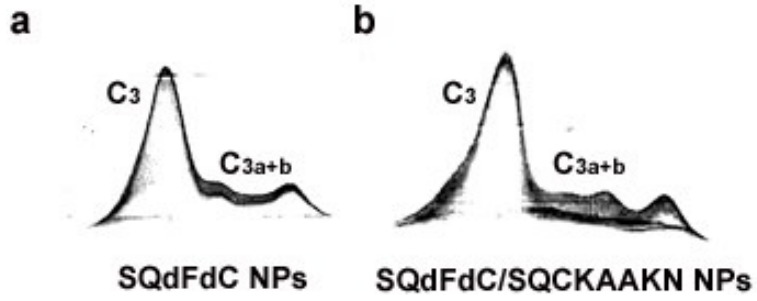

Fig. 5 | Activation of C3 protein of the complement system. 2D electroimmunophoretic profile of complement activation for **(a)** SQdFdC NPs and **(b)** SQdFdC/SQCKAAKN NPs.

In the light of the promising results, we performed a regression trial *in vivo* to assess if SQdFdC/SQCKAAKN NPs were more efficient than SQdFdC NPs or dFdC in blocking tumor growth and angiogenic process on RIP-Tag2 mice, which were previously used for the phage-display screening.[19] RIP-Tag2 mice offer the advantage of both a spontaneous tumor development through multistage tumorigenesis and a well-documented angiogenic switching, in parallel to cancer progression. This well-characterized mouse model represent a suitable and highly reproducible platform to perform pre-clinical trials to test the effects of compounds in regressing tumor growth and in impairing angiogenesis.[28,44-48] In this work we use RIP-Tag2 mice as proof-of-concept model to assess the ability of SQdFdC/SQCKAAKN NPs to regressed the growth of established cancers and, at the same time, to inhibit tumor angiogenesis.
Twelve week-old tumor-bearing RIP-Tag2 mice were injected intravenously (days 0, 3, 7 and 11) with either dFdC (15 mg/Kg), SQdFdC NPs (15 mg/Kg equiv. dFdC) or SQdFdC/SQCKAAKN NPs (15 mg/Kg equiv. dFdC) and compared with saline-treated control mice. All treatments induced a significant reduction of the tumor volume compared with saline treated controls. SQdFdC NPs reduced tumor burden by 32% compared with dFdC, confirming the superior activity of squalenoyl gemcitabine nanoparticles, already demonstrated in other animal tumor models.[49-51] Interestingly, SQdFdC/SQCKAAKN NPs displayed a greater efficacy in impairing tumor growth compared with SQdFdC NPs (by 40%) and with dFdC (by 60 %) (Fig. 6a).

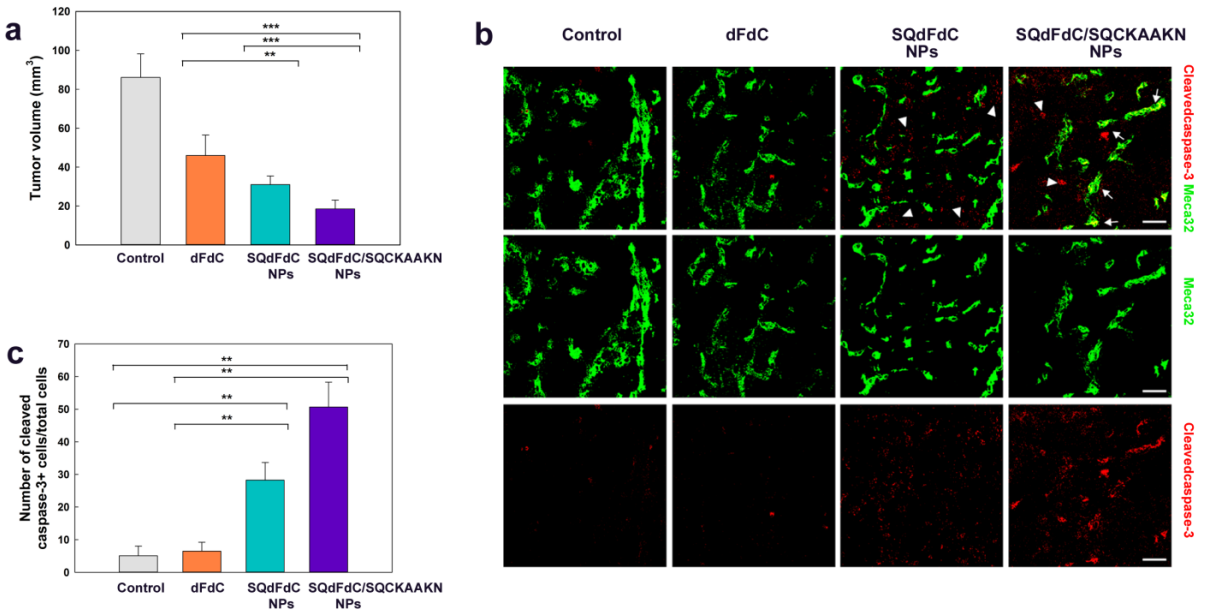

Fig. 6 | Anti-tumor activity and apoptotic index. (a) Total tumor volume in a 4-weeks regression trial in RIP-Tag2 mice. Mice were injected intravenously (days 0, 3, 7 and 11) with either dFdC (15 mg/Kg), SQdFdC NPs (15 mg/Kg equiv. dFdC) or SQdFdC/SQCKAAKN NPs (15 mg/Kg equiv. dFdC) (n=8/group). Values represent mean ± SD. Statistical difference is marked by $^{**}p < 0.01$; $^{***}p < 0.001$). **(b)** Confocal analysis of five fields per mouse from each treatment group immunostained with Meca32 (green) and cleaved caspase-3 (red). Apoptotic cancer cells are indicated with arrow heads and tumor vessels with arrows. Endothelial cells apoptotic rate was detected by colocalization of Meca32 (green) with activated caspase-3 (red). Scale bars: 50 µm. **(c)** Apoptotic index of cleaved caspase-3+ cells on total cells. Values represent mean ± SD. Statistical difference is marked by $^{**}p < 0.01$.

The mechanism underlying the observed anticancer activity of CKAAKN-functionalized NPs was further investigated by assessing the proliferation and apoptosis indexes. Despite the fact that a significant reduction of cancer cell proliferation (anti-Ki67 Ab immune-staining) was observed in all treated groups compared with control (Supplement Fig. S9), the apoptotic rate (anti activated caspase-3 immune-staining) was specifically increased in both nanoparticles-treated groups compared with dFdC and saline-treated ones (Fig. 6b,c). Treatment with NPs increased the apoptotic cell number in tumors by 82% compared with both dFdC and control groups. Remarkably, the treatment with SQdFdC/SQCKAAKN NPs induced a statistically significant increase (by 44%) in active caspase-3 immunostaining, compared with their non functionalized counterpart NPs (Fig. 6c). Noteworthy is that the dramatic increase of apoptosis observed in SQdFdC/SQCKAAKN NPs group was detected not only in cancer cells but also in the tumor blood vessels (Fig. 6b) suggesting that the tumor regression observed with CKAAKN-functionalized nanosized materials resulted from dual activity on both cancer cells and tumor vasculature. To consolidate this hypothesis we further investigated in a more detailed manner the vasculature of the tumors derived from the different treated groups.

By immunostaining with Meca-32 antibody and confocal analysis, it was observed that SQdFdC/SQCKAAKN NPs dramatically reduced the vessel area by 58%, 55% and 57% compared with control, dFdC and non functionalized NPs, respectively (Fig. 7a,b). Along the same line, quantification of α-smooth muscle actin (α-SMA) localized in close proximity to endothelial cells-lined blood vessels revealed also an important increase in SQdFdC/SQCKAAKN NPs-treated animals comparatively with SQdFdC NPs, dFdC and saline treated ones (by 47%, 49% and 45%, respectively) (Fig. 7c,d).

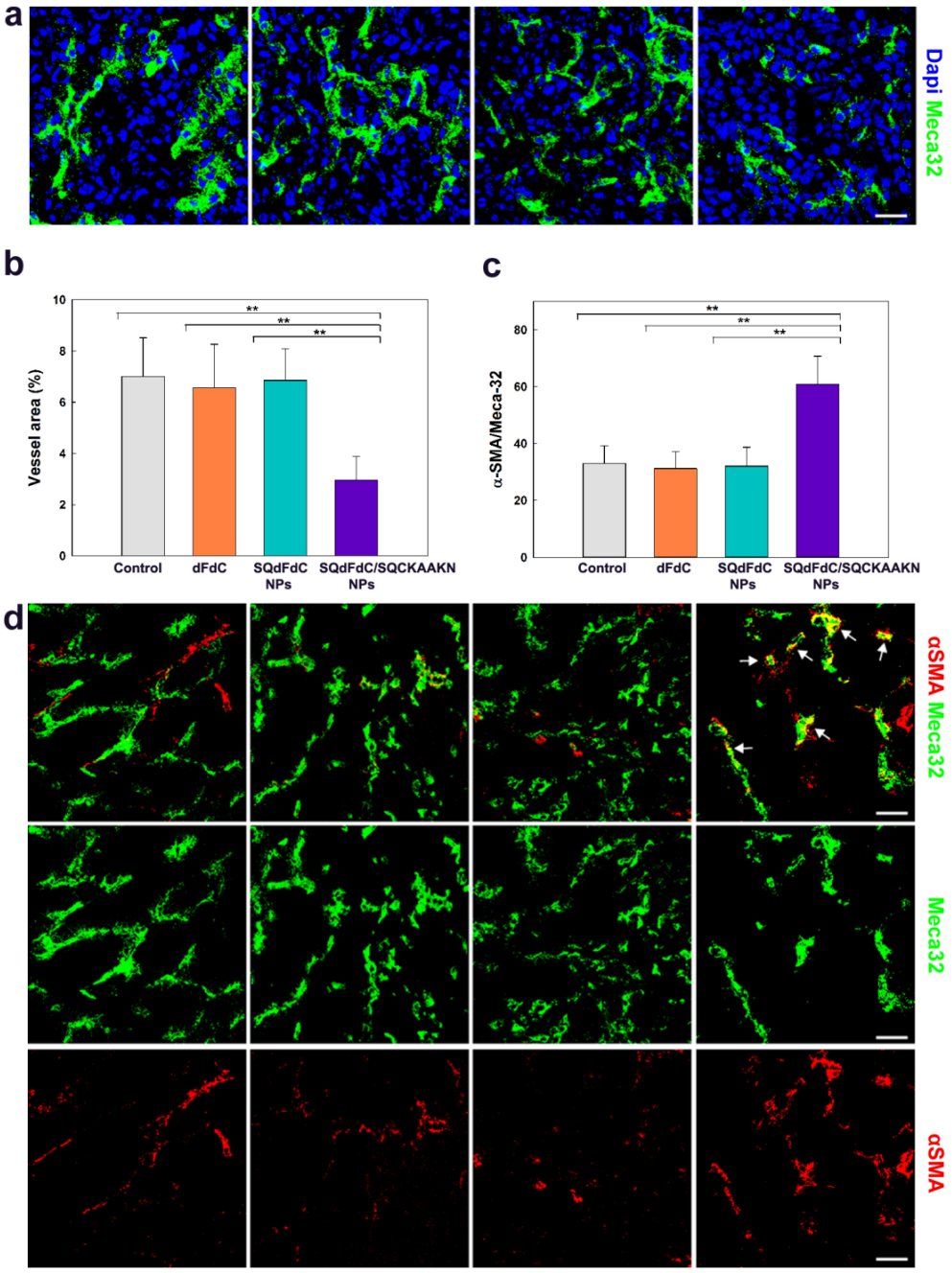

Fig. 7 | Immunohistochemical staining of tumor tissue-vessels and pericyte quantification. **(a)** Representative images (5 fields/mouse) of confocal analysis of Meca32 (green channel) endothelial marker immunostaining in tumor tissues from the different groups of treatment. Nuclei were stained with DAPI (blue channel). Scale bars: 50 μm. **(b)** Percentage of surface area occupied by vessels quantified as Meca32 positive staining. **(c)** Quantification analysis of α-SMA pericyte marker localized in proximity to endothelial cells-lined blood vessels. Values represent mean ± SD. Statistical difference is marked by $^{**}p < 0.01$. **(d)** Tumor vessel pericyte coverage was evaluated as Meca32 (green channel) and α-SMA (red channel) colocalization (arrows). Images are representative of 5 fields per mouse from a total of 8 mice per treatment group. Scale bars: 50 μm.

Increased pericyte coverage and reduction in vascular density are hallmarks of tumor blood vessel normalization. It has been proposed that the duration of the vascular normalization window, that allows more efficient delivery of oxygen and chemotherapeutic drugs into the

tumor tissue, is critical to achieve a long-lasting and successful therapeutic synergy between antiangiogenic and chemotherapeutic drugs.[46,52] These results pointed out that the enhanced antitumor activity observed for the CKAAKN-functionalized squalene-gemcitabine materials reflects by the multiple ability of (i) targeting both tumor and vessel cells, (ii) inhibiting tumor growth and angiogenesis and (iii) normalizing the remaining vasculature as observed with angiogenesis inhibitors .[47,48]

On the basis of previous data indicating the Wnt sharing motifs with the CKAAKN peptide[19] and of our data showing the FZD-5 as putative receptor for CKAAKN peptide-functionalized nanoparticles, we investigated the expression of FZD-5 in RIP-Tag2 tumors. Interestingly, we observed by immunostaining a strong expression of FZD-5 in tumor vasculature but also, although to a lower extent, in cancer cells of end-stage Rip-Tag2 tumors (Fig. 8).

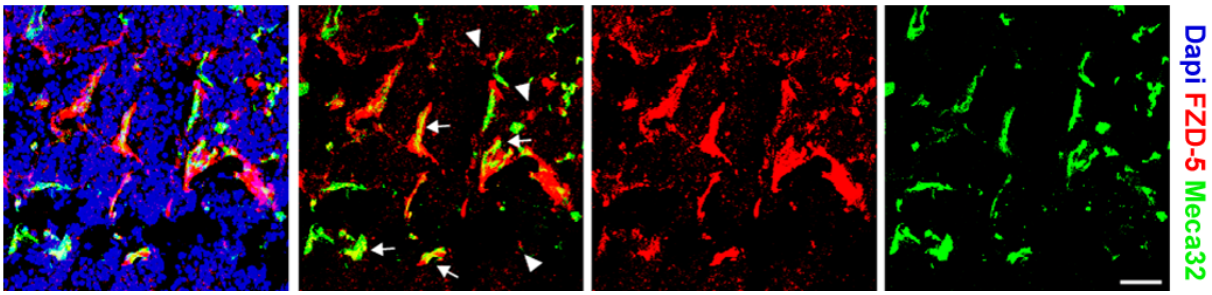

Fig. 8 | Immunocytochemistry analysis and FZD-5 expression in tumor tissue. FZD-5 expression and localization in RIP-Tag2 tumors were assessed by immunofluorescence and confocal analysis. FZD-5 expressed on vessels is shown as co-staining of anti-FZD-5 antibody (red channel) with Meca32 (green channel). Nuclei were stained with DAPI (blue channel). The images shown are representative confocal microscopy of 5 fields per mouse. Scale bars: 50 μm.

These observations strongly suggest that the FZD-5 is the target of SQdFdC/SQCKAAKN NPs *in vivo*, in RIP-Tag2 mice, and that functionalized nanoparticles probably exert their action (that is, anti-tumor and anti-angiogenic effect) by modulating the Wnt-2/FZD-5 signal pathway both in cancer cells and in tumor vasculature.

Conclusion

In a nutshell, we propose here a novel, efficient and easy to prepare peptide-targeted squalene-based nanosized materials for pancreatic cancer treatment, able to specifically interact with both tumor cells and angiogenic vessels and capable of simultaneously promoting pericyte coverage, thus leading to the normalization of the pre-existent vasculature likely improving the tumor accessibility for the therapy. The superior efficacy of peptide-decorated nanoparticles compared with the non functionalized ones in RIP-Tag2 mice and our studies in pancreatic cells suggest the key role of the active targeting in the improvement of the therapeutic efficacy of gemcitabine in experimental pancreatic cancers.
To our knowledge, this is the first successful example of pancreatic cancer targeted nanosized materials with unique selectivity and multiple mechanism of action.

Acknowledgments

The authors warmly thank Julie Mougin and Ghislaine Frébourg (Service of Electron Microscopy from IFR of Integrative Biology, Paris) for the cryo-TEM analysis and Dr. Valerie Nicolas (Service Imagerie-Microscopie Confocale, IFR-141 IPSIT, Châtenay-Malabry, France) for the expert assistance in confocal microscopy. Dr Victoria Franzinetti for her suggestions in revising the manuscript. The research leading to these results has received funding from the European Research Council under the European Community's Seventh Framework Programme FP7/2007-2013 Grant Agreement N°249835; from MIUR - University of Turin “Fondi Ricerca Locale (ex-60%)”; from Associazione Italiana per la Ricerca sul Cancro (AIRC) investigator grants IG (11600); from Fondazione Piemontese per la Ricerca sul Cancro-ONLUS (Intramural Grant) and F.M. was supported by fellowship granted by Fondazione Italiana per la Ricerca sul Cancro (FIRC). The authors acknowledge the Università Italo Francese/Université Franco Italienne for the PhD co-tutoring agreement to S.V.

References

1. Jemal, A.; Siegel, R.; Xu, J.; Ward, E. Cancer statistics, 2010. *CA Cancer J Clin* **2010**, 60, 277-300.
2. Oberstein, P. E.; Saif, M. W. First-line treatment for advanced pancreatic cancer. Highlights from the "2011 ASCO Gastrointestinal Cancers Symposium". San Francisco, CA, USA. January 20-22, 2011. *JOP* **2011**, 12, 96-100.
3. Heinemann, V.; Boeck, S.; Hinke, A.; Labianca, R.; Louvet, C. Meta-analysis of randomized trials: evaluation of benefit from gemcitabine-based combination chemotherapy applied in advanced pancreatic cancer. *BMC Cancer* **2008**, 8, 82.
4. Sultana, A.; Smith, C. T.; Cunningham, D.; Starling, N.; Neoptolemos, J. P.; Ghaneh, P. Meta-analyses of chemotherapy for locally advanced and metastatic pancreatic cancer. *J Clin Oncol* **2007**, 25, 2607-15.
5. Moore, M. J.; Goldstein, D.; Hamm, J.; Figer, A.; Hecht, J. R.; Gallinger, S.; Au, H. J.; Murawa, P.; Walde, D.; Wolff, R. A.; Campos, D.; Lim, R.; Ding, K.; Clark, G.; Voskoglou-Nomikos, T.; Ptasynski, M.; Parulekar, W. Erlotinib plus gemcitabine compared with gemcitabine alone in patients with advanced pancreatic cancer: a phase III trial of the National Cancer Institute of Canada Clinical Trials Group. *J Clin Oncol* **2007**, 25, 1960-6.
6. http://www.accessdata.fda.gov/drugsatfda_docs/appletter/2013/ 021660Orig1s037ltr.pdf.
7. Bildstein, L.; Dubernet, C.; Marsaud, V.; Chacun, H.; Nicolas, V.; Gueutin, C.; Sarasin, A.; Benech, H.; Lepetre-Mouelhi, S.; Desmaele, D.; Couvreur, P. Transmembrane diffusion of gemcitabine by a nanoparticulate squalenoyl prodrug: an original drug delivery pathway. *J Control Release* **2010**, 147, 163-70.
8. Olive, K. P.; Jacobetz, M. A.; Davidson, C. J.; Gopinathan, A.; McIntyre, D.; Honess, D.; Madhu, B.; Goldgraben, M. A.; Caldwell, M. E.; Allard, D.; Frese, K. K.; Denicola, G.; Feig, C.; Combs, C.; Winter, S. P.; Ireland-Zecchini, H.; Reichelt, S.; Howat, W. J.; Chang, A.; Dhara, M.; Wang, L.; Ruckert, F.; Grutzmann, R.; Pilarsky, C.; Izeradjene, K.; Hingorani, S. R.; Huang, P.; Davies, S. E.; Plunkett, W.; Egorin, M.; Hruban, R. H.; Whitebread, N.; McGovern, K.; Adams, J.; Iacobuzio-Donahue, C.; Griffiths, J.; Tuveson, D. A. Inhibition of Hedgehog signaling enhances delivery of chemotherapy in a mouse model of pancreatic cancer. *Science* **2009**, 324, 1457-61.
9. Takakura, Y.; Mahato, R. I.; Hashida, M. Extravasation of macromolecules. *Adv Drug Deliv Rev* **1998**, 34, 93-108.
10. Owens, D. E., 3rd; Peppas, N. A. Opsonization, biodistribution, and pharmacokinetics of polymeric nanoparticles. *Int J Pharm* **2006**, 307, 93-102.
11. Hidalgo, M. Pancreatic cancer. *N Engl J Med* **2010**, 362, 1605-17.
12. Nicolas, J.; Mura, S.; Brambilla, D.; Mackiewicz, N.; Couvreur, P. Design, functionalization strategies and biomedical applications of targeted biodegradable/biocompatible polymer-based nanocarriers for drug delivery. *Chem Soc Rev* **2012**.
13. Valetti, S.; Mura, S.; Stella, B.; Couvreur, P. Rational design for multifunctional non-liposomal lipid-based nanocarriers for cancer management: theory to practice. *Journal of Nanobiotechnology* **2013**, 11, S6.
14. Nichols, J. W.; Bae, Y. H. Odyssey of a cancer nanoparticle: From injection site to site of action. *Nano Today* **2012**, 7, 606-618.
15. Kudgus, R. A.; Szabolcs, A.; Khan, J. A.; Walden, C. A.; Reid, J. M.; Robertson, J. D.; Bhattacharya, R.; Mukherjee, P. Inhibiting the growth of pancreatic adenocarcinoma in vitro and in vivo through targeted treatment with designer gold nanotherapeutics. *PLoS One* **2013**, 8, e57522.

16. Ji, S.; Xu, J.; Zhang, B.; Yao, W.; Xu, W.; Wu, W.; Xu, Y.; Wang, H.; Ni, Q.; Hou, H.; Yu, X. RGD-conjugated albumin nanoparticles as a novel delivery vehicle in pancreatic cancer therapy. *Cancer Biol Ther* **2012**, 13, 206-15.
17. Camp, E. R.; Wang, C.; Little, E. C.; Watson, P. M.; Pirollo, K. F.; Rait, A.; Cole, D. J.; Chang, E. H.; Watson, D. K. Transferrin receptor targeting nanomedicine delivering wild-type p53 gene sensitizes pancreatic cancer to gemcitabine therapy. *Cancer Gene Ther* **2013**, 20, 222-8.
18. Xu, J.; Gattacceca, F.; Amiji, M. Biodistribution and Pharmacokinetics of EGFR-Targeted Thiolated Gelatin Nanoparticles Following Systemic Administration in Pancreatic Tumor-Bearing Mice. *Mol Pharm* **2013**.
19. Joyce, J. A.; Laakkonen, P.; Bernasconi, M.; Bergers, G.; Ruoslahti, E.; Hanahan, D. Stage-specific vascular markers revealed by phage display in a mouse model of pancreatic islet tumorigenesis. *Cancer Cell.* **2003**, 4, 393-403.
20. Reddy, L. H.; Couvreur, P. Squalene: A natural triterpene for use in disease management and therapy. *Adv Drug Deliv Rev* **2009**, 61, 1412-26.
21. Couvreur, P.; Stella, B.; Reddy, L. H.; Hillaireau, H.; Dubernet, C.; Desmaele, D.; Lepetre-Mouelhi, S.; Rocco, F.; Dereuddre-Bosquet, N.; Clayette, P.; Rosilio, V.; Marsaud, V.; Renoir, J. M.; Cattel, L. Squalenoyl nanomedicines as potential therapeutics. *Nano Lett.* **2006**, 6, 2544-8.
22. Willner, D.; Trail, P. A.; Hofstead, S. J.; King, H. D.; Lasch, S. J.; Braslawsky, G. R.; Greenfield, R. S.; Kaneko, T.; Firestone, R. A. (6-Maleimidocaproyl)hydrazone of doxorubicin--a new derivative for the preparation of immunoconjugates of doxorubicin. *Bioconjug Chem* **1993**, 4, 521-7.
23. Fessi, H.; Puisieux, F.; Devissaguet, J. P.; Ammoury, N.; Benita, S. Nanocapsule formation by interfacial polymer deposition following solvent displacement. *International Journal of Pharmaceutics* **1989**, 55, R1-R4.
24. Bertholon, I.; Vauthier, C.; Labarre, D. Complement activation by core-shell poly(isobutylcyanoacrylate)-polysaccharide nanoparticles: influences of surface morphology, length, and type of polysaccharide. *Pharm Res* **2006**, 23, 1313-23.
25. M. Kazatchkine, G. H., U. Nydegger, . Techniques du complément. *INSERM, Paris* **1986**.
26. Vauthier, C.; Persson, B.; Lindner, P.; Cabane, B. Protein adsorption and complement activation for di-block copolymer nanoparticles. *Biomaterials* **2011**, 32, 1646-56.
27. Uhlen, M.; Oksvold, P.; Fagerberg, L.; Lundberg, E.; Jonasson, K.; Forsberg, M.; Zwahlen, M.; Kampf, C.; Wester, K.; Hober, S.; Wernerus, H.; Bjorling, L.; Ponten, F. Towards a knowledge-based Human Protein Atlas. *Nat Biotechnol* **2010**, 28, 1248-50.
28. Hanahan, D. Heritable formation of pancreatic beta-cell tumours in transgenic mice expressing recombinant insulin/simian virus 40 oncogenes. *Nature* **1985**, 315, 115-22.
29. Giraudo, E.; Inoue, M.; Hanahan, D. An amino-bisphosphonate targets MMP-9-expressing macrophages and angiogenesis to impair cervical carcinogenesis. *J Clin Invest* **2004**, 114, 623-33.
30. Zerlin, M.; Julius, M. A.; Kitajewski, J. Wnt/Frizzled signaling in angiogenesis. *Angiogenesis* **2008**, 11, 63-9.
31. Weeraratna, A. T.; Jiang, Y.; Hostetter, G.; Rosenblatt, K.; Duray, P.; Bittner, M.; Trent, J. M. Wnt5a signaling directly affects cell motility and invasion of metastatic melanoma. *Cancer Cell* **2002**, 1, 279-88.
32. Wawrzak, D.; Metioui, M.; Willems, E.; Hendrickx, M.; de Genst, E.; Leyns, L. Wnt3a binds to several sFRPs in the nanomolar range. *Biochem Biophys Res Commun* **2007**, 357, 1119-23.
33. Reulen, S. W.; Dankers, P. Y.; Bomans, P. H.; Meijer, E. W.; Merkx, M. Collagen targeting using protein-functionalized micelles: the strength of multiple weak interactions. *J Am Chem Soc* **2009**, 131, 7304-12.

34. Montet, X.; Funovics, M.; Montet-Abou, K.; Weissleder, R.; Josephson, L. Multivalent effects of RGD peptides obtained by nanoparticle display. *J Med Chem* **2006**, 49, 6087-93.
35. Holland, J. D.; Klaus, A.; Garratt, A. N.; Birchmeier, W. Wnt signaling in stem and cancer stem cells. *Curr Opin Cell Biol* **2013**, 25, 254-64.
36. Schinner, S.; Willenberg, H. S.; Schott, M.; Scherbaum, W. A. Pathophysiological aspects of Wnt-signaling in endocrine disease. *Eur J Endocrinol* **2009**, 160, 731-7.
37. Jones, S.; Zhang, X.; Parsons, D. W.; Lin, J. C.; Leary, R. J.; Angenendt, P.; Mankoo, P.; Carter, H.; Kamiyama, H.; Jimeno, A.; Hong, S. M.; Fu, B.; Lin, M. T.; Calhoun, E. S.; Kamiyama, M.; Walter, K.; Nikolskaya, T.; Nikolsky, Y.; Hartigan, J.; Smith, D. R.; Hidalgo, M.; Leach, S. D.; Klein, A. P.; Jaffee, E. M.; Goggins, M.; Maitra, A.; Iacobuzio-Donahue, C.; Eshleman, J. R.; Kern, S. E.; Hruban, R. H.; Karchin, R.; Papadopoulos, N.; Parmigiani, G.; Vogelstein, B.; Velculescu, V. E.; Kinzler, K. W. Core signaling pathways in human pancreatic cancers revealed by global genomic analyses. *Science* **2008**, 321, 1801-6.
38. Morris, J. P.; Wang, S. C.; Hebrok, M. KRAS, Hedgehog, Wnt and the twisted developmental biology of pancreatic ductal adenocarcinoma. *Nat Rev Cancer* **2010**, 10, 683-695.
39. Katoh, M. WNT2 and human gastrointestinal cancer (review). *Int J Mol Med* **2003**, 12, 811-6.
40. Nel, A. E.; Madler, L.; Velegol, D.; Xia, T.; Hoek, E. M.; Somasundaran, P.; Klaessig, F.; Castranova, V.; Thompson, M. Understanding biophysicochemical interactions at the nano-bio interface. *Nat Mater* **2009**, 8, 543-57.
41. Moghimi, S. M.; Andersen, A. J.; Hashemi, S. H.; Lettiero, B.; Ahmadvand, D.; Hunter, A. C.; Andresen, T. L.; Hamad, I.; Szebeni, J. Complement activation cascade triggered by PEG-PL engineered nanomedicines and carbon nanotubes: the challenges ahead. *J Control Release* **2010**, 146, 175-81.
42. Moghimi, S. M.; Farhangrazi, Z. S. Nanomedicine and the complement paradigm. *Nanomedicine* **2013**, 9, 458-60.
43. Carreno, M. P.; Maillet, F.; Labarre, D.; Jozefowicz, M.; Kazatchkine, M. D. Specific antibodies enhance Sephadex-induced activation of the alternative complement pathway in human serum. *Biomaterials* **1988**, 9, 514-8.
44. Bergers, G.; Javaherian, K.; Lo, K. M.; Folkman, J.; Hanahan, D. Effects of angiogenesis inhibitors on multistage carcinogenesis in mice. *Science* **1999**, 284, 808-12.
45. Teicher, B. A. Tumor models for efficacy determination. *Mol Cancer Ther* **2006**, 5, 2435-43.
46. Bergers, G.; Song, S.; Meyer-Morse, N.; Bergsland, E.; Hanahan, D. Benefits of targeting both pericytes and endothelial cells in the tumor vasculature with kinase inhibitors. *J Clin Invest* **2003**, 111, 1287-95.
47. Maione, F.; Molla, F.; Meda, C.; Latini, R.; Zentilin, L.; Giacca, M.; Seano, G.; Serini, G.; Bussolino, F.; Giraudo, E. Semaphorin 3A is an endogenous angiogenesis inhibitor that blocks tumor growth and normalizes tumor vasculature in transgenic mouse models. *J Clin Invest* **2009**, 119, 3356-72.
48. Maione, F.; Capano, S.; Regano, D.; Zentilin, L.; Giacca, M.; Casanovas, O.; Bussolino, F.; Serini, G.; Giraudo, E. Semaphorin 3A overcomes cancer hypoxia and metastatic dissemination induced by antiangiogenic treatment in mice. *J Clin Invest* **2012**, 122, 1832-48.
49. Reddy, L. H.; Dubernet, C.; Mouelhi, S. L.; Marque, P. E.; Desmaele, D.; Couvreur, P. A new nanomedicine of gemcitabine displays enhanced anticancer activity in sensitive and resistant leukemia types. *J Control Release* **2007**, 124, 20-7.

50. Reddy, L. H.; Renoir, J. M.; Marsaud, V.; Lepetre-Mouelhi, S.; Desmaele, D.; Couvreur, P. Anticancer efficacy of squalenoyl gemcitabine nanomedicine on 60 human tumor cell panel and on experimental tumor. *Mol Pharm* **2009**, 6, 1526-35.
51. Rejiba, S.; Reddy, L. H.; Bigand, C.; Parmentier, C.; Couvreur, P.; Hajri, A. Squalenoyl gemcitabine nanomedicine overcomes the low efficacy of gemcitabine therapy in pancreatic cancer. *Nanomedicine* **2011**, 7, 841-9.
52. Jain, R. K. Normalization of tumor vasculature: an emerging concept in antiangiogenic therapy. *Science* **2005**, 307, 58-62.

Supplementary Data

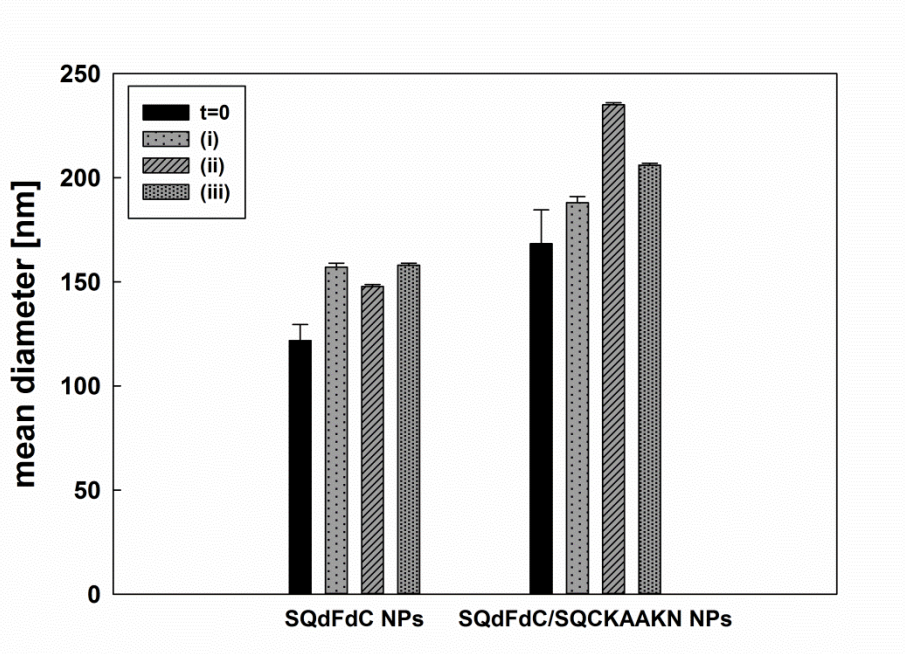

Supplementary Fig. S1: Stability of SQdFdC NPs and SQdFdC/SQCKAAKN NPs. Stability of SQdFdC NPs and SQdFdC/SQCKAAKN NPs after 72 h incubation in (i) water; (ii) 5% w/w dextrose solution; (iii) cell culture medium (DMEM supplemented with 10% of FBS) at 37°C. Values represent ± sd.

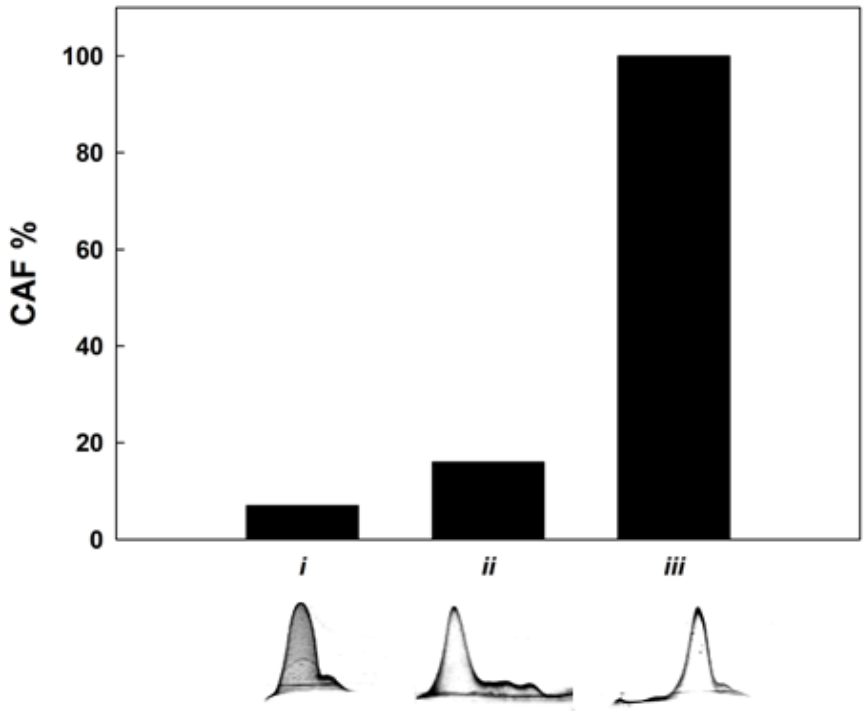

Supplementary Fig. S2: Activation of C3 protein of the complement system. 2D electroimmunophoretic profile of complement activation and C3 protein activation factor (CAF) values for (*i*) negative control (water incubated with serum in VBS-EDTA); (*ii*) control of spontaneous complement activation induced by the experimental conditions (water incubated with serum in VBS^{2+}); (*iii*) positive control for full complement activation (RREP dextran (0.5%)-coated PIBCA nanoparticles incubated with serum in VBS^{2+} at 1000 cm² surface area).

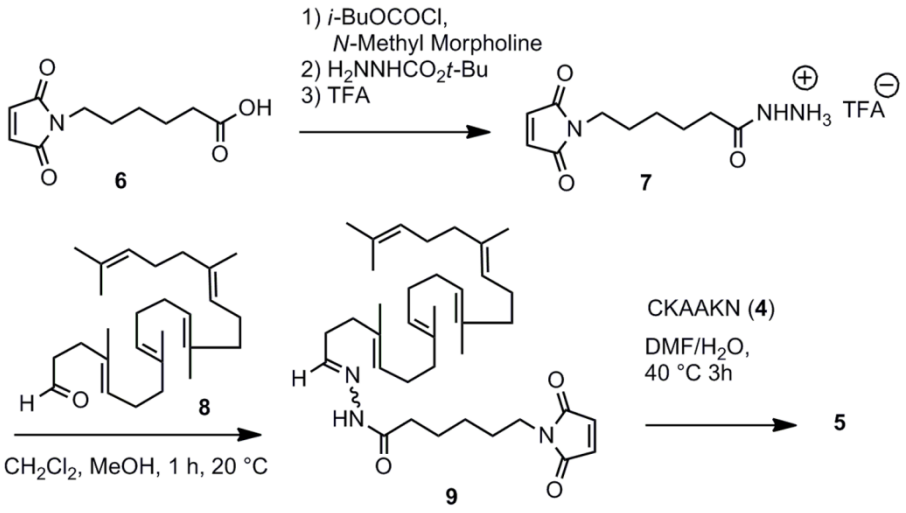

Supplementary Fig. S3: Synthetic scheme for SQCKAAKN. Synthesis of the **(7)** maleimide hydrazide linker and of the **(5)** squalene-peptide conjugate SQCKAAKN.

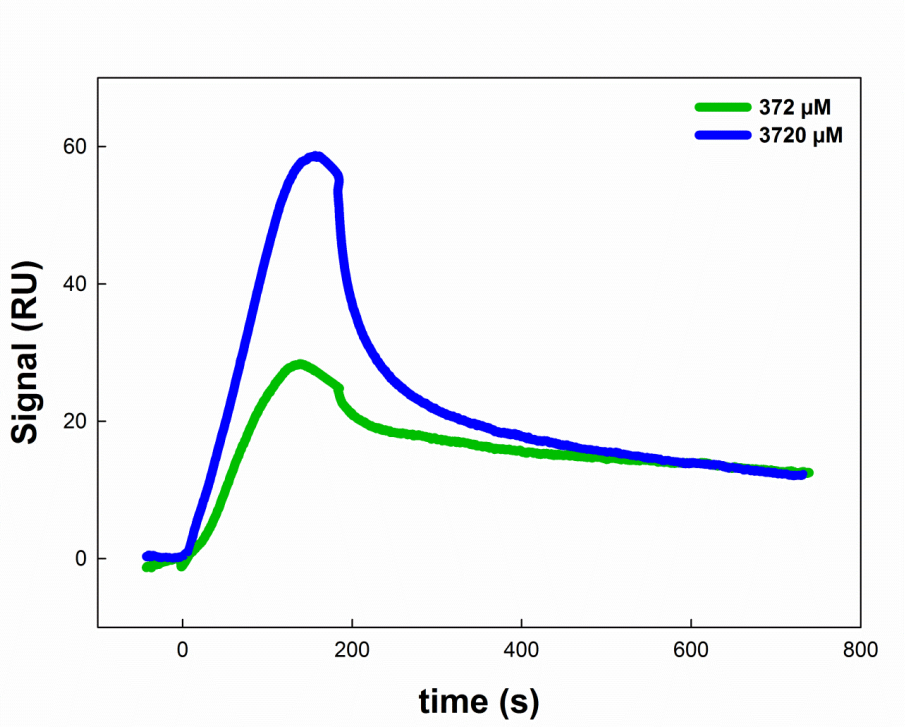

Supplementary Fig. S4: Surface plasmon resonance (SPR) analysis of CKAAKN peptide. SPR sensorgrams (resonance units (RU) *versus* time) of CKAAKN peptide at different concentrations. t=0: sample injection. sFRP-4 was immobilized on two parallel channels of the same sensor chip.

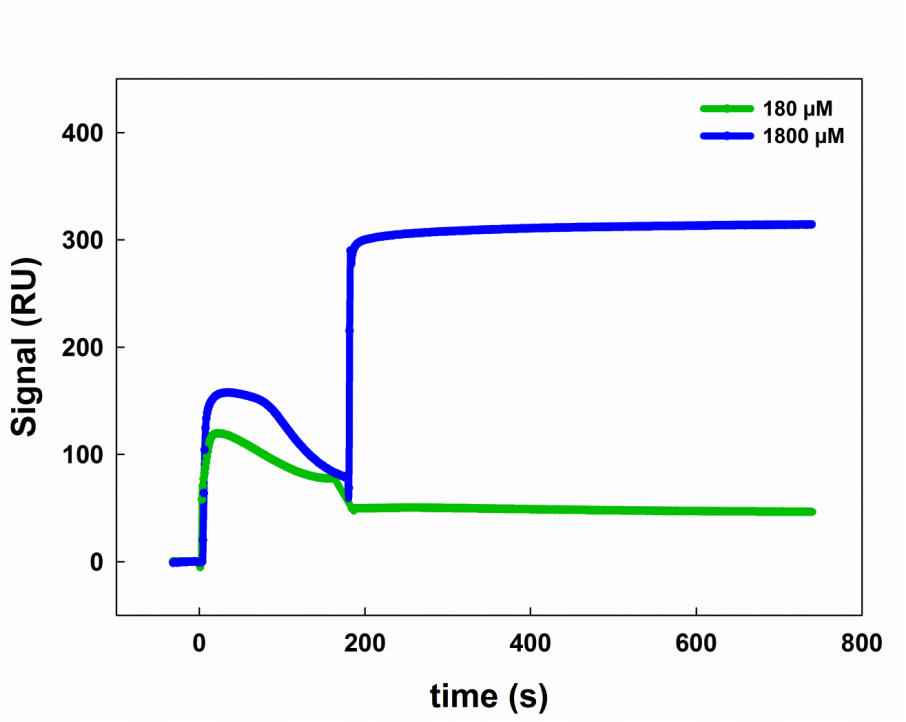

Supplementary Fig. S5: Surface plasmon resonance (SPR) analysis of SQdFdC/SQCKAAKN NPs. SPR sensorgrams (resonance units (RU) *versus* time) of SQdFdC/SQCKAAKN NPs at different concentrations. t=0: sample injection. sFRP-4 was immobilized on two parallel channels of the same sensor chip.

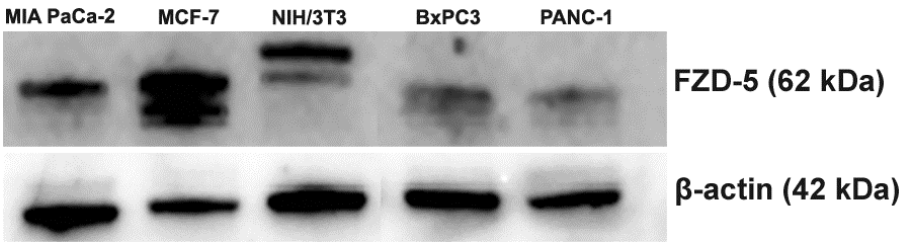

Supplementary Fig. S6: Western blot analysis. Representative Western Blot showing FZD-5 and β-actin expression in different pancreatic cancer and fibroblastic cell lines. MCF-7 cell line was used as a positive control.

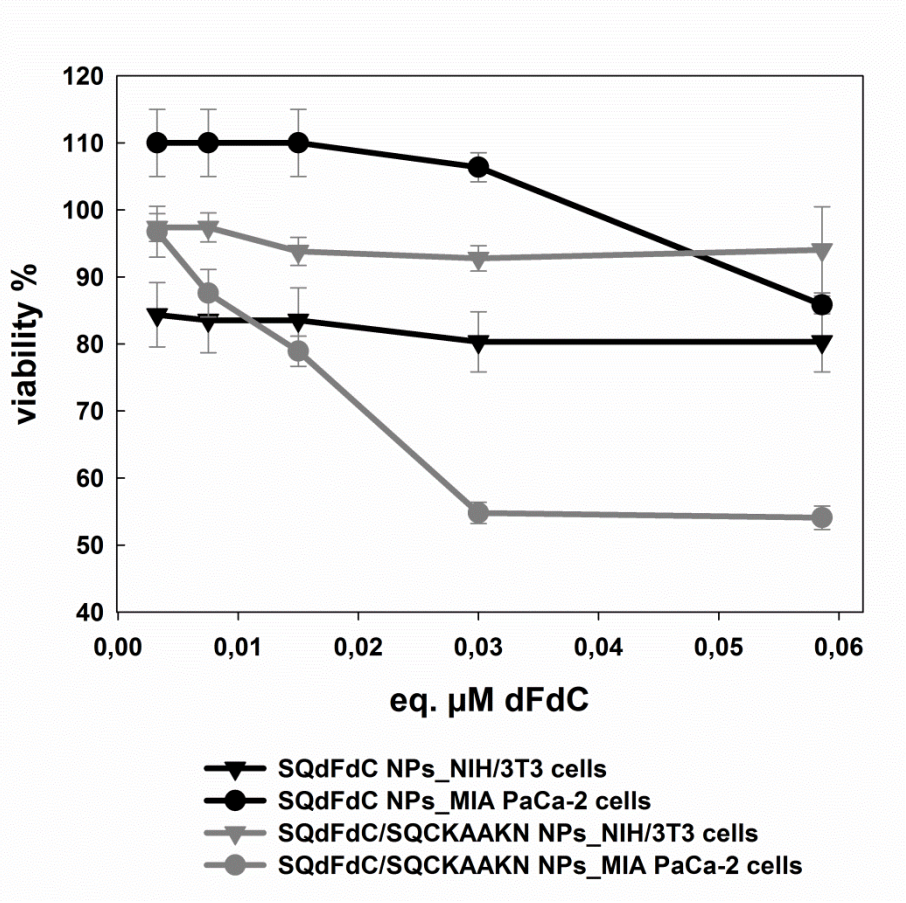

Supplementary Fig. S7: Cytotoxicity of SQdFdC and SQdFdC/SQCKAAKN NPs. Cell viability assay (MTT) of MIA PaCa-2 and NIH/3T3 cell lines treated with increased concentration of SQdFdC or SQdFdC/SQCKAAKN NPs for 72 h. Cytotoxicity of nanoparticles was compared to non-treated cells. Values represent mean ± SEM.

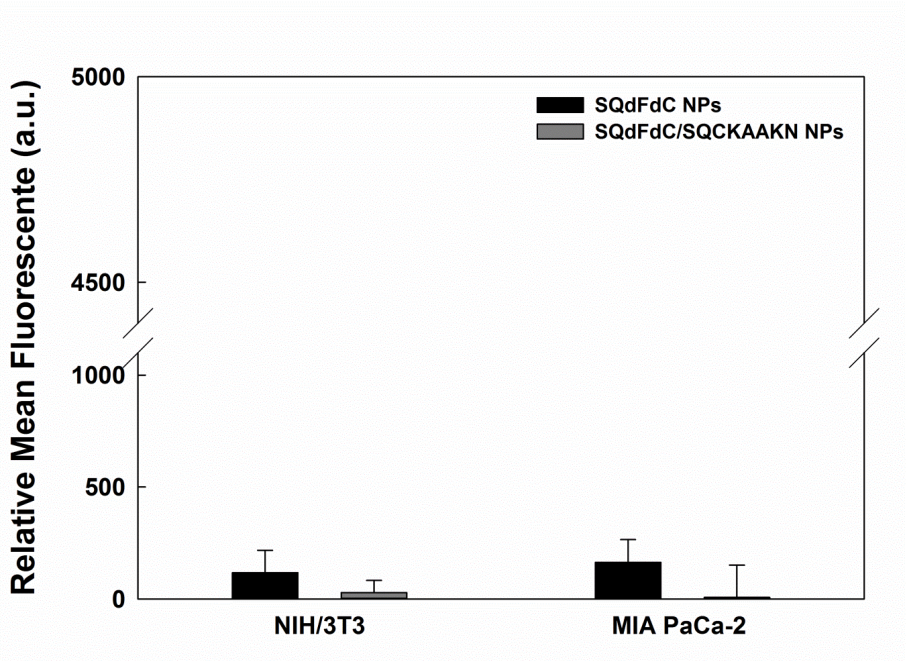

Supplementary Fig. S8: Cellular internalization of SQdFdC and SQdFdC/SQCKAAKN NPs by flow cytometry analysis at 4°C. Quantification of cellular uptake of SQdFdC and SQdFdC/SQCKAAKN NPs in NIH/3T3 and MIA PaCa-2 cell lines at 4°C. Values represent mean ± SEM.

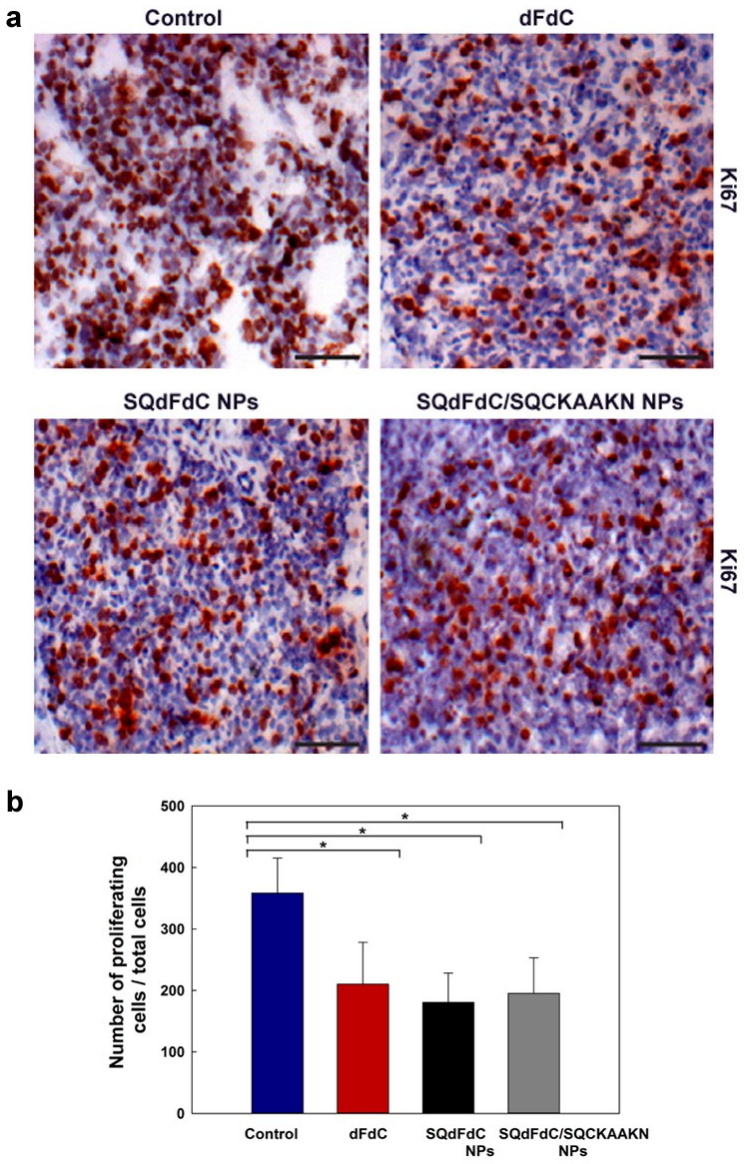

Supplementary Fig. S9: Quantification of proliferation by immunohistochemical staining of tumor tissues. (a) Proliferation level was assessed by immunohistochemistry using the proliferation marker Ki67. Images are representative of five fields per mouse. Scale bars: 50 μm. **(b)** Quantification analysis of Ki67 staining. Bars show the mean of Ki67 positive cells/total cells. Values represent mean ± SD. Statistical difference is marked by $*p < 0.05$.

Chapter 2:

“How to functionalize squalene-based nanoparticles with a peptide: by conjugation before or after nanoparticle formation”

How to functionalize squalene-based nanoparticles with a peptide: by conjugation before or after nanoparticle formation

Sabrina Valetti [a, b], *Barbara Stella* [b], *Magali Noiray* [a], *Didier Desmaële* [a], *Silvia Arpicco* [b], *Franco Dosio* [b], *Simona Mura* [a], *Patrick Couvreur.* [a*]

(Article in preparation)

[a] Université Paris-Sud, Faculté de Pharmacie, 5 rue Jean-Baptiste Clément, 92296 Châtenay-Malabry cedex, France
CNRS UMR 8612, Institut Galien Paris-Sud, 5 rue Jean-Baptiste Clément, 92296 Châtenay-Malabry cedex, France
[b] Dipartimento di Scienza e Tecnologia del Farmaco, Università di Torino, 9 via Pietro Giuria 10125 Torino, Italy

Abstract

A comparative characterization study to evaluate the targeting ability of peptide-decorated squalenoyl gemcitabine (SQdFdC) nanoparticles (NPs), prepared in accordance with different strategies, is herein reported. In particular, the CKAAKN peptide, previously identified as efficient homing device within the pancreatic pathological microenvironment, was conjugated to the nanoparticles by two approaches: (*i*) the targeting moiety was coupled at the surface of preformed SQdFdC nanoparticles, (*ii*) the peptide was firstly reacted with a maleimide group-bearing squalenoyl derivative and the resulting bioconjugate co-nanoprecipitated with SQdFdC. NPs were characterized for mean diameter, zeta potential and stability over time. Then, the specific interaction between the peptide-decorated nanoparticles and the sFRP-4 protein was evaluated by surface plasmon resonance. Despite both the two synthetic strategies allowed to formulate NPs able to interact with the receptor, enhanced target binding and specific avidity was observed only for NPs made by self-assembly of preformed squalenoyl derivatives, which displayed also the highest uptake and cytotoxicity on MIA Paca-2 pancreatic cancer cells.

Introduction

The ability to selectively deliver drugs to tumor cells with minimal interaction with healthy tissues is one of the greatest challenges in chemotherapy. To this aim, suitable ligands able to bind to specific receptors, which are overexpressed on cancer cells and relatively downregulated on healthy ones, have been successfully employed as a valuable strategy to specifically target tumors.[1] By means of high molecular recognition, such "targeted therapy" has improved the balance between efficacy and toxicity of conventional systemic anticancer treatments [2,3] as observed, for instance, in the case of antibody-conjugated chemotherapeutic agents.[3-5] Twenty antibody-drugs are currently included in clinical trials with encouraging results[6] and two conjugates, Adcetris® (Seattle Genetics) and T-DM1® (Genentech), have recently been approved by FDA.[7, 8]

In parallel, the use of targeting ligands, grafted to the surface of nanoscale drug delivery systems (*i.e.*, nanomedicines), seems to be another promising approach.[9] Compared to molecular conjugates, nanocarriers offer the advantage of protection of the drug molecule from degradation, controlled release and distribution. In addition, tuning the number of the ligand molecules at their surface, targeting efficacy might be improved *via* a multivalent binding with the receptor.[10] In the past 30 years, a plethora of targeted nanoparticles functionalized with various ligands belonging to the families of small molecules, polysaccharides, peptides, proteins or even antibodies has been developed.[11,12] Although nanomedicines are gaining more and more attention in cancer therapy[13,14] with 5 examples on the market and 10 in clinical development[15], none of the targeted formulations has been clinically approved and only 5 are in early clinical trials.[15,16] Several functionalization strategies and coupling methods have been developed, each of them exhibiting benefits and drawbacks (for systematic review see[11]). In general, the efficacy of a targeted nanocarrier is governed by (*i*) the nature of the polymer and the ligand, (*ii*) the selected coupling reaction, (*iii*) the disposition of the ligand at the surface and (*iv*) the ligand surface density.[17-22] Two main ligation strategies have been used to display the targeting agents at the surface of nanocarriers: the ligand can either (*i*) be directly coupled in aqueous solution to the surface of preformed nanocarriers or (*ii*) be linked to the nanocarrier components prior to self-assembly into the resulting ligand-decorated nanocarrier (Figure 1a).

The first strategy is generally preferred because: (*i*) the ligand is directly grafted onto the nanoparticle surface and it is available for the receptor recognition, (*ii*) the bulky ligands, like polypeptides, proteins or antibodies, could modify the hydrophilic/lipophilic balance of the carrier components changing the self-assembly properties and therefore the preparation conditions.[11] An undeniable advantage of the second strategy relies on the possibility to control the reaction yield, to purify and characterize the resulting conjugate. However, for proteins or antibodies, the solubilization in organic solvents could cause denaturation thus compromising their affinity for the receptor. In addition, in this approach the ligand could be entrapped in the nanocarrier core during self-assembly and consequently be not available on the nanoparticle surface. Therefore, a comparative study about advantages/disadvantages of each strategy should be done for any new system in order to achieve successful actively targeted nanoparticles.

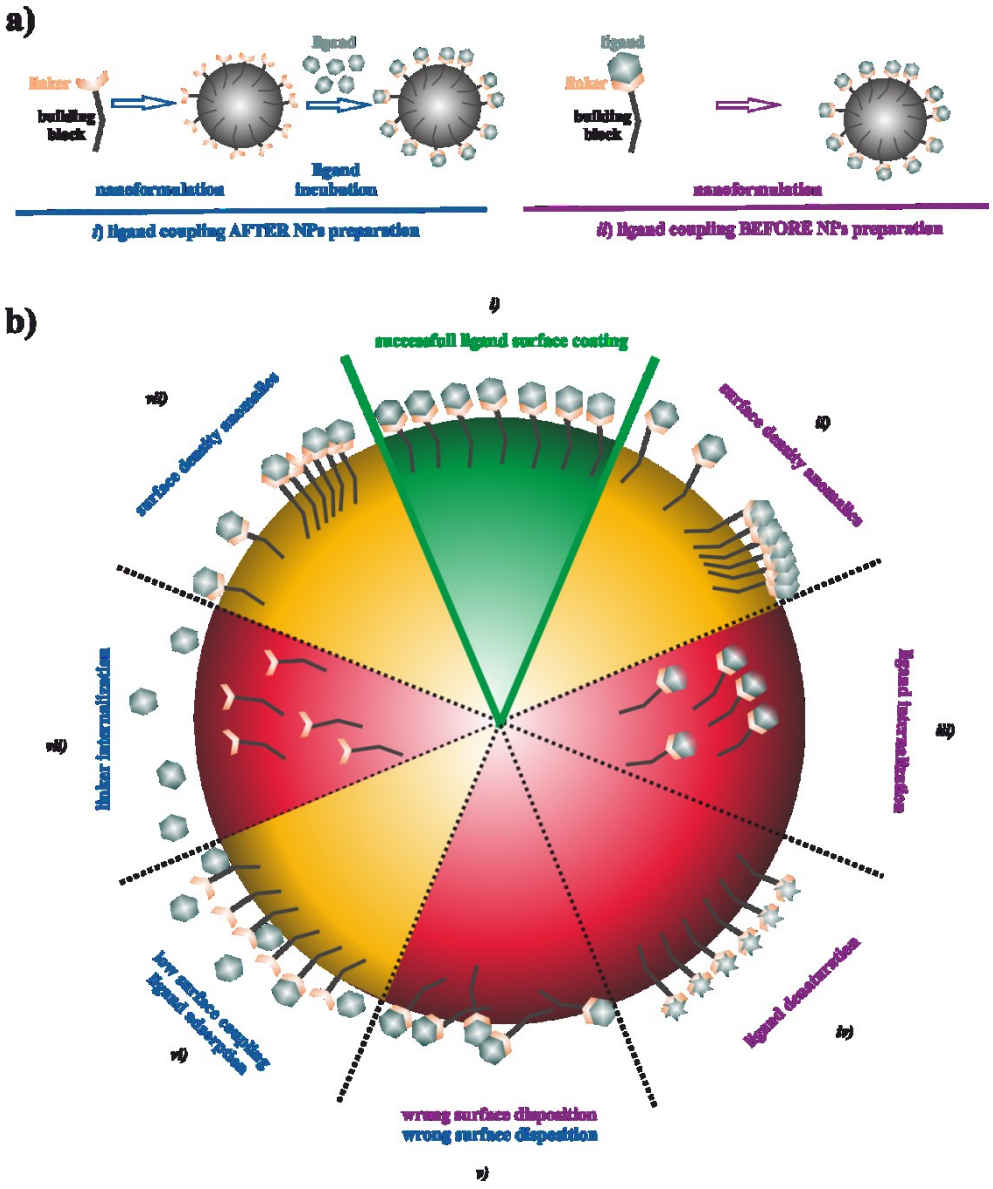

Figure 1. a) Strategies to prepare ligand-functionalized NPs: (*i*) the ligand can be coupled to the surface after nanoparticle formation or (*ii*) the ligand can be directly conjugated to the nanocarrier building material prior to NPs formation. **b)** Schematic representation of possible ligand disposition after both ligation strategies. Blue titles are referred to (*i*) ligand coupling after particles preparation and violet to (*ii*) ligand coupling before carriers preparation. The green segment symbolizes the successful ligand-functionalized nanoparticle, while yellow and red ones correspond to low and inefficient ligand surface coating, respectively.

In this work we report a rational study that investigates both the formulation parameters involved in the nanoparticles preparation and the physico-chemical properties of the resulting nanocarriers with the aim to design ligand-targeted squalene-based nanoparticles showing the highest affinity for pancreatic tumor cells.

The "squalenoylation" approach consists in the linkage of squalene (SQ), a natural triterpene precursor in the sterols biosynthesis, to various drugs. The obtained lipidic bioconjugates are able to self-assemble in aqueous solution to form nanoparticles with high drug payloads.[23] Proof of concept has been provided using gemcitabine (dFdC), which is the first-line therapeutic agent in pancreatic cancer treatment.[24] After intravenous administration squalenoylgemcitabine

(SQdFdC) nanoparticles showed a greater activity than the free drug against different tumor models *(e.g.,*experimental leukemia and pancreatic cancer).[23,25-27] However, the physio-pathological complexity of pancreatic cancer[28] urgently requires the development of targeted therapeutic approaches that would enhance selective nanoparticle internalization by cancer cells avoiding potential side effects.[12]

In this context, functionalized SQdFdC nanoparticles were prepared by using as a targeting agent the CKAAKN peptide, identified as efficient homing device within the pancreatic pathological microenvironment by phage display screening.[29]

Here we performed a comparative study to establish the optimal CKAAKN peptide-SQdFdC nanoparticles ligation strategy. CKAAKN was conjugated to the nanoparticles by the well-explored thiol-maleimide Michael addition coupling strategy either (*i*) by reacting the targeting moiety with preformed nanoparticles obtained with the nanoprecipitation technique (Figure 1a – left panel) or (*ii*) by conjugating the peptide with a squalenoyl derivative and then co-formulating the obtained bioconjugate with the SQdFdC (Figure 1a – right panel). The resulting targeted nanocarriers were characterized for size, zeta potential, stability, receptor binding affinity and *in vitro* behavior.

Materials and Methods

Chemicals

Gemcitabine (2',2'-difluorodeoxycitidine, dFdC) hydrochloride was purchased from Sequoia Research Products Ltd. (UK). CKAAKN peptide was purchased from CASLO Laboratory Aps (Lyngby, Denmark). Squalene, dextrose, maleimide and all other reagents were obtained by Sigma-Aldrich Chemical Co. (Milan, Italy). Squalene derivatives (Figure 2) (4-(*N*)-trisnorsqualenoylgemcitabine (SQdFdC)[23], 6-(maleimidocaproyl)hydrazone of squalene ($SQMal_{lipo}$)[30], 2-[2-(2,5-dioxo-2,5-dihydro-1H-pyrrol-1-yl)ethoxy]ethyl (4E,8E,12E,16E)-4,8,13,17,21-pentamethyl-docosa-4,8,12,16,20-pentaenoate ($SQMal_{hydro}$)[31] were obtained as previously reported. All solvents used were of analytical grade from Carlo Erba Reagenti (Milan, Italy) or VWR (France).

Preparation and characterization of untargeted nanoparticles

SQdFdC, SQdFdC/$SQMal_{lipo}$, SQdFdC/$SQMal_{hydro}$ and $SQMal_{lipo}$ nanoparticles (NPs) were prepared in accordance with the nanoprecipitation technique.[23,32] Practically, for SQdFdC NPs (N0), SQdFdC was dissolved in acetone (**$N0_a$**) or ethanol (**$N0_e$**); the organic solution was then added dropwise under magnetic stirring into MilliQ® water (solvent/water 1:2 v/v). Formation of the nanoparticles occurred spontaneously without using any surfactant. After solvent evaporation under reduced pressure, an aqueous suspension of N0 nanoparticles was obtained (final SQdFdC concentration: 2 mg/mL).
For SQdFdC/$SQMal_{lipo}$ NPs (N1), SQdFdC and $SQMal_{lipo}$ were co-dissolved in acetone (**$N1_a$**) or ethanol (**$N1_e$**) in various SQdFdC/$SQMal_{lipo}$ molar ratios (10:1, 5:1, 2:1). The organic solution was then added dropwise under magnetic stirring into MilliQ® water (solvent/water 1:2 v/v). Formation of the nanoparticles occurred spontaneously without using any surfactant. After solvent evaporation under reduced pressure, an aqueous suspension of $N1_a$ or $N1_e$ nanoparticles was obtained (final SQdFdC concentration: 2 mg/mL).
For SQdFdC/ $SQMal_{hydro}$ NPs (**N2**), SQdFdC and $SQMal_{hydro}$ were co-dissolved in ethanol in various molar ratios (10:1, 5:1). The organic solution was then added dropwise under magnetic stirring into MilliQ® water (ethanol/water 1:2 v/v). Formation of the nanoparticles occurred spontaneously without using any surfactant. After solvent evaporation under reduced pressure, an aqueous suspension of N2 nanoparticles was obtained (final SQdFdC concentration: 2 mg/mL).
For $SQMal_{lipo}$ NPs (**N3**), $SQMal_{lipo}$ was dissolved in acetone at various concentrations. After the addition of the organic solution to MilliQ® water (acetone/water 1:2 v/v) and solvent evaporation, an aqueous suspension of N3 nanoparticles was obtained ($SQMal_{lipo}$ concentration: 0.5, 1 or 2 mg/mL).
The mean particle size and the polydispersity index of all formulations were measured by dynamic light scattering (DLS) with a Nano ZS from Malvern (UK) (173° scattering angle) at 25 °C. The measurements were performed after dilution of the NPs suspensions (1/25 v/v) in MilliQ® water. The NPs surface charge was investigated by zeta potential measurements at 25 °C after dilution with 0.05 mM KCl solution, applying the Smoluchowski equation and using the same apparatus. Each measure was performed in triplicate. The stability of the formulations was evaluated by measuring the size and the zeta potential of the nanoparticles during 7 days of storage at 4 °C.

Preparation and characterization of targeted nanoparticles by coupling CKAAKN peptide to preformed nanoparticles

To obtain CKAAKN-conjugated SQdFdC/SQMal$_{lipo}$ NPs (**N1-P**), the peptide was dissolved in 1 mM degased phosphate buffer at pH 8.2 and then added to N1$_a$ (SQdFdC/SQMal$_{lipo}$ molar ratio 10:1 or 5:1, SQMal$_{lipo}$/peptide molar ratio 1:0.5 or 1:0.25, final SQdFdC concentration: 2 mg/mL). The reaction was carried out for 1 h at room temperature. The CKAAKN-functionalized nanoparticles (N1$_a$-P) were then purified from unreacted peptide by centrifugal filter units (30 kDa) at 14000 *g* for 1 minute (Amicon Ultra-0.5, Millipore). The mean size, the polydispersity index and the zeta potential of purified N1-P were determined at 25 °C by DLS as described above. The stability of the formulations was evaluated by measuring the size and the zeta potential of the nanoparticles during 7 days of storage at 4 °C.

Isothermal titration calorimetry (ITC) analysis of N1 nanoparticles

An isothermal calorimeter (VP-ITC, MicroCal., GE Healthcare Life Sciences) was used to evaluate the interactions between the maleimide (Mal) function and the CKAAKN peptide. The ITC instrument was periodically calibrated either electrically, using an internal electric heater, or chemically by measuring the dilution enthalpy of methanol in water. This standard reaction was in excellent agreement (1-2%) with the MicroCal constructor data.[33,34] In a typical experiment, aliquots of 10 µL of CKAAKN peptide, cysteine (Cys) or lysine in 0.03 M phosphate buffer solution at pH 8.2 (3.1 mM eq. Cys or 12.4 mM eq. lysine) filled into 283 µL syringe were used to titrate a suspension of either N1$_a$ or maleimide in 0.03 M phosphate buffer solution at pH 8.2 (0.31 mM eq. Mal) into the calorimetric cell accurately thermostated at 25 °C. The corresponding heat flows were recorded as a function of time. Intervals between injections were 600 s and agitation speed was 220 rpm. Control experiments with N0$_a$ into the calorimetric cell were done using the equivalent total squalene amount present in N1$_a$. Background of titration consisted on injecting the CKAAKN peptide or Cys in solely phosphate buffer solution placed in the sample cell.
The interaction process was analyzed by models proposed in the Windows-based Origin 7 software package supplied by MicroCal. Based on the concentrations of the two species, the software used a nonlinear least-squares algorithm to fit the series of heat flows to an equilibrium binding equation, providing the best-fit values of the stoichiometry, binding constant (K) and change in enthalpy (ΔH). From these results, the differences in free energy (ΔG) and the entropy (ΔS) were deducted according to the equation:

$$\Delta G = - RT \ln K = \Delta H - T\Delta S$$

Preparation of targeted nanoparticles by coupling CKAAKN to SQMal$_{lipo}$ prior to nanoparticles preparation

To obtain SQdFdC/SQCKAAKN nanoparticles (N4-P), CKAAKN peptide was first conjugated to SQMal$_{lipo}$ to give SQCKAAKN. A mixture of SQMal$_{lipo}$ **(3)** (13.5 mg, 0.0229 mmol) and CKAAKN peptide (**2**) (7.25 mg, 0.0114 mmol) in dimethylformamide DMF/H_2O 3/1 v/v (2 mL) was stirred for 3 h at 40 °C. The reaction mixture was then concentrated under reduced pressure and the crude product was taken into diethyl ether to remove unreacted maleimide. The supernatant was withdrawn after decantation (3 times). In order to eliminate unreacted peptide, the solid was dissolved in methanol and filtered through a sintered glass funnel. The product was obtained as a translucent waxy material (10 mg, 0.0082 mmol, 70% yield); MS (+ESI): *m/z* (%) = 1226.0 (100) $[MH]^+$, 614.5 (2).[30] Then, SQdFdC and SQCKAAKN were dissolved in 0.1 mL of ethanol in various molar ratios (SQdFdC/SQCKAAKN 1:0.1, 1:0.05, 1:0.01). The organic

solution was then added dropwise under magnetic stirring into 1 mL of MilliQ® water (ethanol/water 0.1:1 v/v). After solvent evaporation under reduced pressure, an aqueous suspension of N4-P was obtained (final SQdFdC concentration: 3.4 mg/mL). The mean size, the polydispersity index and the stability of the formulations were determined as described for N1-P. The NPs surface charge was investigated by zeta potential measurements at 25 °C after dilution with 0.05 mM KCl solution or 0.02 M phosphate buffer at pH values ranging from 7.4 to 9.8, applying the Smoluchowski equation and using the same apparatus.

Surface plasmon resonance (SPR) analysis

Interaction analyses were performed on a BIAcore T100 instrument using CM5 Series S sensor chip from GE Healthcare Life Sciences Europe (France). The activation of the carboxymethylated dextran matrix was performed with a mixture of 1:1 *N*-ethyl-*N'*-(3-diethylaminopropyl)-carbodiimide (EDC) 0.1 M / *N*-hydroxysuccinimide (NHS) 0.4 M (GE Healthcare) for 7 min. Running buffer for the immobilization process was 150 mM phosphate buffer, pH 7.4 at a flow rate of 10 µL/min. The sFRP-4 receptor was then injected over the activated surface at 10 µg/mL in 10 mM sodium acetate buffer at pH 4.4 during 7 min, giving an average immobilization level of 2800 resonance units (RU). A solution of 1 M ethanolamine hydrochloride at pH 8.5 was injected during 7 min to block the unreacted sites of the matrix. For reference, an additional blank flow channel was prepared in accordance with the same process without injecting the receptor over the surface. Binding capacities of the functional surfaces were tested with 180 s-injections of a peptide solution, $N1_a$ (SQdFdC/SQMal molar ratio 5:1), $N1_a$-P* (SQdFdC/SQMal/CKAAKN molar ratio 5:1:0.25) or N4-P* (SQdFdC/SQCKAAKN molar ratio 1:0.01) at different concentrations. All experiments were carried out in duplicate at 25 °C in Dulbecco-PBS (D-PBS) running buffer on the InterMol-IPSIT platform (Châtenay-Malabry, France).

Cell culture

MIA PaCa-2 human pancreatic carcinoma cell line was obtained from the American Type Culture Collection (ATCC, France) and maintained as recommended. Briefly, cells were grown in Dulbecco's Modified Eagle Medium (DMEM, Lonza, Belgium) supplemented with 10% heat-inactivated (56 °C, 30 min) fetal bovine serum (FBS), 2.5% heat-inactivated horse serum (Gibco, France) and 50 U/mL penicillin and 50 U/mL streptomycin (Lonza, France). Cells were maintained in a humid atmosphere at 37 °C with 5% CO_2. Cells were used between passage 3 and 12 after thawing.

Cytotoxicity of nanoparticles

The cytotoxicity of NPs was investigated evaluating the mitochondrial activity, using the 3-(4,5-dimethylthiazol-2-yl)-2,5-diphenyl tetrazolium bromide (MTT) test. MIA PaCa-2 cells (1×10^3 cells *per* well) were incubated in 100 µL of complete culture medium in 96-well plates for 24 h. The cells were then treated with 100 µL of a series of concentrations of **$N0_e$** (SQdFdC), **$N1_a$-P*** (SQdFdC/SQMal/CKAAKN molar ratio 5:1:0.25)**, N4-P*** (SQdFdC/SQCKAAKN molar ratio 1:0.01) or free drug for 72 h. At the end of the incubation period MTT (5 mg/mL in D-PBS) was added. Two h incubation later, the culture medium was gently aspirated and replaced by 200 µL of dimethylsulfoxide in order to dissolve the formazan crystals. The absorbance of the solubilized dye was measured spectrophotometrically with a microplate reader at 570 nm (LAB System Original Multiscan MS). The percentage of viable cells in each well was calculated as

the absorbance ratio between treated and untreated control cells. All experiments were set up in triplicate or more to determine means and SD.

Cell internalization of nanoparticles

MIA PaCa-2 cells (50 x 10^3 cells/mL) were cultured in 12-well plates for 24 h to achieve approximately 40% confluence. Fluorescent NPs (untargeted or linked to CKAAKN) were formulated by adding 1% w/w of the hydrophobic green dye cholesteryl BODIPY FL C12 (BChol-green, Life Technologies, Molecular Probes, France) to the organic solution prior to the nanoprecipitation, allowing them to be traked *in vitro*. Cells were then incubated with an aqueous suspension of either BChol-green-labeled N0 (SQdFdC NPs) or BChol-green-labeled $N1_a$-P* (SQdFdC/SQMal/CKAAKN NPs) or BChol-green-labeled N4-P* (SQdFdC/SQCKAAKN NPs) (1 µM eq. dFdC). Free fluorophore was used as control. After 6 h of incubation, cells were washed twice with Dulbecco's PBS and harvested for measurement by flow cytometry (Accuri C6, BD Biosciences, France). The mean fluorescence intensities were collected between 515 and 545 nm, using the 488-nm line of an argon laser for excitation. For all experiments 10000 cells were measured from each sample.
For low temperature experiments, the cells were incubated in the cold room at 4 °C for 6 h. Results were expressed as the ratio of the mean fluorescence intensity of each sample to the mean fluorescence intensity of non-treated cells. This value was then corrected by the fluorescence factor of each NP suspension. All measurements were performed in triplicate or more to determine means and SD.

Results and Discussion

Preparation and characterization of untargeted nanoparticles

In order to obtain stable CKAAKN-functionalized SQdFdC nanoparticles, the formulation of the colloidal system was deeply investigated by varying the preparation conditions. In particular, a maleimide group-bearing squalene derivative able to link the peptide *via* its thiol function was added to SQdFdC (**1**) in various molar ratios. Moreover, between squalene and the maleimide group two different spacers, a lipophilic or a hydrophilic one, were introduced. In the case of the $SQMal_{lipo}$ (**3**)[30], a 6-carbon atom lipophilic chain served as a spacer, while for the $SQMal_{hydro}$ (**4**)[31], a hydrophilic ether chain was inserted (Figure 2).
All NPs were prepared in accordance with the nanoprecipitation technique, using acetone or ethanol as organic solvent and without adding any surfactant. Maleimide-bearing SQdFdC NPs were prepared adding $SQMal_{lipo}$ or $SQMal_{hydro}$.

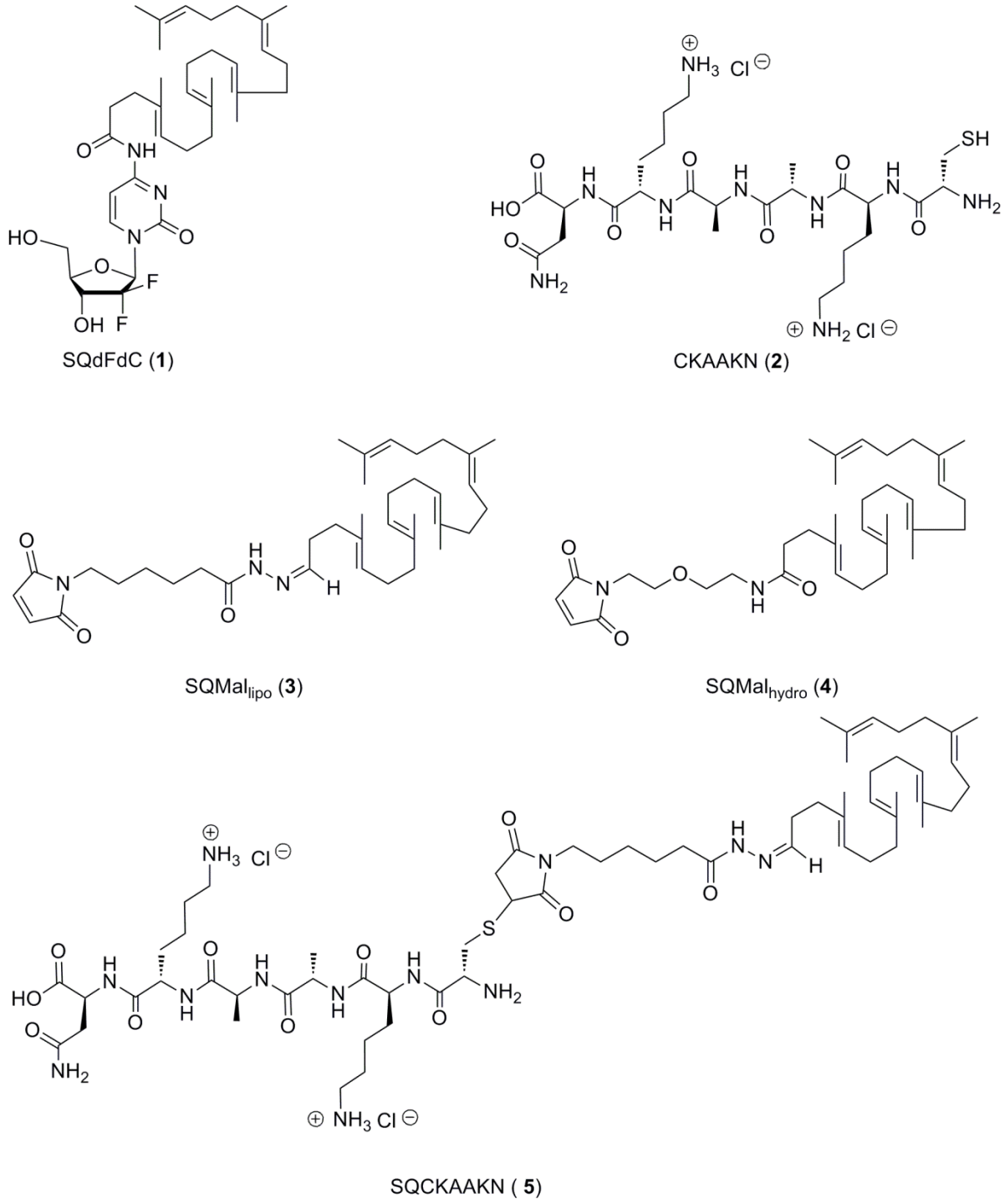

Figure 2. Structure of SQdFdC (**1**), CKAAKN peptide (**2**), SQMal$_{lipo}$ (**3**), SQMal$_{hydro}$ (**4**) and SQCKAAKN (**5**).

SQdFdC and SQMal$_{lipo}$ were co-nanoprecipitated at various SQdFdC/SQMal$_{lipo}$ molar ratios (10:1, 5:1, 2:1) with a constant SQdFdC concentration, giving a suspension of narrow monodispersed NPs (**N1**). Addition of SQMal$_{lipo}$ led to a slight size increase compared to SQdFdC NPs which displayed a mean diameter of 141 nm and 122 nm when prepared in acetone or ethanol, respectively (Table 1).

SQdFdC/SQMal$_{hydro}$ NPs were prepared by co-nanoprecipitation of SQdFdC and SQMal$_{hydro}$ at two molar ratios (10:1, 5:1), with a constant SQdFdC concentration. Ethanol was the best solvent

because acetone was not able to preserve colloidal stability. As for SQdFdC/$SQMal_{lipo}$, these nanoparticles (**N2**) showed a mean diameter lower than 200 nm and a narrow particle size distribution (Table 1). However, the presence of an ether chain between the maleimide and squalene moiety affected the nanoparticle stability, probably due to a modification of the internal inverted hexagonal phase structure of SQdFdC nanoparticles.[35] On the contrary, a higher stability was observed when a lipophilic chain was used as spacer ($SQMal_{lipo}$).
According to these results, the $SQMal_{lipo}$ was preferred to the $SQMal_{hydro}$ for the preparation of peptide-targeted SQdFdC nanoparticles. Among the various SQdFdC/$SQMal_{lipo}$ formulations, the ones prepared in acetone ($\mathbf{N1_a}$) showed higher colloidal stability compared to the $\mathbf{N1_e}$. Using acetone as solvent and a low or medium amount of $SQMal_{lipo}$ (10:1 or 5:1), no precipitation or appreciable size and zeta potential changes were detected after 1-week storage.

Table 1. Nanoparticle composition and characterization.

NPs	*Solvent used in the nanoprecipitation*	*Composition*	*Components molar ratio*	*Mean diameter* (nm ± S.D.)	*Polydispersity index*	*Zeta potential* (mV ± S.D.)	*Stability* at 4 °C (days)
$N0_a$	Acetone	SQdFdC	-	141 ± 42	0.087	-22 ± 4	3
$N0_e$	Ethanol	SQdFdC	-	122 ± 8	0.103	-22 ± 5	3
$N1_a$	Acetone	SQdFdC/$SQMal_{lipo}$	10:1	164 ± 42	0.066	-27 ± 3	7
	Acetone	SQdFdC/$SQMal_{lipo}$	5:1	171 ± 41	0.057	-29 ± 3	7
	Acetone	SQdFdC/$SQMal_{lipo}$	2:1	182 ± 20	0.047	-36 ± 3	3
$N1_{a}$-P	Acetone	SQdFdC/$SQMal_{lipo}$/ CKAAKN	10:1:0.5	281 ± 10	0.134	-15 ± 1	< 3
	Acetone	SQdFdC/$SQMal_{lipo}$/ CKAAKN	10:1:0.25	187 ± 7	0.067	-11 ± 1	< 3
	Acetone	SQdFdC/$SQMal_{lipo}$/ CKAAKN	5:1:0.5	Aggregation	/	/	/
$N1_{a}$-P*	Acetone	SQdFdC/$SQMal_{lipo}$/ CKAAKN	5:1:0.25	245 ± 16	0.141	-10 ± 2	3

$N1_e$	Ethanol	$SQdFdC/SQMal_{lipo}$	10:1	132 ± 9	0.100	-22 ± 7	3
	Ethanol	$SQdFdC/SQMal_{lipo}$	5:1	167 ± 9	0.053	-22 ± 3	3
	Ethanol	$SQdFdC/SQMal_{lipo}$	2:1	Aggregation	/	/	/
N2	Ethanol	$SQdFdC/SQMal_{hydro}$	10:1	183 ± 5	0.055	-16 ± 1	< 3
	Ethanol	$SQdFdC/SQMal_{hydro}$	5:1	177 ± 3	0.053	-25 ± 3	< 3
	Acetone	$SQdFdC/SQMal_{hydro}$	10:1	Aggregation	/	/	/
	Acetone	$SQdFdC/SQMal_{hydro}$	5:1	Aggregation	/	/	/
N3	Acetone	$SQMal_{lipo}$ 0.5 mg/mL	-	600 ± 180	0.091	-56.57 ± 3	7
	Acetone	$SQMal_{lipo}$ 1 mg/mL	-	387 ± 101	0.068	-38.47 ± 3	7
	Acetone	$SQMal_{lipo}$ 2 mg/mL	-	436 ± 148	0.099	-49.81 ± 4	7
N4-P	Ethanol	SQdFdC/SQCKAAKN	1:0.1	186 ± 104	0.032	11 ± 2	< 3

	Ethanol	SQdFdC/SQCKAAKN	1:0.05	897 ± 11	0.332	7 ± 23	< 3
N4-P*	Ethanol	SQdFdC/SQCKAAKN	1:0.01	168 ± 16	0.117	-6 ± 5	3

a NPs formulated using acetone as solvent
e NPs formulated using ethanol as solvent
* Formulations chosen for SPR analysis and *in vitro* studies

$SQMal_{lipo}$ was able to spontaneously self-assemble in water forming nanoparticles (**N3)** having higher mean diameter (400-600 nm) than the one of SQdFdC NPs (Table 1).
Compared to SQdFdC or $SQMal_{lipo}$ NPs, mixed SQdFdC/$SQMal_{lipo}$ NPs showed an intermediate mean diameter with higher colloidal stability, suggesting that the co-nanoprecipitation technique, already used for the preparation of other squalenoyl nanoparticles,[35-37] allowed an efficient incorporation of $SQMal_{lipo}$ in the resulting composite nanoparticles thanks to its squalene chain able to insert in the inner core of nanoparticles. $SQMal_{lipo}$ NPs showed zeta potential values ranging from around -30 to -60 mV. Accordingly, for $N1_a$ (SQdFdC/$SQMal_{lipo}$ NPs prepared using acetone) the zeta potential value gradually decreased (from around -20 to -40 mV) with the increase of $SQMal_{lipo}$ in the formulation (Table 1). When ethanol was used as solvent ($N1_e$), the amount of $SQMal_{lipo}$ did not influence the zeta potential, suggesting that these conditions probably did not allow the presence of maleimide groups on the nanoparticle surface (Figure 1b - *vii*). Although for pure SQdFdC NPs the choice of the solvent did not influence the colloidal characteristics[23,38,39], these results are in concordance with other experiments that highlighted the crucial role of the solvent in the nanoparticle self-organization[40-43] and they further supported the choice of using only the acetone-formulated SQdFdC/$SQMal_{lipo}$ NPs for further investigations.

Preparation and characterization of targeted nanoparticles by coupling CKAAKN peptide to preformed nanoparticles

As mentioned above, the peptide is able to react with the maleimide function of the spacer *via* the cystein thiol group present in its sequence leading to the formation of a stable thioether bond. Moreover, this site of derivatization does not alter the ligand/receptor recognition, because the same function was used for the phage display *in vivo* screening.[29]
Peptide conjugation on preformed nanoparticles allows peptide moieties to be disposed only at the surface of the carriers, thus being more available for the receptor recognition. For this purpose, the peptide thiol group was reacted with maleimide functions of $\mathbf{N1_a}$ (SQdFdC/$SQMal_{lipo}$ molar ratio 10:1 or 5:1, acetone as solvent) in different Mal/peptide molar ratios to obtain $\mathbf{N1_a}$**-P**. Targeted NPs showed a higher mean diameter compared to untargeted ones (Table 1). In addition, in some cases aggregation occurred and/or the stability was very low. The zeta potential value increased with the peptide amount (from -23 to -10 mV) probably due to the presence of two protonable amino groups in the CKAAKN moiety (**2** - Figure 2). SQdFdC/$SQMal_{lipo}$/CKAAKN molar ratio 5:1:0.25 NPs ($\mathbf{N1_a}$**-P*)** showed the highest long-term stability and only this formulation was therefore further studied.
The interaction between the thiol groups and maleimide functions onto $\mathbf{N1_a}$ surface was investigated by isothermal titration calorimetry (ITC) analysis. This technique is widely used in nanotechnology for characterizing thermodynamics and stoichiometry of intermolecular interactions allowing the evaluation of the association constant (K), the stoichiometry, the enthalpy (ΔH) and the entropy (ΔS) from which the Gibbs free energy (ΔG) of the process can be derived.[44-46] The heat flows were determined when peptide aliquots were added to $\mathbf{N0_a}$ (used as control) or $\mathbf{N1_a}$ suspension placed in the titration cell accurately thermostated (Figure 3a). ITC thermograms showed two different signatures: (*i*) a first phenomenon likely related to the non-specific adsorption of the peptide to the nanoparticle surface, (*ii*) a second phenomenon attributed to the interaction with maleimide functions, revealed only in the presence of these groups onto $N1_a$. Such a hypothetical mechanism can be supported by the enthalpograms of the interaction of cysteine and maleimide groups in solution (Figure 3b). Whether the thiol-maleimide Michael addition is happening on the nanoparticle surface (Figure 3b – blue line) or in solution (Figure 3b – black line), the thermodynamics parameters, including the stoichiometry of the interaction, are comparable. Despite the maleimide group is highly specific for thiols, at basic pH some secondary nucleophilic additions from the amine groups present in the two lysines of CKAAKN sequence could take place [47,48], modifying the recognition sequence of the

peptide. For this reason, we also verified that no interactions between lysines and the maleimide groups were established in the same conditions (Figure 3b – grey line).

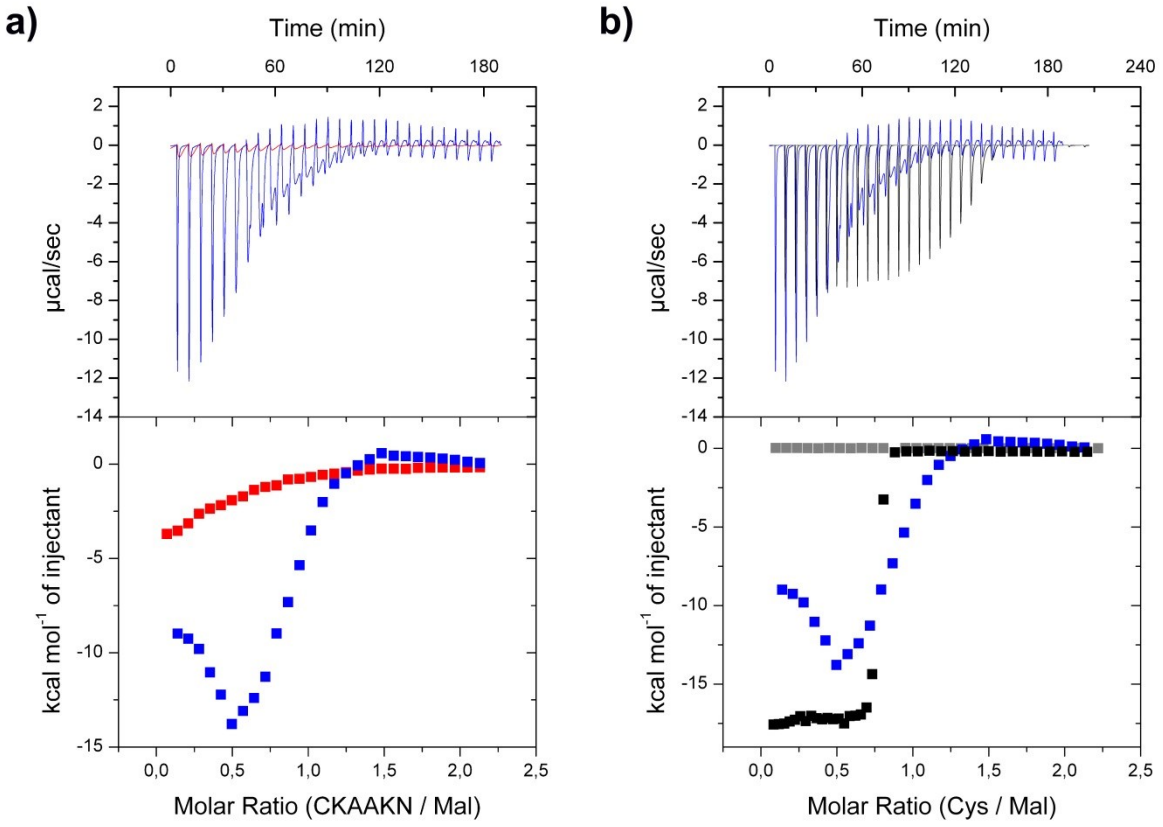

Figure 3. Isothermal titration calorimetry analysis of the interaction between CKAAKN, cysteine (Cys) and maleimide group. The raw and the integrated binding heats are shown in the upper and lower panels, respectively. Heat flows accounting for dilution effects were further subtracted from each experimental heat flow. **a)** ITC thermograms upon injection of CKAAKN solution into either $N0_a$ (red) or $N1_a$ (blue) suspension. **b)** ITC thermograms upon injection of Cys solution into either maleimide solution (black), N1a suspension (blue) or upon injection of lysine into maleimide solution (grey).

Noteworthy is that the Michael addition reaction occurred only from CKAAKN/Mal ratios (N) higher than 0.5, condition that led to the $N1_a$ aggregation likely owing to the instability of peptide scaffold structure at the nanoparticle surface. Thus, since the peptide amount could not be increased, in the case of $N1_a$-P* formulation the ratio used (1:0.25) was not sufficient to obtain a covalent conjugation of the peptide to the nanoparticle surface and we made the hypothesis of the existence of weak noncovalent interactions (demonstrated by ITC in other cases such as bio-molecular recognition or inclusion complexes [44-46]) and that probably the peptide was simply adsorbed at the nanoparticle surface (Figure 1b – *vi*).

Preparation of targeted nanoparticles by coupling CKAAKN to $SQMal_{lipo}$ prior to nanoparticles preparation

In this approach the CKAAKN peptide was previously conjugated to $SQMal_{lipo}$ to give SQCKAAKN bioconjugate (**5**) which was then co-nanoprecipitated with SQdFdC with various

SQdFdC/SQCKAAKN molar ratios (1:0.1, 1:0.05, 1:0.01) leading to formation of targeted NPs (**N4-P)**. In this case only ethanol was used as organic solvent because of the limited solubility of SQCKAAKN in acetone.
The main problem of this synthetic strategy is that the targeting agent could be placed in the nanoparticle core during the nanocarrier formation. Interestingly, the zeta potential gradually increased (from around -22 to +11 mV) with the increase of the percentage of SQCKAAKN in the formulations, suggesting surface distribution of the peptide. As found by DLS analysis, a SQdFdC/SQCKAAKN molar ratio higher than 1:0.01 led to nanoparticle destabilization and aggregation. Hence, SQdFdC/SQCKAAKN 1:0.01 molar ratio NPs (**N4-P***), which showed a decrease of the absolute surface charge compared to untargeted NPs (**N0**) (-6 *vs* -22 mV) and only a slight increase of the mean diameter, were chosen for further investigations. Interestingly, SQdFdC/SQCKAAKN NPs (**N4-P***) showed a marked reduction of the zeta potential value when increasing the pH from 7.4 to 9.8 (Figure 4). This resulted from the deprotonation of the lysine amino groups, suggesting the presence of the peptide onto the surface of the nanoparticles which is a crucial aspect to obtain an efficient cancer cell targeting.

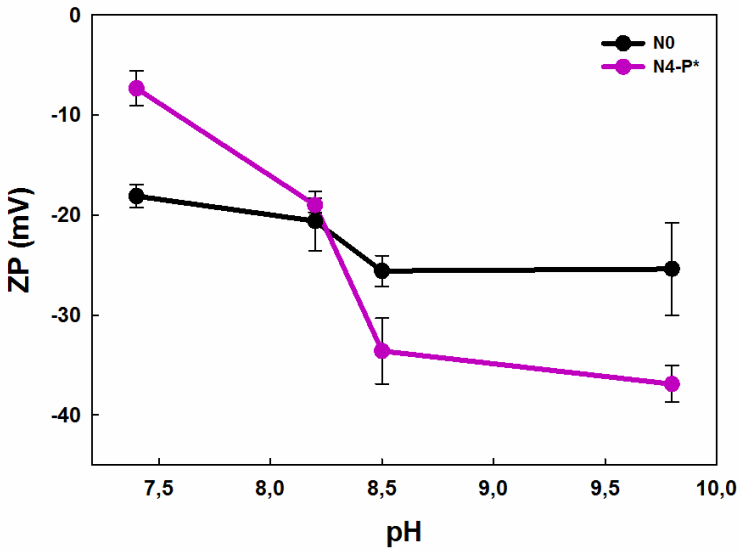

Figure 4. Surface charge of N0 and N4-P* as a function of pH was investigated by zeta potential (ZP) measurement at 25 °C after dilution with 0.02 M phosphate buffer at pH values ranging from 7.4 to 9.8. Values represent mean ± SD, n=3.

Surface plasmon resonance analysis
All the results together suggested that the peptide was associated to preformed nanoparticles by surface adsorption for **N1$_a$-P*** while it was covalently conjugated to the nanoparticle surface for **N4-P***. Covalent conjugation, in contrast to adsorption, ensures a stronger association between nanoparticles and the target, especially after *in vivo* admistration. However, also ligand association to the nanoparticle by weak interactions or surface adsorption has been proven as an alternative strategy to tailor targeted nanoparticles.[49,50] Therefore, both coupling strategies were further investigated and the peptide targeting capability in **N1$_a$-P*** and **N4-P*** was evaluated by analyzing the ability to recognize the biological target receptor by surface plasmon resonance. Since it was reported that the sequence CKA-K shared motifs with the Wnt-2 protein[29], sFRP-4, a secreted frizzled-related protein that binds Wnt-2, was immobilized onto the sensor chip surface.[30,51] Ability of the CKAAKN peptide to specifically interact with the sensor chip-

immobilized sFRP-4 was also verified.[30] Although both **N1$_a$-P*** and **N4-P*** were able to specifically interact with the receptor (which was not the case for untargeted **N1$_a$**), only **N4-P*** enabled to reach a more important plasmonic signal with a dose-response behavior after PBS washing (Figure 5).[30]

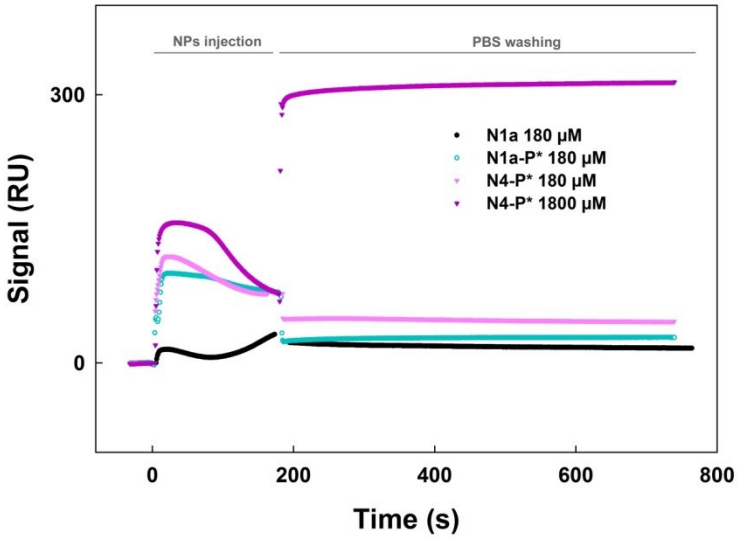

Figure 5. SPR sensorgrams (resonance units (RU) *versus* time) obtained by simultaneous injections of unfunctionalized SQdFdC/SQMal$_{lipo}$ 5:1 NPs (**N1$_a$**) 180 µM, SQdFdC/SQMal$_{lipo}$/CKAAKN 5:1:0.25 NPs (**N1$_a$-P***) 180 µM**,** SQdFdC/SQCKAAKN 1:0.01 NPs (**N4-P***) 180 and 1800 µM over sFRP-4 immobilized on two parallel channels of the same sensor chip.

The enhanced target binding and specific avidity of **N4-P*** suggested that the peptide conjugation prior to nanocarrier formation was more suitable to obtain enhanced binding and avidity that ensures stronger association between nanoparticle and target. This is of significance since earlier studies[18,52-56] showed that the binding of a surface-conjugated nanoparticle to its target is not only relied to the presence of the ligand on nanoparticles surface, but it is a complex mechanism that depends on physico-chemical surface properties in which the ligand content and density at the surface, the hydrophilic/hydrophobic balance and nanoparticle surface charge are also involved.

In vitro tests

In order to confirm the SPR results, the tumor targeting ability as a function of the synthetic strategy was evaluated *in vitro*. The internalization of CKAAKN-functionalized NPs into human pancreatic tumor cells MIA PaCa-2 was evaluated. Cells were incubated for 6 h with BChol-green-labeled **N0**, BChol-green-labeled **N1$_a$-P*** or BChol-green-labeled **N4-P***.

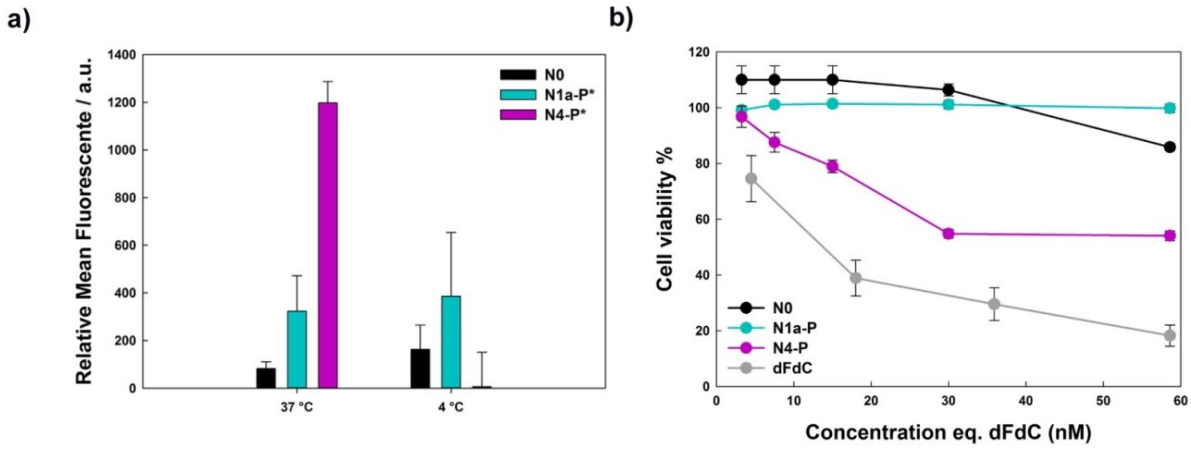

Figure 6. a) Cellular uptake quantification of SQdFdC NPs (**N0)**, SQdFdC/SQMal$_{lipo}$/CKAAKN 5:1:0.25 NPs (**N1$_a$-P***) and SQdFdC/SQCKAAKN 1:0.01 NPs (**N4-P***) after 6-h incubation at 37 and 4 °C. All NPs were labeled with BChol-green and incubated at a final concentration of 1 µM eq. SQdFdC. **b)** Cell viability of cells treated with increasing concentrations of dFdC as free drug (**dFdC**), SQdFdC NPs (**N0**), SQdFdC/SQMal$_{lipo}$/CKAAKN 5:1:0.25 NPs (**N1$_a$-P***) or SQdFdC/SQCKAAKN 1:0.01 NPs (**N4-P*)** for 72 h. Cytotoxicity of nanoparticles was compared to non-treated cells. Values represent mean ± SEM.

Although slight differences were detected after treatment with **N0** and **N1$_a$-P***, remarkably the cell fluorescence intensity after **N4-P*** treatment appeared to be around 14–fold higher compared with both **N0**[30] and **N1$_a$-P*** (Figure 6a). These results clearly indicated a more efficient internalization of **N4-P*** in comparison to **N1$_a$-P*** in MIA PaCa-2 cells.
When cells were incubated at 4 °C, the internalization of **N4-P*** dramatically decreased, suggesting that peptide-NPs were internalized *via* an energy dependent route. The internalization of the nanocarrier is a key issue for the drug to be efficient.[57] Thus, in order to investigate whether the peptide functionalization enabled to achieve an increased drug efficacy compared to the one of untargeted NPs, the *in vitro* cytotoxicity of the different NPs and the free drug was investigated. It is not surprising that all NPs were less cytotoxic than free dFdC due to their prodrug nature. **N4-P*** conducted to an important higher cytotoxicity compared to both **N0** and **N1$_a$-P*** (Figure 6b). It is worth mentioning that for **N4-P*** the half maximal inhibitory concentration (IC$_{50}$) was already reached at 30 nM (eq. dFdC), while untargeted **N0** were not efficient in killing cancer cells in these conditions.[30] These results clearly demonstrated the ability of CKAAKN-functionalized NPs not only to exert a pharmacological activity inside the cell, but also to significantly enhance the cytotoxicity of SQdFdC NPs. As expected, according to the ITC, SPR and internalization results, **N1$_a$-P*** did not improve cytotoxicity in comparison to **N0** treatment, thus suggesting the absence of effective and specific tumor targeting ability when the peptide is only adsorbed at the NP surface.

Conclusions

This study demonstrates that the best strategy to prepare CKAAKN-functionalized SQdFdC NPs relies in the conjugation of the peptide to the $SQMal_{lipo}$ derivative prior nanoparticles formation. Taken together, our results clearly highlight that actively targeted nanoparticles should not be simply designed as largely modular assemblies of scaffold, linker and targeting ligand, but rigorous studies must be performed in order to clarify how different structural components collaborate to determine the real ligand affinity. In a nutshell, the successful functionalization of SQdFdC nanoparticles makes this system a good example to highlight the subtle equilibrium which governs the design of actively targeted NPs able to effectively improve anticancer activity.

Acknowledgements

The authors warmly thank Dr. Emeric Gueneau (GE Healthcare, Life Sciences) for helpful discussion in ITC and SPR analysis. This work was supported by MIUR - University of Turin "Fondi Ricerca Locale (ex-60%)" and by the European Research Council under the European Community's Seventh Framework Programme FP7/2007-2013 Grant Agreement N°249835. The authors acknowledge the Università Italo Francese/Université Franco Italienne for the PhD co-tutoring agreement to S.V.

References

1. Hanahan, D.; Weinberg, R. A. Hallmarks of cancer: the next generation. *Cell* **2011**, 144, 646-74.
2. Krause, D. S.; Van Etten, R. A. Tyrosine kinases as targets for cancer therapy. *N Engl J Med* **2005**, 353, 172-87.
3. Collins, I.; Workman, P. New approaches to molecular cancer therapeutics. *Nat Chem Biol* **2006**, 2, 689-700.
4. Chari, R. V. Targeted cancer therapy: conferring specificity to cytotoxic drugs. *Acc Chem Res* **2008**, 41, 98-107.
5. Dosio, F.; Brusa, P.; Cattel, L. Immunotoxins and anticancer drug conjugate assemblies: the role of the linkage between components. *Toxins (Basel)* **2011**, 3, 848-83.
6. Flygare, J. A.; Pillow, T. H.; Aristoff, P. Antibody-drug conjugates for the treatment of cancer. *Chem Biol Drug Des* **2013**, 81, 113-21.
7. http://www.fda.gov/NewsEvents/Newsroom/PressAnnouncements /ucm268781.htm.
8. http://www.medscape.com/viewarticle/779751.
9. Wang, M.; Thanou, M. Targeting nanoparticles to cancer. *Pharmacol. Res.* **2010**, 62, 90-99.
10. Montet, X.; Funovics, M.; Montet-Abou, K.; Weissleder, R.; Josephson, L. Multivalent effects of RGD peptides obtained by nanoparticle display. *J Med Chem* **2006**, 49, 6087-93.
11. Nicolas, J.; Mura, S.; Brambilla, D.; Mackiewicz, N.; Couvreur, P. Design, functionalization strategies and biomedical applications of targeted biodegradable/biocompatible polymer-based nanocarriers for drug delivery. *Chem Soc Rev* **2013**, 42, 1147-235.
12. Valetti, S.; Mura, S.; Stella, B.; Couvreur, P. Rational design for multifunctional non-liposomal lipid-based nanocarriers for cancer management: theory to practice. *Journal of Nanobiotechnology* **2013**, 11, S6.
13. Peer, D.; Karp, J. M.; Hong, S.; Farokhzad, O. C.; Margalit, R.; Langer, R. Nanocarriers as an emerging platform for cancer therapy. *Nat Nanotechnol* **2007**, 2, 751-60.
14. Davis, M. E.; Chen, Z. G.; Shin, D. M. Nanoparticle therapeutics: an emerging treatment modality for cancer. *Nat Rev Drug Discov* **2008**, 7, 771-82.
15. Cheng, Z.; Al Zaki, A.; Hui, J. Z.; Muzykantov, V. R.; Tsourkas, A. Multifunctional nanoparticles: cost versus benefit of adding targeting and imaging capabilities. *Science* **2012**, 338, 903-10.
16. Lammers, T.; Kiessling, F.; Hennink, W. E.; Storm, G. Drug targeting to tumors: principles, pitfalls and (pre-) clinical progress. *J Control Release* **2012**, 161, 175-87.
17. Bae, Y.; Nishiyama, N.; Kataoka, K. In vivo antitumor activity of the folate-conjugated pH-sensitive polymeric micelle selectively releasing adriamycin in the intracellular acidic compartments. *Bioconjug Chem* **2007**, 18, 1131-9.
18. Tassa, C.; Duffner, J. L.; Lewis, T. A.; Weissleder, R.; Schreiber, S. L.; Koehler, A. N.; Shaw, S. Y. Binding affinity and kinetic analysis of targeted small molecule-modified nanoparticles. *Bioconjug Chem* **2010**, 21, 14-9.
19. Canovi, M.; Markoutsa, E.; Lazar, A. N.; Pampalakis, G.; Clemente, C.; Re, F.; Sesana, S.; Masserini, M.; Salmona, M.; Duyckaerts, C.; Flores, O.; Gobbi, M.; Antimisiaris, S. G. The binding affinity of anti-Abeta1-42 MAb-decorated nanoliposomes to Abeta1-42 peptides in vitro and to amyloid deposits in post-mortem tissue. *Biomaterials* **2011**, 32, 5489-97.
20. Huwyler, J.; Wu, D.; Pardridge, W. M. Brain drug delivery of small molecules using immunoliposomes. *Proc Natl Acad Sci U S A* **1996**, 93, 14164-9.

21. Le Droumaguet, B.; Souguir, H.; Brambilla, D.; Verpillot, R.; Nicolas, J.; Taverna, M.; Couvreur, P.; Andrieux, K. Selegiline-functionalized, PEGylated poly(alkyl cyanoacrylate) nanoparticles: Investigation of interaction with amyloid-beta peptide and surface reorganization. *International Journal of Pharmaceutics* **2011**, 416, 453-460.
22. Fakhari, A.; Baoum, A.; Siahaan, T. J.; Le, K. B.; Berkland, C. Controlling ligand surface density optimizes nanoparticle binding to ICAM-1. *J Pharm Sci* **2011**, 100, 1045-56.
23. Couvreur, P.; Stella, B.; Reddy, L. H.; Hillaireau, H.; Dubernet, C.; Desmaele, D.; Lepetre-Mouelhi, S.; Rocco, F.; Dereuddre-Bosquet, N.; Clayette, P.; Rosilio, V.; Marsaud, V.; Renoir, J. M.; Cattel, L. Squalenoyl nanomedicines as potential therapeutics. *Nano Lett.* **2006**, 6, 2544-8.
24. Oberstein, P. E.; Saif, M. W. First-line treatment for advanced pancreatic cancer. Highlights from the "2011 ASCO Gastrointestinal Cancers Symposium". San Francisco, CA, USA. January 20-22, 2011. *JOP* **2011**, 12, 96-100.
25. Reddy, L. H.; Renoir, J. M.; Marsaud, V.; Lepetre-Mouelhi, S.; Desmaele, D.; Couvreur, P. Anticancer efficacy of squalenoyl gemcitabine nanomedicine on 60 human tumor cell panel and on experimental tumor. *Mol Pharm* **2009**, 6, 1526-35.
26. Reddy, L. H.; Ferreira, H.; Dubernet, C.; Mouelhi, S. L.; Desmaele, D.; Rousseau, B.; Couvreur, P. Squalenoyl nanomedicine of gemcitabine is more potent after oral administration in leukemia-bearing rats: study of mechanisms. *Anticancer Drugs* **2008**, 19, 999-1006.
27. Rejiba, S.; Reddy, L. H.; Bigand, C.; Parmentier, C.; Couvreur, P.; Hajri, A. Squalenoyl gemcitabine nanomedicine overcomes the low efficacy of gemcitabine therapy in pancreatic cancer. *Nanomedicine* **2011**, 7, 841-9.
28. Hidalgo, M. Pancreatic cancer. *N Engl J Med* **2010**, 362, 1605-17.
29. Joyce, J. A.; Laakkonen, P.; Bernasconi, M.; Bergers, G.; Ruoslahti, E.; Hanahan, D. Stage-specific vascular markers revealed by phage display in a mouse model of pancreatic islet tumorigenesis. *Cancer Cell.* **2003**, 4, 393-403.
30. Valetti, S.; Maione, F.; Mura, S.; Stella, B.; Desmaele, D.; Noiray, M.; Vergnaud, J.; Vauthier, C.; Cattel, L.; Giraudo, E.; Couvreur, P. Peptide-functionalized nanoparticles for selective targeting of pancreatic tumor. *Submitted* **2013**.
31. Raouane, M.; Desmaele, D.; Gilbert-Sirieix, M.; Gueutin, C.; Zouhiri, F.; Bourgaux, C.; Lepeltier, E.; Gref, R.; Ben Salah, R.; Clayman, G.; Massaad-Massade, L.; Couvreur, P. Synthesis, characterization, and in vivo delivery of siRNA-squalene nanoparticles targeting fusion oncogene in papillary thyroid carcinoma. *J Med Chem* **2011**, 54, 4067-76.
32. Fessi, H.; Puisieux, F.; Devissaguet, J. P.; Ammoury, N.; Benita, S. Nanocapsule formation by interfacial polymer deposition following solvent displacement. *International Journal of Pharmaceutics* **1989**, 55, R1-R4.
33. Othman, M.; Bouchemal, K.; Couvreur, P.; Gref, R. Microcalorimetric investigation on the formation of supramolecular nanoassemblies of associative polymers loaded with gadolinium chelate derivatives. *Int J Pharm* **2009**, 379, 218-25.
34. Segura-Sanchez, F.; Bouchemal, K.; Lebas, G.; Vauthier, C.; Santos-Magalhaes, N. S.; Ponchel, G. Elucidation of the complexation mechanism between (+)-usnic acid and cyclodextrins studied by isothermal titration calorimetry and phase-solubility diagram experiments. *J Mol Recognit* **2009**, 22, 232-41.
35. Bekkara-Aounallah, F.; Gref, R.; Othman, M.; Reddy, L. H.; Pili, B.; Allain, V.; Bourgaux, C.; Hillaireau, H.; Lepêtre-Mouelhi, S.; Desmaële, D.; Nicolas, J.; Chafi, N.; Couvreur, P. Novel PEGylated Nanoassemblies Made of Self-Assembled Squalenoyl Nucleoside Analogues. *Advanced Functional Materials* **2008**, 18, 3715-3725.
36. Trung Bui, D.; Maksimenko, A.; Desmaele, D.; Harrisson, S.; Vauthier, C.; Couvreur, P.; Nicolas, J. Polymer prodrug nanoparticles based on naturally occurring isoprenoid for anticancer therapy. *Biomacromolecules* **2013**, 14, 2837-47.

37. Bui, D. T.; Nicolas, J.; Maksimenko, A.; Desmaele, D.; Couvreur, P. Multifunctional squalene-based prodrug nanoparticles for targeted cancer therapy. *Chem Commun (Camb)* **2013**.
38. Desmaële, D.; Gref, R.; Couvreur, P. Squalenoylation: A generic platform for nanoparticular drug delivery. *Journal of Controlled Release* **2011**, doi:10.1016/j.jconrel.2011.07.038.
39. Lepeltier, E.; Bourgaux, C.; Rosilio, V.; Poupaert, J. H.; Meneau, F.; Zouhiri, F.; Lepetre-Mouelhi, S.; Desmaele, D.; Couvreur, P. Self-Assembly of Squalene-Based Nucleolipids: Relating the Chemical Structure of the Bioconjugates to the Architecture of the Nanoparticles. *Langmuir* **2013**.
40. Ganachaud, F.; Katz, J. L. Nanoparticles and nanocapsules created using the Ouzo effect: Spontaneous emulsification as an alternative to ultrasonic and high-shear devices. *Chemphyschem* **2005**, 6, 209-216.
41. Yu, W.; Doegito, E. S. T.; Barratt, G.; Fessi, H.; Devissaguet, J. P.; Puisieux, F. A Novel-Approach to the Preparation of Injectable Emulsions by a Spontaneous Emulsification Process. *International Journal of Pharmaceutics* **1993**, 89, 139-146.
42. Bouchemal, K.; Briancon, S.; Perrier, E.; Fessi, H. Nano-emulsion formulation using spontaneous emulsification: solvent, oil and surfactant optimisation. *International Journal of Pharmaceutics* **2004**, 280, 241-251.
43. Legrand, P.; Lesieur, S.; Bochot, A.; Gref, R.; Raatjes, W.; Barratt, G.; Vauthier, C. Influence of polymer behaviour in organic solution on the production of polylactide nanoparticles by nanoprecipitation. *Int J Pharm* **2007**, 344, 33-43.
44. Bouchemal, K. New challenges for pharmaceutical formulations and drug delivery systems characterization using isothermal titration calorimetry. *Drug Discov Today* **2008**, 13, 960-72.
45. Mazzaferro, S.; Bouchemal, K.; Gallard, J. F.; Iorga, B. I.; Cheron, M.; Gueutin, C.; Steinmesse, C.; Ponchel, G. Bivalent sequential binding of docetaxel to methyl-beta-cyclodextrin. *Int J Pharm* **2011**, 416, 171-80.
46. Agostoni, V.; Chalati, T.; Horcajada, P.; Willaime, H.; Anand, R.; Semiramoth, N.; Baati, T.; Hall, S.; Maurin, G.; Chacun, H.; Bouchemal, K.; Martineau, C.; Taulelle, F.; Couvreur, P.; Rogez-Kreuz, C.; Clayette, P.; Monti, S.; Serre, C.; Gref, R. Towards an Improved anti-HIV Activity of NRTI via Metal-Organic Frameworks Nanoparticles. *Adv Healthc Mater* **2013**, 2, 1630-7.
47. Hermanson, G. T. *Bioconjugate Techniques*. First, Academic Press: San Diego, **1996**.
48. Furgeson, D. Y.; Dreher, M. R.; Chilkoti, A. Structural optimization of a "smart" doxorubicin-polypeptide conjugate for thermally targeted delivery to solid tumors. *J Control Release* **2006**, 110, 362-9.
49. Avvakumova, S.; Colombo, M.; Tortora, P.; Prosperi, D. Biotechnological approaches toward nanoparticle biofunctionalization. *Trends Biotechnol* **2014**, 32, 11-20.
50. Occhipinti, E.; Verderio, P.; Natalello, A.; Galbiati, E.; Colombo, M.; Mazzucchelli, S.; Salvade, A.; Tortora, P.; Doglia, S. M.; Prosperi, D. Investigating the structural biofunctionality of antibodies conjugated to magnetic nanoparticles. *Nanoscale* **2011**, 3, 387-90.
51. Wawrzak, D.; Metioui, M.; Willems, E.; Hendrickx, M.; de Genst, E.; Leyns, L. Wnt3a binds to several sFRPs in the nanomolar range. *Biochem Biophys Res Commun* **2007**, 357, 1119-23.
52. Cedervall, T.; Lynch, I.; Lindman, S.; Berggard, T.; Thulin, E.; Nilsson, H.; Dawson, K. A.; Linse, S. Understanding the nanoparticle-protein corona using methods to quantify exchange rates and affinities of proteins for nanoparticles. *Proc Natl Acad Sci U S A* **2007**, 104, 2050-5.

53. Lundqvist, M.; Stigler, J.; Elia, G.; Lynch, I.; Cedervall, T.; Dawson, K. A. Nanoparticle size and surface properties determine the protein corona with possible implications for biological impacts. *Proc Natl Acad Sci U S A* **2008**, 105, 14265-70.
54. Blanchette, C. D.; Fischer, N. O.; Corzett, M.; Bench, G.; Hoeprich, P. D. Kinetic Analysis of His-Tagged Protein Binding to Nickel-Chelating Nanolipoprotein Particles. *Bioconjugate Chem.* **2010**, 21, 1321-1330.
55. Mourtas, S.; Canovi, M.; Zona, C.; Aurilia, D.; Niarakis, A.; La Ferla, B.; Salmona, M.; Nicotra, F.; Gobbi, M.; Antimisiaris, S. G. Curcumin-decorated nanoliposomes with very high affinity for amyloid-beta1-42 peptide. *Biomaterials* **2011**, 32, 1635-45.
56. Choi, C. H.; Alabi, C. A.; Webster, P.; Davis, M. E. Mechanism of active targeting in solid tumors with transferrin-containing gold nanoparticles. *Proc Natl Acad Sci U S A* **2010**, 107, 1235-40.
57. Hillaireau, H.; Couvreur, P. Nanocarriers' entry into the cell: relevance to drug delivery. *Cell Mol Life Sci* **2009**, 66, 2873-96.

Chapter 3:

“Multi-therapeutic nanoparticles for synergistic combined therapy with gemcitabine and tyrosine kinase inhibitor”

Multi-therapeutic nanoparticles for synergistic combined therapy with gemcitabine and tyrosine kinase inhibitor

Sabrina Valetti [a, b], *Eric Buchi* [a], *Didier Desmaële* [a], *Claire Guetin* [a], *Barbara Stella* [b], *Patrick Couvreur* [a], *Simona Mura* [a]

(Article in preparation)

[a] Université Paris-Sud, Faculté de Pharmacie, 5 rue Jean-Baptiste Clément, 92296 Châtenay-Malabry cedex, France
CNRS UMR 8612, Institut Galien Paris-Sud, 5 rue Jean-Baptiste Clément, 92296 Châtenay-Malabry cedex, France

[b] Dipartimento di Scienza e Tecnologia del Farmaco, Università di Torino, 9 via Pietro Giuria 10125 Torino, Italy

Abstract

Combined therapy with gemcitabine and tyrosine-kinase inhibitors (*i.e.,* erlotinib and/or sunitinib), has already demonstrated important benefits in pancreatic cancer treatment. In this view, an attractive approach relies on the use of nanoparticles (NPs) which enable (*i*) the co-existence in a single nanocarrier of drugs with different mechanisms of action and pharmacokinetic profiles and (*ii*) the fine tuning of their release rate overcoming the rapid clearance often observed with free drugs. Taking advantages from the "squalenoylation technology", we designed multi-therapeutic nanoparticles by combining the gemcitabine-squalene bioconjugate (SQdFdC) with erlotinib (Erl) and sunitinib (Sun) by different formulating strategies in accordance to their physico-chemical properties. Cytotoxic activity of combined therapy NPs was evaluated *in vitro* on pancreatic cancer cells. Sun-loaded SQdFdC NPs led to a significant increase of the cell toxicity compared to NPs in monotherapy. Remarkably, the synergistic effect between the two co-loaded drugs and the role of exposure schedule highlighted the advantage offered by the NP-mediated drug-codelivery to achieve a synergistic interaction that led to a reduction of the required effective dose to achieve the same final antitumor effect.

Introduction

Despite the progress in the field of cancer treatments, pancreatic cancer remains a lethal disease for which chemotherapy offers minimal benefit leading to a median survival of less than 6 months and a maximum of 5 years for the 6% of patients.[1] So far, the only potentially curative therapy is surgical resection for which, however, only the 20% of pancreatic cancer patients is eligible, making it the fourth leading cause of cancer-related death in Europe and United States.[2] Gemcitabine (dFdC), a nucleoside analogue that blocks the DNA replication, is currently the first line treatment for advanced pancreatic cancer in the clinical practice in spite of a limited response rate of only 5%.[3, 4] Gemcitabine drawbacks mainly arise from a rapid blood inactivation which dramatically decreases plasma half-life[5] and from the downregulation of its membrane transporter leading to a reduced cellular internalization.[6] In addition, pancreatic cancer cells display accumulation of several genetic alterations[7] responsible of multi-drug resistance phenomena which cause (*i*) an increase of the doses required to achieve the therapeutic effect and (*ii*) the consequent insurgence of intolerable toxicity on healthy tissues. According to this complexity and heterogeneity, the simultaneous co-administration of two or more drugs (*i.e.,* combined therapy (CT)) may be an attractive strategy to realize an effective treatment. Co-delivered drugs, interacting with multiple targets, different signaling pathways and various cell subpopulations, may exert a synergistic effect which could lead to a reduction of the required effective dose of each molecule and the associated side effects. In this context, platinum based agents, taxanes, topoisomerase or tyrosine-kinase inhibitors (TKIs) have been associated to gemcitabine in several clinical trials.[1, 8] TKIs are small-molecule agents that block the activity of tyrosine kinase receptors, which are involved in the regulation of different cell functions (*e.g*., proliferation and migration) and show a crucial role in oncogenesis.[9] For instance, among the various tyrosine kinase receptors, the epidermal growth factor receptors (EGFRs), the vascular endothelial growth factor receptors (VEGFs) and the platelet-derived growth factor receptors (PDGFRs) play a critical role in promoting angiogenesis in solid tumors.[10] Combined therapy with gemcitabine and erlotinib (Erl) (*i.e*., EGFR-TKI) demonstrated statistically significant benefits in overall survival compared to monotherapy[11] and has obtained the FDA approval for pancreatic cancer treatment.[12] In parallel, also the sunitinib (Sun) malate, currently administered in monotherapy for the treatment of advanced renal cell carcinoma, imatinib-refractory gastrointestinal tumor and advanced pancreatic neuroendocrine cancer[13], showed improved efficacy when combined with gemcitabine.[14] Noteworthy is that the sunitinib exerts its anti-tumor and anti-angiogenic action by inhibiting VEGFR1–3 and PDGF receptors,[15-18] whose genetic mutations have been correlated with poor prognosis in pancreatic cancer patients.[19]

However, the specific pharmacokinetic profile and the bioavailability of each drug highly hinder the possibility to achieve a synergistic effect with a conventional combined therapy (*i.e.,* co-administration of two (or more) free drug molecules). In this context, nanotechnology-based combined drug delivery may represent a suitable alternative[20] enabling (*i*) the co-existence in a single nanocarrier of drugs with different mechanisms of action and pharmacokinetic profiles and (*ii*) finely tuning their release rate overcoming the rapid clearance often observed with free drugs.[21] Moreover, this approach holds the promise to modify favorably the biodistribution of each drug and improve their therapeutic efficacy. Emergent evidences showed that treatments with erlotinib and sunitinib as free drugs are associated with severe cutaneous toxicity, mucositis and diarrhea mainly related to their administration *per os*.[22-25] In addition, sunitinib activity versus multiple molecular targets causes side effects on healthy tissues leading to cardiotoxicity, hypertension and neutropenia.[26,27] To overcome these issues, both erlotinib[28-30] and sunitinib-loaded[31,32] nanocarriers have already been prepared, allowing to achieve an higher activity on targeted cancer cells with reduction of toxicity.

In this perspective, we have designed a novel nanoscale drug delivery system for a combined therapy with gemcitabine and TKIs (*i.e.,* erlotinib or sunitinib). We have previously reported the development of a prodrug approach (the so-called "*squalenoylation concept*") by chemically

coupling squalene to gemcitabine. Surprisingly, the gemcitabine-squalene bioconjugate (SQdFdC) demonstrated the ability to self-assemble in aqueous medium in the form of nanoparticles. After intravenous administration, these nanoparticles with a drug loading of almost 50% (w/w) exhibited impressively greater anticancer activity than gemcitabine against different experimental tumor models.[33-36] TKIs exert their action by interacting with the intracellular adenosine triphosphate-binding site of the tyrosine kinase receptors.[15,37,38] According to the impressive uptake of SQdFdC NPs in cancer cells, the proposed combined therapy SQdFdC/TKIs aimed to improve the intracellular concentration of TKIs, thus enhancing their effectiveness and reduce the side effects currently observed in clinical practice. Combined therapy nanoparticles were formulated by two different strategies according to their specific physico-chemical properties. Erlotinib, a quinazoline-based molecule, was encapsulated as a free drug into SQdFdC NPs, while sunitinib, a oxindol-based drug, was covalently conjugated to squalene leading to the formation of a squalenoyl prodrug that was co-formulated with SQdFdC. Cytotoxic activity of nanoparticles was evaluated *in vitro* on pancreatic cancer cells. In addition, the synergistic effect between the two co-loaded drugs and the role of exposure schedule were investigated for their potential relevance for a future preclinical translation.

Materials and Methods

Chemicals and instruments

Erlotinib was purchased from CMS Chemicals (UK). Gemcitabine **(1)** hydrochloride and sunitinib malate were purchased from Sequoia Research Products Ltd (UK). 4-(*N*)-trisnorsqualenoyl-gemcitabine (SQdFdC, **(6)**) was obtained as previously reported.[35] Trisnorsqualene-MePEG (SQPEG, **(8)**) was synthetized by alkylation of the sodium alkoxide of MePEG (MW 2000) with 1,1′,2-trisnorsqualenyl methanesulfonate.[39] Squalene, *p*-toluenesulfonic acid and all other reagents were obtained by Sigma (France). NaHMDS and chloromethyl chlorosulfate were purchased from Alfa Aesar (France). All solvents used were of analytical grade from VWR (France). Diethyl ether and tetrahydrofuran (THF) were distilled from sodium/benzophenone ketyl. Methanol and ethanol were dried over magnesium and distilled. DMF and CH_2Cl_2 were distilled from calcium hydride, under a nitrogen atmosphere.
All reactions involving air- or water-sensitive compounds were routinely conducted in glassware which was flame-dried under a positive pressure of nitrogen.
IR spectra were obtained as solid or neat liquid on a Fourier Transform Bruker Vector 22 spectrometer. Only significant absorptions are listed. The ^1H and ^{13}C NMR spectra were recorded on a Bruker Avance 300 (300 MHz and 75 MHz, for ^1H and ^{13}C, respectively) or a Bruker Avance 400 (400 MHz and 100 MHz, for ^1H and ^{13}C, respectively) spectrometer. Recognition of methyl, methylene, methine, and quaternary carbon nuclei in ^{13}C NMR spectra rests on the J-modulated spin-echo sequence. Mass spectra were recorded on a Bruker Esquire-LC. Analytical thin-layer chromatography was performed on Merck silica gel 60F254 glass precoated plates (0.25 mm layer). Column chromatography was performed on Merck silica gel 60 (230-400 mesh ASTM).

Synthesis and characterization of N-(3-ethynylphenyl)-6,7-bis(2-methoxyethoxy)4-quinazolinaminium p-toluenesulfonate salt (ErlTs salt, (3))

Erl **(2)** (12.5 mg, 31.8 μmol) was added to a methanolic solution of *p*-toluenesulfonic acid (6.04 mg, 31.8 μmol, 1 equiv). The mixture was kept for 10 min at room temperature and then 10 min at -4 °C to facilitate crystals formation. The solvent was taken up to give the erlotinib-tosylate salt **(3)** as a pale yellow solid. The ErlTs salt solubility was tested in water, ethanol and acetone at room temperature.
^1H NMR (300 MHz, CD_3OD) δ = 8.68 (s, 1H, H-2), 8.00 (s, 1H, H-8), 7.86 (br s, 1H, H-2'), 7.73-7.68 (m, 3H, H-4', $TolSO_3$), 7.48-7.41 (m, 2H, H-5', H-6'), 7.26 (s, 1H, H-5), 7.21 (d, 2H, J = 8.4 Hz, $TolSO_3$), 4.38 (t, 4H, J = 4.5 Hz, $CH_3OCH_2CH_2OAr$), 3.90-3.85 (m, 4H, $CH_3OCH_2CH_2OAr$), 3.59 (s, 1H, C≡CH), 3.48 (s, 3H, OMe), 3.46 (s, 3H, OMe), 2.36 (s, 3H, CH_3PhSO_3).

Synthesis and characterization of N-(3-ethynylphenyl)-6,7-bis(2-methoxyethoxy)4-quinazolinaminium trisnorsqualenate salt (ErlSQ salt, (4))

Erl **(2)** (4.9 mg, 12.5 μmol) was added to a methanolic solution of trisnorsqualenoic acid (5 mg, 12.5 μmol, 1 equiv). The mixture was allowed to stir for 10 min at room temperature and then it was concentrated under reduced pressure. The residue was taken into diethyl ether and washed multiple times with water. The resulting organic layer was dried over $MgSO_4$, filtered, concentrated under reduced pressure and dried under vacuum to give the ErlSQ salt **(4)** as a translucent waxy material. The ErlSQ salt solubility was tested in water, ethanol and acetone at room temperature.

^{1}H NMR (300 MHz, $CDCl_3$) a 1:2 ratio between erlotinib and squalenic acid was observed δ = 8.64 (s, 1H, H-2), 7.84 (br s, 1H, H-2'), 7.74 (d, J = 8.4 Hz, 1H, H-4'), 7.54 (t, J = 7.8 Hz, 1H, H-5'), 7.29-7.21 (m, 3 H, H-8, H-5, H-6'), 5.25-5.05 (m, 10 H, CH=C(CH_3)), 4.30 (t, 4H, J = 4.6 Hz, $CH_3OCH_2CH_2OAr$), 3.90-3.82 (m, 4H, $CH_3OCH_2CH_2OAr$), 3.49 (s, 3H, OMe), 3.48 (s, 3H, OMe), 3.09 (s, 1H, C≡CH), 2.46–2.40 (m, 4H, $O_2CCH_2CH_2$), 2.35-2.25 (m, 4H, $O_2CCH_2CH_2$), 2.15-1.90 (m, 32H, =$CHCH_2CH_2C(CH_3)$), 1.67 (s, 6H, =$C(CH_3)_2$), 1.61 (s, 6H, $CH_2C(CH_3)C$=), 1.59 (s, 24H, $CH_2C(CH_3)C$=).

Synthesis and characterization of [(3Z)-3-[(4-{[2-(diethylamino)ethyl]carbamoyl}-3,5-dimethyl-1H-pyrrol-2-yl)methylidene]-5-fluoro-2-oxo-2,3-dihydro-1H-indol-1-yl]methyl (4E,8E,12E,16E)-4,8,13,17,21-pentamethyldocosa-4,8,12,16,20-pentaenoate (SQSun (7))

To an ice-cooled solution of sunitinib **(5)** base (45 mg, 0.11 mmol) in a THF/DMF 4:1 (v/v) mixture (3 mL) was added a solution of NaHMDS (1 M, 0.17 mL, 0.17 mmol). The reaction mixture was stirred for 30 min at 0 °C and a solution of trisnorsqualenic acid chloromethyl ester[40] (61 mg, 0.14 mmol) was then added; the mixture was stirred at room temperature for 24 h. Water (2 mL) was added and the mixture was extracted with AcOEt (3 × 20 mL). The combined organic layers were washed with aqueous sodium bicarbonate, dried over $MgSO_4$ and concentrated under reduced pressure. Purification by chromatography over silica gel (CH_2Cl_2/MeOH/NH_4OH, 94:4:2) gave prodrug **(7)** (41 mg, 44% yield) as a yellow oil. IR (neat, cm^{-1}) □ 3300-3100, 3000-2800, 1742, 1706, 1672, 1625, 1604, 1573, 1541, 1477, 1458,1431, 1383, 1375, 1342, 1312, 1287, 1274, 1242, 1199, 1166, 1151, 1134, 1116, 1090, 1058, 1036, 1000, 968, 953, 922, 906, 848, 798, 765, 749, 735, 670; ^{1}H NMR (300 MHz $CDCl_3$) □ = 13.32 (s, 1H, H-1'), 7.38 (s, 1H, =CHC-2'), 7.18 (dd, J = 8.5 Hz, J = 2.3 Hz, H-4), 7.15 (br s, 1H, NHCO), 7.02 (dd, 1H, J = 8.5 Hz, J = 4.1 Hz, H-7), 6.95-6.85 (dt, 1H, J = 8.8 Hz, J = 2.2 Hz, H-6), 5.90 (d, 2H, J = 3.1 Hz, NCH_2O), 5.20-5.00 (m, 5H, CH=C(CH_3)), 3.70-3.60 (m, 2H, $CONHCH_2CH_2NEt_2$), 2.92 (t, 2H, J = 5.3 Hz, $CONHCH_2CH_2NEt_2$), 2.70 (q, 2H, J = 7.2 Hz, $N(CH_2CH_3)_2$), 2.60 (s, 3H, CH_3C-5'), 2.52 (s, 3H, CH_3C-3'), 2.47-2.24 (m, 6H, $O_2CCH_2CH_2$, $CONHCH_2CH_2NEt_2$), 2.10-1.85 (m, 16 H, =$C(CH_3)CH_2CH_2$), 1.67 (s, 3H, =$CH(CH_3)_2$), 1.59 (s, 9H, =$CH(CH_3)CH_2$), 1.54 (s, 6H, =$CH(CH_3)CH_2$), 1.10 (t, J = 7.2 Hz, 2H, $N(CH_2CH_3)_2$); ^{13}C NMR (300 MHz $CDCl_3$) □ = 173.0 (C, CO_2),168.5 (C, CON), 165.7 (C, CONH), 159.8 (CF, d, JCF = 239,3 Hz, C-5), 139.3 (C, C-5'), 137.1 (C, CH=$C(CH_3)$), 135.1 (C, CH=$C(CH_3)$), 135.0 (C, CH=$C(CH_3)$), 134.9 (C, CH=$C(CH_3)$), 134.8 (C, CH=$C(CH_3)$), 133.7 (C, C-7a), 132.7 (C, CH=$C(CH_3)_2$), 131.5 (C, C-2'), 126.6 (C, d, JCF = 9.2 Hz, C-3a), 126.3 (C, C-3'), 125.4 (CH, CH=C-2'), 124.6 (CH, CH=$C(CH_3)$), 124.4 (2CH, CH=$C(CH_3)$), 124.2 (CH, CH=$C(CH_3)$),123.9 (CH, CH=$C(CH_3)$), 121.7 (C, C-3'), 119.6 (C, C-4'), 112.9 (CH, d, JCF = 24.4 Hz, C-6), 112.8 (CH, d, JCF = 2.8 Hz, C-6), 112.9 (C, C-3), 109.8 (CH, d, JCF = 2.8 Hz, C-7), 105.0 (CH, JCF = 25.6 Hz, C-4), 62.9 (CH_2, OCH_2N), 51.9 (CH_2, $CONHCH_2CH_2NEt_2$), 47.1 ($2CH_2$, $N(CH_2CH_3)_2$), 39.7 (2 CH_2, =$C(CH_3)CH_2CH_2$), 39.5 (CH_2, =$C(CH_3)CH_2CH_2$), 36.2 (CH_2, $CONHCH_2CH_2NEt_2$), 34.3 (CH_2, =$C(CH_3)CH_2CH_2$), 34.2 (CH_2, $O_2CCH_2CH_2$), 32.8 (CH_2, $O_2CCH_2CH_2$), 28.2 (CH_2, =CCH_2CH_2C=), 26.7 ($2CH_2$, =CCH_2CH_2C=), 26.6 (CH_2, =CCH_2CH_2C=), 26.5 (CH_2, =CCH_2CH_2C=), 25.6 (CH_3, =$CH(CH_3)_2$), 23.3 (CH_2, =CCH_2CH_2C=), 17.6 (CH_3, =$CH(CH_3)_2$), 16.1 ($4CH_3$, =$CH(CH_3)CH_2$), 15.9 (CH_3, =$CH(CH_3)CH_2$), 14.2 (CH_3, CH_3C-5'), 11.4 (CH_3, CH_3C-3'), 10.2 ($2CH_3$, $N(CH_2CH_3)_2$); SM : ESI^+, m/z (%), 811.9 (M^+H^+) (100).

Nanoparticles preparation

All nanoparticles (NPs) were prepared in a single step according to the nanoprecipitation technique.[41]

Practically, for Erl-loaded SQdFdC NPs **(SQdFdC/Erl NPs)**, SQdFdC and Erl were co-dissolved in 0,5 mL of ethanol according to various SQ/Erl molar ratios (1:2, 2:1, 4:1). The organic solution was then added dropwise under magnetic stirring into MilliQ® water (ethanol/water 0.5:1 v/v). Formation of the nanoparticles occurred spontaneously without using any surfactant. After solvent evaporation under reduced pression, an aqueous suspension of SQdFdC/Erl NPs was obtained (final SQdFdC concentration: 2 mg/mL). The aqueous suspension was filtered through 1 micron Acrodisc 25 mm glass fiber syringe filters (Sigma, France) to remove Erl crystals.
For ErlTs salt-loaded SQdFdC NPs **(SQdFdC/ErlTs salt NPs)**, SQdFdC and ErlTs salt were co-dissolved in 0,2 mL of ethanol according to various SQdFdC/ErlTs salt molar ratios (5:1, 20:1). The organic solution was then added dropwise under magnetic stirring into MilliQ® water (ethanol/water 0.2:1 v/v). Formation of the nanoparticles occurred spontaneously without using any surfactant. After solvent evaporation under reduced pression, an aqueous suspension of SQdFdC/ErlTs salt NPs was obtained (final SQdFdC concentration: 2 mg/mL). No precipitation of Erl crystals was observed by visual inspection.
For ErlSQ salt-loaded SQdFdC NPs **(SQdFdC/ErlSQ salt NPs)**, SQdFdC and ErlSQ salt were co-dissolved in ethanol at various SQdFdC/ErlSQ salt molar ratios (10:1, 2:1) and completed with 5% w/w of SQPEG. The organic solution was then added dropwise under magnetic stirring into MilliQ® water (ethanol/water 0.2:1 v/v). After solvent evaporation under reduced pression, an aqueous suspension of SQdFdC/ErlSQ salt NPs was obtained (final SQdFdC concentration 2: mg/mL) without any Erl crystals.
For co-assembled **SQdFdC/SQSun NPs**, SQdFdC and SQSun were co-dissolved in ethanol at 1:25 SQdFdC/SQSun molar ratio. The organic solution was then added dropwise under magnetic stirring into MilliQ® water (ethanol/water 0.5:1 v/v). After solvent evaporation under reduced pression, an aqueous suspension of SQdFdC/SQSun NPs was obtained (final SQdFdC concentration: 2 mg/mL).
For **SQdFdC NPs** and **SQSun NPs**, SQdFdC or SQSun were each dissolved in ethanol. The organic solution was then added dropwise under magnetic stirring into MilliQ® water (ethanol/water 0.5:1 v/v). After solvent evaporation under reduced pression, an aqueous suspension of NPs was obtained (final SQdFdC or SQSun concentration: 2 mg/mL).
A physical mixture of **SQdFdC NPs + SQSun NPs** was prepared by mixing SQdFdC NPs and SQSun NPs at 1:1 v/v ratio.

Nanoparticle characterization

The NP diameter was measured by dynamic light scattering (DLS) with a Nano ZS from Malvern (UK) (173° scattering angle) at 25 °C. The measurements were performed after dilution of the NPs suspensions to 1:25 in MilliQ® water. The NP surface charge was investigated by ζ-potential measurement at 25 °C after dilution with 0.05 mM KCl solution applying the Smoluchowski equation and using the same apparatus. Measurements were carried out in triplicate. The colloidal stability of the NPs was investigated by measuring the nanoparticle mean diameter over a period of 15 days at 4°C.

HPLC studies

The amount of Erl loaded into SQdFdC/Erl NPs was determined by HPLC. The chromatographic system consisted of a Waters 1525 Binary LC pump, Waters 2707 Autosampler and a Waters 2998 programmable photodiode-array detector (Waters, Milford, MA 01757,USA) with column temperature controllers (model 7950 column heater and chiller, Jones Chromatography, CO). SUPELCOSIL™ Suplex™ pKb-100 HPLC analytical reversed-phase column 250 x 4.6 mm (5

µm particles) maintained at 30 °C was used as stationary phase, while the mobile phase was acetonitrile/phosphate buffer 0.5 mM (pH = 7.4) 50:50 v/v.
Erl stock solutions were prepared independently in triplicate by dissolving the appropriate amount of drug in ethanol to a final concentration of 5 µg/mL and stored at -20 °C. Calibration standards were freshly prepared by serial dilution of stock solutions in mobile phase at concentration of 100, 200, 500, 1000, 1500, 2000 and 2500 ng/mL. To extract analytes, 100 µL of NPs were dried and then solubilized with 200 µL of methanol, vortexed for 30 s and then sonicated for 60 s. This mixture was analyzed by DLS to verify that the NP structure was dissolved.
A typical HPLC procedure was performed according to procedures previously described with slight modifications.[42,43] Samples, diluted with mobile phase to 50 µL, were injected and eluted isocratically at a flow rate of 1 mL/min. Detection was monitored at 245 and 333 nm for SQdFdC and Erl, respectively.

Cell culture

Human pancreatic carcinoma cell line MIA PaCa-2 was obtained from the American Type Culture Collection (ATCC, France) and maintained as recommended. Briefly, MIA PaCa-2 cells were grown in Dulbecco's Modified Eagle Medium (DMEM) supplemented with 10% heat-inactivated (56 °C, 30 min) fetal bovine serum (FBS) and 2.5% heat-inactivated horse serum (Gibco, France). Medium was further supplemented with 50 U/mL penicillin and 50 U/mL streptomycin (Lonza, France). Cells were maintained in a humid atmosphere at 37 °C with 5% CO_2. Cells were used between passage 3 and 12 after thawing.

Cytotoxicity studies

The *in vitro* cytotoxicity of NPs was investigated through the determination of the mitochondrial activity by MTT [3-(4,5-dimethylthiazol-2-yl)-2,5-diphenyl tetrazolium bromide] viability test. A typical procedure for cytotoxicity study is as follows. 1000 cells were incubated in 100 µL of complete culture medium in 96-well plates for 24 h. The cells were then exposed to the different treatments (*i.e.,* NPs or free drugs). At the end of the incubation period, 20 µL of a 5 mg/mL MTT (Sigma Aldrich, Germany) solution in phosphate buffered saline was added to each well. After 2 h of incubation, the culture medium was gently aspirated and replaced by 200 µL of dimethylsulfoxide in order to dissolve the formazan crystals. The absorbance of the solubilized dye was measured spectrophotometrically with a microplate reader (LAB System Original Multiscan MS, Finland) at 570 nm. The fraction of viable cells was calculated from the absorbance ratio between the treated cells and the average absorbance of the untreated cells.
For cytotoxicity dose-response effect, cells were exposed to a series of concentrations of squalenoyl NPs or free drugs for 72 h.
To evaluate the efficacy of the combined therapies (*i.e.,* SQdFdC in combination with Erl salts or SQSun), cells were incubated with NPs maintaining constant concentration of SQdFdC (0.2 µM). Monotherapies were tested at the equivalent molar concentration.
For sequence-dependent anti-proliferative effect study, cells were incubated with squalenoyl prodrug *(i.e.,* SQdFdC and SQSun) NPs or free drugs *(i.e.,* dFdC and Sun) at concentrations nearly close to their IC_{50}, following different sequences: (*i*) dFdC followed by Sun; cells were treated with dFdC (10 nM) or SqdFdC NPs (0.25 µM). After 24 h of incubation, medium was removed and cells were incubated with Sun (13 µM) or SQSun NPs (4 µM) for additional 24 h followed by 24 h recovery (*i.e.,* drug-free medium); (*ii*) Sun followed by dFdC; cells were treated with Sun (13 µM) or SQSun NPs (4 µM). After 24h of incubation, medium was removed

and cells were incubated with dFdC (10 nM) or SqdFdC NPs (0.25 μM) for additional 24 h followed by 24 h recovery; (*iii*) concurrent treatment; cells were exposed to SQdFdC/SQSun NPs (molar ratio 1:25, 0.25 μM SQdFdC), or a physical mixture of both dFdC (10 nM) and Sun (13 μM) or SQdFdC NPs (0.25 μM) and SQSun NPs (4 μM) for 24 h followed by 48 h recovery (Figure 1).
Initial cell density and incubation time were determined to allow cells to remain in exponential growth and to undergo two cell-doubling times during the assay. All experiments were set up in triplicate or more to determine means and SD.

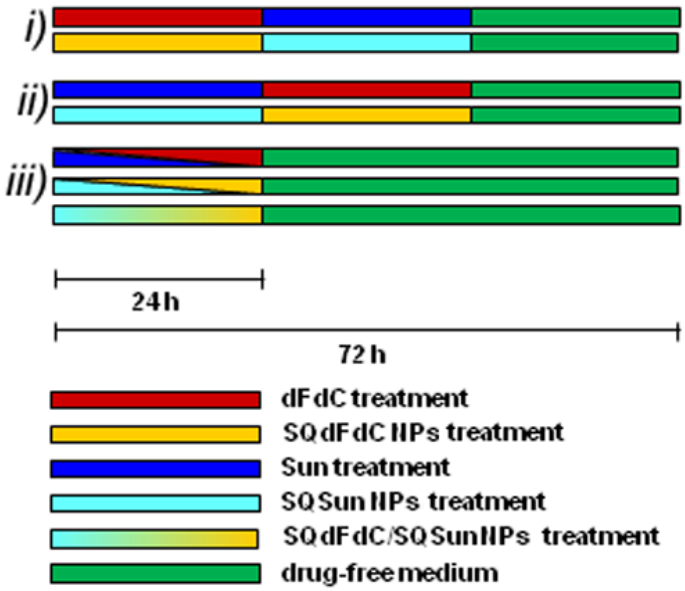

Figure 1. Schematic representation of the sequence-dependent anti-proliferative effect *in vitro* study.

Combined Therapy (CT) analysis

The results of the cytotoxicity dose-response effect of the monotherapy and combined treatments were analyzed according to the method of Chou Talalay by using CalcuSyn software v. 1.0[44] based on the median-effect principle.[45,46]

Results and Discussion

Aiming to realize a concurrent delivery of dFdC and TKI, different formulation strategies have been adopted as a function of the hydrophobic/hydrophilic nature of the chosen molecule (*i.e.,* erlotinib and sunitinib) (Figure 2).

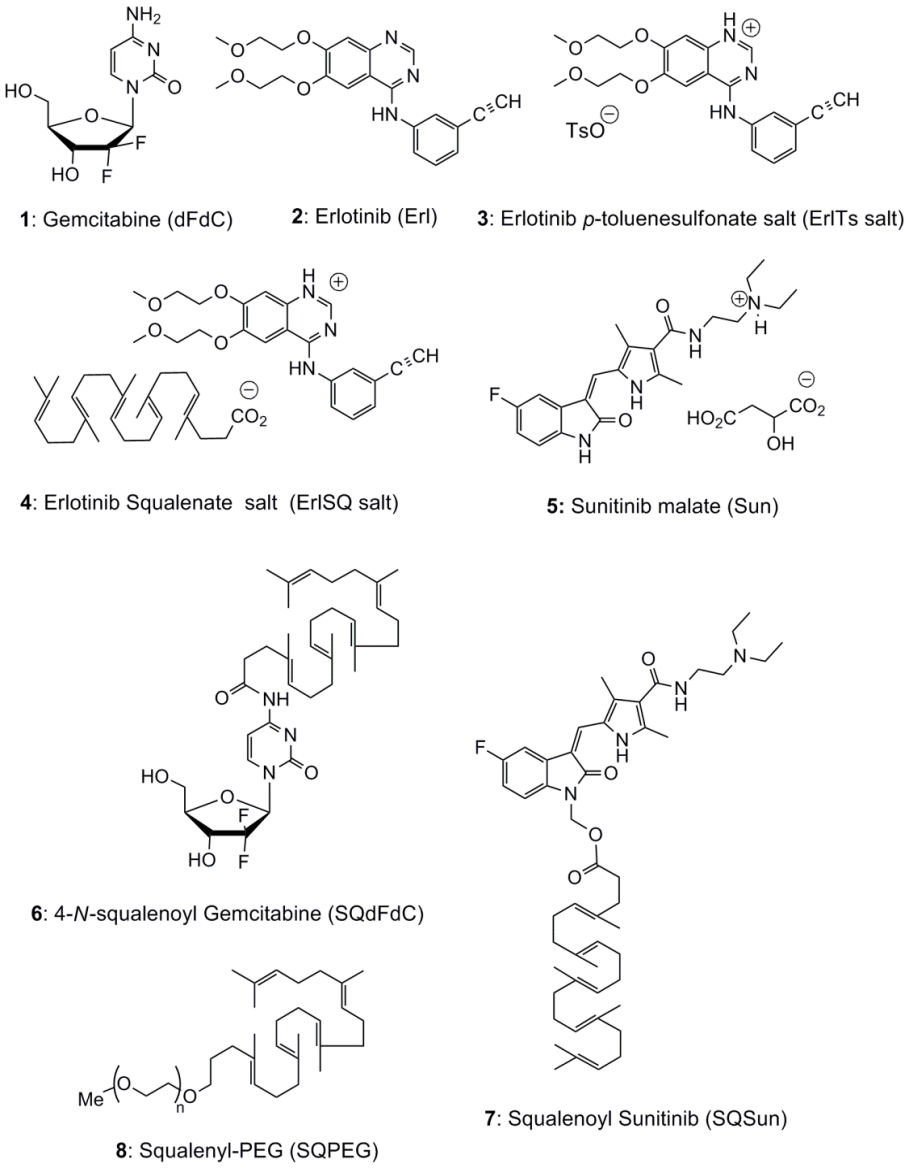

Figure 2. Structure of dFdC **(1)**, Erl **(2)**, ErlTs salt **(3)**, ErlSQ salt **(4)**, Sun **(5)**, SQdFdC **(6),** SQSun**(7)** and SQPEG **(8)**.

Due to the hydrophobicity of erlotinib (logP = 3.032 ± 1.37 at 25 °C[47]), the first approach relied on its physical encapsulation into SQdFdC NPs. SQdFdC **(6)** was synthesized by acylation of the C-4 nitrogen atom of the cytosine nucleus with squalenic acid as reported elsewhere.[35] Erl-loaded SQdFdC NPs were prepared by nanoprecipitation. Non-encapsulated drug immediately precipitated in the aqueous phase forming crystals, since the used concentration was over the

maximal water solubility (0.4 mg/mL).[48] After filtration, the obtained dispersion contained NPs with a mean diameter of 105-130 nm and a narrow particle distribution. NPs displayed a mean ζ-potential value of around -35 mV (Table 1).

NPs	SQdFdC (mol)	Erl (mol)	Mean diameter ± SD (nm)	PDI[a]	Zeta potential ± SD (mV)	Final [Erl] in NPs (µg/mL)	EE%[b]	DL%[c]
SQdFdC/Erl	1	2	130 ± 3	0.12	-33 ± 3	0.5	0.013	0.03
	2	1	105 ± 3	0.12	-33 ± 3	1.5	0.15	0.08
	4	1	107 ± 2	0.10	-34 ± 4	0.9	0.18	0.05
SQdFdC/ErlTs salt	5	1	Aggregation	/	/	/	/	/
	20	1	170 ± 5	0.09	-50 ± 1	61	100	2.9
SQdFdC/ErlSQ salt/ SQPEG	10	1	100 ± 1	0.08	-68 ± 3	60	100	2.9
	2	1	98 ± 2	0.13	-52 ± 2	304	100	14.5

Table 1. Characterization of Erl-loaded SQdFdC NPs. The final SQdFdC concentration in each formulation was 2 mg/mL.
[a] Polydispersity index.
[b] EE% (Encapsulation Efficiency): (Wt/Wi) ×100, where Wt is the total amount of Erl in the nanoparticle dispersion and Wi is the total quantity of Erl added initially during preparation.
[c] DL% (Drug Loading): (weight Erl/weight carrier) x 100.

The final SQdFdC and erlotinib concentrations after NPs filtration was determined by HPLC analysis (Supporting Figure S1). The encapsulation efficiency (EE%) and drug loading (DL%) were lower than 0.1% and 0.2%, respectively, probably as a consequence of the Erl physico-chemical properties (*e.g.*, high melting point ~150 °C[49]) and the thermodynamics and kinetics parameters that control nanoparticle formation during the nanoprecipitation process, which promoted the drug crystallization in the aqueous phase instead of its partition in the lipid (squalene) core. The higher amount of Erl likely led to a more important nucleation process which shifted the equilibrium versus the formation of crystals. According to the amount of drug loaded in the formulation, presumably too low to achieve any synergistic effect between dFdC and Erl, further studies with these formulations were not performed and we moved to the synthesis of an Erl salt. Such approach is commonly used in pharmaceutical technology to improve drug solubility, dissolution rate and bioavailability.[50] Herein, due to the strong acid character (pKa = -1.34) and relative low melting point (m.p.=100-105 °C) of the *p*-toluenesulphonic acid, we prepared a tosylate salt with Erl (pKa =5.32[49]). Currently, tosylate salts of different active molecules are commercially available for oral (*i.e.,* sorafenib- and lapatinib-tosylate) or intravenous (*i.e.*, bretyliumtosylate) administration.[51] The resulting erlotinib-tosylate salt (ErlTs salt **(3)** - Figure 2) allowed avoiding crystallization during the nanoprecipitation process. However, formation of stable NPs occurred with SQdFdC/ErlTs salt molar ratio of 20:1, leading to a drug loading lower than 3% (Table 1). As an alternative, a salt of Erl with the trisnorsqualenic acid (ErlSQ salt **(4)**) was formulated (Figure 2). Remarkably, an important increase of the amount of loaded drug was obtained by co-nanoprecipitation of SQdFdC and ErlSQ salt (molar ratio 2:1) mixed with SQPEG that was used to improve drug loading as reported elsewhere.[52] Also in this case, no crystals were observed in the final NP

formulation. At the used concentrations, both ErlTs and ErlSQ salts were not soluble in water, thus we supposed a total Erl loading. The Erl-salt-based formulations (*i.e.,* SQdFdC/ErlTs salt (20:1) and SQdFdC/ErlSQ salt (2:1) NPs) were then used for the *in vitro* studies. Despite the SQdFdC/ErlTs salt NPs (20:1) showed a lower DL% compared to SQdFdC/ErlSQ salt NPs (2:1), both formulations were investigated to evaluate whether the different salt composition might influence the antitumor activity.

On the other hand, since the hydrophilic character of sunitinib limited the possibility of a successful physical encapsulation, a prodrug approach was applied.

At the outset of this work, we chose to introduce a pH sensitive spacer between the squalene chain and the nitrogen atom of the indoline-2-one moiety. Sunitinib conjugate (SQSun **(7)**) bearing acid sensitive hemi-aminal ester group was thus synthesized (Figure 2). The squalenoyl prodrug was straight forwardly obtained in one step from sunitinib base **(9)** by alkylation with chloromethyl ester of trisnorsqualenic acid **(10)** which was easily available from squalenic acid upon treatment with chloromethyl chlorosulfate.[40] Accordingly, sodium anion of sunitinib was generated by treatment with NaHMDS and then it was condensed with trisnorsqualenic acid chloromethyl ester **(10)** gave the prodrug **(7)** in 44% yield after chromatographic purification (Scheme 1).[53]

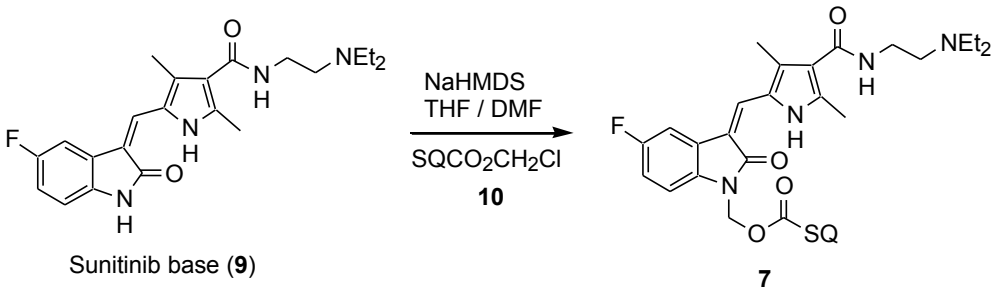

Scheme 1. Synthesis of SQSun (**7**).

The obtained bioconjugate SQSun **(7)** was able to self-assemble in water in form of nanoparticles showing a mean diameter lower than 200 nm and a narrow size distribution (Table 2). In addition, after co-nanoprecipitation of SQdFdC and SQSun, a narrow monodispersed NPs was obtained (SQdFdC/SQSun NPs). For this combined therapy NP, the gemcitabine amount was significantly lower than the one of sunitinib with the aim to realize a "metronomic" chemotherapy, which consists in the continuous administration without extended interruptions of the chemotherapeutic agent at doses inferior to the maximum-tolerated one. Gemcitabine has been already tested in preclinical trials following a "metronomic" schedule avoiding the dose-limiting side effects faced with the traditional protocols[54] and the combination of metronomic chemotherapy with antiangiogenic drugs led to enhanced antitumor efficacy in preclinical studies.[55-57] In this context, the SQdFdC/SQSun molar ratio was chosen in order to have a dFdC/Sun dose combination in accordance with the gemcitabine metronomic treatment[57,58] and sunitinib schedule[14,56,57,59-62] previously reported in literature.

Table 2. Characterization of Sun-loaded SQdFdC NPs. The final SQdFdC concentration in each formulation was 2 mg/mL.

NPs	SQdFdC (mol)	SQSun (mol)	Mean diameter ± SD (nm)	PDI[a]	Zeta potential ± SD (mV)
SQSun	/	1	103 ± 13	0.14	+ 59 ± 1
SQdFdC/SQSun	1	25	123 ± 23	0.16	+ 58 ± 3

[a] Polydispersity index.

The antitumor efficacy of the various NPs (*i.e.*, monotherapy and combined therapy) was evaluated *in vitro* on MIA Paca-2 pancreatic cancer cells. SQSun NPs were able to induce cytotoxicity at the same molar range of Sun free drug (Figure 3a). According to previous experiments, SQdFdC NPs displayed lower cytotoxicity compared to the free drug (Figure 3b).

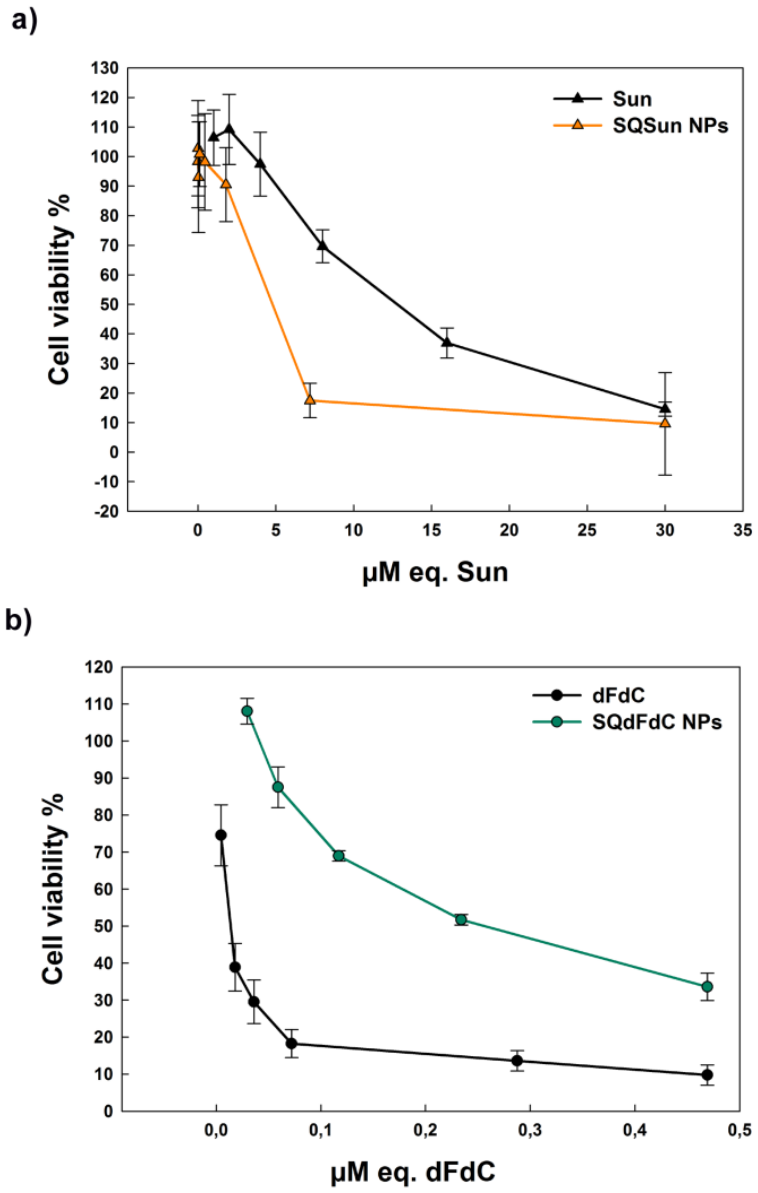

Figure 3. Viability of MIA PaCa-2 cells after exposure to increasing concentrations of **(a)** Sun free drug or SQSun NPs and **(b)** dFdC free drug or SQdFdC NPs for 72 h. Values represent mean ± SD.

In order to assess which combined therapy (i.e., SQdFdC NPs with Erl salts or SQSun) enabled enhancing the SQdFdC antitumor activity, cells were incubated with the different NPs formulations (*i.e.,* SQdFdC/ErlTs salt (molar ratio 20:1), SQdFdC/ErlSQ salt (molar ratio 2:1) NPs and SQdFdC/SQSun (molar ratio 1:25) NPs) at the same SQdFdC concentration (0.2 µM) nearly close the IC_{50} (inhibitory concentration 50%) of SQdFdC (Figure 4a). Not any additive effect was observed after cell exposure to either SQdFdC/ErlTs salt NPs or SQdFdC/ErlSQ salt NPs, compared to SQdFdC NPs or free drugs at the corresponding molar concentration (Figure 4a-c). This could probably rely on the low Erl drug loading. On the other hand, SQdFdC/SQSun NPs led to a significant increase of the cell toxicity (viability ~ 10%) compared with both SQdFdC NPs and SQSun NPs (viability ~ 50%) and the free sunitinib (viability ~ 95%) at the same molar concentration (Figure 4a,d).

According to the results, further studies with Erl-loaded SQdFdC NPs were not performed and we focused our attention only on SQdFdC/SQSun NPs.

Firstly, we investigated the dose-response effect after exposure to mono (*i.e.*, dFdC and Sun or SQdFdC NPs and SQSun NPs) or combined therapies (*i.e.*, dFdC/Sun free drugs combination and SQdFdC/SQSun NPs) in which dFdC/Sun molar ratio was kept constant at 1:25 (Figure 5). The cytotoxic activity of dFdC was significantly increased (around 12 folds) in the SQdFdC/SQSun combined therapy NPs compared to SQdFdC NPs (IC_{50} 0.022 µM *vs* 0.253 µM eq. dFdC) (Figure 5c) while no additive effect was observed in dFdC/Sun free drugs combination in comparison to the dFdC treatment (Figure 5d). Of note, treatment of 0.022 µM of SQdFdC and 0.55 µM of SQSun was not efficient in killing cancer cells in monotherapy (*i.e.,* SQdFdC NPs and SQSun NPs) while led to a viability reduction of 50% in combined therapy (*i.e.,* SQdFdC/SQSun NPs) (Figure 5e). Besides, no increase of the dFdC cytotoxicity was observed when cells were exposed to the combination of dFdC and Sun as free drugs (Figure 5f).

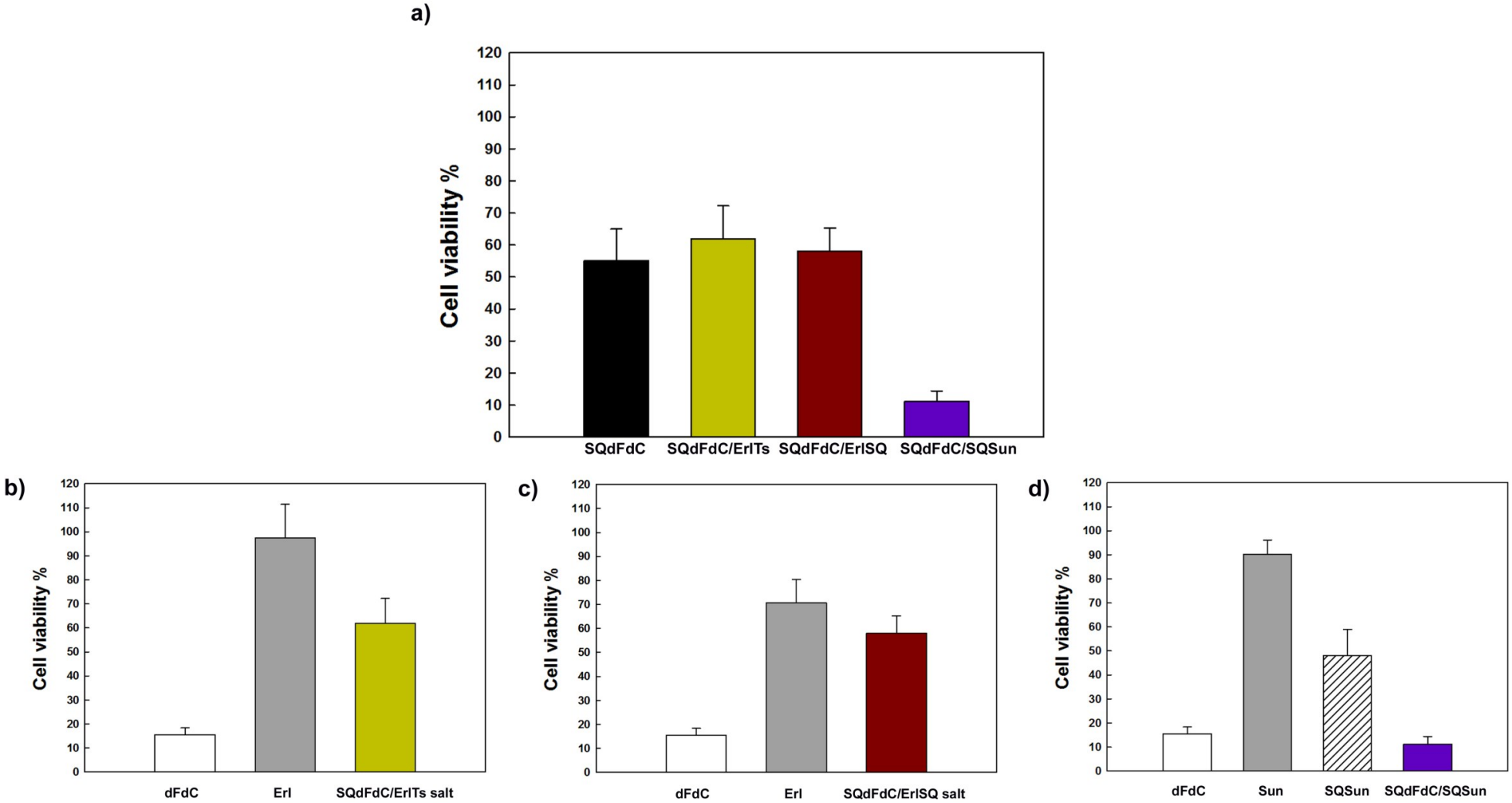

Figure 4. Viability of MIA PaCa-2 cells after exposure for 72 h to different NPs formulations at the same dFdC concentration (0.2 μM) close to the IC_{50} of SQdFdC NPs. **a)** SQdFdC NPs, SQdFdC/ErlTs salt (0.01 μM eq. Erl) NPs, SQdFdC/ErlSQ salt (0.05 μM eq. Erl) NPs or SQdFdC/SQSun (5 μM eq. Sun) NPs; **b)** dFdC, Erl (0.01 μM) and SQdFdC/ErlTs salt NPs (0.01 μM eq. Erl); **c)** dFdC, Erl (0.05 μM) and SQdFdC/ErlTs salt NPs (0.05 μM eq. Erl); **d)** dFdC, Sun (5 μM), SQSun NPs (5 μM eq. Sun) and SQdFdC/SQSun NPs (5 μM eq. Sun). Values represent mean ± SD.

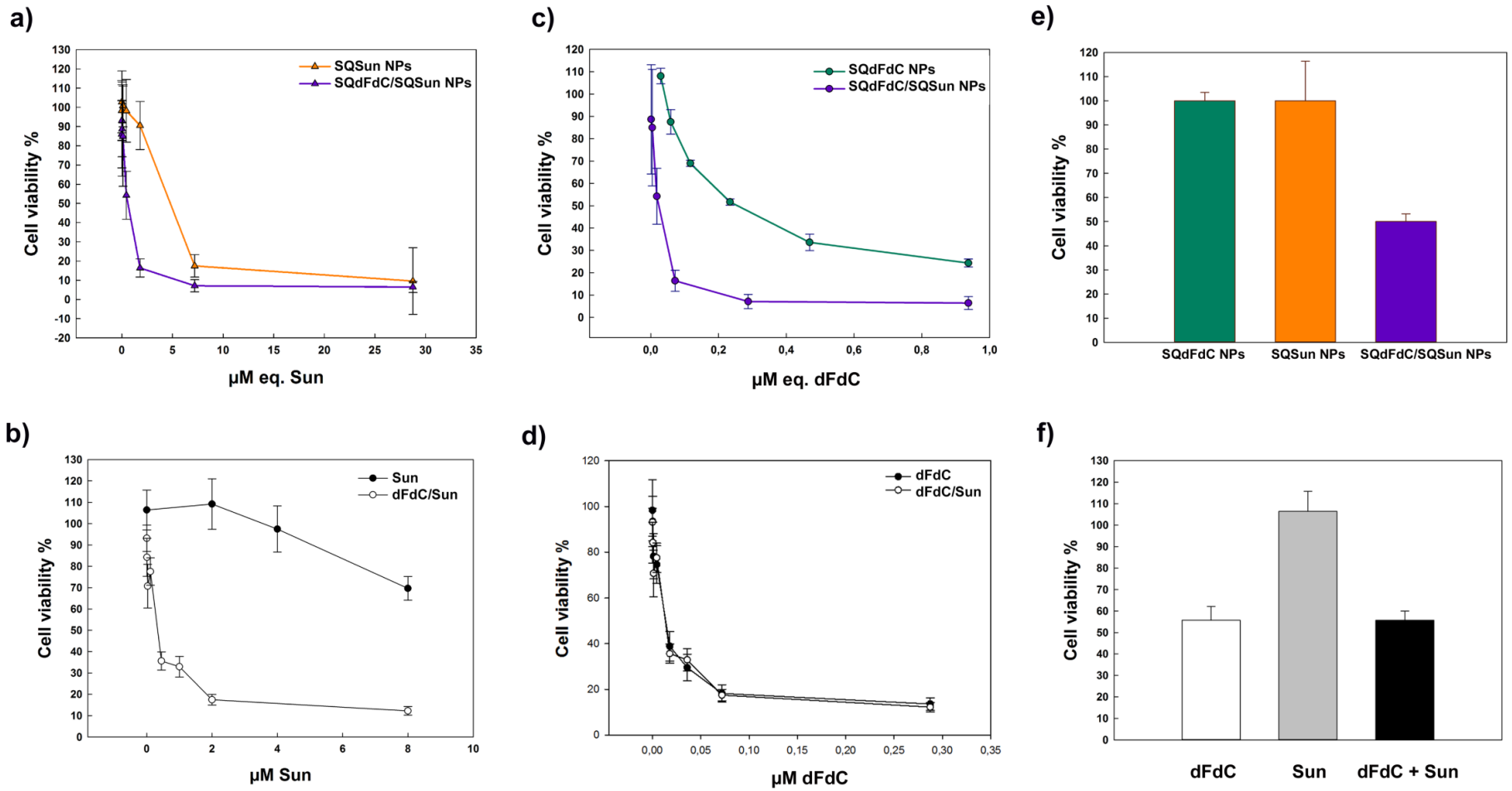

Figure 5. Viability of MIA Paca-2 cells after exposure for 72 h to increasing concentrations of **(a)** SQSun NPs and SQdFdC/SQSun NPs; **(b)** Sun and dFdC/Sun combination; **(c)** SQdFdC NPs and SQdFdC/SQSun NPs; **(d)** dFdC and dFdC/Sun combination. Viability of MIA Paca-2 cells incubated for 72 h with **(e)** SQdFdC/SQSun NPs at concentrations corresponding to the IC_{50} (*i.e.,* 0.022 µM for dFdC and 0.55 µM for Sun), compared with SQdFdC NPs and SQSun NPs at the corresponding molar concentrations; **(f)** dFdC/Sun combination at concentrations corresponding to the IC_{50} (*i.e.,* 0.012 µM for dFdC and 0.3 µM for Sun) compared with dFdC and Sun at the corresponding molar concentrations. dFdC/Sun molar ratio was kept constant at 1:25. Values represent mean ± SD.

Then, we investigated if the viability of pancreatic cancer cells was dependent on the dFdC/Sun drug association timing, which plays a crucial role in the drug interaction and the resulting therapeutic effect in combined therapy.[63,64] To this aim, cells were exposed to different incubation schedules (concurrent and sequential) of free drugs or NPs at concentration close to their IC_{50} (for protocol see Figure 1). Sequential incubation with Sun and dFdC free drugs, or SQdFdC and SQSun NPs, always resulted in a lower cytotoxic effect compared to one of the simultaneous exposure (Figure 6). In addition, concurrent treatment with the physical mixture (SQdFdC NPs + SQSun NPs p.m.) did not show any significant difference compared to the cytotoxic effect induced by each NPs in monotherapy. Noteworthy is that a significant superior cytotoxicity was observed only in the case of SQdFdC/SQSun NPs, suggesting that the superior antitumor activity relied on the exposure to SQdFdC and SQSun in the same nanoparticle (Figure 6). Indeed, the co-deliver of the drugs in the same unit could be an undeniable advantage offered by the nano-technology to enhance the final combined antitumor effect.

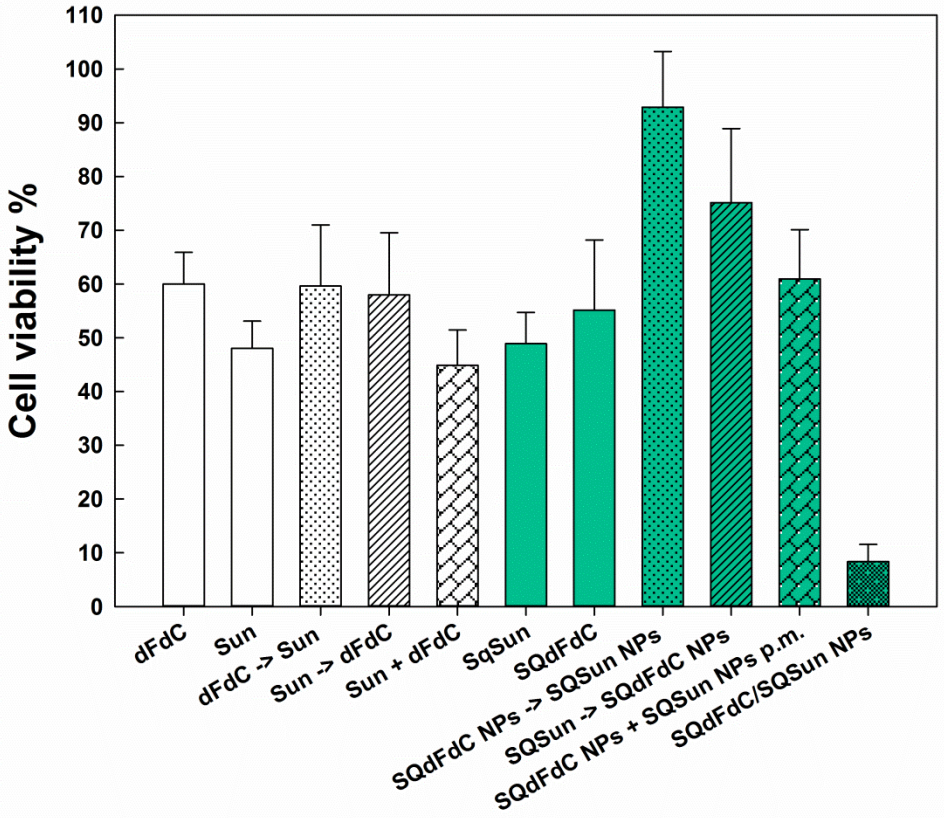

Figure 6. Viability of MIA PaCa-2 cells after exposure to dFdC and Sun free drugs, SQdFdC NPs, SQSun NPs and SQdFdC/SQSun NPs for 24 h. Sequential and concurrent treatments were performed. Concentrations tested are close to the IC_{50} value determined for each component. The symbols "->" and "+" indicates sequential and concurrent incubation, respectively.

According to these promising results, we further investigated the antitumor combined activity of SQdFdC/SQSun NPs in comparison to dFdC/Sun free drugs. Several rigorous drug-combination analysis methods have been developed for analyzing combinations from experimental data.[65-67] Among them, the Chou-Talalay method (for review see[67]) has been proven to be an effective

scientific method to evaluated the synergistic, additive or antagonism interactions between two or more drugs.[68] Thus, a combined drug analysis using the CalcuSyn software[44] based on Chou-Talalay method was performed starting from the dose-response levels depicted in Figure 5 a-d for monotherapies (*i.e.,* dFdC and Sun or SQdFdC NPs and SQSun NPs) or combined therapies (*i.e.,* dFdC/Sun or SQdFdC/SQSun NPs). The simplest drug interaction parameter was the combination index (CI), defined for the pair of drugs A e B as

$$CI = \frac{EDx(A\ pair)}{EDx(A)} + \frac{EDx(B\ pair)}{EDx(B)}$$

Where EDx is the drug concentration that inhibits a cellular function (*i.e.,* cell growth) by x%, for each individual drug (EDx(A) or EDx(B)) or for the drug given as A-B pair (EDx(A pair) or EDx(B pair)). CI allows to quantitatively determine synergistic (CI < 1), additive (CI = 1) and antagonistic (CI > 1) effects for each dose tested in combined therapies.[46]
The CI plot as a function of cytotoxicity (Fa) (e.g., Fa of 0.9 corresponds to 90% of cytotoxicity) was calculated for each dFdC/Sun free or SQdFdC/SQSun NPs pairs (Figure 7). The synergism for dFdC/Sun (Figure 7 – right panel) was higher at low levels of toxicity, according to previously reports.[57] Noteworthy is that only SQdFdC/SQSun NPs (Figure 7 – left panel) showed a synergistic effect also at Fa > 0.8 which is more therapeutically relevant because the chemotherapy are aimed to eradicate the cancer cells working at high level of cytotoxicity.[67] Contrarily, dFdC/Sun displayed an antagonistic effect at high Fa values.

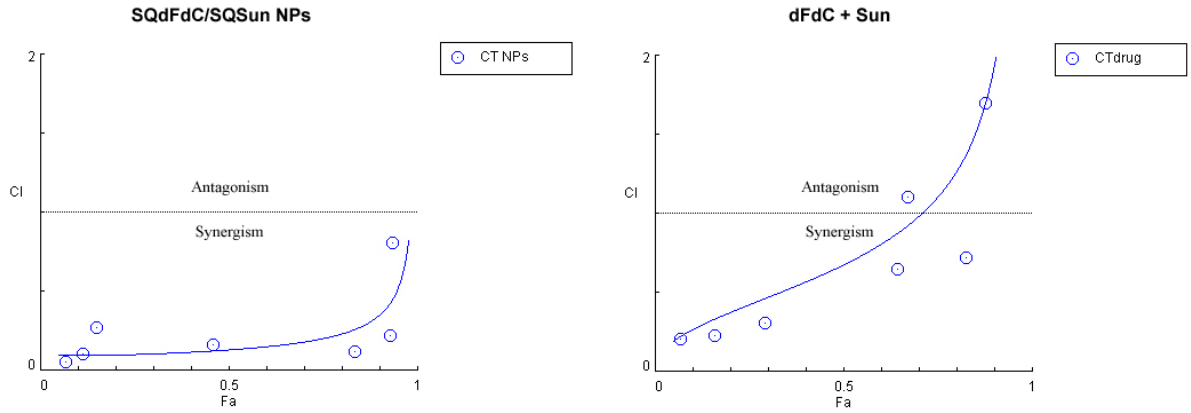

Figure 7. Combination Index plots for SQdFdC/SQSun NPs (CT NPs - left panel) and dFdC/Sun free drugs association (CTdrug - right panel). Combined index (CI) is represented as a function of effect level (Fa). The data points (blue circles) and the correlated simulated curve (blue line) below, at, and above the horizontal line of CI=1 indicate synergistic, additive and antagonistic effect, respectively.

The combined therapy analysis also permitted to calculate the dose-reduction index (DRI), which represents the drug dose reduction to reach a given effect level in combined therapy in

comparison to monotherapy (Table 3). The high DRI values for SQdFdC ($10 \leq DRI \leq 40$) clearly demonstrate that the SQdFdC/SQSun NPs would allow a significant reduction of the dFdC dose, in contrast with dFdC/Sun association, for which the DRI values of dFdC were low. Interestingly, the SQdFdC dose reduction was proportional to the level of cytotoxicity. Of note, in order to obtain the 90% of cytotoxicity, the SQdFdC/SQSun NPs allowed to reduce the dFdC dose around 38 times, which may represent an important advantage enabling to reduce the side toxicity associated to this chemotherapy agent.
These results combined to the CI plot demonstrate the possibility to achieve a higher *in vitro* anticancer synergistic activity taking advantage of a squalene-based nanoparticles combined therapy.

Table 3. DRI (dose-reduction index) values for dFdC, Sun, SQdFdC and SQSun when associated in dFdC/Sun free drugs association or in SQdFdC/SQSun NPs combined therapy.

Fa	0.1	0.2	0.3	0.4	0.5	0.6	0.7	0.8	0.9
DRI dFdC	3.74	2.67	2.14	1.78	1.50	1.27	1.06	0.85	0.60
DRI Sun	2253	680	307	160	88	48	25	11	3.42
DRI SQdFdC	13.81	16.68	18.90	20.95	23.02	25.29	28.02	31.77	38.36
DRI SQSun	42.95	26.38	19.08	14.62	11.47	8.89	6.89	4.98	3.06

Conclusion

Application of the squalenoylation concept enabled the successful design of a novel nanoscale system for combined drug therapy. Association of the two prodrugs in a single nanoparticle resulted in a significant enhanced *in vitro* cytotoxic effect compared to the NPs in monotherapy. In addition, a stronger synergistic effect was observed, leading to an important decrease of the dFdC dose required to attain a certain efficacy level, thus potentially reducing the side effects and resistance phenomena currently associated to the use of gemcitabine in the clinical practice. These promising *in vitro* results open interesting perspectives for application of squalenoyl prodrug-based nanomedicine to pancreatic cancer metronomic treatment.

Acknowledgements

The research leading to these results has received funding from the European Research Council under the European Community's Seventh Framework Programme FP7/2007-2013 Grant Agreement N°249835. The authors acknowledge the Università Italo Francese/Université Franco Italienne for the PhD co-tutoring agreement to S.V.

Supporting Informations

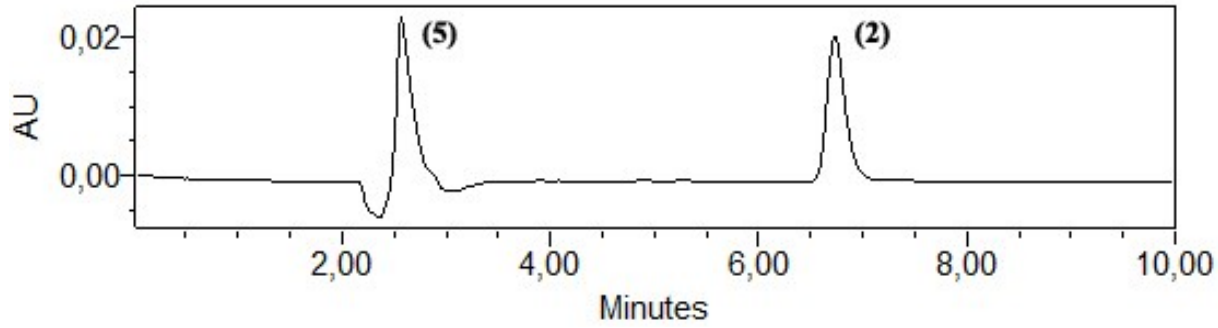

Supporting Figure S1. HPLC identification and separation of SQdFdC **(5)** and Erl **(2)**

References

1. Hidalgo, M. Pancreatic cancer. *N Engl J Med* **2010**, 362, 1605-17.
2. Jemal, A.; Siegel, R.; Xu, J.; Ward, E. Cancer statistics, 2010. *CA Cancer J Clin* **2010**, 60, 277-300.
3. Burris, H. A., 3rd; Moore, M. J.; Andersen, J.; Green, M. R.; Rothenberg, M. L.; Modiano, M. R.; Cripps, M. C.; Portenoy, R. K.; Storniolo, A. M.; Tarassoff, P.; Nelson, R.; Dorr, F. A.; Stephens, C. D.; Von Hoff, D. D. Improvements in survival and clinical benefit with gemcitabine as first-line therapy for patients with advanced pancreas cancer: a randomized trial. *J Clin Oncol* **1997**, 15, 2403-13.
4. Oberstein, P. E.; Saif, M. W. First-line treatment for advanced pancreatic cancer. Highlights from the "2011 ASCO Gastrointestinal Cancers Symposium". San Francisco, CA, USA. January 20-22, 2011. *JOP* **2011**, 12, 96-100.
5. Storniolo, A. M.; Allerheiligen, S. R.; Pearce, H. L. Preclinical, pharmacologic, and phase I studies of gemcitabine. *Semin Oncol* **1997**, 24, S7-2-S7-7.
6. Rauchwerger, D. R.; Firby, P. S.; Hedley, D. W.; Moore, M. J. Equilibrative-sensitive nucleoside transporter and its role in gemcitabine sensitivity. *Cancer Res* **2000**, 60, 6075-9.
7. Jones, S.; Zhang, X.; Parsons, D. W.; Lin, J. C.; Leary, R. J.; Angenendt, P.; Mankoo, P.; Carter, H.; Kamiyama, H.; Jimeno, A.; Hong, S. M.; Fu, B.; Lin, M. T.; Calhoun, E. S.; Kamiyama, M.; Walter, K.; Nikolskaya, T.; Nikolsky, Y.; Hartigan, J.; Smith, D. R.; Hidalgo, M.; Leach, S. D.; Klein, A. P.; Jaffee, E. M.; Goggins, M.; Maitra, A.; Iacobuzio-Donahue, C.; Eshleman, J. R.; Kern, S. E.; Hruban, R. H.; Karchin, R.; Papadopoulos, N.; Parmigiani, G.; Vogelstein, B.; Velculescu, V. E.; Kinzler, K. W. Core signaling pathways in human pancreatic cancers revealed by global genomic analyses. *Science* **2008**, 321, 1801-6.
8. Saif, M. W.; Ruoslahti, E.; Bhatia, S. N.; Sailor, M. J. Pancreatic neoplasm in 2011: an update. *Jop.* **2011**, 12, 316-21.
9. Gschwind, A.; Fischer, O. M.; Ullrich, A. The discovery of receptor tyrosine kinases: targets for cancer therapy. *Nat Rev Cancer* **2004**, 4, 361-70.
10. Hanahan, D.; Weinberg, R. A. Hallmarks of cancer: the next generation. *Cell* **2011**, 144, 646-74.
11. Moore, M. J.; Goldstein, D.; Hamm, J.; Figer, A.; Hecht, J. R.; Gallinger, S.; Au, H. J.; Murawa, P.; Walde, D.; Wolff, R. A.; Campos, D.; Lim, R.; Ding, K.; Clark, G.; Voskoglou-Nomikos, T.; Ptasynski, M.; Parulekar, W. Erlotinib plus gemcitabine compared with gemcitabine alone in patients with advanced pancreatic cancer: a phase III trial of the National Cancer Institute of Canada Clinical Trials Group. *J Clin Oncol* **2007**, 25, 1960-6.
12. http://www.accessdata.fda.gov/drugsatfda_docs/appletter/2013/021660Orig1s037ltr.pdf.
13. Goodman, V. L.; Rock, E. P.; Dagher, R.; Ramchandani, R. P.; Abraham, S.; Gobburu, J. V.; Booth, B. P.; Verbois, S. L.; Morse, D. E.; Liang, C. Y.; Chidambaram, N.; Jiang, J. X.; Tang, S.; Mahjoob, K.; Justice, R.; Pazdur, R. Approval summary: sunitinib for the treatment of imatinib refractory or intolerant gastrointestinal stromal tumors and advanced renal cell carcinoma. *Clin Cancer Res* **2007**, 13, 1367-73.
14. Casneuf, V. F.; Demetter, P.; Boterberg, T.; Delrue, L.; Peeters, M.; Van Damme, N. Antiangiogenic versus cytotoxic therapeutic approaches in a mouse model of pancreatic cancer: an experimental study with a multitarget tyrosine kinase inhibitor (sunitinib), gemcitabine and radiotherapy. *Oncol Rep* **2009**, 22, 105-13.
15. Faivre, S.; Demetri, G.; Sargent, W.; Raymond, E. Molecular basis for sunitinib efficacy and future clinical development. *Nature Reviews Drug Discovery* **2007**, 6, 734-745.

16. Abrams, T. J.; Lee, L. B.; Murray, L. J.; Pryer, N. K.; Cherrington, J. M. SU11248 inhibits KIT and platelet-derived growth factor receptor beta in preclinical models of human small cell lung cancer. *Molecular Cancer Therapeutics* **2003**, 2, 471-478.
17. O'Farrell, A. M.; Abrams, T. J.; Yuen, H. A.; Ngai, T. J.; Louie, S. G.; Yee, K. W. H.; Wong, L. M.; Hong, W.; Lee, L. B.; Town, A.; Smolich, B. D.; Manning, W. C.; Murray, L. J.; Heinrich, M. C.; Cherrington, J. M. SU11248 is a novel FLT3 tyrosine kinase inhibitor with potent activity in vitro and in vivo. *Blood* **2003**, 101, 3597-3605.
18. Mendel, D. B.; Laird, A. D.; Xin, X. H.; Louie, S. G.; Christensen, J. G.; Li, G. M.; Schreck, R. E.; Abrams, T. J.; Ngai, T. J.; Lee, L. B.; Murray, L. J.; Carver, J.; Chan, E.; Moss, K. G.; Haznedar, J. O.; Sukbuntherng, J.; Blake, R. A.; Sun, L.; Tang, C.; Miller, T.; Shirazian, S.; McMahon, G.; Cherrington, J. M. In vivo antitumor activity of SU11248, a novel tyrosine kinase inhibitor targeting vascular endothelial growth factor and platelet-derived growth factor receptors: Determination of a pharmacokinetic/pharmacodynamic relationship. *Clinical Cancer Research* **2003**, 9, 327-337.
19. Chang, Y. T.; Chang, M. C.; Wei, S. C.; Tien, Y. W.; Hsu, C.; Liang, P. C.; Tsao, P. N.; Jan, I. S.; Wong, J. M. Serum vascular endothelial growth factor/soluble vascular endothelial growth factor receptor 1 ratio is an independent prognostic marker in pancreatic cancer. *Pancreas* **2008**, 37, 145-50.
20. Parhi, P.; Mohanty, C.; Sahoo, S. K. Nanotechnology-based combinational drug delivery: an emerging approach for cancer therapy. *Drug Discov Today* **2012**, 17, 1044-52.
21. Ma, L.; Kohli, M.; Smith, A. Nanoparticles for combination drug therapy. *Acs Nano* **2013**, 7, 9518-25.
22. Rock, E. P.; Goodman, V.; Jiang, J. X.; Mahjoob, K.; Verbois, S. L.; Morse, D.; Dagher, R.; Justice, R.; Pazdur, R. Food and Drug Administration drug approval summary: Sunitinib malate for the treatment of gastrointestinal stromal tumor and advanced renal cell carcinoma. *Oncologist* **2007**, 12, 107-13.
23. Berz, D.; Wanebo, H. Targeting the Growth Factors and Angiogenesis Pathways: Small Molecules in Solid Tumors. *J Surg Oncol* **2011**, 103, 574-586.
24. Kiyohara, Y.; Yamazaki, N.; Kishi, A. Erlotinib-related skin toxicities: treatment strategies in patients with metastatic non-small cell lung cancer. *J Am Acad Dermatol* **2013**, 69, 463-72.
25. Mountzios, G.; Syrigos, K. N. A benefit-risk assessment of erlotinib in non-small-cell lung cancer and pancreatic cancer. *Drug Saf* **2011**, 34, 175-86.
26. Di Lorenzo, G.; Autorino, R.; Bruni, G.; Carteni, G.; Ricevuto, E.; Tudini, M.; Ficorella, C.; Romano, C.; Aieta, M.; Giordano, A.; Giuliano, M.; Gonnella, A.; De Nunzio, C.; Rizzo, M.; Montesarchio, V.; Ewer, M.; De Placido, S. Cardiovascular toxicity following sunitinib therapy in metastatic renal cell carcinoma: a multicenter analysis. *Ann Oncol* **2009**, 20, 1535-42.
27. Chu, T. F.; Rupnick, M. A.; Kerkela, R.; Dallabrida, S. M.; Zurakowski, D.; Nguyen, L.; Woulfe, K.; Pravda, E.; Cassiola, F.; Desai, J.; George, S.; Morgan, J. A.; Harris, D. M.; Ismail, N. S.; Chen, J. H.; Schoen, F. J.; Van den Abbeele, A. D.; Demetri, G. D.; Force, T.; Chen, M. H. Cardiotoxicity associated with tyrosine kinase inhibitor sunitinib. *Lancet* **2007**, 370, 2011-9.
28. Marslin, G.; Sheeba, C. J.; Kalaichelvan, V. K.; Manavalan, R.; Reddy, P. N.; Franklin, G. Poly(D,L-lactic-co-glycolic acid) nanoencapsulation reduces Erlotinib-induced subacute toxicity in rat. *J Biomed Nanotechnol* **2009**, 5, 464-71.
29. Vrignaud, S.; Hureaux, J.; Wack, S.; Benoit, J. P.; Saulnier, P. Design, optimization and in vitro evaluation of reverse micelle-loaded lipid nanocarriers containing erlotinib hydrochloride. *Int J Pharm* **2012**, 436, 194-200.
30. Xu, Y.; Karmakar, A.; Heberlein, W. E.; Mustafa, T.; Biris, A. R.; Biris, A. S. Multifunctional magnetic nanoparticles for synergistic enhancement of cancer treatment

by combinatorial radio frequency thermolysis and drug delivery. *Adv Healthc Mater* **2012**, 1, 493-501.
31. Altintas, I.; Heukers, R.; van der Meel, R.; Lacombe, M.; Amidi, M.; van Bergen En Henegouwen, P. M.; Hennink, W. E.; Schiffelers, R. M.; Kok, R. J. Nanobody-albumin nanoparticles (NANAPs) for the delivery of a multikinase inhibitor 17864 to EGFR overexpressing tumor cells. *J Control Release* **2013**, 165, 110-8.
32. Dolman, M. E.; van Dorenmalen, K. M.; Pieters, E. H.; Sparidans, R. W.; Lacombe, M.; Szokol, B.; Orfi, L.; Keri, G.; Bovenschen, N.; Storm, G.; Hennink, W. E.; Kok, R. J. Dendrimer-based macromolecular conjugate for the kidney-directed delivery of a multitargeted sunitinib analogue. *Macromol Biosci* **2012**, 12, 93-103.
33. Reddy, L. H.; Renoir, J. M.; Marsaud, V.; Lepetre-Mouelhi, S.; Desmaele, D.; Couvreur, P. Anticancer efficacy of squalenoyl gemcitabine nanomedicine on 60 human tumor cell panel and on experimental tumor. *Mol Pharm* **2009**, 6, 1526-35.
34. Reddy, L. H.; Ferreira, H.; Dubernet, C.; Mouelhi, S. L.; Desmaele, D.; Rousseau, B.; Couvreur, P. Squalenoyl nanomedicine of gemcitabine is more potent after oral administration in leukemia-bearing rats: study of mechanisms. *Anticancer Drugs* **2008**, 19, 999-1006.
35. Couvreur, P.; Stella, B.; Reddy, L. H.; Hillaireau, H.; Dubernet, C.; Desmaele, D.; Lepetre-Mouelhi, S.; Rocco, F.; Dereuddre-Bosquet, N.; Clayette, P.; Rosilio, V.; Marsaud, V.; Renoir, J. M.; Cattel, L. Squalenoyl nanomedicines as potential therapeutics. *Nano Lett.* **2006**, 6, 2544-8.
36. Rejiba, S.; Reddy, L. H.; Bigand, C.; Parmentier, C.; Couvreur, P.; Hajri, A. Squalenoyl gemcitabine nanomedicine overcomes the low efficacy of gemcitabine therapy in pancreatic cancer. *Nanomedicine* **2011**, 7, 841-9.
37. Silvestri, G. A.; Rivera, M. P. Targeted therapy for the treatment of advanced non-small cell lung cancer: a review of the epidermal growth factor receptor antagonists. *Chest* **2005**, 128, 3975-84.
38. Mendelsohn, J. The epidermal growth factor receptor as a target for cancer therapy. *Endocr Relat Cancer* **2001**, 8, 3-9.
39. Bekkara-Aounallah, F.; Gref, R.; Othman, M.; Reddy, L. H.; Pili, B.; Allain, V.; Bourgaux, C.; Hillaireau, H.; Lepêtre-Mouelhi, S.; Desmaële, D.; Nicolas, J.; Chafi, N.; Couvreur, P. Novel PEGylated Nanoassemblies Made of Self-Assembled Squalenoyl Nucleoside Analogues. *Advanced Functional Materials* **2008**, 18, 3715-3725.
40. Semiramoth, N.; Di Meo, C.; Zouhiri, F.; Said-Hassane, F.; Valetti, S.; Gorges, R.; Nicolas, V.; Poupaert, J. H.; Chollet-Martin, S.; Desmaele, D.; Gref, R.; Couvreur, P. Self-assembled squalenoylated penicillin bioconjugates: an original approach for the treatment of intracellular infections. *Acs Nano* **2012**, 6, 3820-31.
41. Fessi, H.; Puisieux, F.; Devissaguet, J. P.; Ammoury, N.; Benita, S. Nanocapsule formation by interfacial polymer deposition following solvent displacement. *International Journal of Pharmaceutics* **1989**, 55, R1-R4.
42. Lepper, E. R.; Swain, S. M.; Tan, A. R.; Figg, W. D.; Sparreboom, A. Liquid-chromatographic determination of erlotinib (OSI-774), an epidermal growth factor receptor tyrosine kinase inhibitor. *J Chromatogr B Analyt Technol Biomed Life Sci* **2003**, 796, 181-8.
43. Zhang, W.; Siu, L. L.; Moore, M. J.; Chen, E. X. Simultaneous determination of OSI-774 and its major metabolite OSI-420 in human plasma by using HPLC with UV detection. *J Chromatogr B Analyt Technol Biomed Life Sci* **2005**, 814, 143-7.
44. Chou, T. C.; Martin, N. *CompuSyn software for drug combinations and for general dose-effect analysis, and user's guide*, ComboSyn, Inc. Paramus: NJ, 2007.
45. Chou, T. C. Drug combination studies and their synergy quantification using the Chou-Talalay method. *Cancer Res* **2010**, 70, 440-6.

46. Chou, T. C.; Talalay, P. Quantitative analysis of dose-effect relationships: the combined effects of multiple drugs or enzyme inhibitors. *Adv Enzyme Regul* **1984**, 22, 27-55.
47. ACD/Labs. *Advanced Chemistry Development (ACD/Labs) Software V11.02* 1994-2012
48. http://www.accessdata.fda.gov/. http://www.accessdata.fda.gov/.
49. Chandregowda, V.; Venkateswara Rao, G.; Chandrasekara Reddy, G. Convergent Approach for Commercial Synthesis of Gefitinib and Erlotinib. *Organic Process Research & Development* **2007**, 11, 813-816.
50. Stahl, P. H.; Wermuth, C. G. In *Handbook of Pharmaceutical Salts*, ActaWiley-VCH, V. H. C. a., Ed. Zürich, **2011**.
51. Saal, C.; Becker, A. Pharmaceutical salts: A summary on doses of salt formers from the Orange Book. *European Journal of Pharmaceutical Sciences* **2013**, 49, 614-623.
52. Mura, S.; Zouhiri, F.; Lerondel, S.; Maksimenko, A.; Mougin, J.; Gueutin, C.; Brambilla, D.; Caron, J.; Sliwinski, E.; LePape, A.; Desmaele, D.; Couvreur, P. Novel Isoprenoyl Nanoassembled Prodrug for Paclitaxel Delivery. *Bioconjugate Chem.* **2013**, 24, 1840-1849.
53. Buchy, E.; Valetti, S.; Mura, S.; Couvreur, P.; Desmaële, D. Synthesis and cytotoxic activity of self-assembling squalene conjugates of 3-[(pyrrol-2-yl)methylidene]-2,3-dihydro-1H-indol-2-ones anticancer agents. *In preparation* **2014**.
54. Pasquier, E.; Kavallaris, M.; Andre, N. Metronomic chemotherapy: new rationale for new directions. *Nat Rev Clin Oncol* **2010**, 7, 455-65.
55. Browder, T.; Butterfield, C. E.; Kraling, B. M.; Shi, B.; Marshall, B.; O'Reilly, M. S.; Folkman, J. Antiangiogenic scheduling of chemotherapy improves efficacy against experimental drug-resistant cancer. *Cancer Res* **2000**, 60, 1878-86.
56. Pietras, K.; Hanahan, D. A multitargeted, metronomic, and maximum-tolerated dose "chemo-switch" regimen is antiangiogenic, producing objective responses and survival benefit in a mouse model of cancer. *J Clin Oncol* **2005**, 23, 939-52.
57. Tran Cao, H. S.; Bouvet, M.; Kaushal, S.; Keleman, A.; Romney, E.; Kim, G.; Fruehauf, J.; Imagawa, D. K.; Hoffman, R. M.; Katz, M. H. Metronomic gemcitabine in combination with sunitinib inhibits multisite metastasis and increases survival in an orthotopic model of pancreatic cancer. *Mol Cancer Ther* **2010**, 9, 2068-78.
58. Laquente, B.; Lacasa, C.; Ginesta, M. M.; Casanovas, O.; Figueras, A.; Galan, M.; Ribas, I. G.; Germa, J. R.; Capella, G.; Vinals, F. Antiangiogenic effect of gemcitabine following metronomic administration in a pancreas cancer model. *Mol Cancer Ther* **2008**, 7, 638-47.
59. O'Reilly, E. M.; Niedzwiecki, D.; Hall, M.; Hollis, D.; Bekaii-Saab, T.; Pluard, T.; Douglas, K.; Abou-Alfa, G. K.; Kindler, H. L.; Schilsky, R. L.; Goldberg, R. M. A Cancer and Leukemia Group B phase II study of sunitinib malate in patients with previously treated metastatic pancreatic adenocarcinoma (CALGB 80603). *Oncologist* **2010**, 15, 1310-9.
60. Blansfield, J. A.; Caragacianu, D.; Alexander, H. R.; Tangrea, M. A.; Morita, S. Y.; Lorang, D.; Schafer, P.; Muller, G.; Stirling, D.; Royal, R. E.; Libutti, S. K. Combining agents that target the tumor microenvironment improves the efficacy of anticancer therapy. *Clinical Cancer Research* **2008**, 14, 270-280.
61. Cuneo, K. C.; Geng, L.; Fu, A.; Orton, D.; Hallahan, D. E.; Chakravarthy, A. B. SU11248 (sunitinib) sensitizes pancreatic cancer to the cytotoxic effects of ionizing radiation. *Int J Radiat Oncol Biol Phys* **2008**, 71, 873-9.
62. Cumashi, A.; Tinari, N.; Rossi, C.; Lattanzio, R.; Natoli, C.; Piantelli, M.; Iacobelli, S. Sunitinib malate (SU-11248) alone or in combination with low-dose docetaxel inhibits the growth of DU-145 prostate cancer xenografts. *Cancer Lett* **2008**, 270, 229-33.
63. Li, M.; Li, H.; Cheng, X.; Wang, X.; Li, L.; Zhou, T.; Lu, W. Preclinical pharmacokinetic/pharmacodynamic models to predict schedule-dependent interaction between erlotinib and gemcitabine. *Pharm Res* **2013**, 30, 1400-8.

64. Furugaki, K.; Iwai, T.; Shirane, M.; Kondoh, K.; Moriya, Y.; Mori, K. Schedule-dependent antitumor activity of the combination with erlotinib and docetaxel in human non-small cell lung cancer cells with EGFR mutation, KRAS mutation or both wild-type EGFR and KRAS. *Oncol Rep* **2010**, 24, 1141-6.
65. Keith, C. T.; Borisy, A. A.; Stockwell, B. R. Multicomponent therapeutics for networked systems. *Nature Reviews Drug Discovery* **2005**, 4, 71-U10.
66. Zimmermann, G. R.; Lehar, J.; Keith, C. T. Multi-target therapeutics: when the whole is greater than the sum of the parts. *Drug Discovery Today* **2007**, 12, 34-42.
67. Chou, T. C. Theoretical basis, experimental design, and computerized simulation of synergism and antagonism in drug combination studies. *Pharmacol Rev* **2006**, 58, 621-81.
68. Jia, J.; Zhu, F.; Ma, X. H.; Cao, Z. W. W.; Li, Y. X. X.; Chen, Y. Z. Mechanisms of drug combinations: interaction and network perspectives. *Nature Reviews Drug Discovery* **2009**, 8, 111-128.

General Discussion

As a consequence of the extremely complex physiology and the heterogeneity of pancreatic cancer and its microenvironment, successful chemotherapy for this pathology is still an active challenge.[1]

Advanced nanoscale drug delivery systems hold the potential to overcome the limits of traditional treatments and improve chemotherapy efficiency through (*i*) their surface functionalization with ligands that specifically bind receptors mainly expressed on malignant cells[2] and/or (*ii*) the co-delivery in the same system of drug molecules capable to interact in a synergistic fashion with multiple targets countering different biological signaling pathways.[3] However, it has been observed that the choice of ligands not highly specific for pancreatic cancer or a not adequate surface functionalization resulted in limited targeting capacity. Besides, an effective combined drug therapy requires an appropriate drug pair, precise dosage and well defined treatment schedule.

Scientific activity of our research groups is devoted to the design of nanoscale drug delivery systems and much work has been done in the last years using squalene as drug carrier. The "squalenoylation" approach, which consists in the chemical coupling of squalene to biologically active drug molecules, has been firstly applied to gemcitabine (dFdC) as a model anticancer drug. The gemcitabine-squalene bioconjugate demonstrated the ability to self-assemble in the form of nanoparticles (*i.e.*, SQdFdC NPs) which exhibited greater anticancer activity than gemcitabine against different experimental tumor models (*i.e.,* leukemia and pancreatic cancer).[4-7]

In this context, the aim of this study was to further improve the antitumor efficacy of SQdFdC NPs and to propose novel strategies to optimize pancreatic cancer treatment taking into account the specific physio-pathology of this tumor.

One approach consisted in the design of novel peptide-functionalized SQdFdC NPs performing a detailed investigation of both the formulation parameters involved in the nanoparticle preparation and the physico-chemical properties of the resulting nanocarriers.

As an alternative strategy we formulated multi-therapeutic nanoparticles by combining the anticancer SQdFdC bioconjugate to a tyrosine kinase inhibitor; these agents synergistically interact together leading to a reduction of the required effective dose to achieve the same final antitumor effect. SQdFdC **(1)** was synthesized as reported elsewhere[6] by acylation of the C-4 nitrogen atom of the cytosine nucleus with squalene previously modified with an acid function. In addition, during this research work, a small library of squalenoyl prodrugs or derivatives was synthesized (Figure 1).

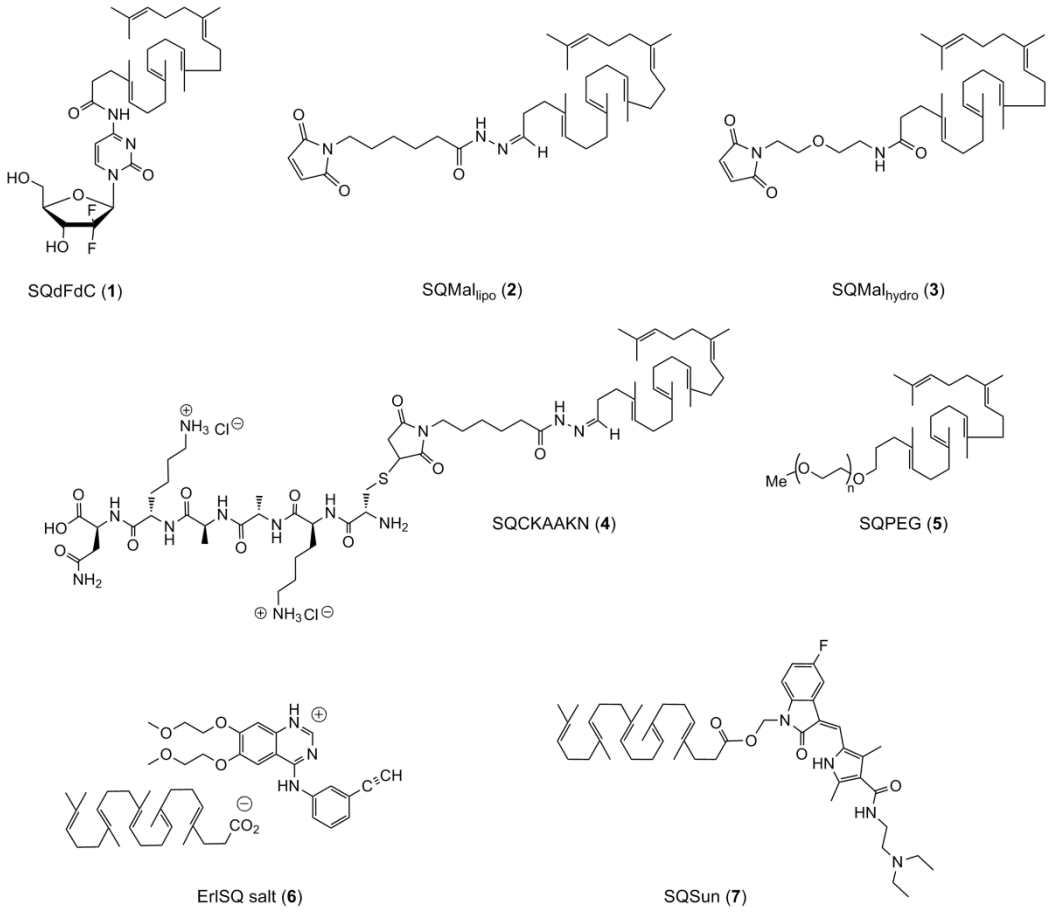

Figure 1. Library of squalenoyl prodrugs or derivatives synthesized in this work.

Peptide-functionalized squalenoyl nanoparticles for selective targeting of pancreatic carcinoma: from the rational design to the antitumor activity evaluation in vitro and in vivo models

Functionalized SQdFdC nanoparticles were prepared by conjugating them to a targeting agent, the CKAAKN peptide, previously identified as efficient homing device within the pancreatic pathological microenvironment by phage display screening.[8]
CKAAKN was conjugated to the nanoparticles by the well-explored thiol-maleimide Michael addition coupling strategy either (*i*) by reacting the targeting moiety with preformed nanoparticles obtained with the nanoprecipitation technique (Figure 2a) or (*ii*) by conjugating the peptide with a squalenoyl derivative and then co-formulating the obtained bioconjugate with SQdFdC (Figure 2b).

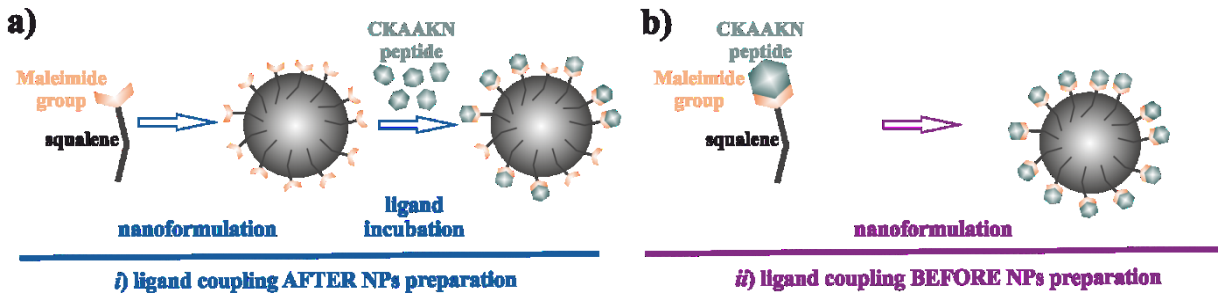

Figure 2. Strategies to prepare peptide-functionalized squalenoyl NPs. The CKAAKN peptide was **a)** coupled to the surface after nanoparticle formation or **b)** directly conjugated to squalene prior to NPs formation.

In accordance with the first strategy, two different maleimide group-bearing squalene derivatives (*i.e.,* $SQMal_{lipo}$ (**2**) and $SQMal_{hydro}$ (**3**)) able to link the peptide *via* its thiol function were co-nanoprecipitated with SQdFdC using acetone or ethanol as organic solvent. The use of the squalene derivative containing a lipophilic spacer and using acetone as solvent allowed to prepare NPs with a good colloidal stability. In addition, this solvent enabled the localization of maleimide groups at the NP surface, thus confirming previous observations related to the role of the organic solvent used during the nanoprecipitation process on the surface properties of the nanoparticles.[9,10-12] Opportunely tuning the ratio between the squalenoyl derivatives and the peptide, stable peptide-decorated NPs (**$N1_a$-P***) were constructed. In this case, the study of the thiol/maleimide group interactions suggested that this coupling strategy enabled only the establishment of weak non covalent interactions between the peptide and the NP surface.
In accordance with functionalization prior nanoparticle assembly strategy, the desired conjugate SQCKAAKN (**4**) was obtained with a satisfactory 70% yield despite the difficulty to allow the highly hydrophilic peptide to react with the lipophilic squalene derivative (Figure 1). SQdFdC/SQCKAAKN NPs (**N4-P*,** molar ratio 1:0.01) displayed the highest colloidal stability. The variation of the NP surface charge as a function of the pH suggested the surface disposition of the peptide during the process of nanoparticles formation.
To further investigate which was the best coupling strategy, the ability of peptide-decorated NPs to recognize the biological target receptor was also investigated.
Interestingly, in SPR experiments the CKAAKN peptide was able to specifically interact with the sensorchip-immobilized sFRP-4 receptor, thus confirming the previous observed homology of the petide with the Wnt-2 protein.[8] Although both **$N1_a$-P*** and **N4-P*** specifically interacted with the receptor (which was not the case for untargeted nanoparticles), only **N4-P*** enabled to reach the most important plasmonic signal with a dose-response behavior (Figure 3).

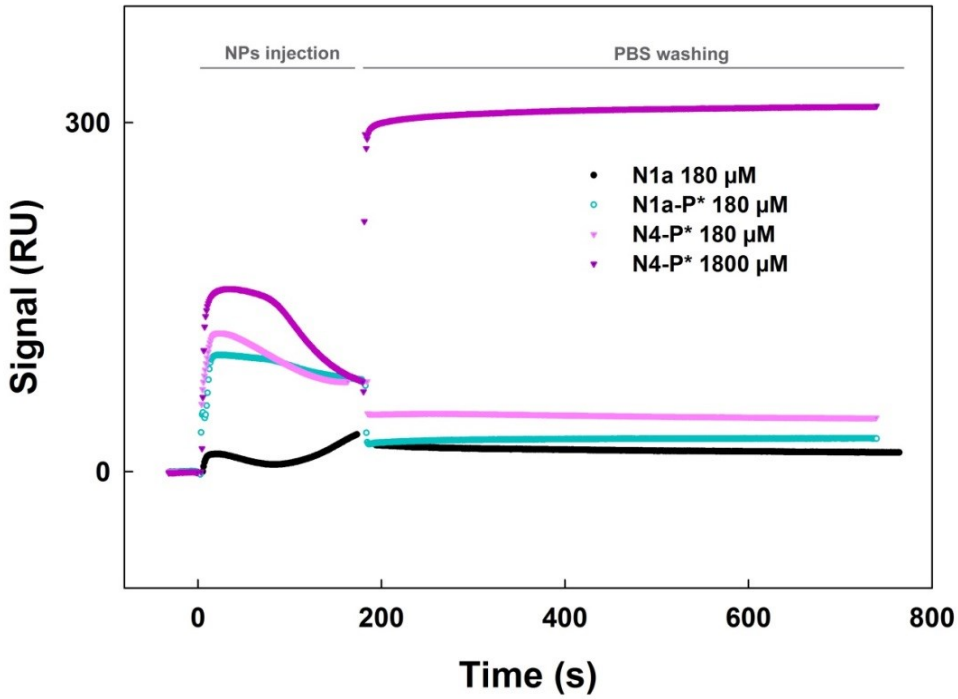

Figure 3. SPR sensorgrams (resonance units (RU) *versus* time) obtained by simultaneous injections of unfunctionalized SQdFdC/SQMal$_{lipo}$ NPs (**N1a**) 180 µM, SQdFdC/SQMal $_{lipo}$ /CKAAKN 5/1/0.25 NPs (**N1$_a$-P*)** 180 µM**,** SQdFdC/SQCKAAKN 1/0.01 NPs (**N4-P*)** 180 and 1800 µM over sFRP-4 immobilized on two parallel channels of the same sensor chip.

This investigation resulted extremely important for several reasons. Firstly, the Wnt-2 signaling pathway was identified as a biological target of the CKAAKN peptide. The overexpression of Wnt-2, which belongs to a family of secreted lipid-modified signaling glycoproteins involved in embryonic development and tissue homeostasis[13], has been recently correlated to tumorigenesis, driving the self-renewal and differentiation of cancer stem cells and promoting the angiogenesis process.[1,13-16] Moreover, recent comprehensive genetic analysis[14,17,18] revealed that the Wnt is one of the 6 signaling pathways always altered in pancreatic carcinomas.[19]

Secondly, the more important ligand-receptor interaction observed with CKAAKN-functionalized nanoparticles, if compared to the free peptide, demonstrated that the affinity of phage-display-derivated peptides can be significantly enhanced thanks to the multivalent interactions offered by a scaffold-like nanosized material in accordance to previous observations.[20,21]

Finally, the enhanced target binding and specific avidity of **N4-P*** suggested that the covalent conjugation of the peptide to squalene prior nanoformulation was the most suitable coupling strategy to ensure stronger association with the target. This hypothesis was confirmed by *in vitro* studies performed in MIA PaCa-2 pancreatic tumor cells revealing a more efficient cellular internalization of **N4-P*** in comparison to **N1$_a$-P*** which led to an increased cytotoxic effect (Figure 4). These results suggested that the peptide coupled to preformed NPs (**N1$_a$-P***) was unstable in biological media, thus inefficient to give good targeting ability.

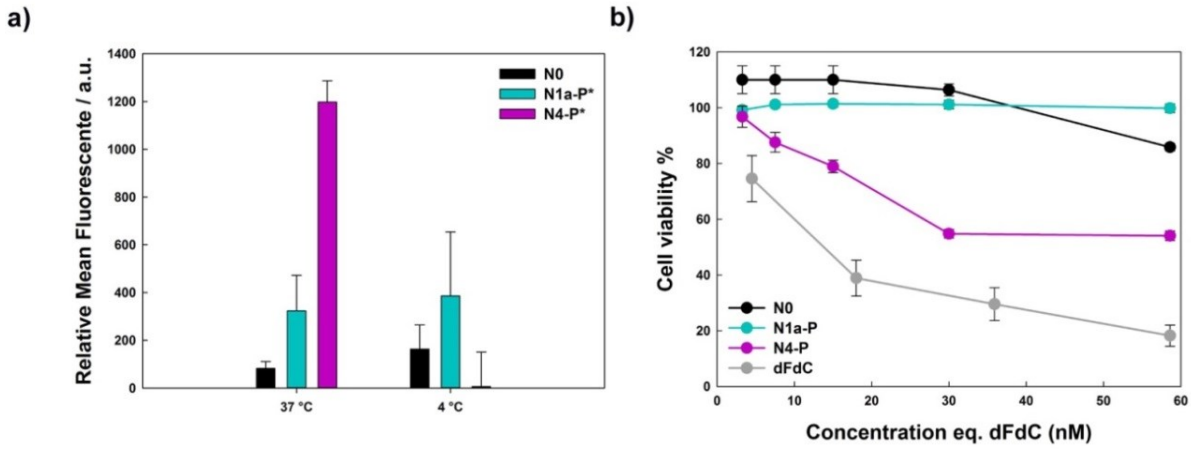

Figure 4. a) Cellular uptake quantification of SQdFdC NPs (**N0)**, SQdFdC/SQMal $_{lipo}$ /CKAAKN 5/1/0.25 NPs (**N1$_a$-P***) or SQdFdC/SQCKAAKN 1/0.01 NPs (**N4-P***) after 6-h incubation at 37 and 4 °C. All NPs were labeled with BChol-green and incubated at a final concentration of 1 µM eq. SQdFdC. **b)** Cell viability of cells treated with increasing concentrations of dFdC as free drug (**dFdC**), SQdFdC NPs (**N0**), SQdFdC/SQMal $_{lipo}$ /CKAAKN 5/1/0.25 NPs (**N1$_a$-P***) or SQdFdC/SQCKAAKN 1/0.01 NPs (**N4-P*)** for 72 h. Cytotoxicity of nanoparticles was compared to non-treated cells. Values represent mean ± SEM.

To further investigate the tumor cell targeting, the interaction of **N4-P*** with healthy cells (i.e., NIH/3T3 fibroblastic cells) was studied and compared to the uptake by MIA PaCa-2 cells. Non functionalized nanoparticles were taken-up by both cell lines in a nonspecific manner, resulting in higher accumulation and cytotoxicity in NIH/3T3 fibroblasts. On the contrary, CKAAKN-functionalized squalene-based nanoparticles were internalized into the cells by a receptor-mediated mechanism, which allowed to achieve highly selective tumor cell uptake and toxicity, while decreasing non-specific accumulation into healthy cells (Figure 5).

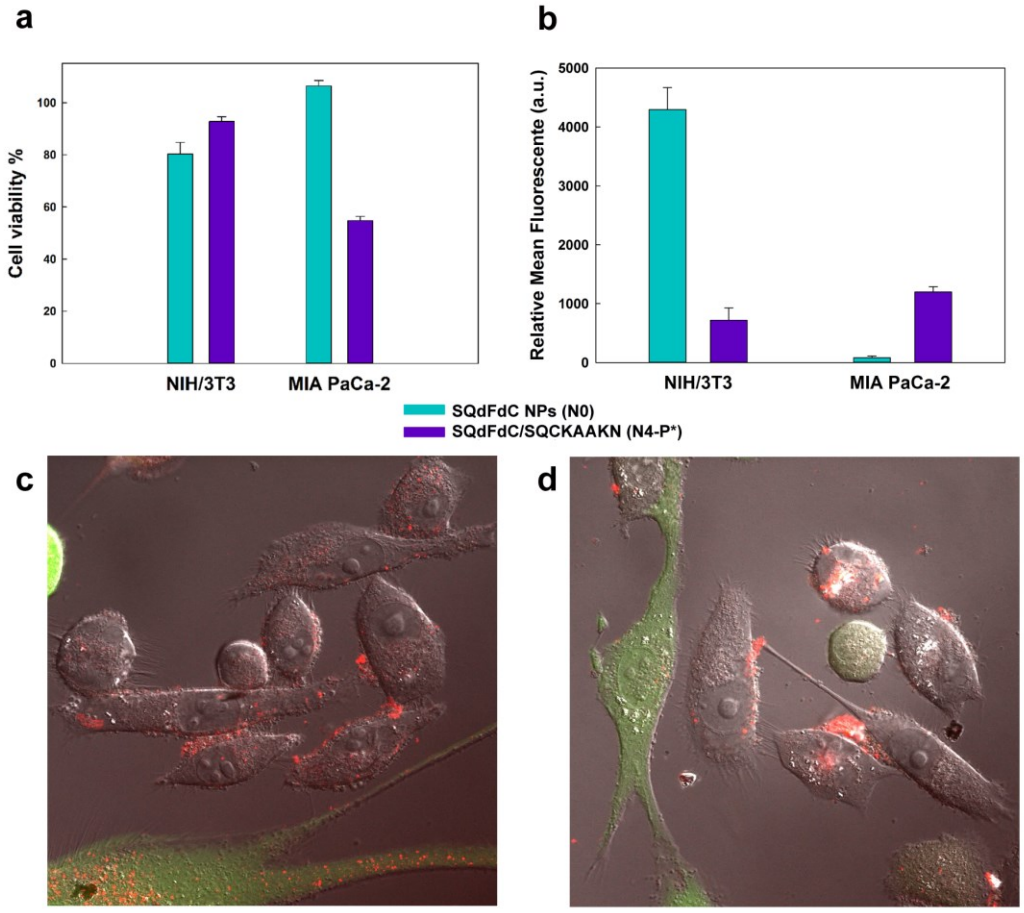

Figure 5. (a) Viability of MIA Paca-2 and NIH/3T3 cells treated for 72 h with SQdFdC NPs (**N0**) and SQdFdC/SQCKAAKN NPs (**N4-P***) (30 nM eq. dFdC). **(b)** Quantification of cellular uptake of BChol-green-labeled SQdFdC NPs (**N0**) and BChol-green-labeled SQdFdC/SQCKAAKN NPs (**N4-P***) in NIH/3T3 and MIA PaCa-2 cells at 37 °C. **(c)** 3D reconstruction images obtained from confocal z scans of a coculture of NIH/3T3 (green) and MIA PaCa-2 cells (unstained) after incubation with BChol-red-labeled SQdFdC NPs (**N0**) and **(d)** BChol-red-labeled SQdFdC/SQCKAAKN NPs (**N4-P***). Values represent mean ± SEM. Scale bars = 20 μm.

Notheworthy is that both types of nanoparticles, either peptide-functionalized or not, resulted to be very weak activators of the complement C3 component, thus supporting the hypothesis of a potentially safe intravenous administration avoiding pseudo-allergic reactions responsible for severe side effects.[22-24] In the light of the promising results, we performed a regression trial *in vivo* on RIP-Tag2 mice, a spontaneously arising model of pancreatic cancer. Interestingly, peptide-functionalized NPs displayed a greater efficacy in impairing tumor growth associated to a dramatic increase of apoptosis in cancer cells and tumor blood vessels and an increased pericyte coverage compared to all other treatment groups (Figure 6). These results pointed out that the enhanced antitumor activity observed for the CKAAKN-functionalized NPs relied on the multiple ability of (*i*) targeting both tumor and vessel cells, (*ii*) inhibiting tumor growth and angiogenesis and (*iii*) normalizing the remaining vasculature as previously observed with angiogenesis inhibitors.

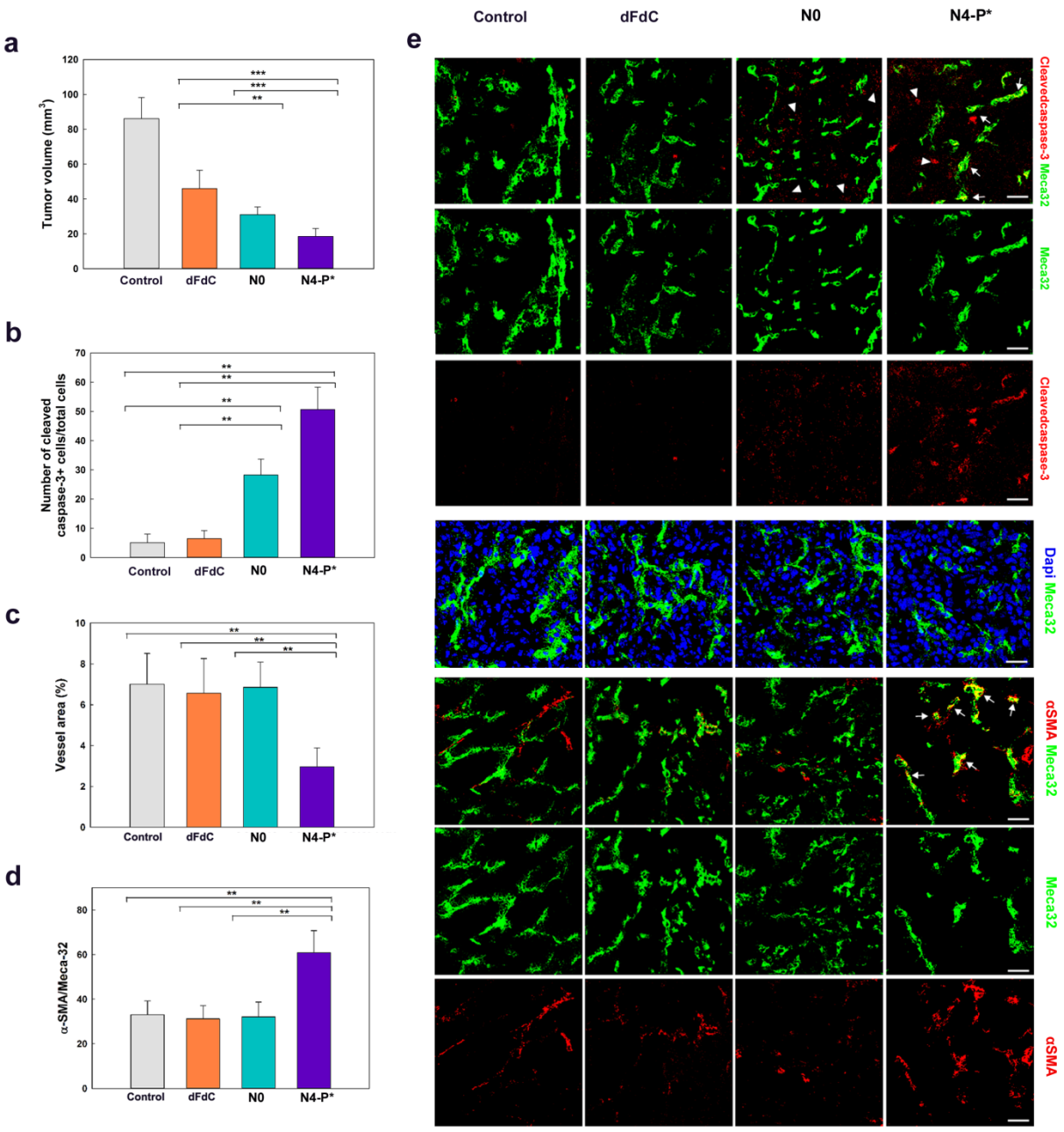

Figure 6. (a) Total tumor volume in a 4-weeks regression trial in RIP-Tag2 mice. (*n*=8/group). **(b)** Apoptotic index of cleaved caspase-3+ cells on total cells. **(c)** Percentage of surface area occupied by vessels quantified as Meca32 (endothelial marker) positive staining. **(d)** Quantification analysis of α-SMA (pericyte marker) localized in proximity to endothelial cells-lined blood vessels. **(e)** Confocal images of each treatment group. Endothelial cells apoptotic rate was detected by colocalization of Meca32 (green - arrows) with cleaved caspase-3+ (red - arrow heads). Nuclei were stained with DAPI (blue). Tumor vessel pericyte coverage was evaluated as Meca32 (green), α-SMA (red) and colocalization (arrows). Values represent mean ± SD. Statistical difference is marked by $^{**}p < 0.01$; $^{***}p < 0.001$. Images are representative of 5 fields per mouse from a total of 8 mice per treatment group. Scale bars: 50 μm.

Squalene-based nanomedicine for synergetic combined therapy between gemcitabine and tyrosine kinase inhibitor

NPs for combined therapy were constructed by combining SQdFdC with erlotinib (Erl) and sunitinib (Sun) (i.e., tyrosine kinase inhibitors). In accordance with their physico-chemical properties, Erl, a hydrophobic molecule, was encapsulated as free drug into SQdFdC NPs, while Sun, due to its hydrophilic nature, was co-nanoprecipited as squalenoyl prodrug.
In all cases, NPs were successfully prepared by simple nanoprecipitation in water of the ethanolic solution of nanoparticle components followed by solvent evaporation under vacuum. For Erl-encapsulating NPs, during the nanoprecipitation process the high melting point of the drug and the thermodynamics/kinetics parameters presumably promoted the drug crystallization in the aqueous phase instead of its partition in the squalene core, thus leading to low encapsulation efficiency and drug loading. The development of two different salts, the erlotinib-tosylate and the erlotinib-squalenate **(6)**, resulted a good approach to hinder the crystallization phenomenon and improve Erl drug loading.
In parallel, the sunitinib conjugate SQSun **(7)**, bearing an acid-sensitive hemi-aminal ester group, was synthetized. Co-nanoprecipitation of the two bioconjugates (SQdFdC and SQSun) led to their self-assembly in a stable single nanoparticle (SQdFdC/SQSun NP) with narrow size distribution.
Then, in order to assess whether the combined therapy (*i.e.,* SQdFdC in combination with Erl-salts or SQSun) could enhance the antitumor activity of SQdFdC, MIA Paca-2 cells were incubated with the different NPs formulations at the same SQdFdC. None additive effect was observed after cell exposure to both Erl-salt-based SQdFdC NPs compared to SQdFdC NPs, probably as consequence of the low Erl drug loading. On the other hand, SQdFdC/SQSun NPs led to a significant increase of the cell toxicity compared with SQdFdC NPs alone (Figure 7b). Of note, treatment of 0.022 µM of SQdFdC and 0.55 µM of SQSun was not efficient in killing cancer cells in monotherapy (*i.e.,* SQdFdC NPs and SQSun NPs) while led to a viability reduction of 50% in combined therapy (*i.e.,* SQdFdC/SQSun NPs) (Figure 7c).

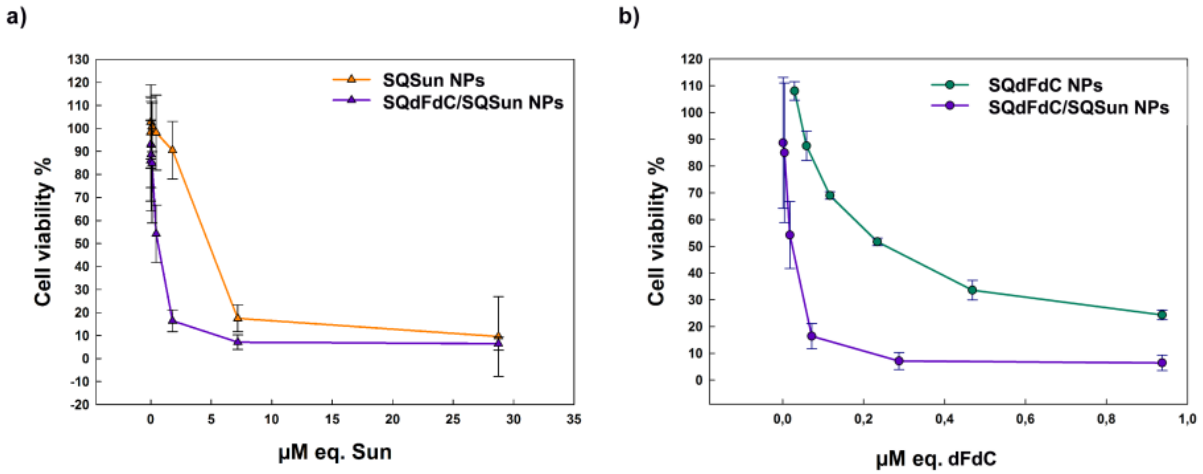

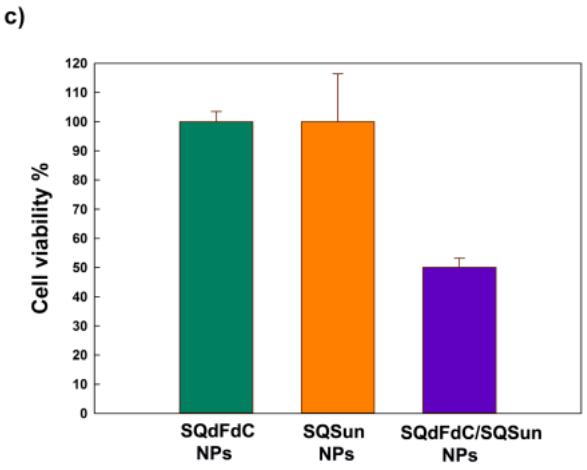

Figure 7. Viability of MIA Paca-2 cells after exposure to increasing concentrations of **(a)** SQdFdC/SQSun NPs and SQSun NPs; **(b)** SQdFdC/SQSun NPs and SQdFdC NPs for 72 h. **(c)** Viability of MIA Paca-2 cells incubated with SQdFdC/SQSun NPs at a concentration corresponding to the IC_{50} (*i.e.,* 0.022 μM for SQdFdC and 0.55 μM for SQSun), compared with the SQdFdC NPs and SQSun NPs at the corresponding molar concentration. Values represent mean ± SD.

A further investigation on the potential influence of the cell exposure timing to the NPs or the free drugs revealed a superior cytotoxicity only in the case of SQdFdC/SQSun NPs. Noteworthy is that the concurrent treatment with the physical mixture (SQdFdC NPs + SQSun NPs) did not show significant difference compared with the cytotoxic effect induced by each NPs in monotherapy, suggesting that the superior antitumor activity relied on the exposure to SQdFdC and SQSun only when they co-exist in the same nanoparticle. Finally, a detailed combined therapy study based on the Chou-Talalay method[25] showed that this greater antitumor activity was due to a strong synergistic interaction. The simplest drug interaction parameter resulted from this analysis was the combination index (CI), which allows to quantitatively determine synergistic (CI < 1), additive (CI = 1) and antagonistic (CI > 1) effects for each dose tested in combined therapies. The CI plot as a function of cytotoxicity (Fa) (e.g., Fa of 0.9 corresponds to 90% of cytotoxicity) was calculated for dFdC/Sun free drugs combination or SQdFdC/SQSun NPs (Figure 8). Noteworthy is that only SQdFdC/SQSun NPs (Figure 8 – left panel) showed a synergistic effect also at Fa > 0.8 which is more therapeutically relevant since the chemotherapy are aimed to eradicate the cancer cells working at high level of cytotoxicity. Contrarily, dFdC/Sun displayed an antagonistic effect at high Fa values (Figure 8 – right panel).

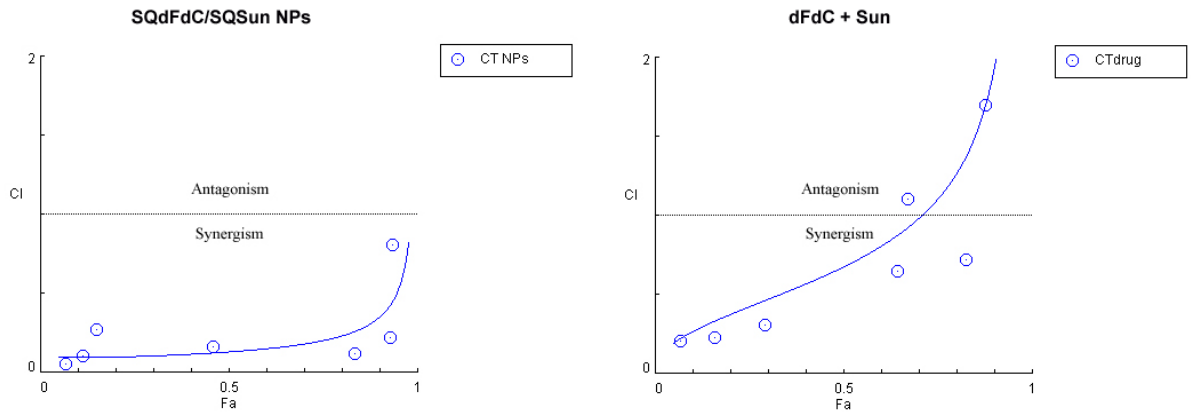

Figure 8. Combination Index plots for SQdFdC/SQSun NPs (CT NPs - left panel) and dFdC/Sun free drugs association (CTdrug - right panel). Combined index (CI) is represented as a function of effect level (Fa). The data points (blue circles) and the correlated simulated curve (blue line) below, at, and above the horizontal line of CI=1 indicate synergistic, additive and antagonistic effect, respectively.

The combined therapy analysis also permitted to calculate the dose-reduction index (DRI), which represents the drug dose reduction to reach a given effect level in combined therapy in comparison to monotherapy. Remarkably, in order to obtain the 90% of cytotoxicity, the SQdFdC/SQSun NPs allowed to reduce the dFdC dose around 38 times, which may represent an important advantage enabling to reduce the side toxicity associated to this chemotherapy agent.
These results combined to the CI plot demonstrate the possibility to achieve a higher *in vitro* anticancer synergistic activity at high cytotoxicity taking advantage of a squalene-based nanoparticles combined therapy.

References

1. Hidalgo, M. Pancreatic cancer. *N Engl J Med* **2010**, 362, 1605-17.
2. Nicolas, J.; Mura, S.; Brambilla, D.; Mackiewicz, N.; Couvreur, P. Design, functionalization strategies and biomedical applications of targeted biodegradable/biocompatible polymer-based nanocarriers for drug delivery. *Chem Soc Rev* **2013**, 42, 1147-235.
3. Ma, L.; Kohli, M.; Smith, A. Nanoparticles for combination drug therapy. *Acs Nano* **2013**, 7, 9518-25.
4. Reddy, L. H.; Renoir, J. M.; Marsaud, V.; Lepetre-Mouelhi, S.; Desmaele, D.; Couvreur, P. Anticancer efficacy of squalenoyl gemcitabine nanomedicine on 60 human tumor cell panel and on experimental tumor. *Mol Pharm* **2009**, 6, 1526-35.
5. Reddy, L. H.; Ferreira, H.; Dubernet, C.; Mouelhi, S. L.; Desmaele, D.; Rousseau, B.; Couvreur, P. Squalenoyl nanomedicine of gemcitabine is more potent after oral administration in leukemia-bearing rats: study of mechanisms. *Anticancer Drugs* **2008**, 19, 999-1006.
6. Couvreur, P.; Stella, B.; Reddy, L. H.; Hillaireau, H.; Dubernet, C.; Desmaele, D.; Lepetre-Mouelhi, S.; Rocco, F.; Dereuddre-Bosquet, N.; Clayette, P.; Rosilio, V.; Marsaud, V.; Renoir, J. M.; Cattel, L. Squalenoyl nanomedicines as potential therapeutics. *Nano Lett.* **2006**, 6, 2544-8.
7. Rejiba, S.; Reddy, L. H.; Bigand, C.; Parmentier, C.; Couvreur, P.; Hajri, A. Squalenoyl gemcitabine nanomedicine overcomes the low efficacy of gemcitabine therapy in pancreatic cancer. *Nanomedicine* **2011**, 7, 841-9.
8. Joyce, J. A.; Laakkonen, P.; Bernasconi, M.; Bergers, G.; Ruoslahti, E.; Hanahan, D. Stage-specific vascular markers revealed by phage display in a mouse model of pancreatic islet tumorigenesis. *Cancer Cell.* **2003**, 4, 393-403.
9. Ganachaud, F.; Katz, J. L. Nanoparticles and nanocapsules created using the Ouzo effect: Spontaneous emulsification as an alternative to ultrasonic and high-shear devices. *Chemphyschem* **2005**, 6, 209-216.
10. Yu, W.; Doegito, E. S. T.; Barratt, G.; Fessi, H.; Devissaguet, J. P.; Puisieux, F. A Novel-Approach to the Preparation of Injectable Emulsions by a Spontaneous Emulsification Process. *International Journal of Pharmaceutics* **1993**, 89, 139-146.
11. Bouchemal, K.; Briancon, S.; Perrier, E.; Fessi, H. Nano-emulsion formulation using spontaneous emulsification: solvent, oil and surfactant optimisation. *International Journal of Pharmaceutics* **2004**, 280, 241-251.
12. Legrand, P.; Lesieur, S.; Bochot, A.; Gref, R.; Raatjes, W.; Barratt, G.; Vauthier, C. Influence of polymer behaviour in organic solution on the production of polylactide nanoparticles by nanoprecipitation. *Int J Pharm* **2007**, 344, 33-43.
13. Holland, J. D.; Klaus, A.; Garratt, A. N.; Birchmeier, W. Wnt signaling in stem and cancer stem cells. *Curr Opin Cell Biol* **2013**, 25, 254-64.
14. Jones, S.; Zhang, X.; Parsons, D. W.; Lin, J. C.; Leary, R. J.; Angenendt, P.; Mankoo, P.; Carter, H.; Kamiyama, H.; Jimeno, A.; Hong, S. M.; Fu, B.; Lin, M. T.; Calhoun, E. S.; Kamiyama, M.; Walter, K.; Nikolskaya, T.; Nikolsky, Y.; Hartigan, J.; Smith, D. R.; Hidalgo, M.; Leach, S. D.; Klein, A. P.; Jaffee, E. M.; Goggins, M.; Maitra, A.; Iacobuzio-Donahue, C.; Eshleman, J. R.; Kern, S. E.; Hruban, R. H.; Karchin, R.; Papadopoulos, N.; Parmigiani, G.; Vogelstein, B.; Velculescu, V. E.; Kinzler, K. W. Core signaling pathways in human pancreatic cancers revealed by global genomic analyses. *Science* **2008**, 321, 1801-6.
15. Morris, J. P.; Wang, S. C.; Hebrok, M. KRAS, Hedgehog, Wnt and the twisted developmental biology of pancreatic ductal adenocarcinoma. *Nat Rev Cancer* **2010,** 10, 683-695.

16. Katoh, M. WNT2 and human gastrointestinal cancer (review). *Int J Mol Med* **2003**, 12, 811-6.
17. Yachida, S.; Jones, S.; Bozic, I.; Antal, T.; Leary, R.; Fu, B. J.; Kamiyama, M.; Hruban, R. H.; Eshleman, J. R.; Nowak, M. A.; Velculescu, V. E.; Kinzler, K. W.; Vogelstein, B.; Iacobuzio-Donahue, C. A. Distant metastasis occurs late during the genetic evolution of pancreatic cancer. *Nature* **2010**, 467, 1114-U126.
18. Campbell, P. J.; Yachida, S.; Mudie, L. J.; Stephens, P. J.; Pleasance, E. D.; Stebbings, L. A.; Morsberger, L. A.; Latimer, C.; McLaren, S.; Lin, M. L.; McBride, D. J.; Varela, I.; Nik-Zainal, S. A.; Leroy, C.; Jia, M. M.; Menzies, A.; Butler, A. P.; Teague, J. W.; Griffin, C. A.; Burton, J.; Swerdlow, H.; Quail, M. A.; Stratton, M. R.; Iacobuzio-Donahue, C.; Futreal, P. A. The patterns and dynamics of genomic instability in metastatic pancreatic cancer. *Nature* **2010**, 467, 1109-1113.
19. Corbo, V.; Tortora, G.; Scarpa, A. Molecular Pathology of Pancreatic Cancer: From Bench-to-Bedside Translation. *Current Drug Targets* **2012**, 13, 744-752.
20. Reulen, S. W.; Dankers, P. Y.; Bomans, P. H.; Meijer, E. W.; Merkx, M. Collagen targeting using protein-functionalized micelles: the strength of multiple weak interactions. *J Am Chem Soc* **2009**, 131, 7304-12.
21. Montet, X.; Funovics, M.; Montet-Abou, K.; Weissleder, R.; Josephson, L. Multivalent effects of RGD peptides obtained by nanoparticle display. *J Med Chem* **2006**, 49, 6087-93.
22. Nel, A. E.; Madler, L.; Velegol, D.; Xia, T.; Hoek, E. M.; Somasundaran, P.; Klaessig, F.; Castranova, V.; Thompson, M. Understanding biophysicochemical interactions at the nano-bio interface. *Nat Mater* **2009**, 8, 543-57.
23. Moghimi, S. M.; Andersen, A. J.; Hashemi, S. H.; Lettiero, B.; Ahmadvand, D.; Hunter, A. C.; Andresen, T. L.; Hamad, I.; Szebeni, J. Complement activation cascade triggered by PEG-PL engineered nanomedicines and carbon nanotubes: the challenges ahead. *J Control Release* **2010**, 146, 175-81.
24. Moghimi, S. M.; Farhangrazi, Z. S. Nanomedicine and the complement paradigm. *Nanomedicine* **2013**, 9, 458-60.
25. Chou, T. C. Theoretical basis, experimental design, and computerized simulation of synergism and antagonism in drug combination studies. *Pharmacol Rev* **2006**, 58, 621-81.

General Conclusion

and
Future Perspectives

This Ph.D. project has been performed within the scientific co-operation between the Dipartimento di Scienza e Tecnologia del Farmaco (University of Turin) and the Institut Galien Paris Sud XI (University of Paris XI) aiming to propose novel nanoscale-based strategies to optimize pancreatic cancer treatment taking into account the specific physio-pathology of this tumor. In order to achieve this aim, the co-tutoring doctorate and the scientific collaboration among research groups was necessary for joining the chemical and technological skills of the University of Turin and those technological and pharmacological of the University of Paris XI.

In this work we have designed peptide-targeted squalene-based nanoparticles suitable for pancreatic cancer treatment, able to specifically interact with both tumor cells and angiogenic vessels and capable of simultaneously promoting pericyte coverage, thus leading to the normalization of the pre-existent vasculature likely improving the tumor accessibility for the therapy. Indeed, a rational study that investigates both the formulation parameters involved in the nanoparticles preparation and the physico-chemical properties highlighted that active targeted nanoparticles should not be simply designed as largely modular assemblies of scaffold, linker and targeting ligand, but rigorous studies must be performed in order to clarify how different structural components collaborate to determine the real ligand affinity.
In a second approach, by combining two therapeutic agents in the same squalene-based nanoparticle we constructed a multi-therapeutic drug delivery system capable to increase the therapeutic index of the combined therapy, opening interesting perspectives for metronomic treatment in pancreatic cancer.

In this view, further studies to investigate the kinetic of *in vitro* drug release, the *in vivo* pharmacokinetic/pharmacodynamic profile, the relevance of the Wnt2 signaling pathway as target for the CKAAKN-functionalized nanoparticles, and the mechanisms responsible for the sequence-dependent anti-proliferative effect for combined therapy nanoparticles have to be conducted to deeply investigate their real potential in the pancreatic cancer treatment.

Abbreviations

ADV	Acoustic droplet vaporization
Bchl	Bacteriochlorophyll
CAF	Complement activating factor
CARPA	Complement activation-related pseudoallergy
Chol	Cholesterol
CI	Combination index
CKAAKN	CKAAKN peptide
CT	Combined therapy
dFdC	Gemcitabine
DiR	1,1'-Dioctadecyl-3,3,3',3'-Tetramethylindotricarbocyanine Iodide
DL%	Drug loading
DLS	Dynamic light scattering
DMEM	Dulbecco's modified eagle medium
DRI	Dose-reduction index
DSPE	Distearoylphosphatidylethanolamine
EE%	Encapsulation Efficiency
EGFR	Epidermal growth factor receptor
EPR	Enhanced permeability and retention
Erl	Erlotinib
ErlSQ salt	N-(3-ethynylphenyl)-6,7-bis(2-methoxyethoxy)4-quinazolinaminium trisnorsqualenate salt
ErlTs salt	N-(3-ethynylphenyl)-6,7-bis(2-methoxyethoxy)4-quinazolinaminium p-toluenesulfonate salt
Fa	Level of cytotoxicity
FA	Folic acid
FBS	Fetal bovine serum
FR	Folic acid receptor
FZD	Frizzled receptor
HA	Hyaluronic acid
HDL	High density lipoprotein
HIFU	High-intensity focused ultrasounds
ICG	Indocyanine green
ITC	Isothermal titration calorimetry
LDL	Low-density lipoprotein
LNC	Lipid nanocapsules
MNP	Magnetic nanoparticle
MRI	Magnetic resonance imaging
NIR	Near infra-red
NP	Nanoparticle
$N0_a$	SQdFdC nanoparticles, acetone as organic solvent
$N0_e$	SQdFdC nanoparticles, ethanol as organic solvent
N1	SQdFdC/$SQMal_{lipo}$ nanoparticles

$N1_a$	$SQdFdC/SQMal_{lipo}$ nanoparticles, acetone as organic solvent
$N1_e$	$SQdFdC/SQMal_{lipo}$ nanoparticles, ethanol as organic solvent
N2	$SQdFdC/SQMal_{hydro}$ nanoparticles
N3	$SQMal_{lipo}$ nanoparticles
N4-P	SQdFdC/SQCKAAKN nanoparticles
PDGFR	Platelet-derived growth factor receptor
PDI	Polydispersity index
PEG	Polyethylene glycol
PET	Positron emission tomography
PFC	Perfluorocarbon
PFOB	Perfluoroctylbromide
QD	Quantum dots nano-crystal
RGD	Arg-Gly-Asp sequence peptide
SLN	Solid lipid nanoparticles
SPIO	Superparamagnetic iron oxide nanoparticle
SPR	Surface plasmon resonance
SQ	Squalene
SQdFdC	4-(N)-1,1',2-Trisnorsqualenoyl-gemcitabine/4-(N)-1,1',2-trisnorsqualenoyl-2',2'-difluoro-2'-dideoxycytidine
SQdFdC/SQCKAAKN NPs	CKAAKN-functionalized squalenoyl-gemcitabine nanoparticles
SQCKAAKN	Michael adduct of CKAAKN and 6-(2,5-dioxo-2,5-dihydro-1H-pyrrol-1-yl)-N'-[(4E,8E,12E,16E)-4,8,13,17,21-pentamethyldocosa-4,8,12,16,20-pentaen-1-ylidene]hexanehydrazide
SQMalhydro	2-[2-(2,5-Dioxo-2,5-dihydro-1H-pyrrol-1-yl)ethoxy]ethyl (4E,8E,12E,16E)-4,8,13,17,21-pentamethyl-docosa-4,8,12,16,20-pentaenoate
$SQMal_{lipo}$	6-(2,5-Dioxo-2,5-dihydro-1H-pyrrol-1-yl)-N'-[(4E,8E,12E,16E)-4,8,13,17,21-pentamethyldocosa-4,8,12,16,20-pentaen-1-ylidene]hexanehydrazide
SQPEG	Trisnorsqualene-MePEG
SQSun	[(3Z)-3-[(4-{[2-(diethylamino)ethyl]carbamoyl}-3,5-dimethyl-1H-pyrrol-2-yl)methylidene]-5-fluoro-2-oxo-2,3-dihydro-1H-indol-1-yl]methyl (4E,8E,12E,16E)-4,8,13,17,21-pentamethyldocosa-4,8,12,16,20-pentaenoate
Sun	Sunitinib
TKI	Tyrosine-kinase inhibitor
US	Ultrasonography
VEGFR	Vascular endothelial growth factor receptor
VLDL	Very low-density lipoprotein
ZP	Zeta potential

Synthèse du projet de thèse

Le cancer pancréatique représente la cinquième cause de décès par cancer dans les pays occidentaux. Son mauvais pronostic (survie à 5 ans inférieure à 3,5 % des cas) est dû à l'absence de facteurs de risques spécifiques interdisant une prévention efficace, et à un diagnostic tardif qui révèle un cancer agressif chez environ 90% des patients.[1] Actuellement, le seul traitement curatif de ce cancer est la chirurgie, mais celle-ci ne peut être envisagée que dans 10 à 15 % des cas.
La gemcitabine (dFdC), un analogue nucléoside bloquant la réplication de l'ADN, est actuellement le traitement pharmacologique de première ligne des cancers pancréatiques localement avancés et/ou métastatiques.[2] Cependant, ce traitement reste palliatif et n'augmente que faiblement le temps de survie. En effet, la gemcitabine, comme tous les principes actifs, est confrontée à de nombreux obstacles tels que le passage des barrières biologiques, la métabolisation et l'élimination plasmatique. Ces barrières mécaniques, physico-chimiques ou enzymatiques rendent l'obtention de concentrations efficaces au niveau du site d'action difficile à atteindre, et conduisent à l'apparition d'effets toxiques au niveau des autres tissus sains, pouvant provoquer l'arrêt du traitement. Par ailleurs, il a été montré que la majorité des cancers pancréatiques sont caractérisés par une vascularisation réduite et une production importante de matrice extracellulaire, qui ensemble réduisent fortement l'accès des médicaments anticancéreux à la tumeur.
L'adressage de molécules thérapeutiques vers l'organe, le tissu ou la cellule malade constitue aujourd'hui un défi majeur pour le traitement des maladies humaines notamment infectieuses, cancéreuses ou d'origine génétique. C'est pour ces raisons que le développement de nanotechnologies, en tant que vecteurs de médicaments, a pris un essor considérable au cours des dernières années. S'appuyant sur le développement de nouveaux matériaux, la recherche galénique a permis d'imaginer des systèmes d'administration sub-microniques capables : (*i*) de protéger la molécule active de la dégradation et (*ii*) d'en contrôler la libération dans le temps et dans l'espace (Figure 1).

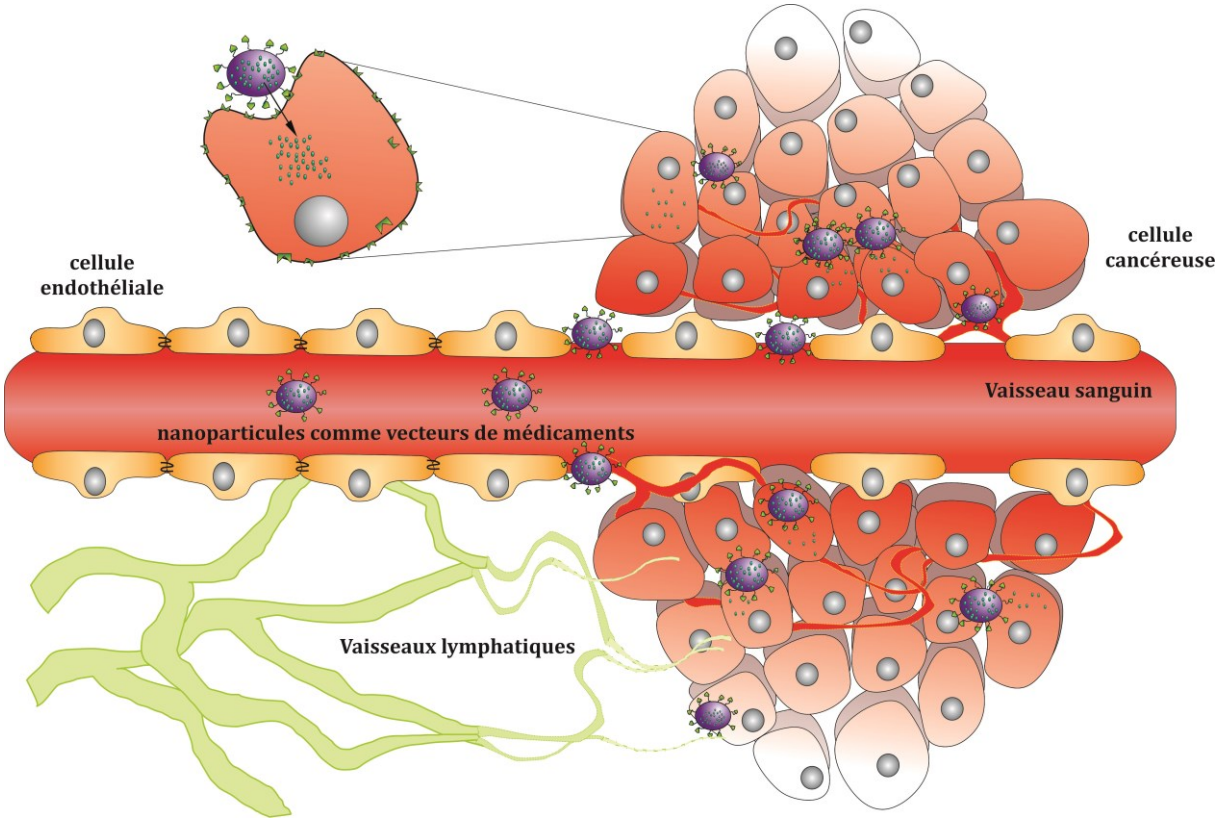

Figure 1 - Adressage de molécules thérapeutiques vers le tissu tumoral à l'aide de nanotechnologies.

Dans ce contexte, la technique de « squalènisation » a été développée en 2006 en collaboration entre le groupe de recherche du Professeur Patrick Couvreur à l'Université Paris Sud-11 et le groupe de recherche du Professeur Luigi Cattel et du Docteur Barbara Stella à l'Université de Turin (Italie). Le concept de squalènisation repose sur le couplage chimique entre le squalène (SQ), un lipide naturel précurseur de la synthèse du cholestérol, et des principes actifs (notamment des molécules anticancéreuses). Les bioconjugués ainsi formés sont alors capables de s'auto-assembler en solution aqueuse pour former des nanoparticules stables de diamètres compris entre 100 et 300 nm. L'exemple de référence dans ce domaine est la nanoparticule de gemcitabine-squalène (SQdFdC) qui a donné lieu à des résultats spectaculaires in vitro sur des lignées de cellules cancéreuses humaines.[3] In vivo, les nanoparticules de gemcitabine-squalène se sont avérées beaucoup plus efficaces que la gemcitabine libre sur des tumeurs solides greffées par voie sous-cutanée ainsi que sur des modèles murins de leucémies agressives métastatiques.[3-6] Au vu de ces résultats encourageants, le projet de thèse a été développé autour de deux axes de recherche. **(I)** Dans un premier temps, les nanoparticules de gemcitabine-squalène ont été fonctionnalisées par un peptide capable de reconnaître et de cibler spécifiquement les cellules cancéreuses pancréatiques (Figure 2I). **(II)** Le deuxième axe de recherche a visé l'encapsulation d'un second principe actif au sein des nanoparticules de gemcitabine-squalène afin de développer le concept de nanoparticule « multi-thérapeutique » (Figure 2II).

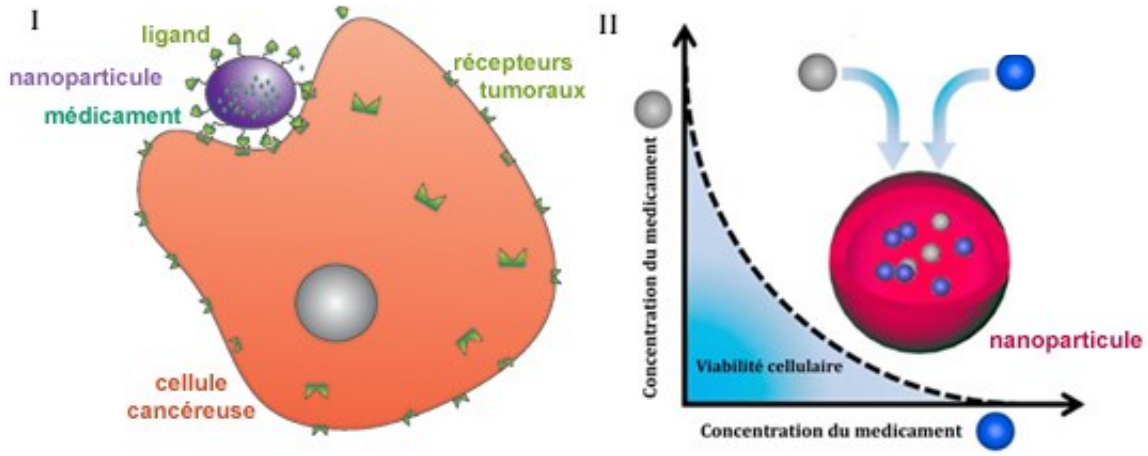

Figure 2 – Axes de recherche développés au cours du projet de thèse: **(I)** réalisation d'une nanoparticule de gemcitabine-squalène fonctionnalisées à l'aide d'un peptide capable de reconnaitre les cellules cancéreuses pancréatiques et **(II)** réalisation d'une nanoparticule multi-thérapeutique pour la délivrance de deux médicaments.

Au vu des aspects pluridisciplinaires de ce projet, la mise en commun des connaissances et des savoirs-faire des deux équipes engagées au sein de la cotutelle a permis de mener à bien ce travail de thèse. Les principaux résultats obtenus sont rapportés dans les deux sections suivantes afin de permettre à l'ensemble de la communauté scientifique francophone d'accéder aux travaux de recherche menés au cours de cette thèse.

(I) Développement d'une nanoparticule de gemcitabine-squalène fonctionnalisée à l'aide d'un peptide capable de cibler les cellules cancéreuses pancréatiques.

Les nanoparticules de squalène-gemcitabine (SQdFdC) ont été fonctionnalisées à l'aide du peptide CKAAKN, préalablement sélectionné comme ligand spécifique des tumeurs pancréatiques.[7] Au cours des travaux de thèse le peptide a ainsi été couplé aux nanoparticules de SQdFdC par le biais de deux stratégies distinctes. Une première stratégie (*i*) a reposé sur le couplage du peptide CKAAKN sur les nanoparticules de SQdFdC préalablement formées (Figure 3a). La seconde stratégie (*ii*) a consisté à coupler le peptide directement sur le squalène pour ensuite le co-nanoprecipiter avec la SQdFdC (Figure 3b). Dans les deux cas, la conjugaison a été réalisée grâce à une addition de Michael entre le groupement thiol présent sur le peptide et un groupement maléimide précédemment introduit sur la chaine du squalène.

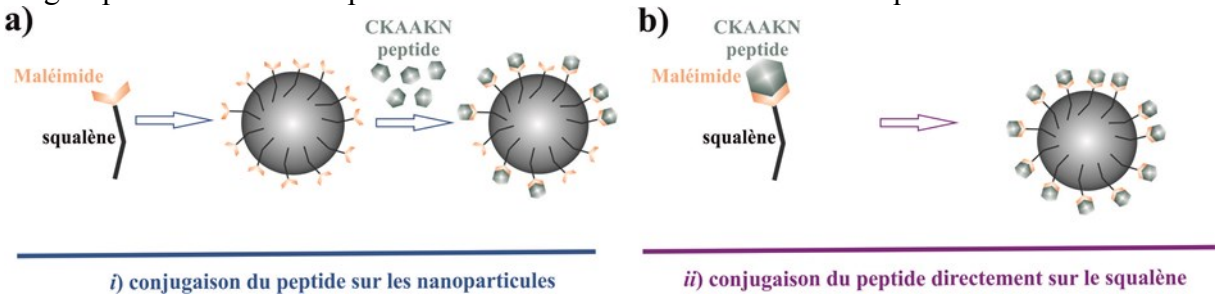

Figure 3 - Stratégies pour la fonctionnalisation des nanoparticules à base de SQdFdC.

Grace à une étude approfondie des paramètres de préparation, une formulation des nanoparticules de SQdFdC fonctionnalisées avec le peptide CKAAKN a été optimisée pour chacune des deux stratégies (la formulation N1a-P* pour la stratégie (*i*) et la formulation N4*-P pour la stratégie (*ii*)).

La capacité des nanoparticules fonctionnalisées à reconnaitre leur cible moléculaire a ensuite été étudiée grâce à la technique de résonance plasmonique de surface (BIACORE). Il a ainsi été montré que le peptide CKAAKN était capable d'interagir spécifiquement avec le récepteur sFRP-4, qui a été identifié comme cible thérapeutique potentielle dans le cancer du pancréas. [1,8] Bien que les deux formulations N1a-P* et N4*-P aient montré une interaction spécifique avec le récepteur sFRP-4, seule la formulation N4-P* a interagi de manière significative et dépendante de la concentration (Figure 4). Aucun signal spécifique n'a été détecté suite à l'injection des nanoparticules de SQdFdC non fonctionnalisées (formulation N1a).

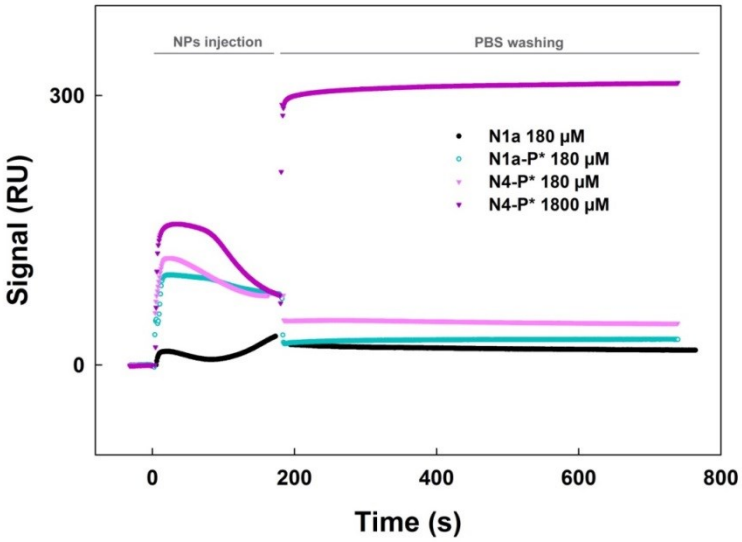

Figure 4 – Analyses des résonances plasmoniques de surface obtenues par injections simultanées des nanoparticules de SQdFdC (N1a), des nanoparticules de SQdFdC fonctionnalisées avec le peptide CKAAKN à l'aide de la stratégie I (N1a-P*) et à l'aide de la stratégie II (N4-P*). Chacune des formulations a été testée à deux concentrations (180 µM et 1800 µM).

La lignée cellulaire cancéreuse pancréatique MIA PaCa-2 a ensuite été sélectionnée pour son expression du récepteur cible sFRP-4 mise en évidence par western blot. Des études de cytotoxicité et d'internalisation cellulaire ont ensuite été réalisées afin d'évaluer l'activité anticancéreuse et démontrer le ciblage actif des deux formulations N1a-P* et N4-P*. Il a ainsi été montré que l'internalisation de la formulation N4-P* par les cellules MIA PaCa-2 était significativement plus importante que l'internalisation de la formulation N1a-P* ou encore que les nanoparticules non fonctionnalisées. Cette augmentation d'internalisation a de plus été complétée par la mise en évidence d'une activité cytotoxique accrue. Ces résultats *in vitro* confirment ainsi que la conjugaison préalable du peptide au squalène avant la nanoformulation est la meilleure stratégie pour obtenir un ciblage sélectif et efficace des cellules pancréatiques et la formulation N4-P* a donc été retenue pour la suite du travail.

L'activité anticancéreuse des nanoparticules de SQdFdC fonctionnalisées a ensuite été testée *in vivo,* sur le modèle murin RIP Tag-2 connu pour développer spontanément des tumeurs pancréatiques. L'efficacité antitumorale de la nanoformulation N4-P* a été évaluée par l'analyse de la régression tumorale et par l'étude histologique des tumeurs, en comparaison avec les nanoparticules de SQdFdC non fonctionnalisées et la dFdC libre.

Les nanoparticules fonctionnalisées avec le peptide ont montré une plus grande activité anticancéreuse par rapport à tous les autres groupes de traitement et une augmentation de l'apoptose à la fois des cellules cancéreuses et des vaisseaux sanguins de la tumeur (Figure 5). Il a aussi été observé une meilleure couverture des péricytes (cellules de support à l'endothélium), ceci permettant une meilleure vascularisation tumorale. Ces résultats indiquent donc que l'activité anti tumorale accrue observée avec les nanoparticules de SQdFdC fonctionnalisées avec le peptide CKAAKN est basée sur la capacité : (*i*) de cibler à la fois les cellules tumorales et endothéliales, (*ii*) d' inhiber la croissance tumorale et l'angiogenèse et (*iii*) de normaliser la vascularisation tumorale pour permettre une meilleure diffusion du nanomédicament.

Ces nouvelles nanoparticules constituent donc un outil prometteur de thérapie anticancéreuse multifonctionnelle.

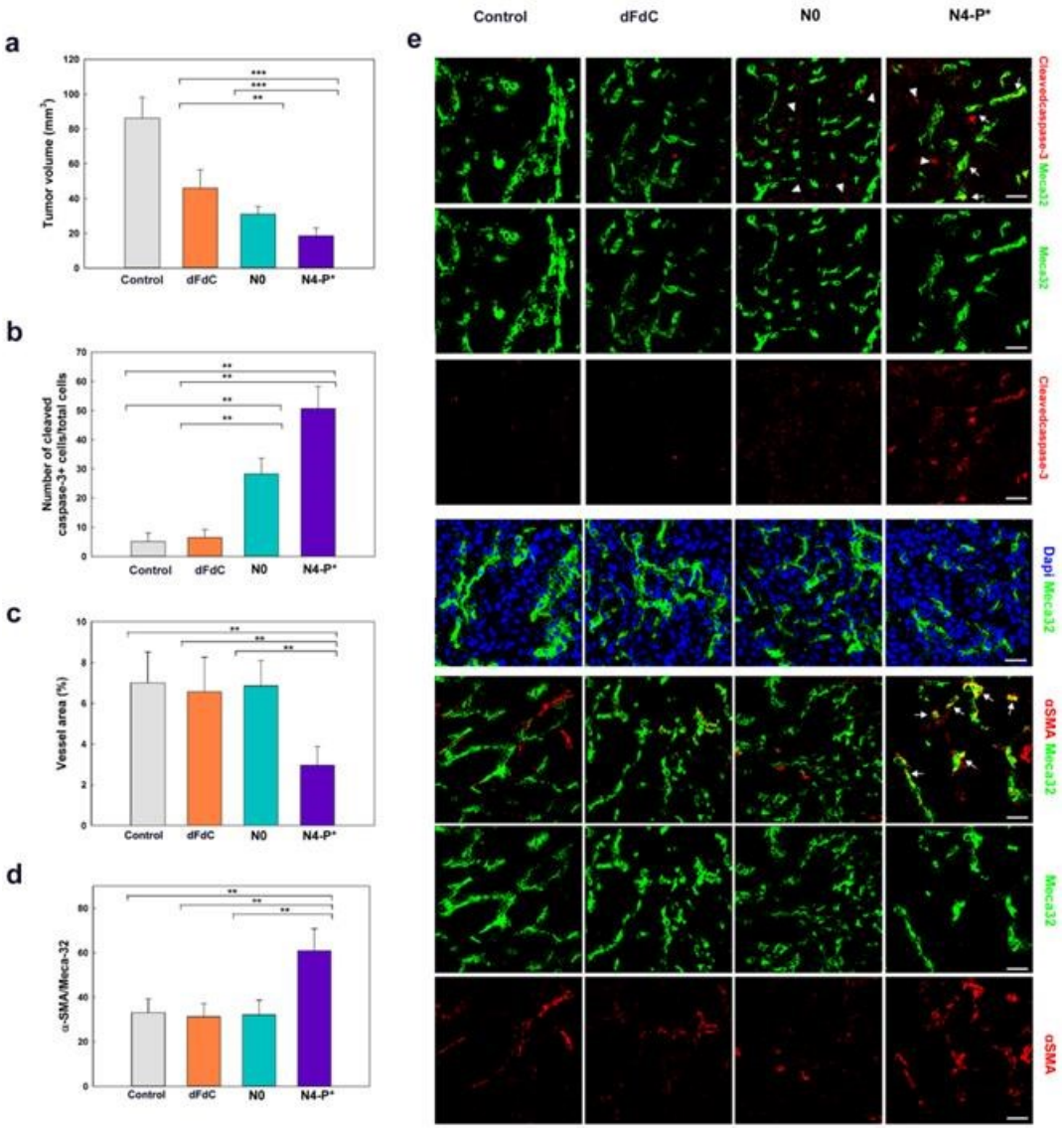

Figure 5 - (a) Croissance tumorale chez les souris RIP-Tag2 en fonction du traitement : contrôle (NaCl 0.9%), dFdC libre (dFdC - 15 mg/kg), N0 (nanoparticules de SQdFdC - 15 mg/kg eq. dFdC), N4-P* (nanoparticules de SQdFdC fonctionnalisées avec le peptide CKAAKN - 15 mg/kg eq. dFdC) (n = 8 animaux/groupe). (b) Indice apoptotique pour tous les traitements, marquage caspase-3 +. (c) Quantification de la surface occupée par les vaisseaux tumoraux pour tous les traitements, marquage Meca32 (marqueur endothélial). (d) Quantification de la surface occupée par les péricytes localisés à proximité des cellules endothéliales pour tous les traitements, marquage α-SMA. Les valeurs représentent la moyenne ± écart-type. La différence statistique est marquée par **p<0,01; ***p<0,001. (e) Images confocales pour tous les traitements. Les taux d'apoptose dans les cellules endothéliales ont été détectés par la colocalisation de Meca32 (vert) avec caspase-3 + (rouge). Les noyaux ont été marqués au DAPI (bleu). La couverture des péricytes des vaisseaux de la tumeur a été évaluée par la colocalisation de Meca32 (vert) et α-SMA (rouge). Les images sont représentatives de 5 champs par souris sur un total de 8 souris par groupe de traitement. Barres d'échelle: 50 µm.

(II) Développement d'une nanoparticule pour la délivrance concommittante de deux médicaments.

Dans le cadre du deuxième axe de recherche, deux inhibiteurs des récepteurs à activité tyrosine kinase, l'erlotinib et le sunitinib, ont été encapsulés dans les nanoparticules de SQdFdC afin de développer deux nanomédicaments chacun alliant une activité cytotoxique et une activité anti-angiogénique. L'encapsulation de chacun des inhibiteurs a été réalisée conformément à leurs propriétés physico-chimiques. L'erlotinib, une molécule hydrophobe, a été encapsulée telle quelle dans les nanoparticules de SQdFdC, alors qu'en raison de son caractère hydrophile, le sunitinib a été conjugué avec le squalène pour permettre son insertion dans les nanoparticules. Grâce à la co-nanoprecipitation de ces molécules, des nanoparticules multi-thérapeutiques ont pu être formées par auto-assemblage moléculaire spontané dans l'eau. Pour l'encapsulation de l'erlotinib, le développement de deux sels entre la molécule et l'acide paratoluènesulfonique (erlotinib tosylate) ou le squalène (erlotinib squalenate) a permis d'augmenter significativement l'efficacité d'encapsulation de la molécule dans les nanoparticules de SQdFdC. En parallèle, le sunitinib a été conjugué au squalène par un groupe hémiaminal (SQSun). La co-nanoprécipitation des deux bioconjugués (SQdFdC et SQSun) a ici aussi permis d'obtenir des nanoparticules caractérisées à l'aide de différentes méthodologies (DLS, microscopie) afin d'en évaluer la taille, la polydispersité et la stabilité. Afin de déterminer si les nanoparticules multi-thérapeutiques (SQdFdC en combinaison avec les sels Erl ou avec le SQSun) pouvaient augmenter l'activité antitumorale des nanoparticules de SQdFdC, les cellules cancéreuses pancréatiques MIA PaCa-2 ont été incubées avec les différentes formulations à des concentrations identiques en SQdFdC. Aucun effet additif cytotoxique n'a été observé après l'incubation des cellules avec les deux formulations contenant la SQdFdC et l'erlotinib (nanoparticules de SQdFdC/erlotinib tosylate et SQdFdC/squalenate), ceci étant probablement dû au faible taux d'encapsulation de l'erlotinib. En revanche, les nanoparticules multi-thérapeutiques à base de SQdFdC et SQSun ont conduit à une augmentation significative de la toxicité cellulaire pas observé dans le cas des deux médicaments sous forme libre (Figure 6).

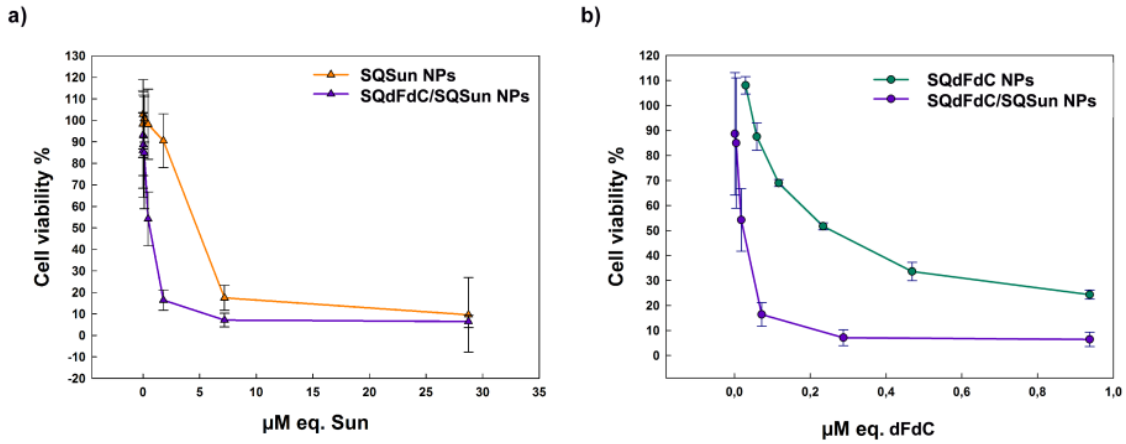

Figure 6 - Viabilité des cellules MIA Paca-2 après exposition à différentes concentrations en (a) nanoparticules de SQdFdC/SQSun (SQdFdC/SQSun NPs) et nanoparticules de SQSun (SQSun NPs); (b) nanoparticules de SQdFdC/SQSun (SQdFdC/SQSun NPs) et nanoparticules de SQdFdC (SQdFdC NPs).

Enfin, une étude détaillée de l'interaction de deux médicaments (Méthode de Chou/Talalay) a montré que l'augmentation significative de la toxicité cellulaire était liée à une action synergique entre la SQdFdC et le SQSun formulés sous forme de nanoparticule. En effet ,cette action synergique n'a pas été observée lorsque les cellules ont été mises en présence des deux médicaments sous forme libre (Figure 7). Cette stratégie de thérapie combinée permet ainsi une réduction significative de la dose de SQdFdC, ce qui représente un avantage majeur pour la

pratique clinique, permettant ainsi de réduire considérablement la toxicité vis-à-vis des tissus sains.

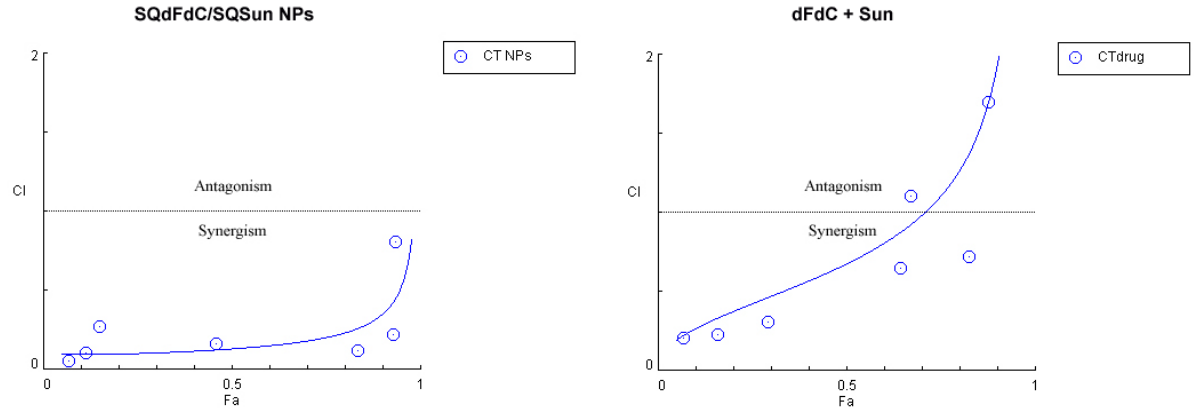

Figure 7 – Evaluation de l'effet synergétique, additif ou antagoniste pour les nanoparticules de SQdFdC/SQSun NPs (gauche) et l'association des médicaments dFdC/Sun sous forme libre (droite). Le *combination index* (CI) est représenté en fonction de l'effet cellulaire (Fa) (un Fa de 0.9 correspondant à 90% de cytotoxicité). La position des points de données (cercles bleus) et de la courbe simulée corrélée (ligne bleue) en-dessous, au niveau et au-dessus de la ligne horizontale (CI=1) indiquent un effet synergétique, additif ou antagoniste respectivement.

A l'issue de ces trois années de thèse, une approche rationnelle et approfondie a donc été proposée, permettant de fonctionnaliser les nanoparticules de SQdFdC à l'aide d'un peptide ciblant la tumeur du pancréas. Il a aussi été montré que la technologie de squalénisation permet de véhiculer deux molécules anticancéreuses au sein d'une même nanoparticule, afin de s'approcher des conditions de multi-thérapie actuellement utilisées en clinique.
Ces avancées ouvrent de nouvelles pistes dans le but d'accroitre l'arsenal contre le cancer du pancréas à l'aide de systèmes nanoparticulaires.

Références

1 Hidalgo, M. Pancreatic cancer. *N Engl J Med* **362**, 1605-1617, doi:10.1056/NEJMra0901557 (2010)

2 http://www.clinicaltrials.gov/

3 Couvreur, P. *et al.* Squalenoyl nanomedicines as potential therapeutics. *Nano Lett.* **6**, 2544-2548 (2006)

4 Reddy, L. H. *et al.* Anticancer efficacy of squalenoyl gemcitabine nanomedicine on 60 human tumor cell panel and on experimental tumor. *Mol Pharm* **6**, 1526-1535 (2009)

5 Reddy, L. H. *et al.* Squalenoyl nanomedicine of gemcitabine is more potent after oral administration in leukemia-bearing rats: study of mechanisms. *Anticancer Drugs* **19**, 999-1006 (2008)

6 Rejiba, S. *et al.* Squalenoyl gemcitabine nanomedicine overcomes the low efficacy of gemcitabine therapy in pancreatic cancer. *Nanomedicine* **7**, 841-849 (2011)

7 Joyce, J. A. *et al.* Stage-specific vascular markers revealed by phage display in a mouse model of pancreatic islet tumorigenesis. *Cancer Cell.* **4**, 393-403 (2003)

8 Jones, S. *et al.* Core signaling pathways in human pancreatic cancers revealed by global genomic analyses. *Science* **321**, 1801-1806 (2008)

Sintesi del progetto di dottorato di ricerca

ll tumore del pancreas è la quinta causa di morte per cancro nei Paesi occidentali. La sua prognosi (sopravvivenza a 5 anni inferiore al 3,5% dei casi) è dovuta all'assenza di fattori specifici di rischio che impediscono una prevenzione efficace e alla diagnosi tardiva che rileva quasi il 90% dei pazienti ad uno stadio aggressivo del tumore. L'unico trattamento terapeutico del cancro del pancreas è la chirurgia, purtroppo possibile solo nel 10-15% dei casi.[1] La gemcitabina (dFdC), un analogo nucleosidico che blocca la replicazione del DNA, è attualmente il trattamento farmacologico di prima linea dei tumori pancreatici in stadi avanzati e/o metastatici.[2] Tuttavia, il trattamento è palliativo con un'aspettativa di vita molto limitata.

L'efficacia terapeutica di una sostanza farmacologicamente attiva è, come noto, strettamente legata al suo comportamento farmacocinetico. Un farmaco dovrebbe raggiungere rapidamente ed in quantità sufficiente il proprio organo bersaglio, restarvi per un periodo di tempo necessario per esplicare la propria azione terapeutica ed essere invece escluso da altri distretti nei quali potrebbe presentare azioni tossiche. Tuttavia, molto spesso la distribuzione di un farmaco nell'organismo non è quella desiderata e la frazione di farmaco che arriva al sito target è insufficiente, mentre esso tende ad accumularsi in altri tessuti con conseguenti effetti tossici. Inoltre, secondo recenti scoperte, la maggior parte dei tumori pancreatici è caratterizzata da ridotto apporto di sangue e da un'elevata produzione di matrice extracellulare, che riducono drasticamente la disponibilità di farmaci a livello tumorale. L'azione della gemcitabina a livello del pancreas è ostacolata non solo dalle suddette barriere biologiche, ma anche dalla degradazione plasmatica e dal metabolismo che diminuiscono le concentrazioni efficaci al sito di azione generando effetti tossici a carico dei tessuti sani.

Una strategia per aumentare la quantità di farmaco in grado di raggiungere l'organo bersaglio e proteggerlo dalla degradazione nell'organismo è l'associazione del principio attivo ad un *carrier* particolato di dimensione submicronica (nanoparticella), in grado d'incorporare il farmaco, di trasportarlo e di rilasciarlo in modo controllato (Figura 1).

Le nanoparticelle sono una categoria di sistemi colloidali di forma sferica per il rilascio controllato di principi attivi, aventi dimensioni inferiori ad 1 micrometro e generalmente costituiti da polimeri o lipidi d'origine sintetica o naturale.

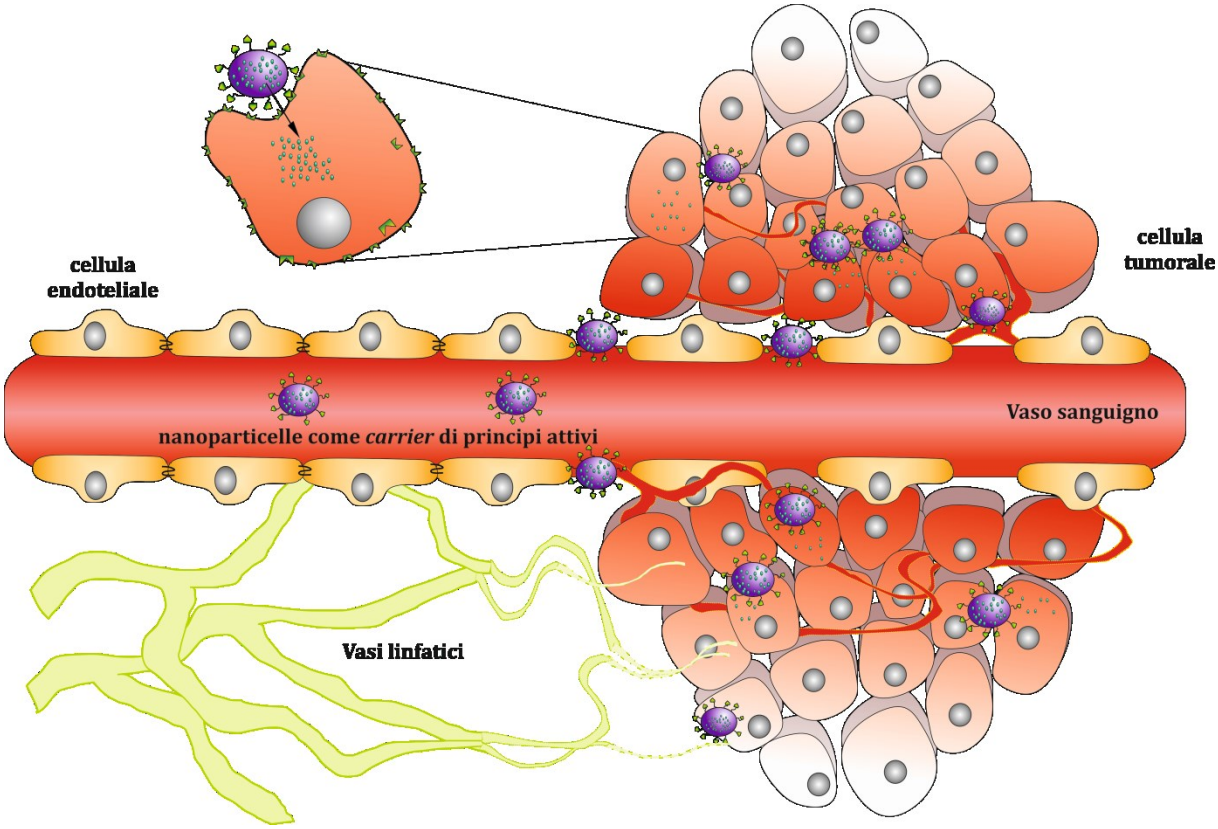

Figura 1 – Veicolazione di un farmaco a livello tumorale tramite le nanoparticelle.

In questo contesto nel 2006 è stato sviluppato il concetto di "squalenizzazione" in collaborazione tra il laboratorio del Professor Patrick Couvreur dell'Università di Parigi Sud-11 (Francia) e il Professor Luigi Cattel e la Dottoressa Barbara Stella dell'Università di Torino. La tecnica della squalenizzazione si basa sulla formazione di un legame chimico covalente tra la molecola dello squalene e diversi principi attivi, con lo scopo di aumentare l'indice terapeutico di questi composti e consentirne una più efficiente somministrazione. I coniugati così ottenuti, si auto-organizzano in modo spontaneo in acqua in nanostrutture con diametro compreso tra 100 e 300 nm, indipendentemente dal principio attivo usato e dal tipo di legame. Il coniugato squalenico della gemcitabina (SQdFdC) è in grado di formare spontaneamente nanoparticelle in acqua grazie alla presenza della porzione idrofobica dello squalene e al conseguente aumento della tensione superficiale delle molecole di SQdFdC.[3] Le nanoparticelle di SQdFdC hanno dimostrato una maggiore citotossicità rispetto alla gemcitabina su diverse linee cellulari tumorali. In parallelo, anche l'attività *in vivo* di nanoparticelle di SQdFdC, testata su modelli animali di leucemia, si è dimostrata superiore a quella del farmaco libero.[3-6]
Sulla base di queste considerazioni, lo scopo di questo progetto è la preparazione di nuove nanoparticelle a base di SQdFdC specifiche per il trattamento del carcinoma pancreatico. In un primo approccio (*i*) la superficie delle nanoparticelle di SQdFdC è stata funzionalizzata con un agente di direzionamento specifico per i recettori espressi sulle cellule tumorali e endoteliali, con lo scopo di aumentare il livello di principio attivo nella cellula tumorale. Nel secondo approccio (*ii*) è stato introdotto un altro farmaco all'interno delle nanoparticelle di SQdFdC, ottenendo condizioni simili alla maggior parte dei protocolli chemioterapici usati in clinica che prevedono farmaci in associazione.

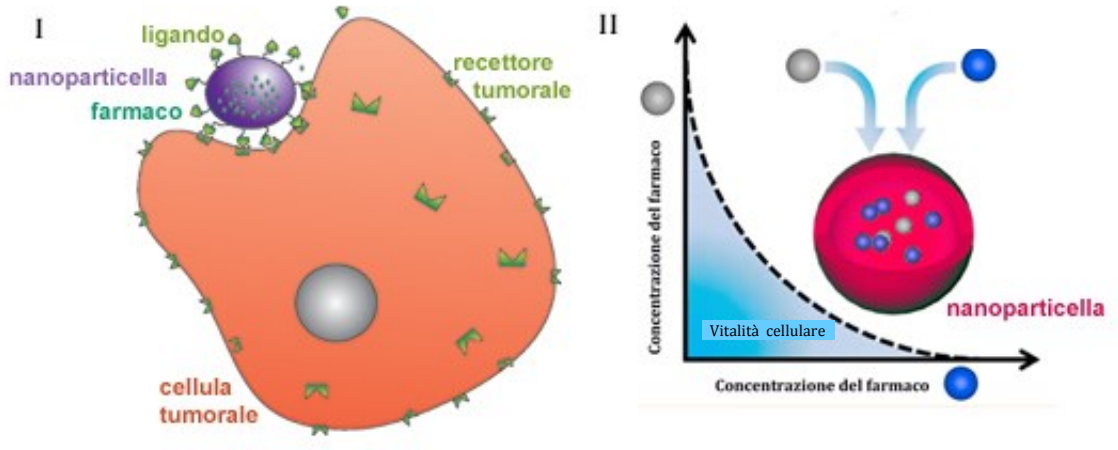

Figura 2 – Progetti del dottorato di ricerca: (I) preparazione di nanoparticelle di SQdFdC direzionate attivamente con un peptide verso il tumore pancreatico e (II) realizzazione di nanoparticelle per la veicolazione di due farmaci in associazione.

I risultati ottenuti sono discussi nelle due sezioni successive. Visti i molteplici aspetti interdisciplinari della ricerca, l'unione delle competenze tecnico-scientifiche e degli strumenti a disposizione di ciascun gruppo ha assunto notevole importanza rendendo la cotutela un punto cruciale per la realizzazione del progetto stesso.

(I) Preparazione di nanoparticelle a base di SQdFdC direzionate con un peptide verso il tumore pancreatico.

Le nanoparticelle di SQdFdC sono state funzionalizzate con il peptide CKAAKN, un esapeptide lineare capace di legarsi in modo selettivo ai vasi tumorali del carcinoma pancreatico.[7] Il peptide è stato inserito sulla superificie delle nanoparticelle tramite due diversi approcci. Il primo approccio (*i*) é basato sulla coniugazione dell'agente di targeting alle nanoparticelle preformate, ovvero tramite reazione direttamente nella sospensione acquosa di nanoparticelle di SQdFdC (Figura 3a). Nel secondo approccio (*ii*) l'agente direzionante é stato coniugato allo squalene prima dell'autoassemblamento delle nanoparticelle di SQdFdC (Figura 3b). In entrambi i casi la coniugazione è stata realizzata grazie all'addizione nucleofila di Michael del gruppo maleimidico (precedentemente introdotto sullo squalene) sul tiolo della cisteina terminale presente nella sequenza peptidica.

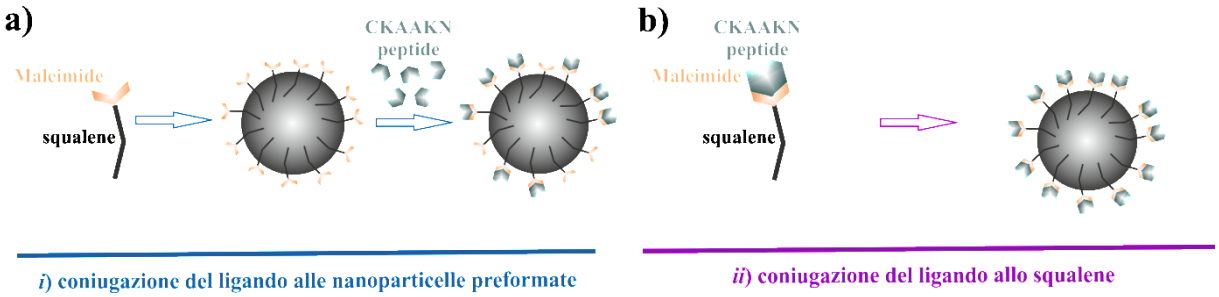

Figura 3 – Strategie di coniugazione del ligando direzionante CKAAKN alle nanoparticelle di SQdFdC.

Grazie ad uno studio approfondito delle condizioni di preparazione delle nanoparticelle, sono state identificate le migliori formulazioni per entrambe le strategie di coniugazione (la formulazione N1a-P* per la strategia (*i*) e la formulazione N4*-P per la strategia (*ii*)).
Successivamente, la tecnica di risonanza plasmonica di superficie ha permesso di comparare la differenza dell'affinità del ligando per il recettore nelle nanoparticelle derivatizzate con il peptide CKAAKN secondo le due strategie. Il peptide è stato in grado di interagire in modo specifico con il recettore sFRP-4, che, assieme alla proteina Wnt-2, è stato identificato come possibile *marker* terapeutico per il cancro del pancreas.[1-8]
Sebbene entrambe le formulazioni N1a-P* e N4*-P siano state in grado di interagire in modo specifico con il recettore sFRP-4, solo con la formulazione N4*-P l' interazione è stata significativa e con un profilo concentrazione-dipendente (Figura 4). Nessun segnale correlato ad un'interazione specifica è stato rilevato in seguito all'iniezione di nanoparticelle di SQdFdC non derivatizzate con il peptide (formulazione N1a).

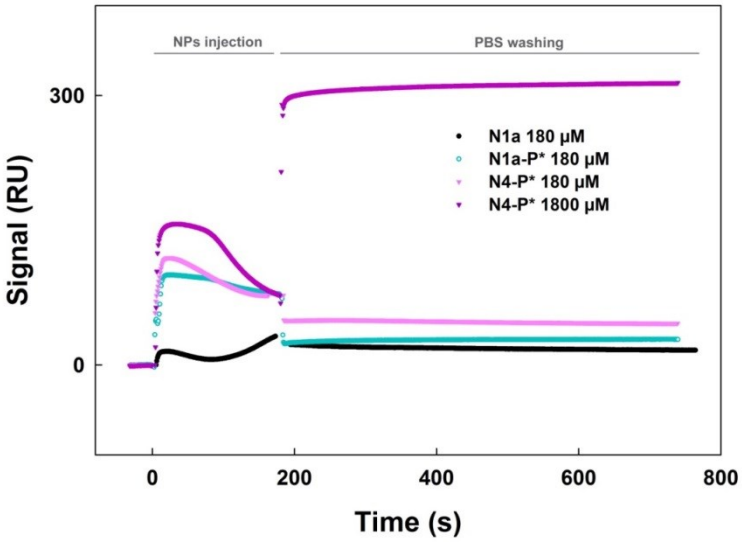

Figura 4 – Curve di risonanza plasmonica di superficie ottenute durante l'interazione tra le nanoparticelle di SQdFdC (N1a), le nanoparticelle di SQdFdC derivatizzate con il peptide con la strategia (*i*) (N1a-P*) e con la strategia (*ii*) (N4-P*) con il recettore sFRP-4 immobilizzato sulla superficie del sensorchip. Ogni formulazione è stata testata a due concentrazioni (180 e 1800 µM).

Successivamente, la linea cellulare tumorale pancreatica umana MIA PaCa-2 è stata selezionata tramite l'analisi western blot per il suo elevato livello di espressione del recettore *target* sFRP-4. Studi di citotossicità e di internalizzazione cellulare sono stati condotti in seguito al fine di valutare *in vitro* l'attività antitumorale ed il direzionamento attivo delle due formulazioni N1a-P* e N4-P*. Una maggiore internalizzazione cellulare è stata osservata per le nanoparticelle N4-P* rispetto alle nanoparticelle N1a-P* e alle nanoparticelle di SQdFC non derivatizzate. I risultati *in vitro* si sono dimostrati coerenti con l'analisi di risonanza plasmonica di superficie: la coniugazione del peptide CKAAKN con lo squalene prima dell'autoassemblamento delle nanoparticelle offre la migliore stategia di derivatizzazione.
L'attività antitumorale della formulazione N4-P* è stata in seguito approfonditamente studiata grazie ad esperimenti *in vivo* condotti su topi Rip1-Tag2, un modello transgenico di topi con tumore delle isolette pancreatiche. Gli esperimenti sono stati condotti (in collaborazione con l'Istituto per la Ricerca e la Cura del Cancro di Candiolo) su gruppi di 8 animali trattati rispettivamente con la soluzione fisiologica, la gemcitabina, le nanoparticelle di SQdFdC e le nanoparticelle di SQdFdC direzionate con il peptide (N4-P*). Alla fine del trattamento si è calcolato il volume del tumore e sono state prelevate sezioni di tessuto da analizzare per ogni gruppo di animali. Per il trattamento con le nanoparticelle direzionate con il peptide CKAAKN è stata osservata una riduzione del volume tumorale medio pari al 60 e al 40% rispettivamente rispetto al trattamento con la gemcitabina libera e con le nanoparticelle di SQdFdC non direzionate (Figura 5). L'analisi dei tessuti al microscopio di immunofluorescenza ha rilevato la presenza di apoptosi sia nelle cellule tumorali sia in quelle endoteliali. Inoltre, la morfologia dei vasi ha chiaramente sottolineato una diminuzione delle ramificazioni e del numero dei vasi e un aumento della copertura pericitica in seguito al trattamento con le nanoparticelle direzionate. Tale riduzione della densità e della tortuosità dei vasi, unita all'aumento della copertura pericitica, è stata indicata come *marker* di normalizzazione dei vasi tumorali, che conduce ad una migliore penetrazione di ossigeno e farmaci ai tessuti. Questi risultati insieme suggeriscono che l'efficacia antitumorale delle nanoparticelle di SQdFdC direzionate con il peptide CKAAKN sia dovuta alla loro capacità multipla (*i*) di indurre apoptosi sia nelle cellule tumorali sia in quelle

endoteliali, (*ii*) di ridurre la crescita tumorale e l'angiogenesi e (*iii*) di normalizzare i vasi tumorali, permettendo una migliore penetrazione del farmaco nel tessuto.
Queste nuove nanoparticelle costituiscono, quindi, uno strumento promettente per la chemioterapia del carcinoma pancreatico.

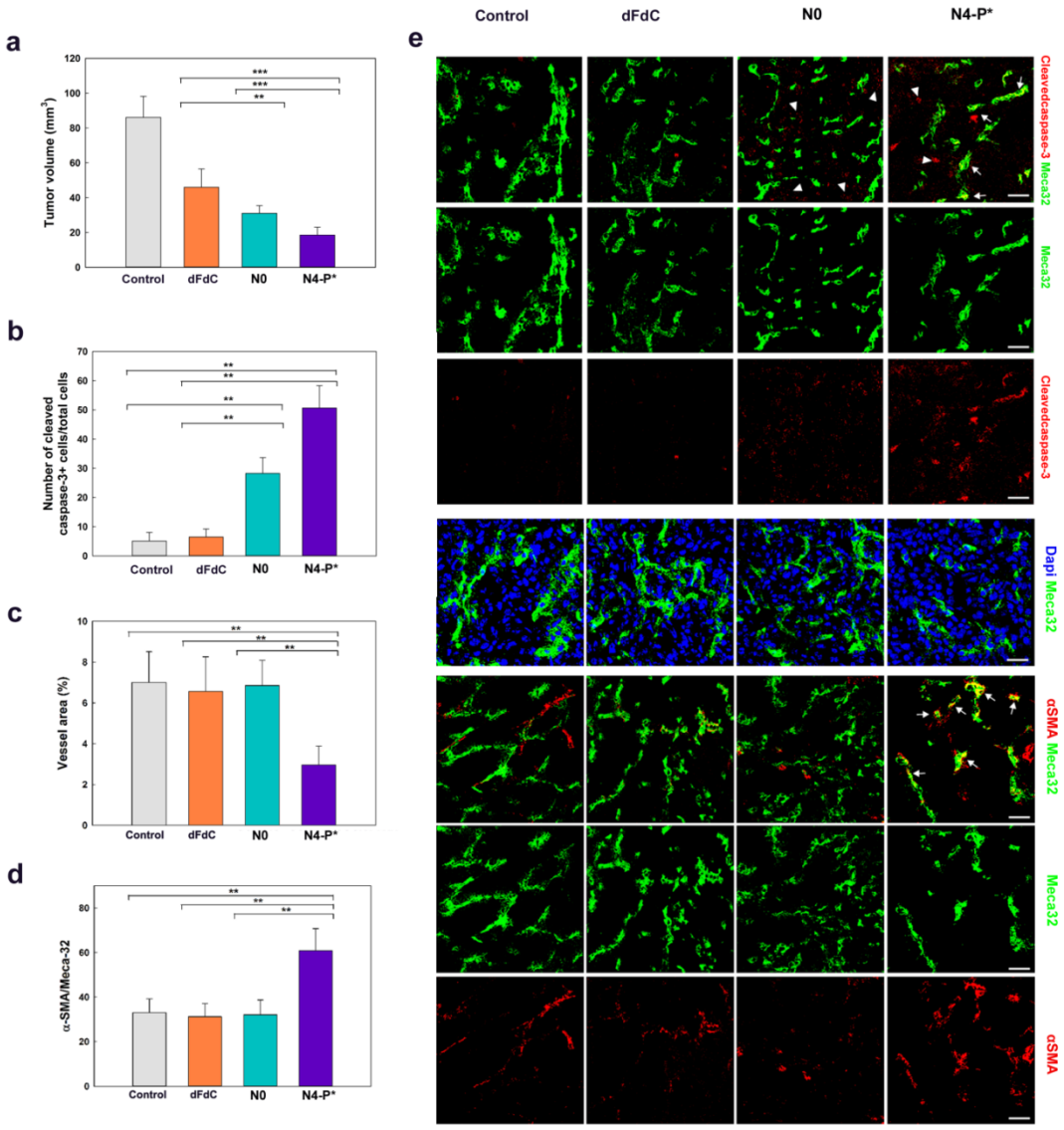

Figura 5 - (a) Crescita tumorale nei topi RIP1-Tag2 a seconda del trattamento: controllo (soluzione fisiologica, NaCl 0.9%), gemcitabina libera (dFdC - 15 mg/kg), N0 (nanoparticelle di SQdFdC - 15 mg/kg eq. dFdC), N4-P* (nanoparticelle di SQdFdC derivatizzate con il peptide CKAAKN - 15 mg/kg eq. dFdC) (*n* = 8 animali/gruppo). (b) Indice apoptotico per tutti i gruppi di trattamento, caspasi-3+ come *marker*. (c) Superficie occupata dai vasi tumorali per tutti i trattamenti, Meca32 come *marker*. (d) Superficie occupata dai periciti in prossimità delle cellule endoteliali per tutti i trattamenti, Meca32 come *marker*. I valori rappresentano la media ± la deviazione standard. La significatività statistica è indicata come **p<0,01; ***p<0,001. (e) Immagini al microscopio confocale per tutti i trattamenti. L'indice apoptotico nelle cellule endoteliali è identificato tramite la colocalizzazione di Meca32 (verde) e caspasi-3+ (rosso). I nuclei sono marcati con il *marker* DAPI (blu). La copertura pericitica dei vasi tumorali è stata valutata tramite la colocalizzazione di Meca32 (verde) e α-SMA (rosso). Le immagini sono rappresentative di ogni gruppo di trattamento. Scala: 50 µm.

(II) Preparazione di nanoparticelle per la veicolazione di due farmaci.

Lo scopo della seconda parte del progetto di ricerca consiste nella preparazione di nanoparticelle squaleniche veicolanti insieme due farmaci antitumorali, al fine di raggiungere condizioni terapeutiche simili a quelle attualmente in clinica. La combinazione di più farmaci, infatti, trova impiego nella maggior parte dei protocolli chemioterapici usati in clinica. Due inibitori dei recettori tirosin chinasici, l'erlotinib e il sunitinib, sono stati incapsulati nelle nanoparticelle di SQdFdC per ottenere due tipi di nanoparticelle, ciascuno avente attività insieme citotossica ed antiangiogenica. L'incapsulazione dei due inibitori è stata realizzata con tecniche diverse in base alle caratteristiche chimico-fisiche delle molecole. L'erlotinib, molecola idrofoba, è stata incapsulata nella matrice idrofobica delle nanoparticelle di SQdFdC, mentre il sunitinib è stato coniugato chimicamente allo squalene (ottenendo un composto anfifilico, SQSun), poiché è troppo idrofilo per poter essere incorporato nelle nanoparticelle.
Tramite la co-nanoprecipitazione di SQdFdC e dei due inibitori, si sono formate nanoparticelle multifunzionali in acqua, come per gli altri derivati squalenici. Al fine di aumentare ulteriormente l'idrofobia e, quindi, l'efficacia d'incapsulazione dell'erlotinib nelle nanoparticelle di SQdFdC, esso è stato salificato con l'acido squalenico e con l'acido paratoluensolfonico. Sono stati ottenuti due sali, l'erlotinib squalenato e l'erlotinib tosilato. Per ogni formulazione sono stati studiati il diametro medio, la carica superficiale e la stabilità nel tempo tramite diverse tecniche. Al fine di determinare se le nanoparticelle multiterapeutiche (SQdFdC in associazione con i sali di erlotinib o con lo SQSun) abbiano un'attività antitumorale più elevata delle nanoparticelle di SQdFdC, le cellule tumorali pancreatiche MIA PaCa-2 sono state incubate con le diverse formulazioni. Non é stato osservato alcun effetto citotossico additivo dopo incubazione delle formulazioni di SQdFdC contententi i sali dell'erlotinib (nanoparticelle di SQdFdC/erlotinib tosilato e SQdFdC/erlotinib squalenato), probabilmente per la bassa quantità di inibitore incorporato. Le nanoparticelle a base di SQdFdC e SQSun hanno invece condotto ad un aumento significativo della citotossicità non riscontrato a seguito dall'associazione dei farmaci liberi (dFdC/Sun) (Figura 6).

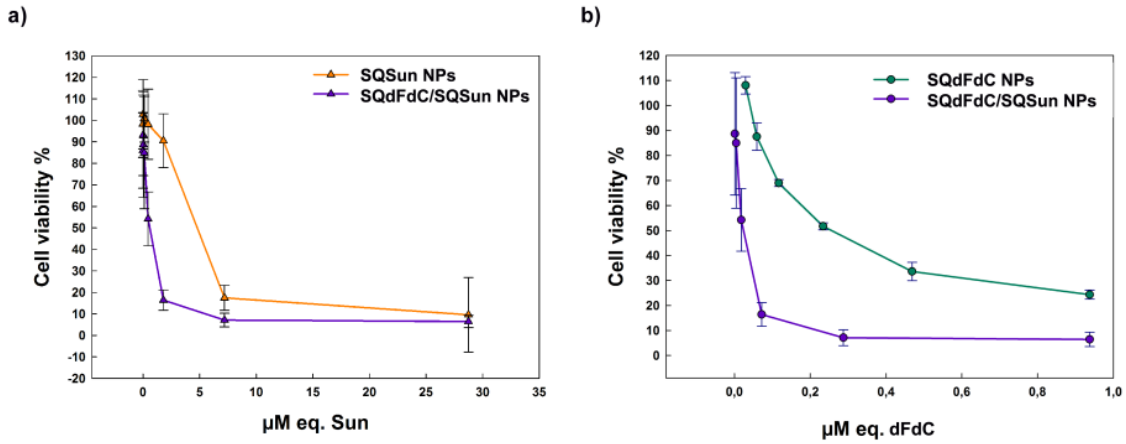

Figura 6 – Vitalità delle cellule MIA Paca-2 dopo esposizione a diverse concentrazioni di (a) nanoparticelle di SQdFdC/SQSun (SQdFdC/SQSun NPs) e nanoparticelle di SQSun (SQSun NPs); (b) nanoparticelle di SQdFdC/SQSun (SQdFdC/SQSun NPs) e nanoparticelle di SQdFdC (SQdFdC NPs).

Infine, uno studio dettagliato sulle interazioni tra i due farmaci con il metodo di Chou/Talalay ha dimostrato che l'aumento significativo della tossicità cellulare può essere ricondotto ad un'azione sinergica tra la SQdFdC e lo SQSun formulati nelle stesse nanoparticelle. Tale azione sinergica non è stata osservata quando le cellule sono state incubate con l'associazione dei due farmaci liberi (dFdC/Sun) (Figura 7). Questa strategia di combinazione di più farmaci ha inoltre permesso una riduzione della quantità di SQdFdC, che rappresenta un grande vantaggio per la pratica clinica, perché permette di diminuire la tossicità verso i tessuti sani.

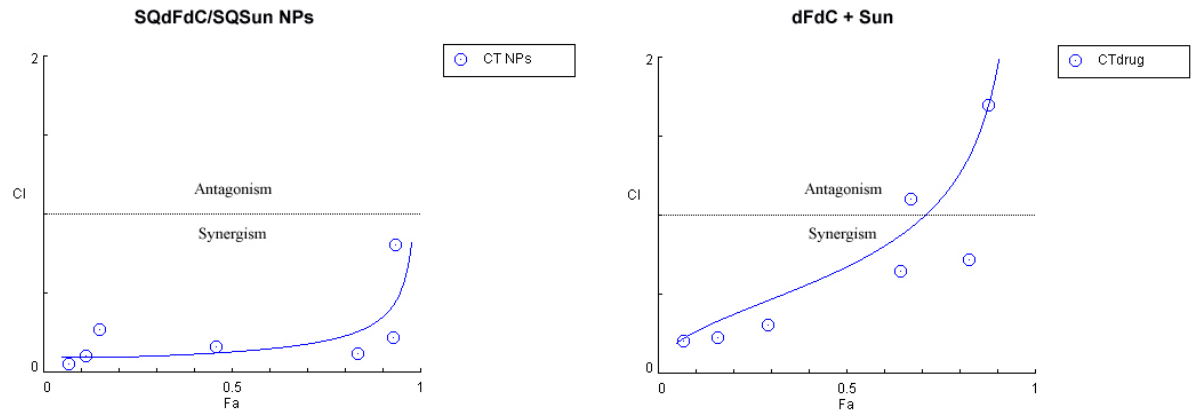

Figura 7 – Studio dell'effetto sinergico, additivo o antagonistico per le nanoparticelle di SQdFdC/SQSun e per l'associazione dFdC/Sun sotto forma di farmaci liberi con il metodo di Chou/Talalay. Il *combination index* (CI) é riportato in funzione dell'effetto cellulare (Fa) (Fa di 0,9 corrisponde al 90% della citotossicità). La posizione dei dati (cerchi blu) e della curva di simulazione correlata (linea blu) sotto, all'altezza e al di sotto della linea orizzontale (CI=1) indica, rispettivamente, un effetto sinergico, additivo o antagonistico.

Nel corso dei tre anni di dottorato di ricerca è stato proposto un approccio razionale e approfondito che ha permesso di derivatizzare le nanoparticelle di SQdFdC con un peptide in grado di direzionare le nanoparticelle verso il carcinoma pancreatico. Inoltre, è stata proposta una strategia per veicolare due molecole antitumorali nelle stesse nanoparticelle al fine di realizzare condizioni simili agli attuali protocolli clinici. Queste nuove nanoparticelle possono essere considerate, un promettente e versatile strumento nel campo della terapia del carcinoma pancreatico.

Riferimenti bibliografici

1 Hidalgo, M. Pancreatic cancer. *N Engl J Med* **362**, 1605-1617 (2010).

2 http://www.clinicaltrials.gov

3 Couvreur, P. *et al.* Squalenoyl nanomedicines as potential therapeutics. *Nano Lett.* **6**, 2544-2548 (2006).

4 Reddy, L. H. *et al.* Anticancer efficacy of squalenoyl gemcitabine nanomedicine on 60 human tumor cell panel and on experimental tumor. *Mol Pharm* **6**, 1526-1535 (2009).

5 Reddy, L. H. *et al.* Squalenoyl nanomedicine of gemcitabine is more potent after oral administration in leukemia-bearing rats: study of mechanisms. *Anticancer Drugs* **19**, 999-1006 (2008).

6 Rejiba, S. *et al.* Squalenoyl gemcitabine nanomedicine overcomes the low efficacy of gemcitabine therapy in pancreatic cancer. *Nanomedicine* **7**, 841-849 (2011).

7 Joyce, J. A. *et al.* Stage-specific vascular markers revealed by phage display in a mouse model of pancreatic islet tumorigenesis. *Cancer Cell.* **4**, 393-403 (2003).

8 Jones, S. *et al.* Core signaling pathways in human pancreatic cancers revealed by global genomic analyses. *Science* **321**, 1801-1806 (2008).

Self-Assembled Squalenoylated Penicillin Bioconjugates: An Original Approach for the Treatment of Intracellular Infections

Nicolas Sémiramoth,[†,#] Chiara Di Meo,[†,#] Fatima Zouhiri,[†] Fatouma Saïd-Hassane,[†] Sabrina Valetti,[†] Roseline Gorges,[§] Valérie Nicolas,[⊥] Jacques H. Poupaert,[∥] Sylvie Chollet-Martin,[§] Didier Desmaële,[‡] Ruxandra Gref,[†] and Patrick Couvreur[†,*]

[†]Faculty of Pharmacy, UMR CNRS 8612, University of Paris-Sud XI, 5 Rue Jean-Baptiste Clément, 92296 Châtenay-Malabry Cedex, France, [‡]Faculty of Pharmacy, UMR CNRS 8076 Biocis, University of Paris-Sud XI, 5 Rue Jean-Baptiste Clément, 92296 Châtenay-Malabry Cedex, France, [§]Faculty of Pharmacy, INSERM UMRS 996, University of Paris-Sud XI, 5 Rue Jean-Baptiste Clément, 92296 Châtenay-Malabry Cedex, France, [⊥]Faculty of Pharmacy, INSERM IFR 141, University of Paris-Sud XI, 5 Rue Jean-Baptiste Clément, 92296 Châtenay-Malabry Cedex, France, and [∥]Louvain Drug Research Institute, UCLouvain, Avenue E. Mounier 73, B-1200 Brussels, Belgium. [#]Equally contributing first authors.

ABSTRACT We describe here new nanoparticles based on the bioconjugation of penicillin G to squalene in order to overcome severe intracellular infections by pathogen bacteria whose mechanism of resistance arises from the poor intracellular diffusion of several antibiotics. Two different squalene—penicillin G conjugates were synthesized (pH-sensitive and pH-insensitive), and their self-assembly as nanoparticles was investigated through morphology and stability studies. These nanoparticles had a size of 140 ± 10 nm (polydispersity index of 0.1) and a negative charge, and they did not display any supramolecular organization. Furthermore, they were found stable in water and in different culture medium. The cellular uptake and localization of these fluorescently labeled nanoparticles were explored on the macrophage cell line J774 by flow cytometry and confocal microscopy analysis. The squalenoylated nanoparticles were found to be cell internalized through clathrin-dependent and -independent endocytic pathways. Moreover, they induced an improved intracellular antibacterial activity on the facultative intracellular pathogen *S. aureus*, compared with free penicillin G, despite the absence of co-localization between the bacteria and the nanoparticles in the cells. This study suggests that the bioconjugation of an antibiotic to a squalene template could be a valuable approach for overcoming the antibiotic resistance due to intracellular bacterial infections.

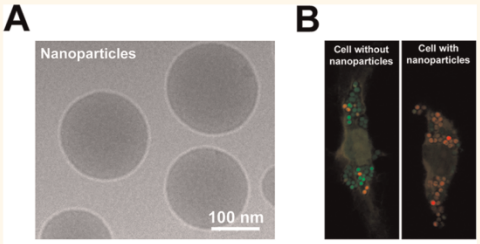

Nanoparticles made of Penicillin G-Squalene bioconjugates (A) efficiently kill intracellular bacteria (live bacteria in green, dead bacteria in red) (B)

KEYWORDS: nanoparticle · squalene · antibiotic · penicillin G · intracellular infections

Major problems associated with severe bacterial infections are related to the existence of intracellular pathogens and to the acquisition of antibiotic resistance by these bacteria. In fact, several obligatory and facultative intracellular bacteria are able to survive and multiply within phagocytic cells, which become reservoirs of pathogenic bacteria, giving rise to chronic infections.[1]

Therefore, there is a tremendous interest in improving antibiotics' entry within cells, in order to treat these intracellular infectious diseases.[2] In particular, many efforts have been made in the last decades in order to find a useful carrier for the intracellular delivery of beta-lactam antibiotics. These antibiotics are, indeed, widely used to treat infections caused by various pathogens, but they have low intracellular uptake in phagocytic cells because of their weak acidic character (*i.e.*, they are ionized at neutral physiological pH), and they do not diffuse spontaneously through cell membranes. Nanoparticulate carriers have been considered to transport antibiotics into phagocytic cells,[3] and in particular, antibiotic-loaded liposomes have been extensively studied.[4] Also, Couvreur *et al.* synthesized polyalkylcyanoacrylate nanoparticles (NPs) loaded with ampicillin for the treatment of *Listeria* and *Salmonella* spp. intracellular infections.[5,6] These nanoparticles allowed the antibacterial activity of the antibiotic against intracellular infections to increase by 120 times *in vivo*, due to the improved cellular uptake and to the accumulation of the antibiotic-loaded nanoparticles within the reticuloendothelial system (RES). However, the drug loading was poor, which necessitated the administration of high amounts of polymer to reach sufficient intracellular concentrations of the antibiotic. This has resulted in some toxicity and side effects, due to intracellular overloading of the cyanoacrylic polymer.

In order to overcome this important toxicological limitation, we have synthesized

* Address correspondence to patrick.couvreur@u-psud.fr.

Received for review December 16, 2011 and accepted April 6, 2012.

Published online April 06, 2012
10.1021/nn204928v

© 2012 American Chemical Society

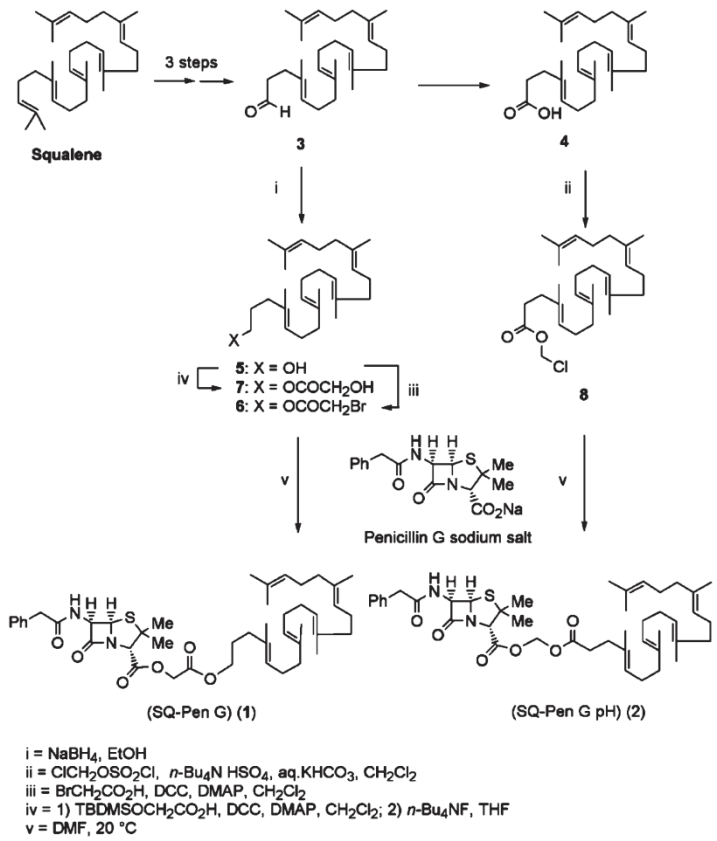

Scheme 1. Synthetic scheme of penicillin G squalenyl conjugates 1 and 2.

here new amphiphilic derivatives based on benzylpenicillin (PNG) linked to squalene (Sq) through pH-sensitive or pH-insensitive chemical bonds. The two bioconjugates differed in the nature of the linker between the hydrophobic chain and the penicillin G polar head. In the first compound, the ester bond was less labile than in the second, which was hydrolyzable in a pH-dependent manner. Remarkably, these new bioconjugates were able to spontaneously self-assemble in aqueous media as NPs, yielding impressive antibiotic loading (44 wt %). Noteworthy, the unique property of the natural lipid squalene to allow the formation of nanoparticles after conjugation was already observed with gemcitabine, an anticancer compound.[7]

This paper also investigates the morphology of the obtained NPs, their cell uptake, and their improved antibacterial activity against intracellular infections by *Staphylococcus* strain.

RESULTS AND DISCUSSION

Synthesis of Squalenyl–Penicillin G Conjugates. The squalenyl conjugate SqPNG (**1**) and the pH-sensitive one, SqPNG-pH (**2**), were synthesized by alkylation of the carboxylate function of penicillin G (**4**) with bromoacetate **6** and chloromethyl ester **8**, respectively, according to Scheme 1. Thus, 1,1′,2-trisnorsqualene alcohol (**5**) was first prepared in four steps from squalene *via* the trisnorsqualene aldehyde according to the Prestwich procedure.[8] Condensation of **5** with bromoacetic acid using N,N′-dicyclohexylcarbodiimide (DCC) as coupling agent led to the corresponding bromoester **6** in 70% yield. Coupling of penicillin G (PNG) sodium salt with bromoacetate **6** took place smoothly in DMSO to provide conjugate **1** in 34% yield. However, simple esters of penicillin are usually not prodrugs of β-lactam antibiotics since the ester bond is not easily cleaved. In contrast, acyloxymethyl esters such as pivampicillin are known to be extremely sensitive to chemical and enzymatic hydrolysis.[9,10] Therefore, we prepared the new conjugate **2** designed to release penicillin G within acidic subcellular organelles such as lysosomes. The chloromethyl ester of 1,1′,2-trisnorsqualenic acid (**8**) was first prepared upon treatment of trisnorsqualenic acid (**4**)[8] with chloromethanesulfonyl chloride.[11] Subsequent alkylation of the sodium salt of penicillin G afforded conjugate **2** in 49% yield. Both squalenoyl conjugates **1** and **2** were found quite stable, surviving chromatographic purification over silica gel and were fully characterized by spectroscopic methods. Since enzymatic hydrolysis of **1** is likely to release hydroxyacetic acid

squalenyl ester **7**, an authentic sample of this material was synthesized by DCC coupling of *tert*-butyldimethylsilyloxy-acetic acid[12] with 1,1′,2-trisnorsqualene alcohol (**6**) followed by nBu_4NF cleavage of the silyl protecting group.

NPs' Physico-chemical Characterization. *NPs' Formation and Stability.* Both SqPNG and SqPNG-pH compounds showed the capability to spontaneously self-assemble as NPs in water by nanoprecipitation from ethanolic solutions.

The SqPNG NPs' average diameter was 140 ± 10 nm with a very low polydispersity index of around ~0.1, and their *Z*-potential was about −50 mV. The NP suspensions, whatever their concentration (from 0.16 to 10 mg/mL), were found to be very stable in different storage conditions (*i.e.*, 2 weeks at 37 °C, several weeks at 25 °C, and more than 1 month at 4 °C; see Figure 1 in the Supporting Information). Moreover, after 7 months, NMR analysis of SqPNG NP suspensions (10 mg/mL) showed that the chemical structure of the derivative was still intact within the nanoparticles. The SqPNG-pH NPs showed a comparable average size and *Z*-potential (about 150 nm and −50 mV) with SqPNG NPs, but, despite a close chemical structure, they displayed a less remarkable stability, which lasted for only 7−8 days (see Figure 2 in the Supporting Information).

Similarly, we have constructed fluorescently labeled SqPNG NPs by solubilizing the fluorochrome cholesteryl-BODIPY (0.5 wt %) in the ethanolic solutions of either SqPNG or SqPNG-pH before nanoprecipitation in water; these fluorescent NPs were shown to be stable in water (see Figure 3 in the Supporting Information). In cell culture medium, however, due to the presence of serum proteins, the average diameter of the NPs increased by about 20 nm, being stable for the 24 h duration of the experiment (see Figure 4 in the Supporting Information), and the *Z*-potential rose to about −20 mV.

NPs' Morphological Analysis. Cryo transmission electron microscopy (CryoTEM) analysis was performed on a SqPNG NP suspension and revealed a spherical and regular shape of the NPs (Figure 1A). Further TEM analysis after freeze-fracture has allowed the investigation of the NPs' internal morphology. It was discovered that they did not display any supramolecular organization (Figure 1B). X-ray diffraction studies by SAXS and WAXS have also confirmed the absence of any crystal structure, contrary to previously synthesized squalenoylated gemcitabine and squalenoylated 2′,3′-dideoxycytidine (ddC) nanoassemblies.[13]

Molecular Modeling. Molecular modeling studies were undertaken on SqPNG and SqPNG-pH bioconjugates (compounds **1** and **2**) featuring double-ester arrangements as pro-drug interconnecting moieties.

The initial models were built using the ChemDraw structure of **1** and **2**, which were converted to 3D models using Chem3D software. These two models were initially energy-minimized *in vacuo* using the AM1[14] semiempirical method present in the HyperChem package and subsequently submitted to a sequence of 50 short molecular dynamics trajectories (10 ps under the molecular mechanics method OPLS, *i.e.*, optimized potentials

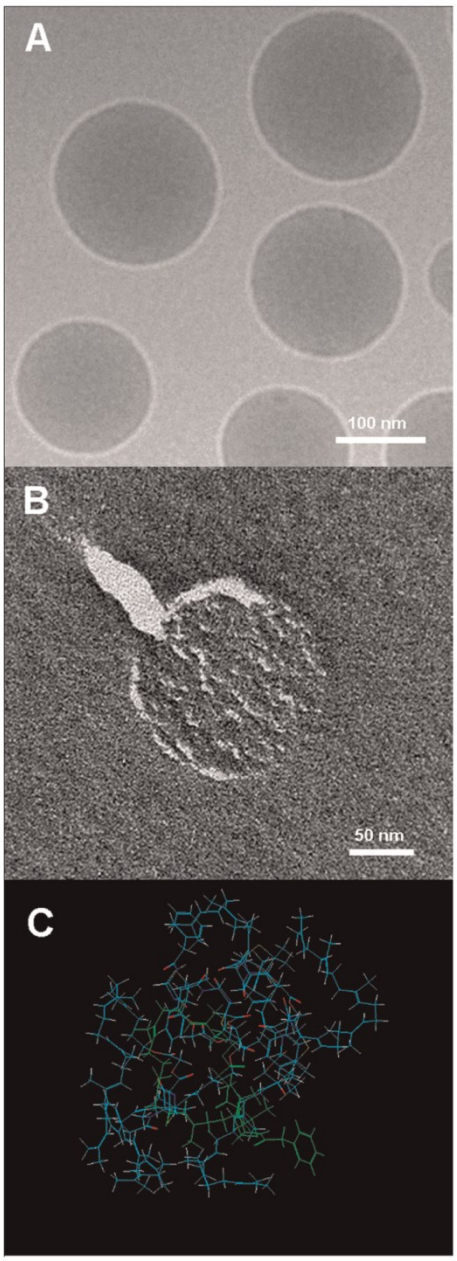

Figure 1. Morphological appearance of SqPNG NPs upon CryoTEM (A) and TEM after freeze-fracture (B). Results of energy minimization using the AM1 method on a stack of SqPNG molecules (C): total energy of the complete assembly $\Delta H = -1183.93$ kcal/mol (AM1); energy of the selected (green) molecule $\Delta H = -193.44$ kcal/mol (AM1); energy of the nonselected (blue) molecules $\Delta H = -979.95$ kcal/mol (AM1); binding energy = total − Σ(partial)= −20.52 kcal/mol. To depict the conformation of a single SqPNG molecule, one molecule is shown in green.

for liquid simulations,[15] followed by energy minimization using the AM1 method in order to sample the conformational space of **1** and **2**). These calculations indicated that extended linear conformations of the squalene side chain were favored over conformers showing a bend somewhere along the lipophilic side chain.

For both **1** and **2**, the lowest ΔH linearly extended conformation models were selected for further studies. It should be noted at this stage that no significantly different ΔH values were obtained for **1** and **2**.

Duplex models of **1** and **2** were built by assembling the above selected conformers in a parallel or antiparallel mode. Using the same approach as for the single entities, it was found that the antiparallel mode was energy favored; this applied for both duplex 1:1 and duplex 2:2 models.

Finally, quintuplex models featuring 5 units of **1** or **2** were assembled using the antiparallel mode and were subjected to a sequence of 10 molecular dynamics trajectories (10 ps under molecular mechanics method OPLS) followed by energy minimization using the AM1 method. The lowest ΔH system was energy-analyzed as shown in Figure 1C.

The same process applied to quintuplex **1** gave a slightly lower (although statistically not significant) binding energy on the order of -15 ± 5 kcal/mol ($n = 10$) compared to 20 ± 5 kcal/mol ($n = 10$) for quintuplex **2**. This trend was difficult to further substantiate, although slight differences were found at the level of the electrostatic potential values of the heteroatoms, especially around the oxygen's double ester moieties.

As can be seen from inspection of these figures, the carbonyl double bonds of **1** were slightly more polarized than those of **2**.

In an effort to study the effect of water solvation, we examined also **1** and **2** in a periodic box of water molecules. Various attempts were made to evidence hydrogen bond formation between water and solutes **1** and **2**. In a very few frames, we were able to evidence a single hydrogen bond and this mainly at the level of the amide oxygen. This bond was also very weak. In other words, both **1** and **2** are highly lipophilic compounds, and within the nanoparticles formed by addition of either ethanolic solution of **1** or **2** to water, structuring by water as often observed previously is very unlikely. Clearly, these entities are mainly stabilized by strong hydrophobic forces.

Direct Antibacterial Activity of NPs. The antibacterial activity of SqPNG NPs was investigated against several bacterial strains, both sensitive and resistant to PNG. PNG and other β-lactam antibiotics prevent the interpeptidoglycan linkage of the bacterial wall, causing the arrest of bacterial multiplication.[16] The controlled and targeted release of PNG is therefore essential to prevent the extracellular release of low concentrations of antibiotic, leading to the emergence of bacterial resistance.[17–19]

TABLE 1. Minimum Inhibitory Concentration of PNG and SqPNG NPs in Several Bacterial Strains

	minimum inhibitory concentration (MIC)	
bacterial strain	penicillin G (μg/mL)	SqPNG NPs (μg/mL)
Enterococcus faecalis ATCC 29212	4	>128
Escherichia coli ATCC 8739	128	>128
Listeria monocytogenes ATCC 15313	>128	>128
Proteus vulgaris ATCC 13315	16	>128
Serratia marcescens ATCC 13880	>128	>128
Shigella sonnei ATCC 25931	64	>128
Staphylococcus aureus MRSA ATCC 33591	64	>128
Staphylococcus aureus ATCC 55585	0.03	2
Pseudomonas aeruginosa ATCC 9027	>128	>128
Streptococcus pneumoniae ATCC 33400	0.12	>128
Salmonella typhimurium ATCC 13311	2	>128
Streptococcus pyogenes ATCC 12344	0.06	16

We quantified the minimum inhibitory concentration for proliferation of bacteria (MIC) of free PNG and of SqPNG NPs. Results, reported in Table 1, clearly show the absence of any significant antibiotic activity of SqPNG NPs against all the tested strains except for *Staphylococcus aureus* and *Streptococcus pyogenes*, probably because PNG was not released from NPs in these experimental conditions.

Noteworthy, *Streptococcus pyogenes* ATCC 12344 and *Staphylococcus aureus* ATCC 55585 displayed high sensitivity toward PNG and NPs. To explain these results, it was calculated that if only about 4% of PNG release occurred, this would be enough to obtain a MIC of 16 μg/mL for *S. pyogenes* ATCC 12344 and 2 μg/mL for *S. aureus* ATCC 55585.

In the same way, SqPNG-pH NPs were tested against *S. aureus* ATCC 55585 and showed a lower MIC (0.125 μg/mL) than SqPNG NPs (2.00 μg/mL), although still higher than free PNG (0.03 μg/mL), probably due to the lower stability of SqPNG-pH compared with SqPNG, resulting in more PNG being released in the bacteria culture media after 18 h of incubation.

Uptake of NPs by J774 Cells. The ability of SqPNG and SqPNG-pH NPs to be internalized by macrophages was studied, using the cell line J774, a murine macrophage model commonly used.[20–22] In order to study the kinetics of the NP internalization, fluorescent BODIPY-cholesterol tagged NPs were incubated with J744 macrophages and cell fluorescence was analyzed by flow cytometry in comparison to untreated cells. We observed (Figure 2) that both types of NPs were internalized after 2 h of incubation; SqPNG reached a maximum at 6 h, while fluorescence of SqPNG-pH NPs continued to increase during the 24 h incubation

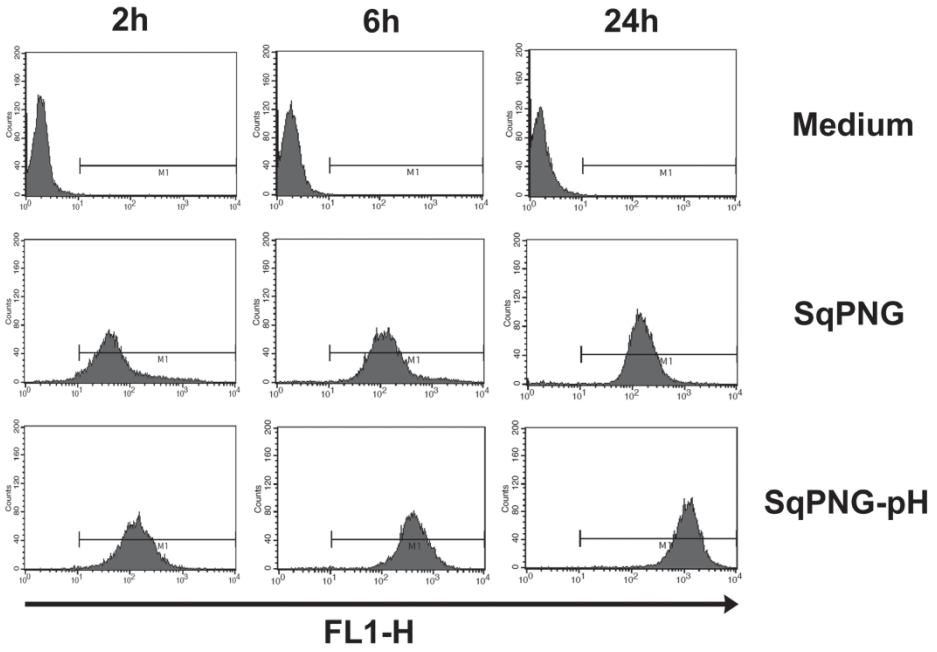

Figure 2. Kinetics of NP (either SqPNG or SqPNG-pH) internalization in J774 macrophages by flow cytometry. Cells were incubated with NPs during 2, 6, and 24 h in RPMI1640 + 0.5% v/v FBSd. The green fluorescence from BODIPY-labeled NPs was read in FL1-H.

[SqPNG: 6 h MFI = 130, 24 h MFI = 153; SqPNG-pH: 6 h MFI = 409, 24 h MFI = 1112 (MFI = mean fluorescence intensity)]. These results evidenced that NPs were differently internalized by macrophages depending on the linkage (*i.e.*, pH-sensitive or pH-insensitive) between squalene and PNG. Moreover, it was observed that NPs were also significantly internalized by PLB-985, a human myeloid cell line differentiated in neutrophil-like[23] (see Figure 5 in the Supporting Information). SqPNG-pH NP internalization was confirmed using confocal microscopy (Figure 6 in the Supporting Information). We can see pictures of the median plane of cells treated with SqPNG-pH fluorescent NPs; the observed green spots were clearly located in the cytosol. Moreover, we have performed an additional experiment using a membrane fluorescent marker (phycoerythrin-conjugated anti-CD11b, an antibody against CD11b coupled to phycoerythrin) to check if there is (or not) co-localization with the fluorescently labeled NPs. The results clearly indicated that the major fraction of the SqPNG-pH NPs was cell-internalized and not localized on the surface of the cell membrane (Figure 9 in the Supporting Information). The absence of fluorescence signals focused at the cell surface suggested that NPs of SqPNG-pH were internalized by the J774 macrophages and concentrated in intracellular compartments. These results are in accordance with the well-known macrophages' role in removal of NPs from the blood.[24]

Intracellular Bactericidal Effect of NPs. As *S. aureus* is known to invade and survive in macrophages,[25] based on the previous data (Table 1), the PNG-sensitive *S. aureus* ATCC 55585 strain was chosen as a model to study the intracellular bactericidal effect of the PNG-based NPs. Experimental conditions were chosen using a variant of the gentamicin protection assay, in order to keep only the intracellular bacteria alive while maintaining at least 95% of cell viability over the 24 h of the assay. This has been measured by trypan blue assay, since the MTT assay could not be performed with infected cells. Practically, cells were preincubated with different NP formulations maintaining similar PNG concentrations (20 μg/mL) and then infected with *S. aureus* bacteria for 2 h. After 6 h of treatment with gentamicin (to remove extracellular bacteria), we observed (Figure 3A) that control PNG-unloaded NPs (obtained by nanoprecipitation of the Sq-est 7) as well as free PNG had no antimicrobial activity on intracellular bacteria. On the contrary, both tested NPs displayed a significant effect in reducing the number of intracellular bacteria, which was more pronounced for the NPs with a pH-sensitive linker between squalene and penicillin G (*i.e.*, SqPNG-pH NPs induced a 78% decrease in viable intracellular bacteria). After 24 h of treatment with gentamicin, the bactericidal profile was slightly different. Indeed, free PNG induced a 56% decrease of bacterial viability, whereas SqPNG-pH NPs were still more effective in killing intracellular bacteria (*i.e.*, 87% reduction). As previously described,

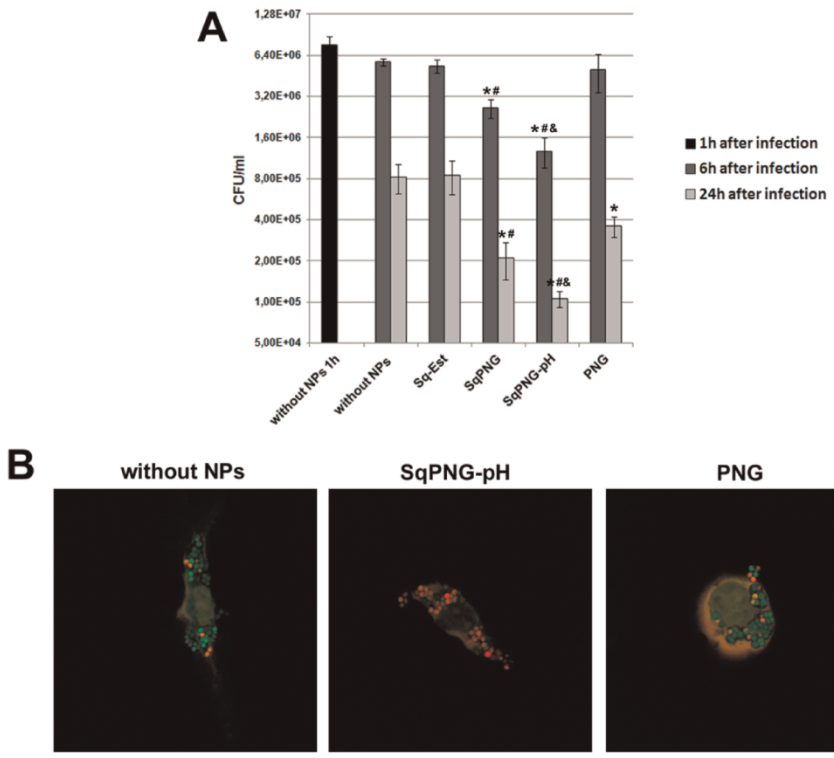

Figure 3. (A) CFU of intracellular *S. aureus* of cells treated with free PNG, SqPNG NPs, or SqPNG-pH NPs, all at 20 μg/mL equiv PNG (*i.e.*, 50 μg/mL total weight for the NP formulations). Experimental conditions: after treatment (6 h), J774 cells were washed and allowed to engulf *S. aureus* at a multiplicity of infection (MOI) of 10 for 2 h. To remove the extracellular bacteria, J774 macrophages were then washed again and incubated with gentamicin (50 μg/mL) during 1 (black), 6 (gray), or 24 (light gray) hours. Cell lysates were plated onto BHI/agar for CFU enumeration after 24 h. The data show three independent experiments (means $\pm$ SD). $^{*}p < 0.05$ compared with "without NPs"; $^{\#}p < 0.05$ compared with PNG; $^{\&}p < 0.05$ compared with SqPNG. (B) Confocal fluorescence microscopy images of viable bacteria in J774 cells. J774 cells were pretreated with NPs then infected with *S. aureus* and fixed with paraformaldehyde, permeabilized with 0.2% Triton X-100, and double-labeled with propidium iodide and Syto9 (LIVE/DEAD BacLight kit). Viable *S. aureus* cells are stained in green, while red signals represent dead bacteria.

the decrease of the number of intracellular bacteria following free PNG treatment after 24 h hours may be explained by the cooperative effect of gentamicin and PNG allowing a small amount of PNG to indeed diffuse intracellularly.[17] The fact that there was no difference, after 6 h, in the intracellular bacterial counts between the untreated cells, the cells treated with the PNG-unloaded NPs (*i.e.*, Sq-Est), and the PNG incubated free clearly suggested that the pure squalene NPs (Sq-Est) did not induce any antibacterial effect and that free PNG had no intracellular bactericidal effect at this time point, likely because of insufficient diffusion into cells.[26] Our data clearly suggested that PNG NPs improved the cell penetration of the antibiotic, which allowed the rise of a significant bactericidal effect. Moreover, the better antibacterial activity of SqPNG-pH NPs *versus* SqPNG NPs may be reasonably explained by the acid-sensitive linkage in SqPNG-pH NPs, which could trigger a more efficient release of penicillin G in the cells.

We further investigated the influence of the different treatments on the intracellular bacterial viability by staining the bacteria with the LIVE/DEAD BacLight kit, which allowed to differentiate between live and dead *S. aureus* (by staining the latter with a red fluorophore and the viable bacteria with a green fluorophore)[27] (Figure 3B). Clearly, free PNG did not induce any significant mortality of intracellular *S. aureus*, unlike SqPNG-pH NPs, which gave rise to many red bacteria, the same ratio as colony-forming unit (CFU) enumeration.

It has, however, to be noted that if SqPNG-pH NPs showed a dramatic ability to kill most of the intracellular *S. aureus* (*i.e.*, 87%) in comparison with all the other treatments, they failed in killing all the intracellular bacteria after 24 h. This may be attributed either to insufficient intracellular PNG release from NPs to kill all bacteria or to the low metabolic state of a fraction of the intracellular bacteria, which may prevent an antibiotic effect,[26,28] or to both events. This deserves further investigations to further improve the antibiotic treatment toward these intracellular bacteria.

Mechanism of NP SqPNG-pH Internalization. Even though phagocytosis is a well-known uptake mechanism of

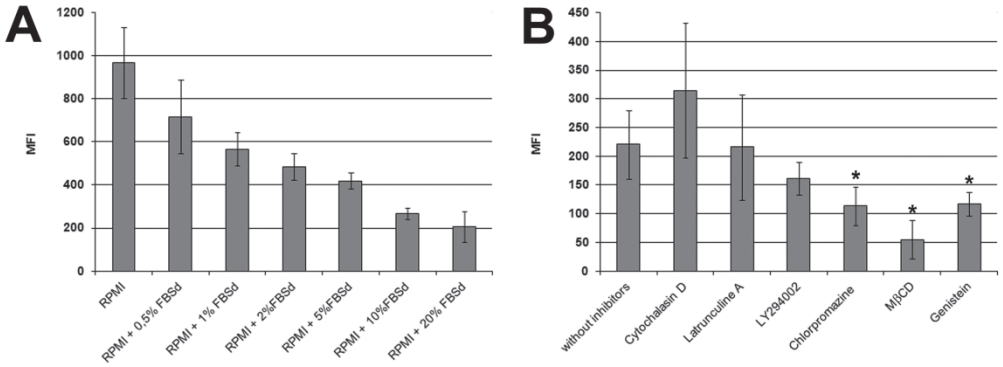

Figure 4. Influence of decomplemented fetal bovine serum (FBSd) on the internalization of SqPNG-pH NPs in J774 cells by flow cytometry. Cells were incubated with 100 μg/mL NPs during 6 h (A). Internalization in J774 cells of SqPNG-pH NPs in the presence of endocytosis inhibitors (flow cytometry). Cells were preincubated 1 h with or without inhibitors, then with 25 μg/mL of NPs during 6 h in RPMI1640 + 0.5% v/v FBS (B). The green fluorescence of cholesteryl-BODIPY in the NPs is read in FL1-H.

macrophages, these cells are also capable of clathrin-dependent or -independent endocytosis.[29,30] These different mechanisms impact the cell internalization kinetics and the intracellular trafficking of the NPs, both parameters that influence the effectiveness of the carried drug.

In the context of treating intracellular infections, targeting a subcellular compartment is a relevant goal to achieve since the co-localization of NPs with bacteria in the same intracellular compartments should enhance the local concentration of the delivered antibiotic and improve the efficiency.[31] To dissect the mechanism underlying NP internalization in our model, we used different pharmacologic inhibitors of endocytosis pathways[32] and observed by cytometry their effect on the internalization of SqPNG-pH NPs. We have also investigated the effect of decomplemented serum (FBSd) on the NP uptake, as serum contains several opsonins able to increase cell internalization (Figure 4A).

Interestingly, it was found that increasing the concentration of decomplemented fetal bovine serum (FBSd) induced a significant decrease in the NP cell capture. Since the complement activation, principally responsible for inducing phagocytosis of particles, was absent in our experimental conditions, it is likely that other proteins, including those with a dysopsonin activity, may adsorb onto the surface of SqPNG-pH NPs.[33] The plasma proteome is, indeed, expected to contain many proteins, and 50 have been identified in association with various NPs.[34−37] Dysopsonins such as albumin and some apolipoproteins are considered to promote prolonged circulation times of NPs in the blood.[38−40] It has been suggested that dysopsonins, naturally occurring substances that inhibit phagocytic ingestion, usually by altering the surface properties of the phagocyte or particle or both, thereby interfering with opsonization or altering the metabolic activity of the phagocyte, may regulate the uptake of NPs.[39] In our case, it is possible that the hydrophobicity and rigidity of SqPNG-pH NPs increased the amount of bounded proteins such as albumin, apolipoproteins, or fibrinogen.[24,41−44] This deserves, however, further experimental clarification.

Different inhibitors were used to inhibit various entrance routes for the NPs: (i) phagocytosis and macropinocytosis (cytochalasin D, latrunculin A, LY294002) and (ii) clathrin- (chlorpromazine) and (iii) clathrin-independent (methyl-β-cyclodextrin (MβCD), genistein) pathways. Figure 4B clearly shows that several endocytosis pathways, including clathrin endocytosis, coexist for SqPNG-pH NP internalization, as already shown before with other types of NPs.[45]

In a nutshell, the negative effect of the serum combined with the absence of influence of phagocytosis inhibitors on NP cell capture allowed us to conclude that J774 did not use the same pathway of internalization for pathogens and squalenoylated NPs.

Intracellular Localization of NPs *versus* Bacteria in J774. To investigate the intracellular distribution of NPs, SqPNG-pH NPs labeled with BODIPY-cholesterol were incubated with J774 macrophages for 6 h and then treated with LysoTracker, a marker of late endosomal and lysosomal vesicles (Figure 5A). Only a partial co-localization of NPs with the fluorescent lysosomal marker was observed, which correlated with our previous findings that NPs employed different endocytosis pathways for cell internalization.

In order to investigate if NPs located or not with intracellular bacteria, we stained *S. aureus* with a high concentration of propidium iodide (red), whereas NPs were tagged with BODIPY-cholesterol (green). Treated cells were then observed by confocal microscopy (Figure 5B). It was observed that NPs and *S. aureus* were found in different intracellular compartments.

The question that arises is how to explain the ability of SqPNG-pH NPs to kill intracellular bacteria (Figure 3), knowing that they distribute in different intracellular vesicles than bacteria (Figure 5B). The suggested

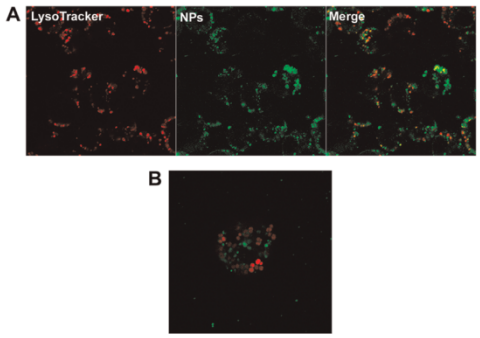

Figure 5. (A) J774 macrophages incubated with fluorescent SqPNG-pH NPs (green) at 6 h, then with LysoTracker Red DND-99 (40 nM) for 5 min and observed by confocal microscopy. Yellow color indicates the lysosomal localization of the NPs. (B) Localization of SqPNG-pH NPs and *S. aureus* ATCC55585 in J774 cells. J774 pretreated with fluorescent SqPNG-pH NPs (green) and then infected with stained IP *S. aureus* ATCC55585 (red) before fixation with paraformaldehyde (at 6 h post-treatment with gentamicin) and observed by confocal microscopy.

mechanism results from the ability of PNG to cross the intracellular endolysosomal membranes after being released in the acidic environment of the lysosomes (Figure 5A).

As depicted in Figure 6, biological membranes are permeable only to the uncharged form of antibiotics. Thus, PNG, being a weak acid ($pK_a = 2.74$), is negatively charged (A^-) at neutral physiological pH. In this form, PNG cannot diffuse into the infected cells, which explains the poor antimicrobial activity of this antibiotic toward intracellular bacteria. The squalenoylated PNG-loaded nanoparticles did not follow this single-membrane diffusion process but entered into the cells through endocytotic pathways, including

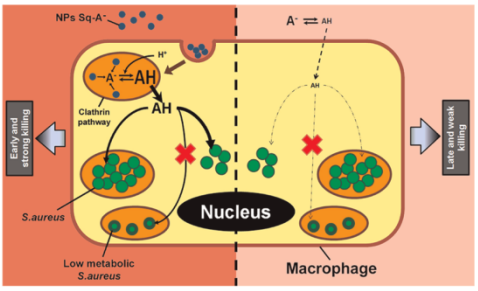

Figure 6. Schematic representation of the proposed mechanism of SqPNG-pH NP bactericidal activity inducing early and efficient killing of intracellular *S. aureus*.

clathrin-dependent endocytosis, as demonstrated in this study (see Figure 4). Thus, SqPNG-pH NPs further accumulated in acidic late endosomes and lysosomes (different from bacterial ones), where their pH-sensitivity triggered the release of free PNG. In the acidic compartments, this antibiotic became protonated (AH) and therefore capable of crossing intracellular membranes and allowing further interaction with intracellular *S. aureus*.[46−48]

CONCLUSION

Two bioconjugates of penicillin G with squalene, using either a pH-sensitive (SqPNG-pH) or a pH-insensitive linker (SqPNG), were synthesized and found to spontaneously form stable nanoparticles.

The SqPNG-pH nanoparticles have proved to induce fast and significant killing of *S. aureus*-infected J774 cells. This approach opens interesting perspectives to combat invasive bacterial infections of macrophages such as *S. aureus*, which represents a worldwide public health concern and a major burden for the dairy industry.[25]

MATERIALS AND METHODS

Materials and Instrumentation. Penicillin G, squalene, and bromoacetic acid were purchased from Sigma-Aldrich Chemical Co., France. Phosphate-buffered solution (PBS) without $CaCl_2$ and $MgCl_2$, RMPI 1640 containing L-glutamine and 25 mM HEPES, and fetal bovine serum (FBS) were purchased from Dulbecco.

Propidium iodide was obtained from Invitrogen (Cergy-Pontoise, France). The following signaling inhibitors were obtained from Sigma: the tyrosine kinase inhibitor genistein, the phosphatidylinositol 3-kinase (PI3K) inhibitor LY-294002, the lipid raft-modifying drug methyl-β-cyclodextrin (MβCD), the clathrin endocytic pathway inhibitor chlorpromazine, and the actin cytoskeleton inhibitors cytochalasin D and latrunculine A. Cholesteryl BODIPY FL C12 (cholesteryl 4,4-difluoro-5,7-dimethyl-4 bora-3a,4°-diaza-5-indacene-3-dodecanoate) and LysoTracker Red DND-99 were Invitrogen Molecular Probes products. In all biological experiments, Milli-Q water (Millipore Synergy 185) was used. Other chemicals obtained from commercial suppliers were used without further purification.

IR spectra were obtained on solid or neat liquid on a Fourier transform Bruker Vector 22 spectrometer. Only significant absorptions are listed. Optical rotations were measured on a Perkin-Elmer 241 polarimeter at 589 nm. The ^1H and ^{13}C NMR spectra were recorded on a Bruker Avance 300 (300 and 75 MHz for ^1H and ^{13}C, respectively) or a Bruker Avance 400 (400 and 100 MHz for ^1H and ^{13}C, respectively) spectrometer. Recognition of methyl, methylene, methine, and quaternary carbon nuclei in ^{13}C NMR spectra rests on the *J*-modulated spin−echo sequence. Mass spectra were recorded on a Bruker Esquire-LC. Analytical thin-layer chromatography was performed on Merck silica gel $60F_{254}$ glass precoated plates (0.25 mm layer). Column chromatography was performed on Merck silica gel 60 (230−400 mesh ASTM). Diethyl ether and tetrahydrofuran (THF) were distilled from sodium/benzophenone ketyl. Methanol and ethanol were dried over magnesium and distilled. Benzene, toluene, DMF, and CH_2Cl_2 were distilled from calcium hydride, under a nitrogen atmosphere. All reactions involving air- or water-sensitive compounds were routinely conducted in glassware that was flame-dried under a positive pressure of nitrogen.

Synthesis of Bromoester (6). To a solution of 1,1′,2-trisnorsqualenyl alcohol **5** (500 mg, 1.3 mmol) in anhydrous CH_2Cl_2 (6 mL) was added bromoacetic acid (216 mg, 2.01 mmol) and 4-dimethylaminopyridine (DMAP) (10 mg, 0.08 mmol). The mixture was cooled to 0 °C, and DCC (317 mg, 1.95 mmol) was added portionwise. After being stirred at room temperature for 18 h, the reaction mixture was filtered through a cake of Celite. The solid was washed with a small amount of CH_2Cl_2.

The filtrate was concentrated under reduced pressure, and the residue was purified by chromatography on silica gel using elution with AcOEt/cyclohexane, 1:4. to give bromoester **6** as a colorless oil (460 mg, 70% yield). IR (neat, cm^{-1}): ν 2960−2850, 1739, 1700, 1448, 13821276, 1381. ^1H NMR (300 MHz, $CDCl_3$): δ 5.18−5.07 (m, 5 H), 4.14 (t, J = 6.4, 2 H), 3.82 (s, 2 H), 2.16−1.98 (m, 18 H), 1.70 (quint, J = 8.0 Hz, 2 H), 1.68 (s, 3 H), 1.53 (s, 15 H). ^{13}C NMR (75 MHz, $CDCl_3$): δ 167.2 (C), 135.0 (C), 134.8 (2C), 133.2 (C), 131.2 (C), 125.3 (CH), 124.4 (2 CH), 124.2 (2 CH), 65.9 (CH_2), 39.7 (2 CH_2), 39.6 (CH_2), 35.5 (CH_2), 28.2 (2 CH_2), 27.8 (CH_2), 26.6 (CH_2), 26.5 (2 CH_2),25.8 (CH_2), 25.6 (CH_3), 17.6 (CH_3), 16.0 (3 CH_3), 15.8 (CH_3).

Synthesis of Chloromethyl Ester (8). To a solution of 1,1′,2-trisnorsqualenic acid (**4**) (400 mg, 1.0 mmol) and n-Bu_4NHSO_4 (34 mg, 0.1 mmol) in CH_2Cl_2 (2 mL) was added a solution of $KHCO_3$ (300 mg, 3.0 mmol) in water (2 mL). The reaction mixture was vigorously stirred, and chloromethylsulfonyl chloride (185 mg, 1.15 mmol) was added dropwise. After being stirred for 1 h, CH_2Cl_2 (10 mL) was added. The organic phase was separated, washed with brine, dried over magnesium sulfate, and concentrated under reduced pressure to leave a pale yellow oil, which was used directly in the next step (382 mg, 81%). IR (neat, cm^{-1}): ν 2980−2845, 1768, 1710,1440, 1377, 1123, 1044. ^1H NMR ($CDCl_3$, 300 MHz): δ 5.69 (s, 1 H, OCH_2Cl), 5.20−5.00 (m, 5 H, HC═C(Me)), 2.60−2.40 (m, 2 H), 2.05−2.20 (m, 2H), 2.10−1.80 (m, 18 H), 1.68 (s, 3 H, C═$C(CH_3)_2$), 1.60 (s, 15 H, HC═$C(CH_3)$). ^{13}C NMR ($CDCl_3$, 100 MHz): δ 171.3 (C, CO_2), 135.1 (C), 134.9 (C), 134.8 (C), 132.5 (C), 131.2 (C), 125.6 (CH), 124.4 (CH), 124.4 (CH), 124.2 (2CH), 68.5 (CH_2, OCH_2Cl), 39.7 (2 CH_2), 39.5 (CH_2), 34.1 (CH_2), 32.8 (CH_2), 28. (2CH_2), 26.7 (CH_2), 26.6 (CH_2), 26.5 (CH_2), 25.7 (CH_3), 17.6 (CH_3), 16.0 (3CH_3), 15.9 (CH_3). MS (+APCI): m/z 449.3 (100%) $[M + H]^+$.

Synthesis of Squalenyl Conjugates. (SqPNG) (**1**): A mixture of penicillin G sodium salt (50 mg, 0.15 mmol) and 1,1′,2-trisnorsqualenyl bromoacetate (**3**) (113 mg, 0.22 mmol) in dry DMF (0.75 mL) was stirred at room temperature for 48 h. The reaction mixture was then concentrated under reduced pressure (0.05 Torr), and the residue was purified by chromatography on silica gel eluting with AcOEt/cyclohexane, 1:4, to give the bioconjugate **1** as a colorless, viscous oil (58 mg, 56% yield). $[\alpha]_D$ = +213.3 (EtOH, c 0.45). IR (neat, cm^{-1}): ν 3400−3100, 2931, 2854, 1789, 1753, 1691, 1659, 1495, 1453, 1375, 1295, 1199, 1177, 1152, 1130, 1075,1028. ^1H NMR (400 MHz, $CDCl_3$): δ 7.42−7.20 (m, 5 H), 6.10 (d, J = 9.1 Hz, 1 H, CONH), 5.65 (dd, J = 9.1, 4.2 Hz, 1 H, H-6), 5.50 (d, J = 4.2 Hz, 1 H, H-5), 5.20−5.10 (m, 5 H, HC═$C(CH_3)$), 4.75 (d, J = 15.8 Hz, 1 H, OCH_2CO_2), 4.58 (d, J = 15.8 Hz, 1 H, OCH_2CO_2), 4.43 (s, 1 H, H-2), 4.13 (t, J = 6.7 Hz, 2 H, $CO_2CH_2CH_2$), 3.63 (s, 2 H, $PhCH_2CO$), 2.12−1.92 (m, 18 H), 1.73 (quint, J = 8.0 Hz, 2 H), 1.68 (s, 3 H, C═$C(CH_3)_2$), 1.60 (s, 15 H, C═$C(CH_3)$), 1.57 (s, 3 H, $SC(CH_3)_2$), 1.50 (s, 3 H, $SC(CH_3)_2$). ^{13}C NMR (100 MHz, $CDCl_3$): δ 173.7 (C, CO), 170.3 (C, CO), 167.0 (C, CO), 166.9 (C, CO), 135.1 (C), 134.9 (C), 133.8 (C), 133.2 (C), 131.2 (C), 129.5 (2CH), 129.1 (2CH), 127.6 (CH), 125.4 (CH), 124.4 (2 CH), 124.2 (2CH), 70.3 (CH, C-2), 67.9 (CH, C-5), 65.4 (CH_2, $CO_2CH_2CH_2$), 64.6 (C, C-3,), 61.2 (CH_2, OCH_2CO_2), 58.5 (CH, C-6), 43.3 (CH_2, $PhCH_2$), 39.7 (CH_2), 39.6 (CH_2), 35.5 (CH_2), 31.1 (CH_3, $SC(CH_3)_2$), 28.2 (3 CH_2), 26.7 (CH_3), 26.7 (CH_2), 26.6 (3 CH_2), 25.7 (CH_3), 17.7 (CH_3), 16.0 (3 CH_3), 15.8 (CH_3). MS (-APCI): m/z (%) 760 (100) $[M - H]^-$.

(SqPNG-pH) (**2**): A mixture of penicillin G sodium salt (180 mg, 0.50 mmol) and trisnorsqualenic acid chloromethyl ester (**8**) (230 mg, 0.51 mmol) in DMF (3 mL) was stirred at room temperature for 4 d. The reaction mixture was concentrated under reduced pressure, and the residue was taken into water. The mixture was extracted with CH_2Cl_2. The combined organic extracts were washed with brine, dried over $MgSO_4$, and concentrated under reduced pressure. Chromatographic purification on silica gel eluting with cyclohexane/AcOEt, 4:1, afforded conjugate **2** as a colorless oil (182 mg, 49%). $[\alpha]_D$ = +137.4 (EtOH, c 1.4). IR (neat, cm^{-1}): ν 3034, 2927, 2851, 1792, 1768, 1738, 1678, 1451, 1373, 1296, 1241, 1116, 1046, 985, 909. ^1H NMR ($CDCl_3$, 300 MHz): δ 7.40−7.25 (m, 5 H, Ph), 6.07 (br s, 1 H, NH), 5.80 (d, J = 5.5 Hz, 1 H, OCH_2O), 5.74 (d, J = 5.5 Hz, 1 H, OCH_2O), 5.65 (dd, J = 9.1 Hz, J = 4.2 Hz, 1 H, H-6), 5.49 (d, d, J = 4.3 Hz, 1 H, H-5), 5.20−5.02 (m, 5 H, HC═$C(CH_3)$), 4.38 (s, 1 H, H-2), 3.63 (s, 2 H, $PhCH_2$), 2.48−2.40 (m, 2 H, $COCH_2CH_2$), 2.30−2.25 (m, 2 H, $COCH_2CH_2$), 2.14−1.90 (m, 16 H, ═$CHCH_2CH_2C(CH_3)$), 1.68 (s, 3 H, $(CH_3)_2C$═), 1.58 (s, 15 H, CH_3), 1.44 (s, 3 H, $C(CH_3)_2$), 1.43 (s, 3 H, $C(CH_3)_2$). ^{13}C NMR ($CDCl_3$, 100 MHz): δ 173.4 (C, CO), 171.7 (C, CO), 170.3 (C, CO), 166.3 (C, CO), 135.1 (C, ═$C(CH_3)$), 134.8 (C, ═$C(CH_3)$), 134.7 (C, ═$C(CH_3)$), 133.7 (C, Ph), 132.5 (C, ═$C(CH_3)$), 131.2 (C, ═$C(CH_3)_2$), 129.5 (2CH, Ph), 129.1 (2CH, Ph), 127.6 (CH, Ph), 125.5 (CH, HC═$C(CH_3)$), 124.4 (CH, HC═C-(CH_3)), 124.3 (CH, HC═$C(CH_3)$), 124.2 (2CH, HC═$C(CH_3)$), 79.5 (CH_2, OCH_2O), 69.9 (CH, C-2), 68.0 (CH, C-5), 64.4 (C, C-3), 58.8 (CH, C-6), 43.3 (CH_2, $PhCH_2$), 39.7 (2 CH_2, ═$C(CH_3)CH_2$), 39.4 (CH_2, ═$C(CH_3)CH_2$), 34.0 (CH_2, $COCH_2CH_2$), 32.7 (CH_2, $COCH_2CH_2$), 31.6 (CH_3, $SC(CH_3)_2$), 28.2 ($2CH_2$, ═$CHCH_2$),), 26.7 (CH_2, ═$CHCH_2$),), 26.6 (CH_2, ═$CHCH_2$), 25.6 ($2CH_3$, ═$C(CH_3)_2$, $SC(CH_3)_2$), 17.6 (CH_3), 16.0 ($3CH_3$), 15.8 (CH_3). MS (+APCI): m/z 747.5 (30) $[M + H]^+$; 721.5 (100), 572.4 (40) $[M - PhCH_2CH$═C═$O + H]^+$.

NP Formation, Characterization, and Stability. In a typical procedure, 4 mg of SqPNG or 4 mg of SqPNG-pH was dissolved in 0.5 mL of ethanol and added dropwise to 1 mL of distilled water, giving rise to the spontaneous formation of nanoparticles. Ethanol was then evaporated under vacuum using a Rotavapor to obtain an aqueous suspension of SqPNG or SqPNG-pH NPs.

Similarly, Sq-Est (**7**) NPs were obtained using the same procedure as described above for SqPNG and SqPNG-pH derivatives. Sq-Est NPs were used as negative control in antibacterial tests.

In order to check the absence of free, nonassembled SqPNG or SqPNG-pH conjugates in solution, SqPNG and SqPNG-pH NPs were ultracentrifugated at 40 000 rpm for 120 min, and the supernatant was analyzed by HPLC (H5C18-25 M INTERCHROM C18 Hypersil 5 μm, 250 × 4,6 mm column, eluent CH_3OH/H_2O, 95:5, λ_1 = 208 nm and λ_2 = 260 nm); for both SqPNG and SqPNG-pH, less than 1% was found free in the supernatant.

The size and the polydispersity of NPs at various dilutions and in different storage conditions (in suspension in water at 4, 25, and 37 °C, and in RPMI medium at 37 °C) were determined at 20 °C by quasi-elastic light scattering using a nanosizer (Zetasizer Nano 6.12, Malvern Instruments Ltd., UK). The selected angle was 173°, and the measurement was made after dilution to 1:25 of the NP suspension in Milli-Q water. The Z-potential was determined using a Zetasizer (Zetasizer 4, Malvern Instruments Ltd., UK), after dilution of 1 mL of the NPs suspension in 1 mL of KCl (1 mM).

Preparation of Fluorescent NPs. Fluorescently labeled NPs were obtained by nanoprecipitation in water of an ethanolic solution of SqPNG or SqPNG-pH (4 mg/mL) containing 0.5% w/w of the hydrophobic green dye cholesteryl BODIPY FL C12. The solvent was then evaporated under vacuum; the centrifugation of fluorescent NPs and the spectrofluorimetric analysis of the supernatant showed the absence of free fluorochrome in solution, showing that cholesteryl BODIPY FL C12 was associated with PNG NPs. In further experiments, fluorescent NPs were not ultracentrifuged, and the size and polydispersity were determined in different storage conditions (*i.e.*, NP suspension in water at 4 °C or in RPMI 5% FBSd at 37 °C).

Cryogenic Transmission Electron Microscopy. The morphology of SqPNG NPs was investigated by cryogenic transmission electron microscopy analysis or by transmission electron microscopy after freeze-fracture (FFTEM).

For CryoTEM, 4 μL of a concentrated SqPNG NPs suspension (10 mg/mL) was deposited onto a perforated carbon film mounted on a 200 mesh electron microscopy grid. The homemade carbon film hole dimensions were about 2 mm in diameter. Most of the drop was removed with a blotting filter paper, and the residual thin films remaining within the holes were vitrified after immersion in liquid ethane using a guillotine-like frame. The specimen was then transferred, using liquid nitrogen, to a cryospecimen holder and observed using a JEOL FEG-2010 electron microscope. Micrographs were recorded at 200 kV under low-dose conditions at a magnification of 40 000 on SO-163 Kodak film. Micrographs were digitized using a film scanner (Super Coolscan 8000 ED, Nikon), and analysis was made using ImageJ software.

For FFTEM observations, a drop of the sample was placed on a copper support, immediately frozen in liquid propane, and then kept in liquid nitrogen. Fracturing and shadowing were performed in a Balzers BAF 400 freeze-etching unit. The replicas were washed in THF and in distilled water and placed on copper grids. Observations were made under a TEM JEOL 100SX.

Antibacterial Activity of the NPs. The antibacterial activity of SqPNG NPs was investigated against several bacterial strains, both sensitive and resistant to penicillin G. The antibacterial activities were carried out in a quantitative assay based on dilution method, using Mueller-Hinton medium (with 10% v/v of FBSd when needed), and the MIC was determined for SqPNG NPs, SqPNG-pH, and free PNG as positive control.

The analysis was conducted preparing various dilutions of penicillin G and NPs from 128 to 0.015 μg/mL in different test tubes (final volume 1 mL) inoculated with equal quantities of bacterial culture (5×10^5 bacteria/mL). After incubation at 37 °C for 18 h, the turbidity of the solutions was examined. The first test tube, in dilution order, which presented a clear solution, was that which contained the minimum inhibitory concentration of the antibiotic. Results were also confirmed by bacterial plating on agar.

Macrophage Cell Line. The J774 murine cell line was used as macrophage model. The cells were grown in RPMI-1640 medium (BioWhittaker, Walkerville, MD, USA) supplemented with 10% v/v fetal bovine decomplemented serum (Cambrex BioSciences, Verviers, Belgium) at 37 °C in humidified air containing 5% CO_2. The cells were scraped to avoid cell confluence.

Bacterial Culture. The penicillin-sensitive *S. aureus* (strain ATCC55585) stock cultures were maintained in 20% glycerol at −80 °C. Before experiments, the bacteria were transferred onto fresh brain heart infusion (BHI)/agar (Difco, Invitrogen, Cergy-Pontoise, France) and incubated at 37 °C for 24 h. For each experiment, bacteria were subcultured in BHI (medium) at 37 °C for 18 h. The day of the experiment, the bacteria were washed twice with sterile PBS, counted in a Salumbini chamber, and adjusted to 1×10^7 bacteria/mL in RPMI-1640 medium supplemented with 10% v/v FBSd.

NP Internalization in J774 Cells. About 5×10^5 J774 cells were put on 24-well tissue-culture plates with (for microscopy) or without (cytometry) glass coverslips and incubated during the night (around 12 h) at 37 °C in humidified air containing 5% CO_2 to ensure cell adherence. Cells were then washed with RPMI 1640 + 0.5% v/v FBSd and incubated with 100 μg/mL of the different fluorescent NPs (*i.e.*, SqPNG or SqPNG-pH) in RPMI 1640 with 0.5% v/v FBSd during 2, 6, and 24 h (37 °C, 5% CO_2). Different concentrations of FBSd (0.5%, 1%, 2%, 5%, 10%, 20%) in the cell culture medium have been used to study the influence of decomplemented serum on the cell internalization of SqPNG-pH NPs (incubation time of 6 h). Different pharmacological inhibitors (cytochalasin D 5 μg/mL, latrunculine A 100 nM, LY294002 25 μM, chlorpromazine 25 μM, MβCD 2 mM, genistein 100 μM) have also been used to investigate NPs' phagocytotic/endocytotic pathways.[32] Practically, the cells were preincubated 1 h with one of the above-mentioned inhibitors before further incubation (6 h) with SqPNG-pH NPs (at 25 μg/mL in RPMI 1640 with 0.5% v/v FBSd at 37 °C and 5% CO_2). For flow cytometry, cells were washed with PBS and then treated with 0.25% trypsin for 10 min at 37 °C and 5% CO_2. Afterward, cells were vigorously dispersed and washed with RPMI 1640 + 10% FBSd. After centrifugation at 1500 rpm for 5 min in cytometry tubes, cells were resuspended with 400 μL of a solution of paraformaldehyde (PFA) 1% w/v in PBS and kept on ice until flow cytometry. A FACSCalibur flow cytometer equipped with a 15 mV, 488 nm argon laser (Becton Dickinson, San Jose, CA, USA) was used. The data were analyzed with CellQuest software. Fluorescence was recorded with a constant photomultiplier gain, and the results were expressed as the mean fluorescence intensity on a four-decade logarithmic scale.

Intracellular Antimicrobial Activity of NPs. *Nanoparticle Incubation Step.* About 5×10^5 J774 cells were incubated on 24-well tissue-culture plates during the night (around 12 h) at 37 °C in humidified air containing 5% CO_2 to ensure cell adherence. The next day, cells were washed with RPMI 1640 + 0.5% v/v FBSd and then incubated for 6 h in the same cell culture medium (37 °C, 5% CO_2) with or without different treatments (*i.e.*, 20 μg/mL of PNG, 50 μg/mL of SqPNG, which was equivalent to 20 μg/mL PNG or 50 μg/mL SqPNG-pH NPs, also equivalent to 20 μg/mL of PNG). Squalene-ester NPs (Sq-Est) (50 μg/mL) were used as control in the same conditions.

S. aureus Infection Step. After NP treatment cells were washed twice with 1 mL of RPMI 1640 + 10% v/v FBSd in order to eliminate extracellular NPs and free PNG. Then, 500 μL of *S. aureus* suspension (ATCC55585) in the same medium was added at 10^7 bacteria/mL (multiplicity of infection, MOI = 10) and incubated for 2 h (37 °C, 5% CO_2). To remove nonphagocytosed bacteria, J774 cells were washed and any extracellular bacteria were killed by further incubation in RPMI 1640 medium containing gentamicin (50 μg/mL). After 1, 6, and 24 h of incubation, cells were washed again with RPMI 1640 + 10% v/v FBSd and lysed by treatment with ice-cold water during 1 h. The lysates were plated at serial dilutions in sterile PBS on BHI/agar plates. The plates were incubated at 37 °C overnight, and the number of formed colonies was evaluated following the usual methodologies.[27,49,50]

For confocal microscopy studies, J774 cells were treated then infected in similar conditions as explained previously. Thereafter, the cells were washed with 1 mL of PBS, fixed with 1% PFA, and permeabilized with 0.2% Triton-X100. They were then brought into the mix of the LIVE/DEAD BacLight bacterial viability kit (Molecular Probes) for 15 min in the dark.[27] After washing with 1 mL of PBS, J774 cells were observed with an inverted Zeiss (Jena, Germany) LSM-510 META confocal laser scanning microscope.

Localization of NPs. For intracellular localization studies, 5×10^5 cells were treated with fluorescent NPs for 6 h, washed with PBS, and incubated with 1 mL of LysoTracker Red DND-99 solution (40 nM)[51] in RPMI medium (5 min at 37 °C, 5% CO_2). After washing, the coverslips were mounted and the fluorescence was immediately examined with an inverted Zeiss (Jena, Germany) LSM-510 META confocal laser scanning microscope equipped with an argon laser and helium neon laser (Plan-Apochromat 63× objective lens NA 1.40, oil immersion).

To visualize *S. aureus* in confocal microscopy, bacteria were incubated for 1 h at 37 °C with a high concentration of IP and washed three times with PBS before the infection step was performed as explained before. After 6 h of incubation with gentamicin, cells were washed three times with PBS, then fixed with 3% PFA at room temperature for 15 min. The washed coverslips were mounted, and the fluorescence was examined with an inverted Zeiss (Jena, Germany) LSM-510 META confocal laser scanning microscope.

Conflict of Interest: The authors declare no competing financial interest.

Acknowledgment. The research leading to these results has received funding from the European Research Council under the European Community's Seventh Framework Programme FP7/2007-2013 (grant agreement no. 249835).

Supporting Information Available: Detailed experimental section [PLB-985 culture; cytotoxicity assay; localization of NPs compared to CD11b membrane], supporting references, and supporting Figures S1 to S9. This material is available free of charge *via* the Internet at http://pubs.acs.org.

REFERENCES AND NOTES

1. Laskay, T.; van Zandbergen, G.; Solbach, W. Neutrophil Granulocytes--Trojan Horses for Leishmania Major and Other Intracellular Microbes? *Trends Microbiol.* **2003**, *11*, 210–214.
2. Abeylath, S. C.; Turos, E. Drug Delivery Approaches to Overcome Bacterial Resistance to Beta-Lactam Antibiotics. *Expert Opin. Drug Delivery* **2008**, *5*, 931–949.
3. Pinto-Alphandary, H.; Andremont, A.; Couvreur, P. Targeted Delivery of Antibiotics Using Liposomes and Nanoparticles: Research and Applications. *Int. J. Antimicrob. Agents* **2000**, *13*, 155–168.
4. Drulis-Kawa, Z.; Dorotkiewicz-Jach, A. Liposomes as Delivery Systems for Antibiotics. *Int. J. Pharm.* **2010**, *387*, 187–198.
5. Pinto-Alphandary, H.; Balland, O.; Laurent, M.; Andremont, A.; Puisieux, F.; Couvreur, P. Intracellular Visualization of Ampicillin-Loaded Nanoparticles in Peritoneal Macrophages Infected *in Vitro* with *Salmonella Typhimurium*. *Pharm. Res.* **1994**, *11*, 38–46.

6. Forestier, F.; Gerrier, P.; Chaumard, C.; Quero, A. M.; Couvreur, P.; Labarre, C. Effect of Nanoparticle-Bound Ampicillin on the Survival of Listeria Monocytogenes in Mouse Peritoneal Macrophages. *J. Antimicrob. Chemother.* **1992**, *30*, 173–179.
7. Couvreur, P.; Stella, B.; Reddy, L. H.; Hillaireau, H.; Dubernet, C.; Desmaele, D.; Lepetre-Mouelhi, S.; Rocco, F.; Dereuddre-Bosquet, N.; Clayette, P.; *et al*. Squalenoyl Nanomedicines as Potential Therapeutics. *Nano Lett.* **2006**, *6*, 2544–2548.
8. Sen, S. E.; Prestwich, G. D. Squalene Analogues Containing Isopropylidene Mimics as Potential Inhibitors of Pig Liver Squalene Epoxidase and Oxidosqualene Cyclase. *J. Med. Chem.* **1989**, *32*, 2152–2158.
9. Daehne, W.; Frederiksen, E.; Gundersen, E.; Lund, F.; Morch, P.; Petersen, H. J.; Roholt, K.; Tybring, L.; Godtfredsen, W. O. Acyloxymethyl Esters of Ampicillin. *J. Med. Chem.* **1970**, *13*, 607–612.
10. Jansen, A. B.; Russell, T. J. Some Novel Penicillin Derivatives. *J. Chem. Soc.* **1965**, *65*, 2127–2132.
11. Baltzer, B.; Binderup, E.; von Daehne, W.; Godtfredsen, W. O.; Hansen, K.; Nielsen, B.; Sorensen, H.; Vangedal, S. Mutual Pro-Drugs of Beta-Lactam Antibiotics and Beta-Lactamase Inhibitors. *J. Antibiot. (Tokyo)* **1980**, *33*, 1183–1192.
12. Klein, L. L.; Yeung, C. M.; Kurath, P.; Mao, J. C.; Fernandes, P. B.; Lartey, P. A.; Pernet, A. G. Synthesis and Activity of Nonhydrolyzable Pseudomonic Acid Analogues. *J. Med. Chem.* **1989**, *32*, 151–160.
13. Couvreur, P.; Reddy, L. H.; Mangenot, S.; Poupaert, J. H.; Desmaele, D.; Lepetre-Mouelhi, S.; Pili, B.; Bourgaux, C.; Amenitsch, H.; Ollivon, M. Discovery of New Hexagonal Supramolecular Nanostructures Formed by Squalenoylation of an Anticancer Nucleoside Analogue. *Small* **2008**, *4*, 247–253.
14. Dewar, M. J.; Storch, D. M. Alternative View of Enzyme Reactions. *Proc. Natl. Acad. Sci. U. S. A.* **1985**, *82*, 2225–2229.
15. Jorgensen, J. H.; Swenson, J. M.; Tenover, F. C.; Barry, A.; Ferraro, M. J.; Murray, P. R.; Reller, L. B. Development of Interpretive Criteria and Quality Control Limits for Macrolide and Clindamycin Susceptibility Testing of *Streptococcus Pneumoniae*. *J. Clin. Microbiol.* **1996**, *34*, 2679–2684.
16. Holten, K. B.; Onusko, E. M. Appropriate Prescribing of Oral Beta-Lactam Antibiotics. *Am. Fam. Physician* **2000**, *62*, 611–620.
17. Briones, E.; Colino, C. I.; Lanao, J. M. Delivery Systems to Increase the Selectivity of Antibiotics in Phagocytic Cells. *J. Controlled Release* **2008**, *125*, 210–227.
18. Hamilton-Miller, J. M. Antibiotic Resistance from Two Perspectives: Man and Microbe. *Int. J. Antimicrob. Agents* **2004**, *23*, 209–212.
19. Martinez, J. L.; Fajardo, A.; Garmendia, L.; Hernandez, A.; Linares, J. F.; Martinez-Solano, L.; Sanchez, M. B. A Global View of Antibiotic Resistance. *FEMS Microbiol. Rev.* **2009**, *33*, 44–65.
20. Balland, O.; Pinto-Alphandary, H.; Pecquet, S.; Andremont, A.; Couvreur, P. The Uptake of Ampicillin-Loaded Nanoparticles by Murine Macrophages Infected with *Salmonella Typhimurium*. *J. Antimicrob. Chemother.* **1994**, *33*, 509–522.
21. Balland, O.; Pinto-Alphandary, H.; Viron, A.; Puvion, E.; Andremont, A.; Couvreur, P. Intracellular Distribution of Ampicillin in Murine Macrophages Infected with *Salmonella Typhimurium* and Treated with (3h)Ampicillin-Loaded Nanoparticles. *J. Antimicrob. Chemother.* **1996**, *37*, 105–115.
22. Lemarchand, C.; Gref, R.; Passirani, C.; Garcion, E.; Petri, B.; Muller, R.; Costantini, D.; Couvreur, P. Influence of Polysaccharide Coating on the Interactions of Nanoparticles with Biological Systems. *Biomaterials* **2006**, *27*, 108–118.
23. Semiramoth, N.; Gleizes, A.; Turbica, I.; Sandre, C.; Marin-Esteban, V.; Gorges, R.; Servin, A.; Chollet-Martin, S. Afa/Dr-Expressing, Diffusely Adhering *Escherichia Coli* Strain C1845 Triggers F1845 Fimbria-Dependent Phosphatidylserine Externalization on Neutrophil-Like Differentiated Plb-985 Cells through an Apoptosis-Independent Mechanism. *Infect. Immun.* **2010**, *78*, 2974–2983.
24. Owens, D. E., 3rd; Peppas, N. A. Opsonization, Biodistribution, and Pharmacokinetics of Polymeric Nanoparticles. *Int. J. Pharm.* **2006**, *307*, 93–102.
25. Garzoni, C.; Kelley, W. L. *Staphylococcus Aureus*: New Evidence for Intracellular Persistence. *Trends Microbiol.* **2009**, *17*, 59–65.
26. Barcia-Macay, M.; Seral, C.; Mingeot-Leclercq, M. P.; Tulkens, P. M.; Van Bambeke, F. Pharmacodynamic Evaluation of the Intracellular Activities of Antibiotics against *Staphylococcus Aureus* in a Model of Thp-1 Macrophages. *Antimicrob. Agents Chemother.* **2006**, *50*, 841–851.
27. Kubica, M.; Guzik, K.; Koziel, J.; Zarebski, M.; Richter, W.; Gajkowska, B.; Golda, A.; Maciag-Gudowska, A.; Brix, K.; Shaw, L.; *et al*. A Potential New Pathway for *Staphylococcus Aureus* Dissemination: The Silent Survival of *S. Aureus* Phagocytosed by Human Monocyte-Derived Macrophages. *PLoS One* **2008**, *3*, e1409.
28. Melter, O.; Radojevic, B. Small Colony Variants of *Staphylococcus Aureus*--Review. *Folia Microbiol. (Praha)* **2010**, *55*, 548–558.
29. Kiss, A. L.; Geuze, H. J. Caveolae Can Be Alternative Endocytotic Structures in Elicited Macrophages. *Eur. J. Cell Biol.* **1997**, *73*, 19–27.
30. Perry, D. G.; Daugherty, G. L.; Martin, W. J., 2nd Clathrin-Coated Pit-Associated Proteins Are Required for Alveolar Macrophage Phagocytosis. *J. Immunol.* **1999**, *162*, 380–386.
31. Rajendran, L.; Knolker, H. J.; Simons, K. Subcellular Targeting Strategies for Drug Design and Delivery. *Nat. Rev. Drug Discovery* **2010**, *9*, 29–42.
32. Ivanov, A. I. Pharmacological Inhibition of Endocytic Pathways: Is It Specific Enough to Be Useful? *Methods Mol. Biol.* **2008**, *440*, 15–33.
33. Aggarwal, P.; Hall, J. B.; McLeland, C. B.; Dobrovolskaia, M. A.; McNeil, S. E. Nanoparticle Interaction with Plasma Proteins as It Relates to Particle Biodistribution, Biocompatibility and Therapeutic Efficacy. *Adv. Drug Delivery Rev.* **2009**, *61*, 428–437.
34. Dobrovolskaia, M. A.; Patri, A. K.; Zheng, J.; Clogston, J. D.; Ayub, N.; Aggarwal, P.; Neun, B. W.; Hall, J. B.; McNeil, S. E. Interaction of Colloidal Gold Nanoparticles with Human Blood: Effects on Particle Size and Analysis of Plasma Protein Binding Profiles. *Nanomedicine* **2009**, *5*, 106–117.
35. Goppert, T. M.; Muller, R. H. Protein Adsorption Patterns on Poloxamer- and Poloxamine-Stabilized Solid Lipid Nanoparticles (Sln). *Eur. J. Pharm. Biopharm.* **2005**, *60*, 361–372.
36. Kim, H. R.; Andrieux, K.; Delomenie, C.; Chacun, H.; Appel, M.; Desmaele, D.; Taran, F.; Georgin, D.; Couvreur, P.; Taverna, M. Analysis of Plasma Protein Adsorption onto Pegylated Nanoparticles by Complementary Methods: 2-De, Ce and Protein Lab-on-Chip System. *Electrophoresis* **2007**, *28*, 2252–2261.
37. Thode, K.; Luck, M.; Semmler, W.; Muller, R. H.; Kresse, M. Determination of Plasma Protein Adsorption on Magnetic Iron Oxides: Sample Preparation. *Pharm. Res.* **1997**, *14*, 905–910.
38. Goppert, T. M.; Muller, R. H. Adsorption Kinetics of Plasma Proteins on Solid Lipid Nanoparticles for Drug Targeting. *Int. J. Pharm.* **2005**, *302*, 172–186.
39. Moghimi, S. M.; Muir, I. S.; Illum, L.; Davis, S. S.; Kolb-Bachofen, V. Coating Particles with a Block Co-Polymer (Poloxamine-908) Suppresses Opsonization but Permits the Activity of Dysopsonins in the Serum. *Biochim. Biophys. Acta* **1993**, *1179*, 157–165.
40. Ogawara, K.; Furumoto, K.; Nagayama, S.; Minato, K.; Higaki, K.; Kai, T.; Kimura, T. Pre-Coating with Serum Albumin Reduces Receptor-Mediated Hepatic Disposition of Polystyrene Nanosphere: Implications for Rational Design of Nanoparticles. *J. Controlled Release* **2004**, *100*, 451–455.
41. Cedervall, T.; Lynch, I.; Lindman, S.; Berggard, T.; Thulin, E.; Nilsson, H.; Dawson, K. A.; Linse, S. Understanding the Nanoparticle-Protein Corona Using Methods to Quantify Exchange Rates and Affinities of Proteins for Nanoparticles. *Proc. Natl. Acad. Sci. U. S. A.* **2007**, *104*, 2050–2055.

42. Carrstensen, H.; Muller, R. H.; Muller, B. W. Particle Size, Surface Hydrophobicity and Interaction with Serum of Parenteral Fat Emulsions and Model Drug Carriers as Parameters Related to Res Uptake. *Clin. Nutr.* **1992**, *11*, 289–297.
43. Muller, R. H.; Ruhl, D.; Luck, M.; Paulke, B. R. Influence of Fluorescent Labelling of Polystyrene Particles on Phagocytic Uptake, Surface Hydrophobicity, and Plasma Protein Adsorption. *Pharm. Res.* **1997**, *14*, 18–24.
44. Norman, M. E.; Williams, P.; Illum, L. Human Serum Albumin as a Probe for Surface Conditioning (Opsonization) of Block Copolymer-Coated Microspheres. *Biomaterials* **1992**, *13*, 841–849.
45. Sahay, G.; Alakhova, D. Y.; Kabanov, A. V. Endocytosis of Nanomedicines. *J. Controlled Release* **2010**, *145*, 182–195.
46. Renard, C.; Vanderhaeghe, H. J.; Claes, P. J.; Zenebergh, A.; Tulkens, P. M. Influence of Conversion of Penicillin G into a Basic Derivative on Its Accumulation and Subcellular Localization in Cultured Macrophages. *Antimicrob. Agents Chemother.* **1987**, *31*, 410–416.
47. Tulkens, P. M. Intracellular Distribution and Activity of Antibiotics. *Eur. J. Clin. Microbiol. Infect. Dis.* **1991**, *10*, 100–106.
48. Andersen, O. S. Elementary Aspects of Acid-Base Permeation and pH Regulation. *Ann. N.Y. Acad. Sci.* **1989**, *574*, 333–353.
49. Vaudaux, P.; Waldvogel, F. A. Gentamicin Antibacterial Activity in the Presence of Human Polymorphonuclear Leukocytes. *Antimicrob. Agents Chemother.* **1979**, *16*, 743–749.
50. Trouillet, S.; Rasigade, J. P.; Lhoste, Y.; Ferry, T.; Vandenesch, F.; Etienne, J.; Laurent, F. A Novel Flow Cytometry-Based Assay for the Quantification of *Staphylococcus Aureus* Adhesion to and Invasion of Eukaryotic Cells. *J. Microbiol. Methods* **2011**, *86*, 145–149.
51. Toyooka, K.; Takai, S.; Kirikae, T. *Rhodococcus Equi* Can Survive a Phagolysosomal Environment in Macrophages by Suppressing Acidification of the Phagolysosome. *J. Med. Microbiol.* **2005**, *54*, 1007–1015.

Remerciements
Acknowledgement
Ringraziamenti

A la fin de ces trois années de thèse, j'adresse mes plus vifs remerciements à toutes les personnes de l'UMR CNRS 8612 et de l'Université de Turin pour l'aide dans le développement de ce projet de thèse. En particulier merci au Prof. Elias Fattal pour m'avoir accueillie et donné la possibilité de travailler dans un cadre de travail pluridisciplinaire, dynamique, agréable et amusant, facteurs très importants pour le bon déroulement du projet.

Un grand merci à mes directeurs de thèse.
En premier lieu, au Prof. Patrick Couvreur pour m'avoir accueillie au sein de son équipe, pour la confiance, l'énergie et l'optimisme, pour sa rigueur scientifique et méthodologique.
Merci au Dr Barbara Stella, pour les précieux conseils scientifiques et personnels, pour les corrections ponctuelles et la patience.
Merci au Dr Simona Mura pour le dynamisme et la présence, la disponibilité et la réactivité aux problèmes scientifiques et techniques de tous les jours ainsi que pour la révision du manuscrit.
Merci au Prof. Luigi Cattel pour m'avoir proposé et promu dans ce projet de thèse en cotutelle et pour toute la confiance et les conseils personnels qu'il m'a donné.

I would like to thank to Prof. Gert Storm, Dr Gianfranco Pasut and Prof. Giampaolo Tortora who accept to be part of the jury of my defense and kindly offer time and energy to review my thesis.

Un sincère merci au Dr Didier Desmaële, pour m'avoir accueillie et dirigée dans le monde de la chimie organique avec la passion qui lui est propre. Pour les conseils à la fois simples et précieux et pour ne pas s'être empêché de faire avec moi des blagues en français même s'il fallait me les expliquer une fois sur deux…

Merci à Magali Noiray, pour son importante aide manuelle et scientifique avec les manips d'interactions moléculaires (BIACORE et ITC) et m'avoir donné courage et motivation dans les moments difficiles.

Merci au Dr Juliette Vergnaud, pour les analyses biochimiques et les autres discussions fructueuses qui m'ont permis d'apprendre importantes astuces pour améliorer mes rapports avec les cellules cancéreuses.

Merci au Dr Christine Vauthier pour m'avoir appris avec méthode et patience l'électrophorèse bidimensionnelle et la manip d'activation du complément dans excellentes conditions matérielles.

Merci au Dr Claire Guetin, pour m'avoir fait découvrir la chimie analytique, pour la disponibilité, l'aide et la sympathie au cours des toutes les analyses HPLC.

Merci à Eric Buchi pour la synthèse du squalene sunitinib ainsi qu'à Fatima et Sinda pour leur gentillesse et l'aide pratique pendant les « journées chimiques » en Tour D3.

A special thanks to Federica Maione and Enrico Giraudo (Institute for Cancer Research at Candiolo) for the in vivo experiments in RIP1-Tag2 mice model.

Mes remerciements à tous les statutaires de l'équipe 7 pour leur disponibilité et les conseils pendant ou dehors des réunions d'équipe. Merci aussi à Nicolas Tsapis et Hervé Hillaireau pour rendre la collaboration et l'échange scientifique dans l'unité simple et agréable.

Un énorme merci à toute la troupe doctorants/postdocs/masters de l'UMR CNRS 8612.

Infine un immenso grazie a Erica, mamma e papà per aver sollecitato, sostenuto e promosso il mio percorso universitario. Per aver compreso e appoggiato questa scelta, sebbene fosse difficile anche per loro, e aver condiviso i sacrifici e il coraggio di chi non si ferma a metà percorso ma arriva fino alla fine delle proprie ambizioni.

BONUS Remerciements / Acknowledgement / Ringraziamenti

Un BIG merci à le fanclub doctorants/post docs/masters de l'Institut Galien Paris-Sud pour les bons moments scientifiques (ou pas du tout scientifiques) passé ensemble.

En particulier merci à toutes les personnes qui ont animé l'ancien bureau D5-114 pendant les 10 mois de mon séjour M2/Erasmus et les 3 années (*grosso modo*) du doctorat. Parce que de fois on passait si beaucoup de temps ensemble qu'il parait de n'être jamais rentre à la maison d'un jour à l'autre…

En fin c'était agréable de partager avec vous les moments délicats du « n=3 », les week-ends-manips, les jours festifs-manips, les dimanches ensoleillés(oui, ca arrive si rarement à Paris…)-manips, les chiantes-manips, les manips avec les cellules qui font les «cellules chiantes», la traversée de tout Paris dans l'heure de embouteillage pour apporter le colis à l'aéroport car M.FedEx avait oublié, les stress «FedEx n'est pas encore arrivé?» qui a suivi, la douleur aiguë de mon pied à reste sous la barrière pour les animaux sauvages de la fac (tu reste après 22h:ongle cassé pour 1 an), et puis beaucoup des autres choses que maintenant je ne rappelle pas.

Pour balancer des noms … ordre très approximatif ☺ …
Merci à Alice pour l'amitié et l'aide concrète dans les moments plus difficiles, le même pour Vianney avec sa pincée de folie quotidienne jamais démesuré, et Thomas et son approche zen, et Nadou pour les cours d'informatique/« entreprise féminine ». Merci aussi pour l'école de français!
Merci aussi à Thais pour l'amitié e sa sensibilité et pour les samedi passé ensemble sur Paris et/ou en culture cells (T-u a-s c-o-m-m-e-n-cé l-a t-h-è-s-e…), à Giovanna pour le souris gratuit et « le sue perle di saggezza », à Tanguy, pour l'admirable niveau de tolérance absolu, à Leticia pour le pragmatisme et pour les très bons moments passe ensemble, à Nadia pour la « rationalité pacifique », Gopan qui aime bien le mot manoscritti…
Et encore à la folle Laura l'espagnol, Acarilia, les trois viking Adam, Christian, Morits, Trung (trois pas quatre), Felix, Patricia, Dunja. Sans oublier les remerciements à les « vieux » (qui plus qui moins) de l'Umr, Sophie avec laquelle j'ai partagé le premier jour et aussi le dernier de cette aventure, Brambilla (ER Pistola), Dario (ehi, comé?), Vale, Violeta, Silvia, Giovanni, Cristina, Chiara, Lucien, j'ai oublié, Nicolas, Stefano, le rat, les deux dents, les momies d'Égypt.

Merci aussi à Dominique, Patricia, Christian, Sylvie, Anne Marie, Marie Claire et Claire.

Et vu les trois années de thèse sont aussi trois année de vie (car il y a eu des moments ou il n'y avait pas gros différences entre la vie et la thèse)…

je voudrais unir à ce remercîments aussi la Cite Universitaire, les américains de la Fondations de Etat Unis et les suédois de la Maison de la Suède. Riccardo, Anna (x3), Marie, Otto, Alfred, Sofia, Ingrid, Cindy, Amélie et son arnaque du fabuleux destin, Cupido che prima o poi colpirà il bersaglio giusto per me, Bob Dylan, Lou Reed che non ce l'ha fatta a vedermi dottorata, the pale blue eyes and so on…
Ah oui, Cri, Ire, Sara, Elisabetta, Anya, Laura et mon amour TGV avec les chefs du train très compréhensibles.

E Grazie a te, Concentrazione, che non mi hai mollato. Un'ultimo sforzo e poi mandiamo Stress in vacanza e ci riposiamo per un po'.